Step-wise differentiation of cerebral organoids towards hippocampal and choroid plexus progeny by sustained expression of early NSC stage-specific microRNA-20b

Inaugural Dissertation

to obtain the academic degree
Doctor rerum naturalium (Dr. rer. nat.)

submitted to the Department of Biology, Chemistry, Pharmacy of

Freie Universität Berlin

by
Sneha Arora

2021

The research work for this dissertation was performed from March 2015 to June 2021 under the supervision of Dr. Yechiel Elkabetz at the Max Planck Institute for Molecular Genetics in Berlin, Germany. The dissertation was submitted in June 2021 to the Department of Biology, Chemistry and Pharmacy of the Freie Universität Berlin, Germany.

1st Reviewer: Prof. Dr. Katja Nowick
Freie Universität Berlin

2nd Reviewer: Prof. Dr. Mathias F. Wernet
Freie Universität Berlin

Date of Defense: 27/09/2021

ACKNOWLEDGEMENTS

I would like to thank and express my deepest gratitude to my research supervisor Dr. Yechiel Elkabetz for giving me the opportunity to work in his lab and guiding me throughout these five years. I am very grateful to him to provide me the opportunity to explore the role of microRNAs in neural stem cells, under his careful and constant supervision. I would also like to show my gratefulness for the patience he has shown in both good and bad times during all these years of my PhD.

Secondly, I would like to thank Prof. Dr. Katja Nowick and Prof. Dr. Mathias F. Wernet for accepting to be my supervisor and thesis reviewer for my PhD dissertation.

I would like to thank our collaborator Dr. Markus Haffner from NIH for his inputs and discussions and for all the small RNA sequencing data.

I would like to thank my lab colleague Daniel Rosebrock for the computational analysis for the work without him it would have been difficult to finish these research goals. I would also like to thank Amèlia Aragonés Hernández for sharing her views and thoughtful discussions. Apart from the scientific discussions, I am also grateful to both of them to be like second family here in Germany. Thank you, guys, for all the help, support, and being a part of my PhD journey.

I would like to thank Dr. Yakey Yaffe for his fruitful discussions and for his jokes, which always improved my mood. I would also like to thank Anastasios Balaskas for all the productive discussion regarding the project. I am also thankful to my good friend Rotem Volkman from Tel Aviv University, who was there for me during the initial phase of my PhD. I always respected his views and suggestions. It was pleasure working with him and will always remember him.

I would like to thank my husband and ex-colleague Dr. Naresh Mutukula for teaching me the tissue culture during the initial phase of PhD, collaborating with me during the initial experiments for this project. A big thanks for always been there and emotionally supporting me during the difficult times. I will always be grateful to you for being a

constant support during these years. A huge hug and special thanks for being a part of my life.

I would like to thank FACS, RNA-Sequencing and Imaging facility of MPIMG, Berlin and Tel Aviv University for all the help and support. I would also like to thank all the department Meissner colleagues for all the support and comments during department meetings.

Finally, I would like to thank my family — my father – Praveen Arora, my mother – Lovely Arora and my brother – Prateek Arora for their unconditional love and support during the ups and downs of my life. I would also like to thank my in-law's family for always being there and motivating me to finish this journey. This would not have been possible without my family's constant support. Words fall short to express my love and gratitude to them.

Table of Contents

Acknowledgements **3**

Table of Contents **5**

Abstract (English) **8**

Abstract (Deutsch) **10**

1. Introduction **12**

1.1 Early mammalian embryonic development 12

1.2 Nervous System development 13

1.3 In vivo neural induction and patterning 17

1.4 Morphogens in neural induction and patterning 21

1.4.1 Transforming Growth Factor (TGF)-β Superfamily 21

1.4.2 Bone morphogenetic protein (BMP) Signaling 22

1.4.3 Activin/Nodal TGF- β Signaling 22

1.4.4 WNT Signaling 23

1.5 Pluripotent stem cells (PSCs) 24

1.6 Neural stem cells (NSCs) 25

1.7 NSCs in cortex and corticogenesis 25

1.8 Brief overview of in vitro neural induction and corticogenesis (2D neural rosettes and 3D brain organoids) using PSCs 31

1.9 Identification, isolation and characterization of consecutive neural stem cells *in* vitro 32

1.10 Classification of small RNAs in animals 35

1.11 MicroRNAs 36

1.11.1 Transcription Regulation 37

1.11.1.1 The Canonical pathway for microRNA biogenesis 38

1.11.1.2 The Non-canonical pathway for microRNA biogenesis 39

1.12 Transcription of microRNA 41

1.12.1 miRNA gene families and nomenclature 41

1.13 MicroRNAs in early embryogenesis 42

1.14 MicroRNAs in embryonic stem cells 43

1.15 miRNAs in NSCs self-renewal, differentiation and fate determinant 43

1.15.1 Self-renewal and proliferation 43

1.15.2 Cell fate determinant 45

1.16 miR-17~92 cluster and family 47

2. Materials and Methods **51**

2.1 Reagents 51

2.2 Molecular Biology application kits 52

2.3 Cell lines 53

2.4 Reagents preparation 53

2.5 Generation and culturing of hESCs line 55

2.6 Generation and culturing of hiPSCs line 55

2.7 Neural induction and rosette formation from pluripotent stem cells (EB protocol) 57

2.8 Derivation of cerebral organoids from human pluripotent stem cells 60

2.9 RNA isolation 63

2.10 Preparation of cDNA 65

2.11 small RNA Sequencing 66

2.12 Cloning of hsa-miR-20b-5p into LT3GEPIR plasmid 67

2.13 Cloning of CCND1 in a lentiviral vector 68

2.14 Midi-Prep plasmid isolation kit 69

2.15 Virus generation in HEK cells 70

2.16 Titer calculation for viral particles and hiPSCs line generation 71

2.17 Genomic DNA isolation 72

2.18 Integration copy number Analysis 73

2.19 Quantitative PCR (qPCR) analysis 73

2.20 cDNA preparation for microRNA 75

2.21 Matrigel Induction protocol 79

2.22 Immunostainings 79

2.23 Measurements and statistical analysis 81

2.24 Bulk RNA sequencing 81

2.25 Preparation and sequencing of RNA-Seq Libraries 81

2.26 RNA dataset and processing, normalization and analysis 83

2.26 Single cell RNA-Seq procedure 82

2.27 Single cell library preparation 83

2.28 Single cell RNA-Seq data processing, dataset alignment and cell population identification 83

3. Results **85**

3.1 Long term propagation, consecutive isolation and characterization of Neural Stem cells (NSCs) using Triple-i (SBNX) method 85

3.2 Identification of stage specific miRNAs in cortical neural progenitors 87

3.3 Generation of inducible stable hsa-miR-20b expressing line 94

3.4 Single Cell RNA Sequencing of day 13 organoids reveals upregulation of WNT family proteins in NSCs of miR-20b overexpressed organoids 96

3.5 Single Cell RNA Sequencing of day 30 mir20b overexpressing organoids revealed inhibition of non-telencephalic fates along with increase in hippocampal NSCs 100

3.6 miR-20b overexpressing organoids on day 30 exhibit reduced number of cortical NSCs and IP populations, while showing an increase in cortical neurons 101

3.7 miR-20b overexpressing organoids exhibited a decrease in ventricular zone (VZ) expansion and poorly defined sub-ventricular zone (SVZ) 109

3.8 Single cell transcriptome analysis of day 50 miR-20b overexpressing organoids display emergence of caudal cortical fates such as cortical hem derived hippocampal as well as choroid plexus fates 116

3.9 miR-20b overexpressing organoids exhibited an emergence of choroid plexus and hippocampal cell types in later stage of development 122

3.10 Overexpression of miR-20b causes downregulation of its target gene CCND1 in cortical NSCs and IPs..... 124

3.11 Generation of inducible stable hsa-miR-20b and CCND1 expressing line 126

3.12 Rescue of the cytoarchitectural phenotype along with change in identity towards hippocampal fates in CCND1-compensating, miR-20b overexpressing organoids 126

3.13 Single Cell RNA sequencing reveals significant increase in hippocampal stem cell populations in CCND1-compensating miR-20b overexpressing organoids 131

3.14 Over expression of miR-20b induces an early ectoderm fate in 2D monolayer neural differentiation system 136

4. Discussion **139**

5. Bibliography..... **145**

6. Abbreviations..... **164**

7. List of Publications **167**

8. Declaration of Independence..... **168**

Abstract (English)

Pluripotent stem cells (PSCs) have the ability to undergo indefinite self-renewal while giving rise to the three germ layers. This remarkable capacity has turned PSCs to be a fundamental cell source for regenerative medicine research and applications. The derivation of induced pluripotent stem cells (iPSCs) over a decade ago has sparked a widespread enthusiasm and opportunity for personalized autologous cell-based therapies in a wide array of diseases. However, the development of optimized disease models and iPSC-derived products heavily relies on the generation of homogenous culture systems for the cell type of interest, which currently presents one of the major hindrances towards the use of PSC derivatives in therapeutic applications.

The cerebral cortex is an excellent example of a tissue with enormous heterogeneity that introduces immense challenges for *in vitro* disease models and therapeutic applications. Our lab mainly focuses on studying the development of the cerebral cortex, particularly investigating the development of cortical neural stem cells (NSCs). Our goal is to devise approaches for the differentiation of PSCs into founder NSC building blocks. We put particular emphasis on achieving high purity that will enable studying authentic cell fate decisions that are associated with regional patterning, self-renewal and differentiation processes that shape the cortex. A homogeneous early cortical population will also enable extracting a more reliable molecular identity of those cells, which can then be used for meaningful disease modeling and for devising sophisticated approaches to induce or maintain self-renewal of such populations *in vitro*.

However, recent research from our lab has shown that current methods to derive early cortical progenitors from PSCs are highly diverse and yield heterogeneous populations containing both cortical and non-cortical cell types. This results in heterogeneous founder NSC populations, limiting their use as a universal pure NSC source. To overcome this hurdle, our lab established a streamlined method known as Triple-i paradigm to derive homogenous starting cortical progenitors both in neural rosettes (2D) and in organoids (3D) platforms.

The main objectives of this thesis are to identify early signals that modulate temporal and regional fates within developing founder cortical NSC populations, focusing on

small non-coding RNA (miRNAs), which are known to be key regulators of many developmental processes including stem cell proliferation and lineage specifications. These miRNAs guide the early development in a spatiotemporal manner by regulating the expression of multiple gene networks at the post-transcriptional level. They are abundantly expressed in the developing neural tube that eventually gives rise to different regions of central nervous system, including the cerebral cortex. However, it is unknown whether they have the capacity to specify a particular brain region in the cortex such as archicortex that consists of cortical hem, hippocampus and choroid plexus.

In this study, we have identified a miRNA important for the specification of archicortex and interrogated its role in cell fate specification using a battery of molecular and cellular studies. First, we employed *in vitro* human embryonic stem cell-based models (2D monolayer and 3D cerebral organoid) for the derivation of founder neural stem cell and their progression. We then identified a list of miRNAs that are specifically expressed in this early neural stem cell stage, among which we found hsa-miR-20b-5p to be one of the highly expressed microRNAs in early NSCs derived under both monolayer culture and cerebral organoids.

Second, by overexpressing hsa-miR-20b-5p in cerebral organoids, we provided evidence that this miRNA is involved in the stepwise specification of choroid plexus of archicortex, by caudalizing the early cortical NSC, due to modulation of WNT and BMP signalling components. In addition, cellular immunostainings displayed a characteristic presence of giant but thin single- layer vesicles positive for choroid plexus markers in miR-20b overexpressing organoids, as opposed to pseudostratified cortical neural rosettes in wildtype organoids. Furthermore, we showed that co-overexpression of miR-20b with of its main target CCND1, lead to the generation of cortical hem/hippocampus organoids.

Altogether, through an extensive miRNA-sequencing, single cell RNA-sequencing and cellular immunofluorescence studies, we revealed the expression of hsa-miR-20b-5p in early neural stem cells, its role in the specification of the archicortex lineages and its part as a cell fate modulator for converting cortical organoids towards choroid plexus structures.

Zusammenfassung (Deutsch)

Pluripotente Stammzellen (PSCs) haben die Fähigkeit, sich auf unbestimmte Zeit selbst zu erneuern und dabei die drei Keimblätter hervorzubringen. Diese bemerkenswerte Fähigkeit hat PSCs zu einer grundlegenden Zellquelle für die Forschung und Anwendungen der regenerativen Medizin gemacht. Die Gewinnung von induzierten pluripotenten Stammzellen (iPSCs) vor über einem Jahrzehnt hat eine weit verbreitete Begeisterung geweckt und Möglichkeiten für personalisierte autologe zellbasierte Therapien bei einer Vielzahl von Krankheiten aufgedeckt. Die Entwicklung optimierter Krankheitsmodelle und von iPSC abgeleiteter Produkte hängt jedoch stark von der Erzeugung homogener Kultursysteme für den bestimmten Zelltyp ab, was derzeit eines der Haupthindernisse für den Einsatz von PSC-Derivaten in therapeutischen Anwendungen darstellt.

Die Großhirnrinde ist ein hervorragendes Beispiel für ein Gewebe mit enormer Heterogenität, das für In-vitro-Krankheitsmodelle und therapeutische Anwendungen immense Herausforderungen mit sich bringt. Unser Labor konzentriert sich hauptsächlich auf die Untersuchung der Entwicklung der Großhirnrinde, insbesondere der Entwicklung von kortikalen neuralen Stammzellen (NSCs). Unser Ziel ist es, Ansätze zur Differenzierung von PSCs in Gründer-NSC-Bausteine zu entwickeln. Wir legen besonderen Wert darauf, eine hohe Reinheit zu erreichen, die es ermöglicht, authentische Entscheidungen über das Zellschicksal zu untersuchen, die mit den regionalen Mustern, Selbsterneuerung und Differenzierungsprozessen verbunden sind, die den Kortex formen. Eine homogene frühe kortikale Population wird es auch ermöglichen, eine zuverlässigere molekulare Identität dieser Zellen zu bestimmen, die dann für aussagekräftige Krankheitsmodelle und für die Entwicklung fortgeschrittener Ansätze zur Induktion oder Aufrechterhaltung der Selbsterneuerung solcher Populationen in vitro verwendet werden kann.

Jüngste Forschungen aus unserem Labor haben jedoch gezeigt, dass aktuelle Methoden zur Ableitung früher kortikaler Vorläufer aus PSCs sehr vielfältig sind und heterogene Populationen ergeben, die sowohl kortikale als auch nicht-kortikale Zelltypen enthalten. Dies führt zu heterogenen Gründer-NSC-Populationen, die nur beschränkt als universelle reine NSC-Quelle dienen können. Um diese Hürde zu überwinden, hat unser Labor eine optimierte Methode namens Triple-i-Paradigma entwickelt, um homogene kortikale Ausgangsvorläufer sowohl in neuronalen Rosetten (2D) als auch in Organoiden (3D) abzuleiten.

Die Hauptziele dieser Arbeit sind die Identifizierung von frühen Signalen, die zeitliche und regionale Schicksale innerhalb sich entwickelnder kortikaler NSC-Populationen modulieren. Dabei liegt der Fokus auf kleinen nicht-kodierenden RNAs (miRNAs), die wichtige Regulatoren vieler Entwicklungsprozesse sind, wie Stammzellproliferation und Zelltyp-Spezifizierung. Diese miRNAs steuern die frühe Entwicklung in Raum und Zeit, indem sie die Expression mehrerer Gennetzwerke auf posttranskriptioneller Ebene regulieren. Sie werden reichlich im sich entwickelnden Neuralrohr exprimiert,

aus dem schließlich verschiedene Regionen des zentralen Nervensystems, einschließlich der Großhirnrinde, hervorgehen. Es ist jedoch nicht bekannt, ob sie in der Lage sind, eine bestimmte Hirnregion im Kortex zu spezifizieren, wie z.B. den Archicortex, der aus kortikalem Saum, Hippocampus und Plexus choroideus besteht.

In dieser Studie haben wir eine miRNA identifiziert, die für die Spezifikation des Archicortex wichtig ist, und ihre Rolle bei der Spezifikation des Zellschicksals mit einer Reihe von molekularen und zellulären Studien untersucht. Zunächst verwendeten wir in vitro-Modelle auf der Basis von humanen embryonalen Stammzellen (2D-Monolayer und 3D-zerebrales Organoid) zur Ableitung von neuralen Gründerstammzellen und deren Progression. Wir identifizierten eine Reihe miRNAs, die spezifisch in diesem frühen neuralen Stammzellstadium exprimiert werden. Unter anderem identifizierten wir hsa-miR-20b-5p als eine der hochexprimierten miRNAs in frühen NSCs, die entweder aus Monolayer-Kulturen oder zerebralen Organoiden stammen.

Zweitens lieferten wir durch die Überexpression von hsa-miR-20b-5p in zerebralen Organoiden den Nachweis, dass diese miRNA an der schrittweisen Spezifizierung des Plexus choroideus des Archicortex beteiligt ist, indem sie die frühen kortikalen NSC durch die Modulation von WNT- und BMP-Signalkomponenten kaudalisiert. Darüber hinaus zeigten zelluläre Immunfärbungen ein charakteristisches Vorhandensein von riesigen, aber dünnen einschichtigen Vesikeln, die – im Gegensatz zu pseudostratifizierten kortikalen neuralen Rosetten in Wildtyp-Organoiden – positiv für Plexus choroideus-Marker in miR-20b-überexprimierenden Organoiden waren. Darüber hinaus haben wir gezeigt, dass die Ko-Überexpression von miR-20b mit seinem Hauptziel CCND1 zur Bildung von kortikalen Hem-/Hippocampus-Organoiden führt.

Insgesamt haben wir durch umfangreiche miRNA-Sequenzierung, Einzelzell-RNA-Sequenzierung und zelluläre Immunfluoreszenzstudien die Expression von hsa-miR-20b-5p in frühen neuralen Stammzellen, seine Rolle bei der Spezifizierung der Archicortex-Linien und seine Rolle als Zellschicksalsmodulator zur Umwandlung von kortikalen Organoiden in Strukturen des Plexus choroideus aufgedeckt.

1. INTRODUCTION

1.1 Early mammalian embryonic development

Embryonic development is initiated by fertilization of an oocyte by sperm, which leads to the formation of a zygote. This single celled zygote undergoes a series of mitotic cell divisions to form the blastocyst and simultaneously moves from the fallopian tubule to the uterus where it gets implanted into the endometrium. The first cell differentiation event in the blastocyst is the establishment of two distinct cell lineages: i) an outer layer of trophoectoderm (TE) which generates an extra embryonic tissue engages in implantation of blastocyst to mother uterus and ii) inner cell mass (ICM) which gives rise to the embryo. It is only after implantation, ICM cells differentiate into three germ layers namely ectoderm, mesoderm and endoderm in a highly organized process known as gastrulation (Marikawa and Alarcon, 2009) (Figure 1). Due to limitations of studying human embryogenesis, much of our knowledge of mammalian early-stage embryogenesis and germ layer formation has come from mouse embryos. It is believed that much of the lineage decision processes are similar to what occurs during human embryogenesis. At E6.5 stage of mouse development, gastrulation begins with the formation of the primitive streak from the posterior side of the embryo. The pluripotent epiblast cells from the posterior end migrate through the primitive streak and give rise to the mesendoderm, which in turn give rise to the mesoderm and definitive endoderm. The single cell layer of anterior epiblast cells which do not ingress are referred as the early ectoderm. (Tam and Behringer, 1997). The anterior/proximal region of the ectodermal layer at E7.0 has transient potential to differentiate into either epidermis which generates skin or neuroectoderm that generates neural tissue depending on the level of BMP signaling. (Figure 2) (Li et al., 2013) Based on the knowledge gained from *in vivo* studies many *in vitro* studies later on developed protocols to derive neural lineages from pluripotent stem cells (PSCs) (Blauwkamp et al., 2012; Gadue et al., 2006; Tchieu et al., 2017; Tropepe et al., 2001; Watanabe et al., 2005; Zhang et al., 2001a; Zimmer et al., 2016)

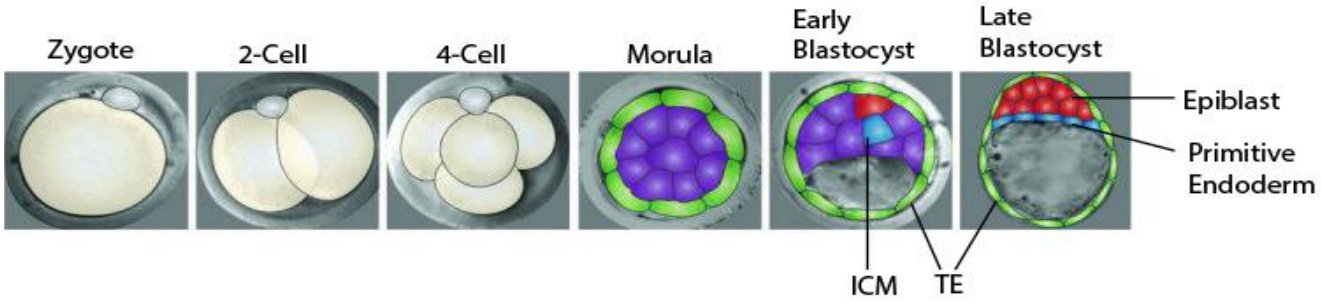

Figure 1: Stages of mammalian embryogenesis (Pre-implantation)

After fertilization, zygote undergoes series of symmetrical cell divisions and generates blastocyst which consist of inner cell mass (ICM) and trophectoderm (TE). ICM later gives rise to three germ layers i.e., ectoderm, mesoderm,and endoderm. These three germ layers give rise to different tissues in mammalian body, Modified from (Hadjantonakis)

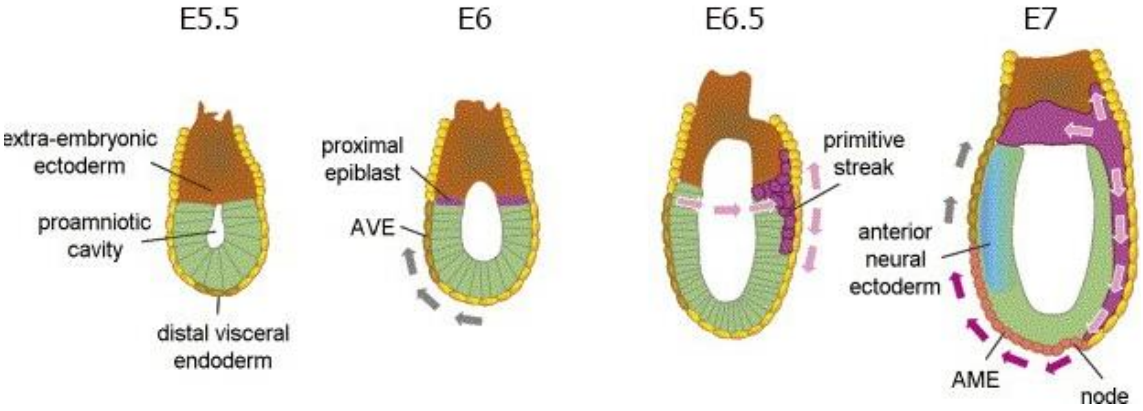

Figure 2: Stages of mammalian embryogenesis (post-implantation)

After implantation during E5.5, the embryo becomes cylindrical and begins the formation of visceral endoderm and extra-embryonic ectoderm. At E6.5, formation of primitive streak begins. At E7, ingression of cells from primitive streak give rise to mesoendoderm and early ectoderm. Adapted from (Marikawa, 2006).

1.2 Nervous system development

Embryo consist of three distinct germ layers: ectoderm, mesoderm, and endoderm. Of which ectoderm will differentiate into the nervous system and the epidermis. During 3rd and 4th week of gestation, formation of neural tube starts and is a complex morphogenic process regulated by variety of signaling molecules. This process of formation of neural tube is called neurulation. The process of neurulation starts with the thickening of ectoderm, followed by trench like structure formed in the mid-region of the ectoderm called neural groove. These neural grooves are flanked by neural

folds which finally fuses together leading to closure of the neural tube which later on detaches from the overlying ectoderm and gave rise to neural crest cells which migrate to different regions. (Nikolopoulou et al., 2017; Singh S.;, 2020) (Figure 3).

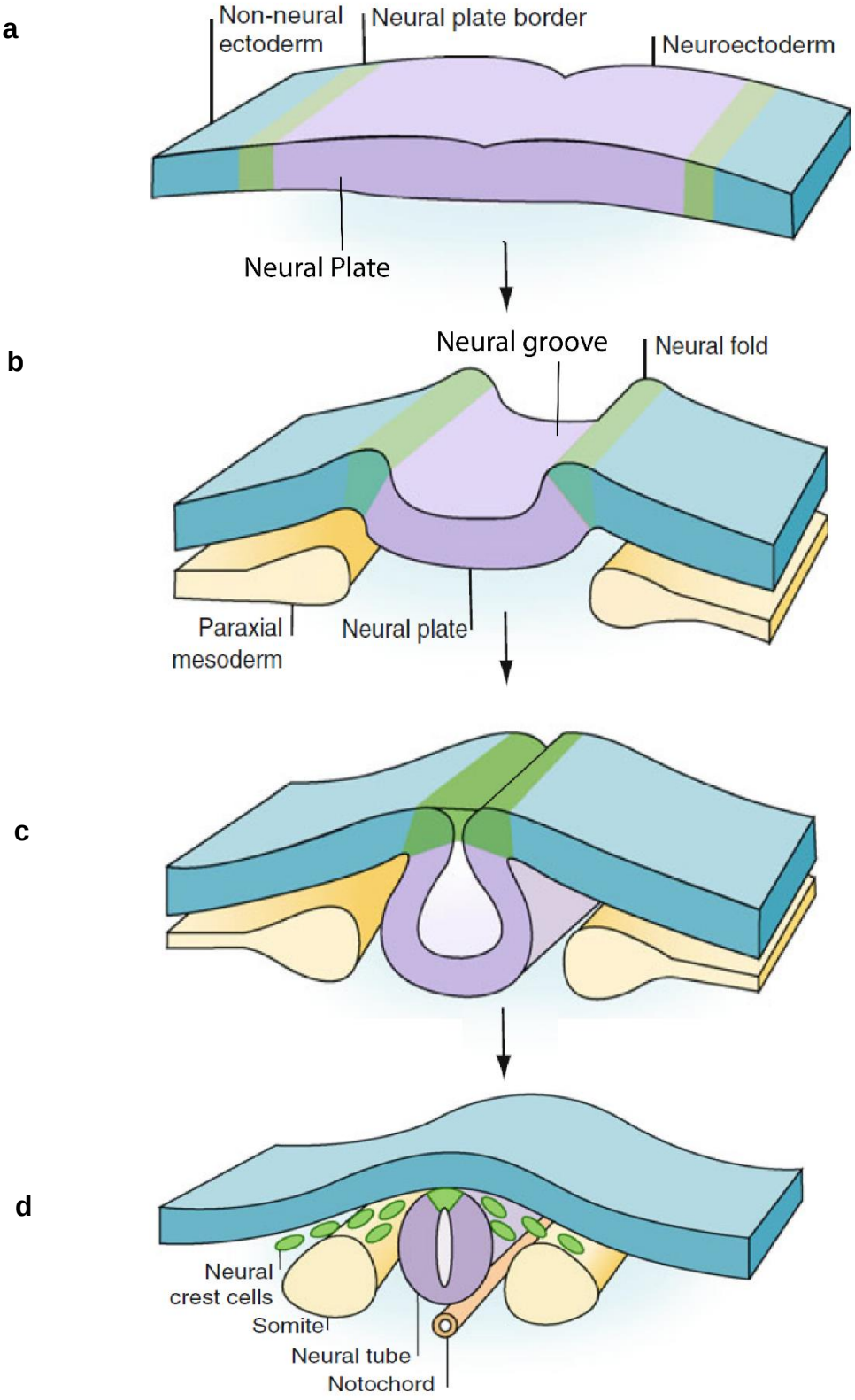

Figure 3: Stepwise process of neurulation

a) Thickening of ectoderm to form neural plate.

b) Formation of trench like structure called neural groove and appearance of neural folds

c) Convergence of neural folds to form neural tube.

d) Detachment of neural tube and formation of neuroectodermal layer. Modified from (Gammill and Bronner-Fraser, 2003)

Neural tube fusion begins in the middle of the embryo and moves cranially and caudally. The cranial open end of the tube is called anterior (rostral) neuropore and caudal open end is the posterior (caudal) neuropore. The anterior and caudal neuropore closes on or before day 26 of gestation. The neural tube thereafter undergoes an expansion leading to the formation of three primary brain vesicles of the central nervous system: forebrain (prosencephalon), midbrain (mesencephalon) and hindbrain (rhombencephalon). These primary vesicles continue to develop and give rise to secondary vesicles where the prosencephalon sub-divides into anterior telencephalon (future neocortex) and posterior diencephalon, which will then form the thalamic and hypothalamic structures of the brain. Telencephalon consists of dorsal telencephalon (dorsal neocortex), medial telencephalon (hippocampaus/cortical hem), and ventral telencephalon (the caudal part of telencephalon there is a structure called choroid plexus, which generates cerebrospinal fluid (CSF) and act as a blood brain barrier (BBB). In the ventral part of neocortex named as ventral telencephalon give rise to basal ganglia and interneurons which migrate to the neocortex (Campbell and Gotz, 2002). The rhombencephalon also further divides into anterior metencephalon (pons and cerebellum) and posterior myelencephalon (medulla) (Ishikawa et al., 2012) (Figure 4). The cerebral cortex consists of neocortex and allocortex. The neocortex (isocortex) constitutes 90% of the cerebral cortex and is a more recently evolved structure of the cerebral cortex characterized by the presence of varieties of NSCs and six-layers of cortical neurons. The allocortex is characterized by the presence of three predominant layers and comprises only 10% of the cerebral cortex. It is subdivided into paleocortex and archicortex. While the archicortex is the portion of allocortex that forms the hippocampus (cortical hem) also known as medial telencephalon, the paleocortex is the region of allocortex that relates to the olfactory system, pyriform cortex, and amyglada (Strominger et al., 2012)

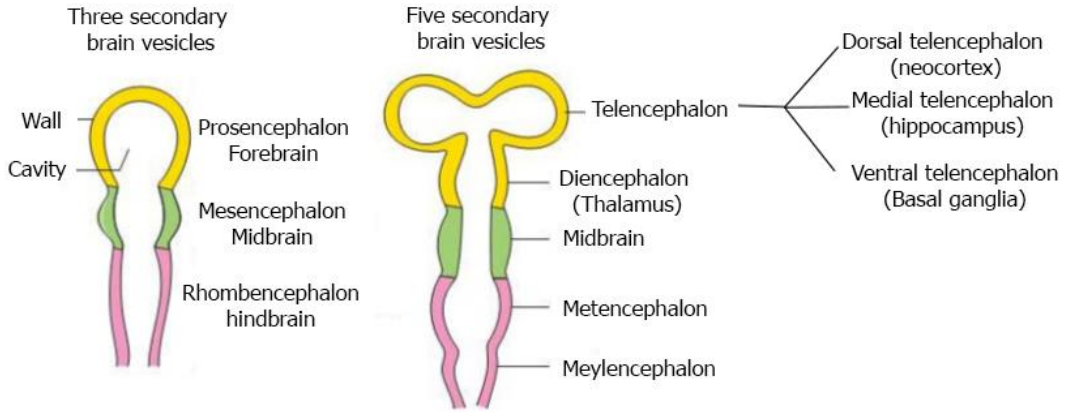

Figure 4: Primary and Secondary brain vesicles development

Primary vesicle stage has three brain regions. During development brain continue to develop and give rise to secondary vesicle which has five regions. (Modified from Development of the Nervous system).

1.3 *In vivo* neural induction and patterning

In 1924, classical experiments of Mangold and Spemann gave fundamental insights into how the neural plate is established and elucidated the role of organizers in inducing the neural tissue (Mangold, 1933). They transplanted a tissue from dorsal blastopore lip (located in the dorsal mesoderm) of a pigmented newt gastrula into ventral region of a non-pigmented newt gastrula, and observed that donor tissue induced a second nervous system (Mangold, 1933)(Figure 5). This tissue which has the capacity to generate whole nervous system is known as Spemann organizer. Spemann and Mangold also showed that later stage gastrula organizer will induce only posterior regions and thus postulated the existence of separate organizers in space and time for inducing different regions of the nervous system along the anterior-posterior axis (Eyal-Giladi, 1954; Mangold, 1933). The organizer releases bone morphogenetic protein (BMP) pathway inhibitors (chordin, and noggin) that induces neural tissue (Hemmati-Brivanlou and Melton, 1994; Lamb and Harland, 1995). However, in 1952, Peter Nieuwkoop postulated another theory for anterior-posterior axis formation, which states that an activation factor causes neuralization of ectoderm. The neuralized tissue in default differentiates into anterior neural structures such as forebrain in the absence of any signaling pathway. While caudalizing factors (WNT,

FGF and RA) are required to act on this previously generated neuralized tissue, to give rise to posterior neural parts like hindbrain and spinal cord (Cox and Hemmati-Brivanlou, 1995; Durston et al., 1989; Gerhart, 1999; Kiecker and Niehrs, 2001; Lumsden and Krumlauf, 1996; Nieuwkoop, P.D., 1952; Nieuwkoop, 1952; [CSL STYLE ERROR: reference with no printed form.]). Despite of growing evidence which favours Nieuwkoop's theory, this concept still remained controversial and unclear (Fraser, 2004).

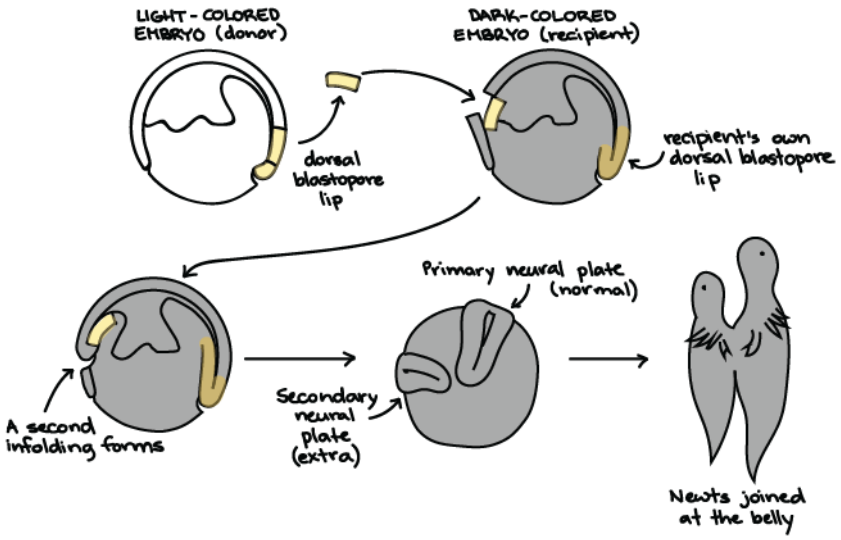

Figure 5: Transplantation experiment of Spemann-Mangold manifesting organizer activity in newt blastopore lip tissue

Transplantation of dorsal blastopore lip tissue from a light pigmented newt *Triturus taeniatus* to non-pigmented *Triturus cristatus*. Transplanted blastopore lip tissue exerted an organizing activity in the surrounding host tissue and induces a whole secondary axis in the embryo. (Adapted from Khan academy)

Similar structures as Spemann organizer namely Henson node, embryonic shield and node has been shown in other vertebrates such as chick, zebrafish and mouse respectively. It has been proved that the role of organizer is evolutionary conserved (Beddington, 1994; Waddington, 1933). However, in mice, transplantations studies have demonstrated that the node (organizer) lacks the information for generating entire neural axis (Beddington, 1994; Tam and Behringer, 1997; Tam and Steiner,

1999). When an early gastrula organizer was transplanted it could give rise to only posterior regions, lacking anterior fates (Beddington, 1994; Tam and Steiner, 1999) indicating lack of information for entire axis generation. Studies in mice at E5.5, have shown that cells from distal region of embryo known as distal visceral endoderm migrate to the future anterior region of the embryo, establishing an additional organizer known as anterior visceral endoderm (AVE) (Beddington and Robertson, 1998; Srinivas, 2006; Takaoka et al., 2007). These AVE cells express specific genes like Otx2, Lhx1, Dkk1, Cerebrus1, Noggin and Lefty which are important for anterior forebrain formation. (Acampora et al., 1998; Hiramatsu et al., 2013; Miura et al., 2010; Perea-Gomez et al., 2002; Rhinn et al., 1999; Yamamoto et al., 2004)(Figure 6a). Some of the transcripts which are generated by the AVE cells are inhibitors of BMP, TGF- β, WNT signalling pathways, thus in turn helps in the formation of anterior fates. It has also been shown that anterior neural fates are determined by synergist effect of AVE, Spemann organizer (node) and axial mesendoderm (Foley et al., 2000). All together these early experimental studies have shed light on the early neural induction and patterning. (Figure 6b).

a

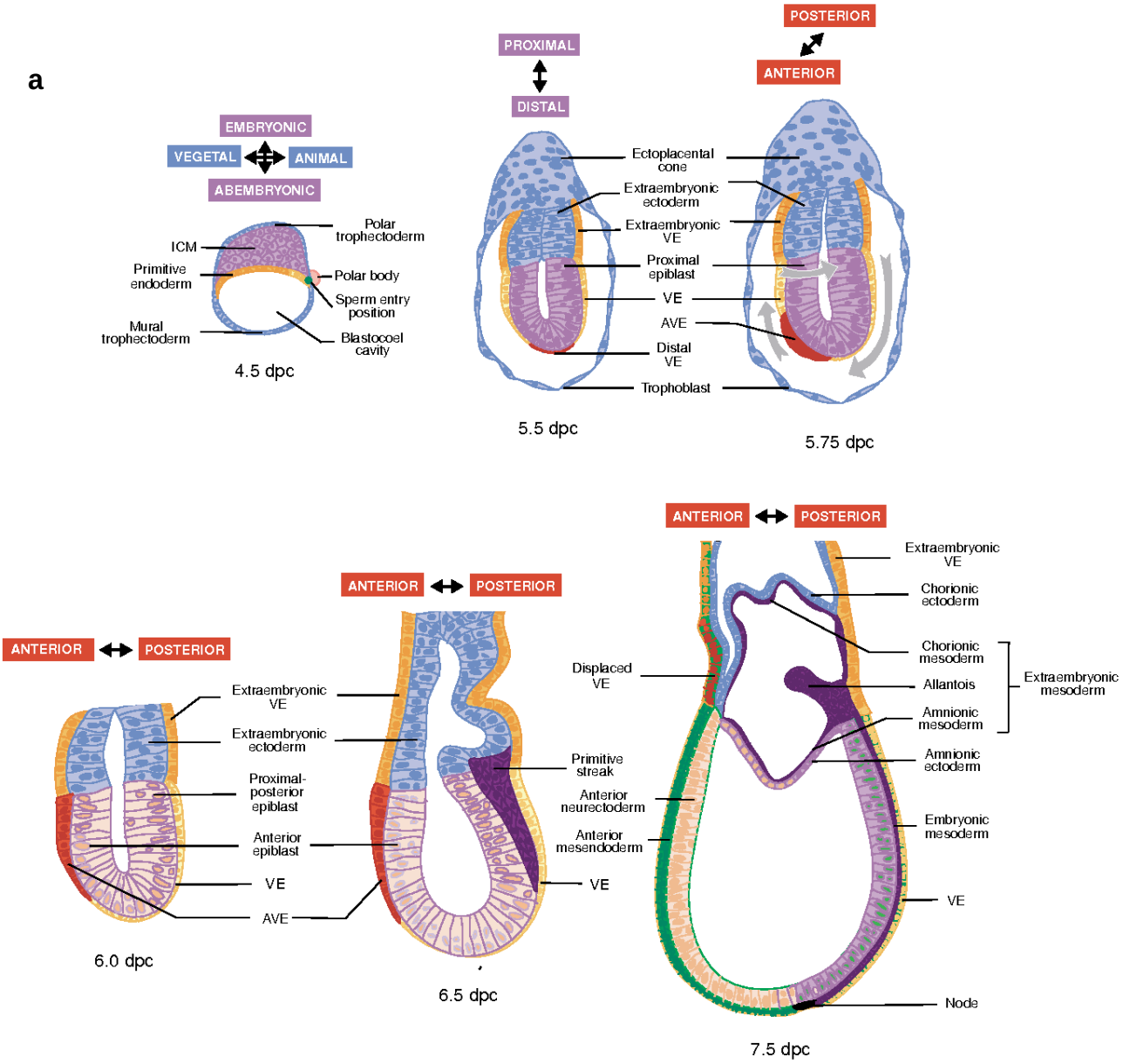
EMBRYONIC
VEGETAL
ANIMAL
ABEMBRYONIC
ICM
Primitive endoderm
Polar trophectoderm
Polar body
Sperm entry position
Mural trophectoderm
Blastocoel cavity
4.5 dpc
PROXIMAL
DISTAL
POSTERIOR
ANTERIOR
Ectoplacental cone
Extraembryonic ectoderm
Extraembryonic VE
Proximal epiblast
VE
AVE
Distal VE
Trophoblast
5.5 dpc
5.75 dpc
ANTERIOR
POSTERIOR
Extraembryonic VE
Extraembryonic ectoderm
Proximal-posterior epiblast
Anterior epiblast
VE
AVE
6.0 dpc
Primitive streak
Anterior neurectoderm
Anterior mesendoderm
6.5 dpc
Displaced VE
Chorionic ectoderm
Chorionic mesoderm
Allantois
Amnionic mesoderm
Extraembryonic mesoderm
Amnionic ectoderm
Embryonic mesoderm
Node
7.5 dpc

b

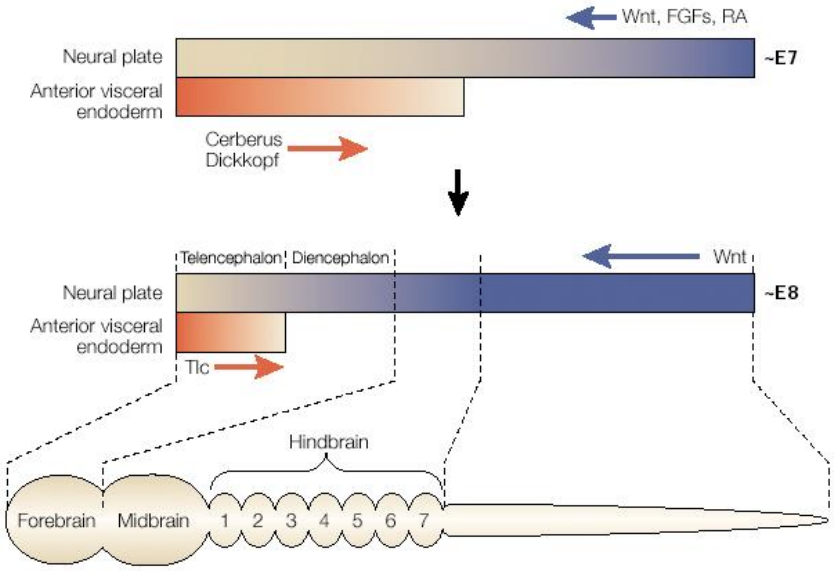

Figure 6: Overview and specification of anterior-posterior in post-implantation mouse embryos.

a) By E4.5 the blastocyst is ready to implant in the uterus and at this stage it is made up of epiblast cells and two extra-embryonic tissue. By E5.5 extra-embryonic ectoderm is formed which is in continuation to epiblast and lumen is formed. These tissues are surrounded by visceral endoderm which is derived from primitive endoderm. A subset of visceral endoderm cells is specified as DVE (distal visceral endoderm) and AVE (anterior visceral endoderm), which migrate towards the epiblast extra embryonic ectoderm boundary to determine the future anterior side. Future anterior and posterior brain regions are specified in neuroectoderm overlying AVE and ADE/AME (anterior definitive endoderm/anterior mesoendoderm) whereas the posterior regions became neuroectoderm overlying the notochord plate.

b) AVE secrets Wnt and nodal antagonist hence creating a gradient of wnt and nodal signaling that leads to the specification of anterior-posterior axis. An array of signalling molecule gradient that confers anterior-posterior regions in brain. Adapted from (Biology; Lu et al., 2001).

1.4 Morphogens in neural induction and patterning

Paracrine morphogens such as Cerebrus/Lefty, Noggin, Dkk-1 plays an important role in the inhibition of signaling cascades, leading to neural pattering *in vivo*. The following signaling pathways are inhibited in order to induce neurulation process.

1.4.1 TGF-beta superfamily

There are more than 30 structurally related members of this superfamily, which play important roles in the neurodevelopmental interactions. Three of the most widely used members of this family are: TGF-β, BMP, and Nodal/Activin.

In TGF-β signaling pathway, TGF-β ligand first binds to a type-II receptor dimer, which then recruits type-I receptor forming a heterotetrameric receptor ligand complex. Type-II receptor catalyzes phosphorylation of serine residues of type-I receptor, which then phosphorylates Smad proteins initiating Smad protein signaling cascades. Smad-1/2/3/5/8 are the receptor regulated Smads known as R-Smads. Smad-2/3 are activated by Nodal/Activin signals while Smad1/5/8 are activated in response to BMP signaling. These R-Smads bind to a common Smad protein i.e., Smad4 forming R-Smad/Smad-4 complex, which then translocates into the nucleus and regulate gene expression. Smad6/7 are inhibitory Smads which inhibit the signaling pathways (Figure 7a).

1.4.2 BMPs (Bone Morphogenetic Protein) Signaling

Studies have identified the release of BMP antagonist such as noggin, chordin, and follistatin from notochord or Spemann organizer, which prevent the binding of BMP4 molecule to its receptor, there by inhibiting BMP pathway in the overlying ectoderm and thus induces the ectoderm into neural plate. (Levine and Brivanlou, 2007). Previous studies, in mice with deficient BMP-1a receptor exhibit premature neural induction at pre-gastrula stage (Di-Gregorio et al., 2007). Mice with mutant Noggin and Chordin fail to form proper forebrain (Bachiller et al., 2000). All these studies implied the valuable role of BMP inhibition in neural patterning (Figure 7b).

1.4.3 Nodal/Activin Signaling

BMP signaling is not the sole player in neural patterning, studies have established the role of other TGF-β family members such as Nodal/Activin in neural induction. Nodal mutant mice displayed increased neuroectoderm specification (Camus et al., 2006). It has been shown that overexpression of cerebrus, lefty in mESCs and mutant with Cripto -/- (coreceptor for TGF and Nodal signaling) display increased neural induction (Bouwmeester et al., 1996; Inui et al., 2012; Liguori et al., 2003). These studies altogether have shown the indispensable role of TGF-β signaling in achieving neural induction.

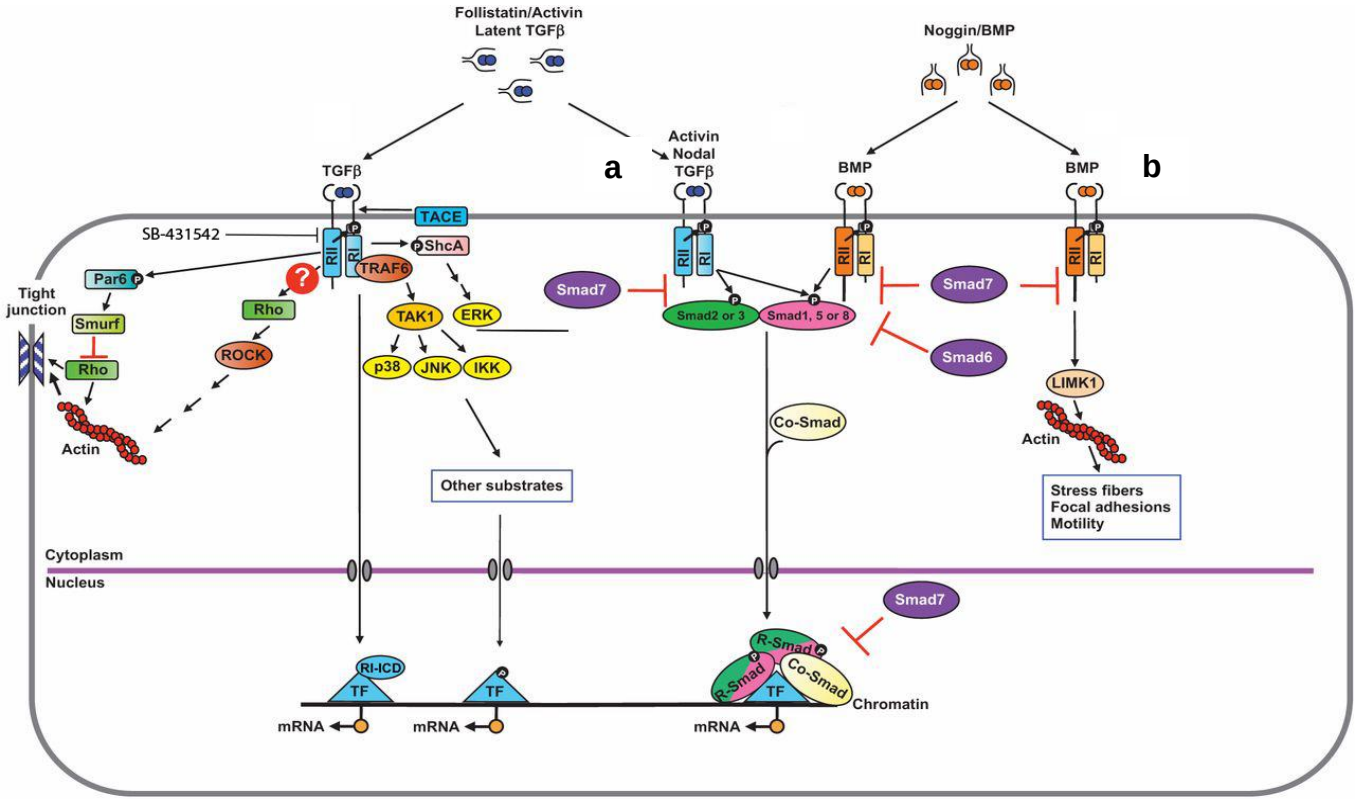

Figure 7: TGF-beta, BMP and Nodal signaling pathway.

Binding of TGF-beta (a) molecule or BMP ligands (b) to its respective receptor type 1 and II leads to heterodimerization and activation of Smad2/3 and Smad 1/5/8 respectively. Activated R-Smad binds to Smad4 and translocate into the nucleus and activate transcription of targeted genes. Modified from (Zhang and Newfeld, 2013)

1.4.4 WNT Signaling

WNT signaling also plays important role in determining anterior neural fates. In chicks, ectoderm explants meant to become anterior forebrain when exposed to Wnt molecules transformed into posterior neural fates. (Nordstrom et al., 2002). Beta-catenin mutant in zebrafish, shown increased Wnt levels, leading to the transformation of telencephalic fates into posterior diencephalic tissues (Heisenberg et al., 2001). In mice, loss of WNT inhibitor Dickkopf (Dkk1), prevents anterior forebrain formation (Mukhopadhyay et al., 2001). Loss of Wnt receptor Lrp5/6 displayed the expansion of anterior neuroectoderm (Kelly et al., 2004). Mice mutant which doesn't express Wnt1 lacks midbrain (McMahon et al., 1992; Thomas and Capecchi, 1990). The presence of consequent Wnt gradient from highest dorsally and lowest ventrally has been shown for proper brain axis formation (Megason SG). Overall, these studies have shown the role of Wnt signaling in cell proliferation and anterior-posterior neural fate specification.

1.5 Pluripotent Stem Cells (PSCs)

In 1981, mouse embryonic stem cells (mESCs) have been isolated and cultured *in vitro* from ICM of the mouse blastocyst (Evans and Kaufman, 1981; Martin, 1981). In 1998, human embryos, produced by invitro fertilization technique, were obtained and grown till blastocyst stage. The inner cell mass from these blastocysts was isolated, dissociated and cultured *in vitro* on mouse embryonic fibroblast and grown indefinitely as human embryonic stem cells (hESCs) (Thomson, 1998). Several studies have been done to understand the self-renewal and differentiation capacity of these ESCs which led to the identification of transcription factors (TFs) that are directly linked to the cell renewal and pluripotency property of these cells (Mitsui et al., 2003; Niwa et al., 1998). The two unique properties of stem cells i.e. self-renewal, and differentiation potential towards distinct cell types make them an indispensable tool for developmental, and regenerative studies. But, the use of hESCs were limited due to ethical, technological and tissue availability concerns. Also, for cell replacement therapies immune rejection should be kept under consideration.

Studies using somatic cell nuclear transfer (SCNT) technique has postulated/indicated the presence of factors in oocytes and ESCs that can reprogram a somatic cell to pluripotent like state (Cowan et al., 2005; Gurdon, 1962; Tada et al., 2001; Wilmut et al., 1997). In 2006, the ground breaking discovery by Yamanaka group where they have demonstrated the use of TFs to reprogram mouse fibroblast cells into induced pluripotent stem cells (iPSCs) and a year later they successfully derived human iPSCs from human fibroblast (Takahashi and Yamanaka, 2006). They have used four transcription factors Oct4, Sox2, Klf4, and c-Myc to reprogram the fibroblast to iPSCs. These iPSCs hold a great potential to generate patient specific PSCs that will be highly useful for therapeutic purposes. These cells thus circumvent ethical concerns regarding the use of ESCs (Hamazaki et al., 2017; Robinton and Daley, 2012). However, these cells look alike ESCs but still need extensive characterization as their epigenetic reprogramming is still questionable. (Baghbaderani et al., 2016; Bilic and Izpisua Belmonte, 2012). Nonetheless, iPSCs provide an unlimited source to derive and study different cell types which are inaccessible to obtain.

1.6 Neural Stem Cells (NSCs)

Neural Stem Cells are self-renewing multipotent stem cells that can give rise to neurons, astrocytes and oligodendrocytes (Cattaneo and McKay, 1990; Gage, 2000). Studies in xenopus, chick and mice have shown the importance of inductive or inhibitory factors (TGF, BMP and WNT signaling) for the acquisition of A-P and D-V axis. After the procurement of neural fate, the neural tube consists of one-layer thick neuroepithelial cells (NE cells) whose nuclei are arranged from the inner luminal site to outer surface leading to pseudostratified epithelial organization (Sauer, 1935). In mammalian nervous system, it is unclear that stem cells derived from the given region of the embryonic brain are different from those derived from the same structures in the adult brain (Gage, 2000) It has been shown from the heterochronic transplantation studies that early neural stem cells have broad differentiation potential and can give rise to different neuronal subtypes while later neural stem cells have restricted potential (Frantz and McConnell, 1996; Gage and Temple, 2013; Temple, 2001). Collectively, these findings indicate that the NSCs have restricted developmental potential both spatially and temporally and this dynamic nature of NSCs plays an important role in generating heterogenous neural cell types in the developing central nervous system (Gage and Temple, 2013). Therefore, further studies need to be accomplished for dissecting the *in vivo* and *in vitro* heterogeneity using specific markers proteins.

1.7 Neural stem cells in cortex and corticogenesis:

Neocortex is the recently evolved and most complex part of brain with enormous cell diversity, functionality and connectivity (Florio and Huttner, 2014; Lui et al., 2011). This recently evolved structure is considered to be basis for our increased cognitive abilities. Human neocortex is about ~1000 times larger and the surface is highly convoluted (gyrencephalic) featuring fissures (gyri) and ridges (sulci) compared to smooth mouse neocortex (lissencephalic) (Figure 8). Key parameters thought to be considered for the expansion of human neocortex is the increased proliferative capacity of neural stem and progenitor cells (Rakic, 2009). Extensive work over the last decade has identified a diversity of neural stem cell types (Malatesta et al., 2000; Miyata et al., 2004; Noctor et al., 2001). Neuroepithelial cells (NE) are the earliest neural stem cells present in the neural tube lining the ventricles as a pseudostratified neuroepithelium. NE maintain a characteristic apicobasal polarity with one end

anchored to ventricular surface by means of tight and adherens junctions (Aaku-Saraste et al., 1996; Manabe et al., 2002; Zhadanov et al., 1999) and the other end to pial basal lamina by integrins (Graus-Porta et al., 2001; Radakovits et al., 2009). The nuclei of NE cells undergo a characteristic migration pattern during cell cycle in which the nuclei of NE cells migrate from apical surface to basal surface during G1 phase, undergoes DNA duplication at the basal surface and then return to apical surface to undergo mitosis at the ventricles. This process is called as interkinetic nuclear migration (INM) (Figure 9) (Sauer and Walker, 1959; Taverna et al., 2014)(which helps to accommodate increased number of NE cells per unit ventricular surface ultimately conferring the neuroepithelium its pseudostratification. NE initially undergoes symmetric division to expand its pool and then shifts to asymmetric division generating radial glial (RG) cells. These RG cells retain some NE characteristics (apical-basal polarity, INM) and starts expressing astroglial markers (Campbell and Gotz, 2002). Radial glial cells loose tight junctions and express adherence junctions at their apical endfoot (Aaku-Saraste et al., 1996). As these RG cells divide at apical surface of ventricles, they are also referred to as apical radial glia (aRG) or apical progenitors. Apical radial glial cells undergo both symmetric and asymmetric divisions. During neurogenic phase, they primarily undergo asymmetric division to generate one aRG and a daughter differentiated cell—either neuron or intermediate progenitor (IP). IP cells are transit amplifying self-consuming progenitors undergo one or two rounds of mitosis in sub-ventricular zone (SVZ) and generate neurons (Delaunay et al., 2017). IP's are non-epithelial progenitor cells expresses a transcription factor Eomes or Tbr2 on their way to SVZ (Englund et al., 2005). In comparison to mouse (non-primate), ferret and primate brains consists of a thickened outer SVZ (OSVZ) layer comprising of another undifferentiated and self-renewing neural progenitor known as outer radial glia (oRG) or basal radial glia (bRG) with a long radial basal process {Hansen D et al., Nature 2010}. In lissencephalic brains such as mice, these bRGs are scarce with low proliferative capacity while in gryencephalic primate brains, bRGs are abundant with high proliferative potential (Fietz et al., 2010; Hansen et al., 2010). Thus, these bRGs are now widely considered to be instrumental for neocortical expansion (Lui et al., 2011; Sousa et al., 2017). In line with this concept, recent studies showing genes might responsible for human neocortex expansion such as ARHGAP11B, and NOTCH2NL are indeed operating in bRG promoting their proliferation (Florio et al., 2018; Suzuki et al., 2018). Similar to aRG, the bRG cells express *SOX2, PAX6* and *NESTIN* while

in addition also express more specific genes such as *HOPX, LIFR* and *PTPRZ* (Pollen et al., 2015).

During corticogenesis, neurons are produced from aRG, bRG and IPs in successive waves generating an organized six layered cortical plate (CP) in an inside-out pattern with early-born neurons occupying the deep layers (DL) while late-born neurons migrate to upper superficial layers (UL) (Figure 10) (Cooper, 2008; Englund et al., 2005; Hansen et al., 2010; Kwan et al., 2012). Early born are the Cajal-Retzius (CR) and subplate neurons. The Cajal-Retzius neurons release a secreted protein known as Reelin, which act as an important cue for the rest of the cortical plate formation (D'Arcangelo et al., 1995). The initial aRGs that generates CR neurons doesn't express Foxg1. Thereafter, the aRGs start expressing Foxg1 and repress CR neurons and initiate the program that regulates the subsequent laminar fates {(Kumamoto and Hanashima, 2014). Neurons subtype specification is progressive and fine-tuned along with the differentiation of post-mitotic neurons. Transcription factors such as Tbr1, Fefz2, Sox5 and Ctip2, and Tle4 are vital for DL neuron subtype specification while Cux1, Satb2, and Brn1/2 promote UL neuron identity (Lodato and Arlotta, 2015; Toma and Hanashima, 2015). In addition to cell intrinsic factors, external cues from DL neurons involved in neural progenitor shift to UL neurons. For example, Sip1 mediated Ntf3 suppression is involved in neuron-progenitor feedback loop (Parthasarathy et al., 2014; Seuntjens et al., 2009).

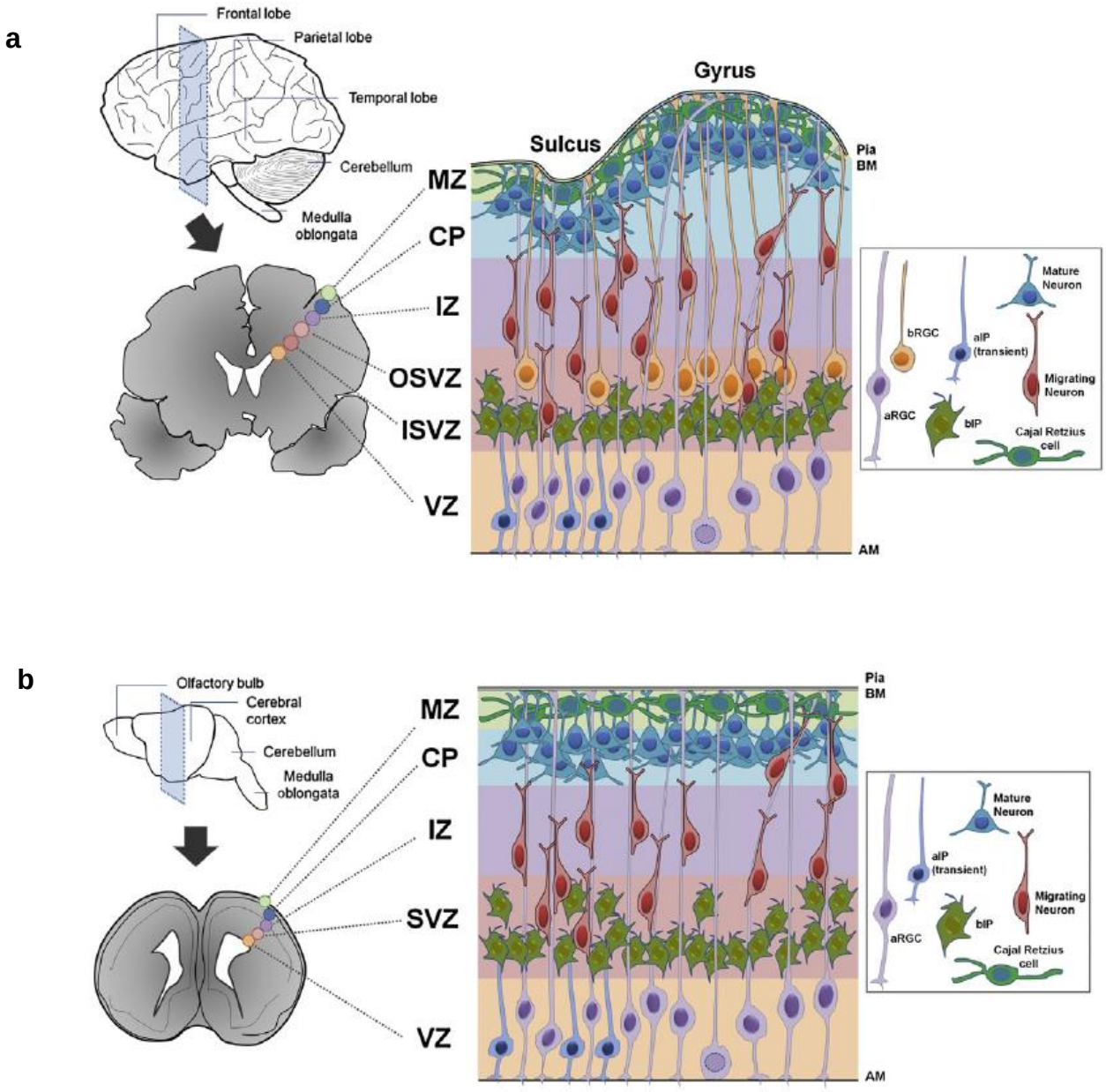

Figure 8: Cortical development in gyrencephalic and lissencephalic brains.

a) Lateral view of an adult gyrencephalic brain (top left) and a coronal view of developing brain slice (lower left). Different colour circles indicate developing cortical region (indicated on the right). The location of each cell-types presents in developing brain region are illustrated in right panels. The basal radial glial cells (bRGCs) are mainly present in gyrencephalic species and they are localized within the outersubventricular zone (OSVZ).

b) Lateral view of an adult lissencephalic brain (top left) and a coronal view of developing brain slice (lower left). Cortical region has been differentially coloured and specified on the right. The location of developing cortical cell-types of each region is illustrated on the right panel. In both figures the

interkinetic nuclear migration of RGCs in the ventricular zone (VZ) and neuronal migration are represented. The division of the subventricular zone (SVZ) into an inner (ISVZ) and outer (OSVZ) region, and the presence of sulci and gyri, are the main organizational differences between the human and mouse. Adapted from (Romero et al., 2018)

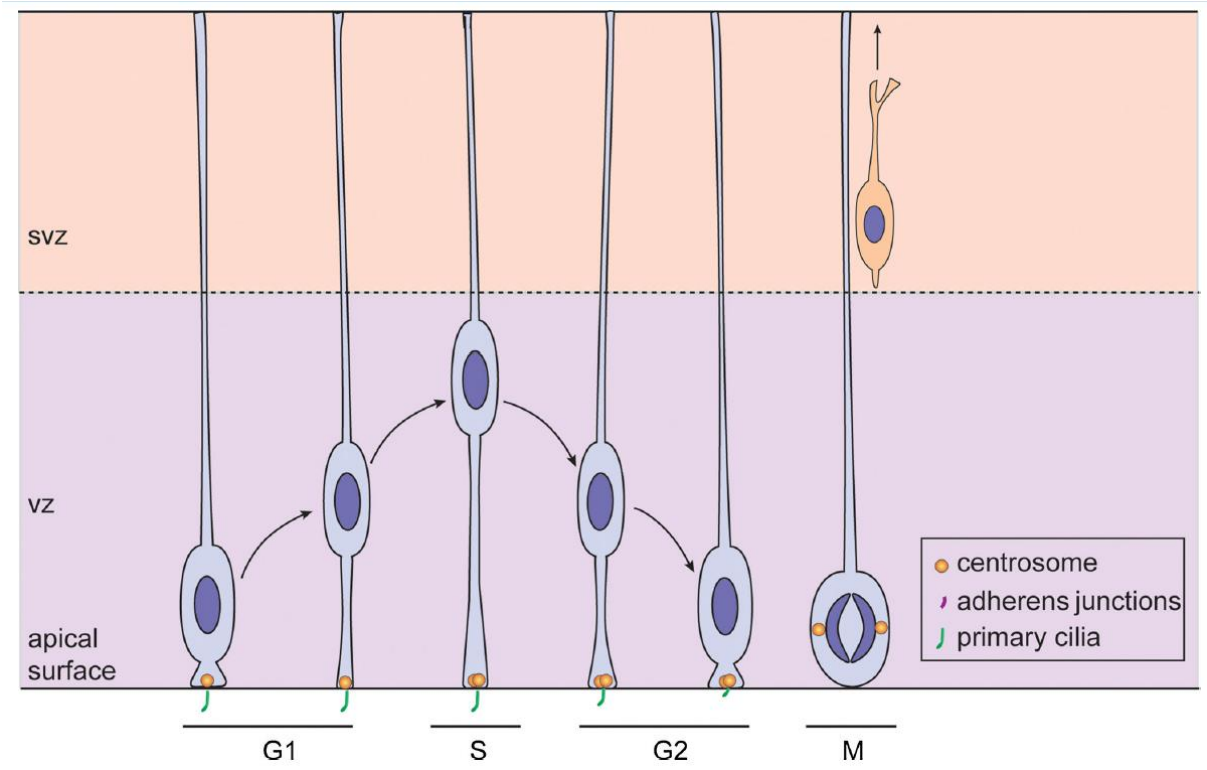

Figure 9: Interkinetic nuclear migration of apical radial glial cell during cell cycle progression. During G1 phase of cell cycle, the nucleus of radial glial cell migrates from apical site to basal site of ventricular zone (VZ) and then reach a basal position at S phase. During S-Phase, the nucleus undergoes basal location followed by basal to apical migration in G2 phase of cell cycle, then entering M-phase at the apical surface. The cell division can be symmetric (formation of two apical radial glial) or asymmetric (apical radial glial and intermediate progenitor/neuron). Adapted from (Laguesse et al., 2015)

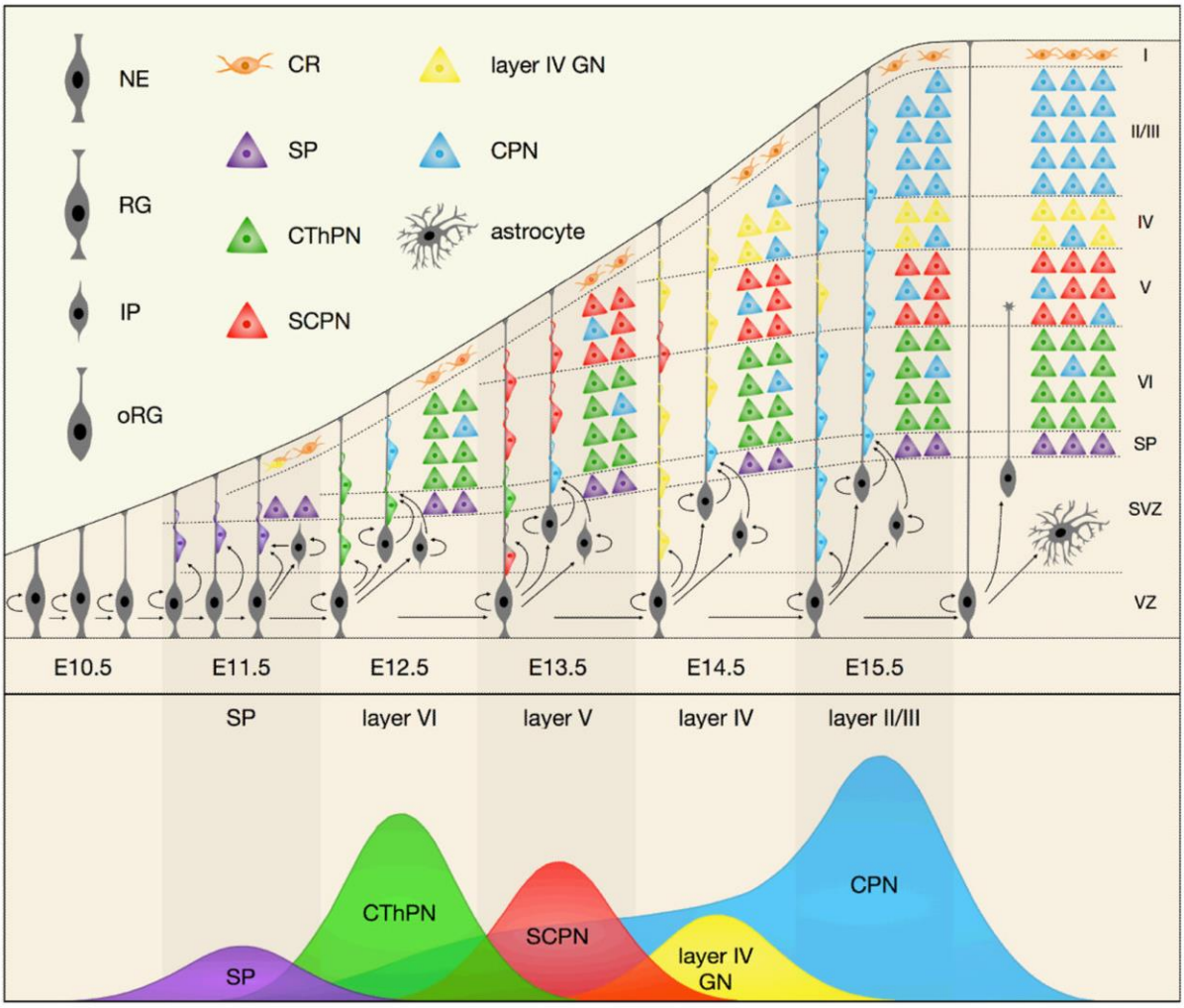

Figure 10: Cortical lamination in mouse neocortex

Schematic representation of sequential generation of neural stem cells and neurons over the course of mouse embryonic development. a. Around E11.5, neuroepithelium (NE) give rise to apical radial glial cells (aRGs). At the same time, aRGs give rise to intermediate progenitors (IPs) and outer radial glial cells (oRG) and populate the subventricular zone (SVZ) and act as transit amplifying cells to increase the neuronal production. At E15.5, radial glial transition from neurogenic to astrogenic neural progenitors. Cajal-reticulus cells generate directly from NE or from non-cortical areas migrate into layer I, while other projection neurons are born from VZ/SVZ and migrate along radial glial processes to populate at the cortical plate. b. Generation of neurons happens in an orderly fashion. At around E11.5 subplate neurons forms (SP), with corticothalamic projection neuron (CThPN) and subcerebral projection neurons (SCPN) generating at E12.5 and 13.5 respectively. Layer IV granular neurons forms during E14.5. While collosal projection neurons (CPN) starts from E12.5 and along with CThPN and SCPN they migrate to the deep layer. Adapted from (Greig et al., 2013)

1.8 Brief overview of *in vitro* neural induction and corticogenesis (2D neural rosettes and 3D brain organoids) using PSCs

PSCs have the capacity to form an aggregate in suspension culture called as the embryoid bodies (EB), which can generate three germ lineages spontaneously (Desbaillets et al., 2000; Itskovitz-Eldor et al., 2000). These EBs when cultured in the presence of FGF2 generated the neural tube-like structures known as neural rosettes (Zhang et al., 2001b). These neural rosette (2D culture) precursors in turn generated neurons, astrocytes and oligodendrocytes upon further differentiation. Starting with this initial study to the recently emerged complex 3D brain organoid technology, neural induction methods have undergone many different modifications with the inclusion of small molecule inhibitors, extra-cellular matrix (matrigel and hydrogels), and sophisticated 3D bioreactors—altogether to enhance the neural induction and homogeneity of generated cortical cell populations. Though the complexity of 2D cultures is lower in comparison to 3D organoids, neural rosettes helped us a great deal in understanding and characterizing (at molecular and cellular levels) different neural progenitors and their differentiated daughter neuronal cells (Edri et al., 2015; Elkabetz and Studer, 2008; Ziller et al., 2015; Ziv et al., 2015). In addition to EB formation, PSCs have the ability to undergo neural induction in the absence of serum and growth factors (Tropepe et al., 2001; Ying et al., 2003). Combining these two features (serum free and EB), Watanabe and colleagues developed SFEB cultures (serum free culture of embryoid bodies like culture) which efficiently differentiated PSCs into telencephalic identities (Watanabe et al., 2005). The SFEB culture is then modified into quick SFEB (SFEBq) allowing quick aggregates in low adhesion U-bottom 96-well plate (Eiraku et al., 2008). This technique allowed to produce uniform aggregates (EBs), and yielded better reproducibility and higher neuronal differentiation capacity. Later studies started the addition of exogenous inhibitors to the cultures with the knowledge gained from *in vivo* conditions of brain positions (anterior-posterior and dorsal-ventral positions of neural tube). For example, Wnt and retinoic acids were used to induce posterior regions whereas the inhibition of Wnt is required for anterior regions. Subsequently, SFEBq culture method underwent another modification with the inclusion of matrigel (ECM proteins) for embedding the quick aggregates, resulted in a robust and expanded fluid filled neuroepithelium vesicle generation termed as brain organoids (Lancaster et al., 2013; Quadrato et al., 2017). However, this technique is reported to produce heterogeneous and highly variable brain organoids consisting of different

brain tissues (Cortex, hippocampus, choroid plexus, thalamus, and retina etc) by means of natural and spontaneous self-organization properties of stem cells. Later on, some studies aimed to generate desired brain regional organoids with high purity by the addition of exogenous small molecule inhibitors (Kadoshima et al., 2013; Mariani et al., 2012; Pasca et al., 2015; Qian et al., 2016). Recently, in our lab we have developed a brain organoid derivation method using small molecule inhibitors of BMP, TGF-beta and WNT pathway (Mutukula N*, 2021) that generated superior cortical organoids with high purity and reproducibility in comparison to all the previously known cortical organoid derivation methods. These *in vitro* 3D brain organoids in turn recapitulates many features of *in vivo* brain structure and composition. For example, these 3D brain organoid structures contain neuroepithelium with apico-basal polarity and ventricle like cavities. Similar to *in vivo,* NSC forms the lining of neuroepithelial vesicles (like VZ) and produce EOMES +ve IPs and neurons that migrate basally to form SVZ and CP. Especially, the order of neurogenesis is also conserved *in vitro* with deep layer neurons are born first followed by upper layer neurons like in the case of *in vivo*. Though the layer formation is obscure compared to *in vivo* neocortex but still follows the inside-outside pattern formation.

1.9 Identification, isolation and characterization of consecutive neural stem cells *in vitro*

Neural stem cells (NSCs) are self-renewing multipotent progenitors functioning as building blocks of central nervous system (CNS) development. The complex and well-orchestrated development of the cerebral cortex involves extensive changes in the properties and cell fate potential of these building blocks, which are translated into distinct NSC types that consecutively emerge and function throughout cortical development. Currently, the generation of these NSC types almost strictly depends on generating an early starting population and observing its progression *in vitro*, with no ability to control the transition between the stages. Therefore, revealing mechanisms that drive transition through these different NSC types is of great importance to the understanding of how we derive NSC cultures in the laboratory. In our lab, we previously dissected the entire cortical differentiation process *in vitro* from neuroepithelial cells towards distinct RG cell types. Specifically, we identified five consecutive rosette stages in culture corresponding to developmentally distinct types

of RGCs using HES5::eGFP H9 line (Edri et al., 2015; Ziller et al., 2015). We sorted for Notch signalling marker HES5 for isolating different NSC stage cells and then identified, characterized these stages such as Neuroepithelium (NE) NSC stage which divide symmetrically and then give rise to Early radial glial (E-RG) rosettes (day 14 in culture) contain highly proliferative NSCs exhibiting broad differentiation potential and minimal differentiation propensity in culture (Edri et al., 2015). As development progress in culture, E-RG NSCs generates a stage termed as Mid radial glial (M-RG) rosettes (day 35 in culture), which is characterized by decreased stemness and increased tendency to differentiate into neurons. As culture proceed *in vitro*, M-RG rosettes (beyond day 55) loose its rosettes cytoarchitecture, resulted in further decrease in number of NSCs and transition from neurogenic potential to astrogenic potential (Figure 11). We further broadly dissected the regulatory networks involved in differentiating PSCs to different stages of NSCs by performing extensive transcriptional and epigenetic characterization coupled with computational analysis (Edri et al., 2015). These analyses resulted in a comprehensive NSC type specific molecular signature.

Our lab mainly focuses on studying the development of the cerebral cortex, particularly investigating the development of cortical NSCs. We are interested in devising approaches for differentiation of PSCs into NSC building blocks, with emphasis on achieving high purity that will enable studying authentic cell fate decisions that are associated with regional patterning, self-renewal and differentiation processes that shape the cortex. A homogeneous early cortical population will also enable extracting more reliable molecular identity of that population, which can then be used for meaningful disease modeling and for devising sophisticated approaches to induce or maintain self-renewal of such populations *in vitro*.

However, recent research from our lab has shown that methods to derive homogenous early cortical progenitors from PSCs are highly diverse and yield heterogenous populations containing both cortical and non-cortical populations. This results in heterogeneous founder NSC populations that introduce major challenges to study them as a universal pure NSC platform. To overcome this hurdle our lab established a streamlined method known as Triple-i paradigm to derive homogenous starting cortical progenitors both in neural rosettes (2D) and organoids (3D) platforms. In this

study, we have shown that Triple-i paradigm consistently enriches for cortical cell types and suppresses non-cortical identity. We successfully modelled cortex specific microcephaly defects using Triple-i paradigm. Thus, creating a rich cortical cell-repertoire is critical for meaningful disease modelling (Mutukula N*, 2021). The main objectives of this thesis is to identify early signals (microRNAs) that modulate temporal and regional fates within developing founder cortical NSC populations.

It has been already shown that overexpression of specific microRNA and genes can induce cell fate conversion from fibroblast to neurons (Cheng et al., 2009; Thomas P. Naidich Pedro Pasik; Treutlein et al., 2016; Visvanathan et al., 2007; Yoo et al., 2011)and PSCs to astrocytes (Tchieu et al., 2017). This indicates that identification of specific regulators microRNAs/ genes which play an important role in changing cell fate between different NSCs and different regions in cortex will bring a wide range of opportunities for generating these specific cell types from different sources for both basic as well as future therapeutic application.

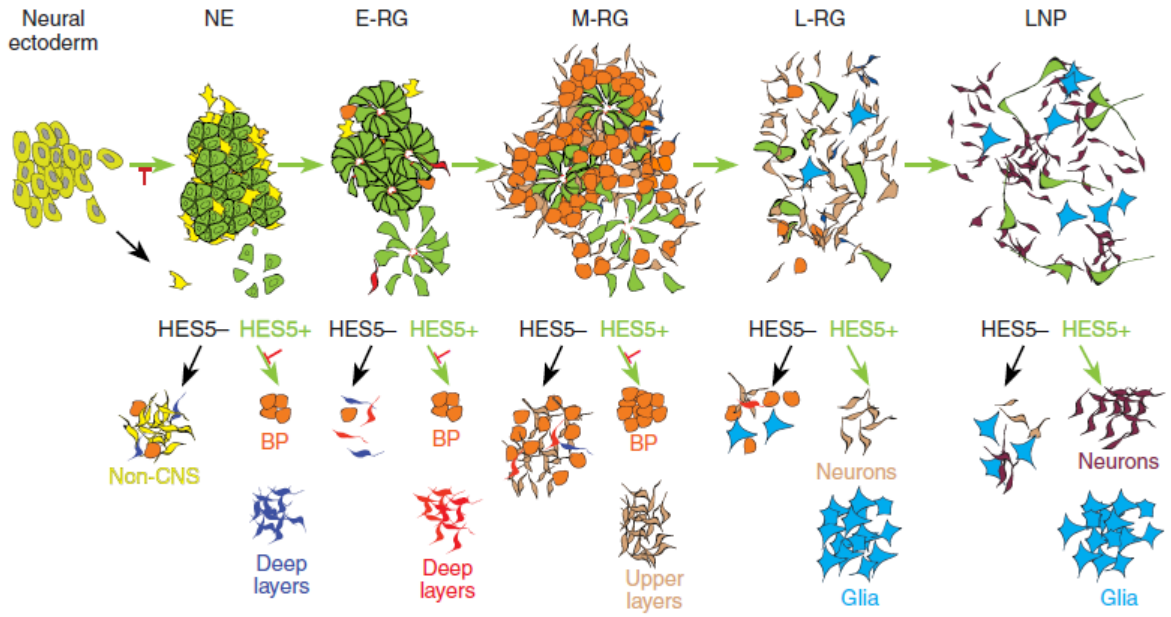

Figure 11: Schematic representation of Neural Stem cells progression.

Neuroectodermal cells of CNS give rise to NE cells by activating Notch and HES5 expression, while non-CNS cells lack this activation. In proliferative culture condition, HES5+ NE cells progress and give rise to HES5+ E-RG cells and their respective deep layer neurons such as TBR1, FEZF2 and CTIP2. These HES5+ E-RG progress in culture condition and give rise to M-RG NSCs which give rise to upper layer neurons such as CUX1, CUX2 and SATB2. Later after M-RG, rosette lose their integrity and generates late radial glial (L-RG) and long-term progenitors (LNP) and these are adult NSCs which are HES+ have both neurogenic and astrogenic potential and generates glial cell types. Horizontal green arrows mark transition in a Notch-dependent manner. Diagonal green and black arrows mark HES5+ and HES5- cells, respectively, subjected to differentiation following FACS-based separation. When differentiated under Notch inhibitor culture condition (red bar-headed lines). Adapted from (Edri et al., 2015)

1.10 Classification of small RNAs in animals

There are three main types of small silencing RNAs: i) microRNAs (miRNAs) ii) siRNAs and iii) PIWI-interacting RNAs (piRNAs) (Ghildiyal and Zamore, 2009; Ha and Kim, 2014; Kim et al., 2009). siRNAs (~21 nucleotides long) are derived from processing of long double stranded RNA structures by Dicer enzyme. They are mostly involved in post-transcriptional suppression of transcripts and transposons, and also contribute to the anti-viral defense (Ghildiyal and Zamore, 2009; Ha and Kim, 2014; Kim et al., 2009). piRNAs (~24 nucleotides long) processing are not dependent on RNase III protein but are derived from single stranded precursors processed by Zucchini

enzymes (also known as mitrochondrial cardiolipin hydrolysase enzyme in humans). The major role of piRNAs is to silence transposable elements in germline cells. There are two subclasses of Argonaute proteins (AGO and PIWI), siRNAs and miRNAs are associated with AGO proteins, whereas piRNAs bind to PIWI proteins (Ghildiyal and Zamore, 2009; Ha and Kim, 2014; Kim et al., 2009). The work in this project is on microRNAs (miRNAs) hence it is described in much more detail.

1.11 MicroRNAs

MicroRNAs are small (20~22 ntd in length) endogenous, evolutionarily conserved non-coding RNAs that mediate post-transcriptional regulation of gene expression (Bartel, 2004). A single microRNA can target several hundreds of target genes, and so far, there are thousands of microRNAs which has been discovered in mammalian genome (Kozomara and Griffiths-Jones, 2014), indicating that these microRNA molecules play important role in controlling transcriptional networks (Guo et al., 2010; Hafner et al., 2010; Helwak et al., 2013). The 5'end sequences of the microRNA binds to its complement target sequence present in the 3' UTR of the messenger RNA (mRNA) and hence repressing translation. It is also shown that microRNA binding to its target mRNA triggers the recruitment of mRNA decay factors, leading to mRNA destabilization, degradation which result in decrease in the expression level of the protein (Bhaskaran and Mohan, 2014). There are reports which have shown that microRNAs can interact with other regions like 5'UTR, coding sequence, and gene promoters [Broughton JP, Cell 2016]. Additionally, microRNAs have been shown to activate gene expression under certain conditions (Vasudevan, 2012). Recent studies have proposed that microRNAs are shuttled between subcellular compartments to control the rate of transcription and translation (Makarova et al., 2016).

microRNAs were first discovered in 1993 by Lee and collegues in the nematode C. elegans (Lee et al., 1993). During a genetic screening experiment in *C. elegans* they found the downregulation of a protein known as LIN-14 which is essential for the progression from first larval stage (L1) to L2. They further investigated and observed that the downregulation of the LIN-14 is dependent on a second gene called lin-4. Interestingly, the transcribed product of lin-4 generates 2 small RNAs approximately 21 and 61 nucleotides in length. The 61-nucleotide sequence server as the precursor stem loop for the shorter RNA. Later the same group, along with Wightman et al (Lee

et al., 1993; Wightman et al., 1993) discovered that the smaller RNA had antisense complementarity to the multiple sites in the 3'UTR of the lin-14 mRNA, thereby causing the translational repression of lin-14 and subsequently affecting the progression in *C.elega*ns development.

It was thought that this novel method of regulation is exclusive for C.elegans. In 2000, two groups discovered that a small RNA, let-7, was essential for development of later larval stage to adult stage in the C.elegans (Rodriguez et al., 2007; Slack et al., 2000). Interestingly, homologues of this gene were afterward discovered in many organisms, including humans [Pasquinelli AE et al., Nature 2004]. This period and later was marked by deluge of information where many laboratories cloned numerous microRNAs from many organisms and found evolutionarily conserved microRNAs in animals and plants. This effort leads to set up of an online repository in 2002 named as "miRbase" for potential microRNA sequences, annotation, nomenclature and target prediction information.

1.11.1 Transcription regulation

miRNA sequences are located within various regions in the genome. In humans, the majority of canonical miRNA are encoded by introns of non-coding or coding transcript, but some are also encoded by exogenic regions. Several miRNA loci which are located in close proximity, constituting a poly-cistronic transcriptional unit. This poly-cistronic miRNA is called "miRNA cluster" and these miRNA cluster are generally co-transcribed, but the individual miRNA can be regulated post-transcriptionally. For example, one of the conserved miRNA cluster 'mir-100~let-7~mir-125' plays important role in developing bilateral animal. In embryonic stem cells (ESCs) and in cancer cells, only let-7 miRNA from this cluster is suppressed post-transcriptional to maintain the cells in pluripotent state (Lee et al., 2004; Roush and Slack, 2008).

miRNA promoters have not yet been identified for most miRNA genes but they can be inferred from collective data analysis of Chip-seq (chromatin immunoprecipitation followed by sequencing), CpG island analysis and RNA sequencing (Ozsolak et al., 2008). About half of the identified miRNA are intragenic and processed from the introns of the protein coding genes and thus share the same host promoter, while

intergenic miRNAs are regulated independently of the host gene and by their own promoters (Kim and Kim, 2007; de Rie et al., 2017).

The transcription of miRNA genes is carried out by RNA Pol II and is controlled by RNA Pol II associated transcription actor and epigenetic regulators (Cai et al., 2004; Lee et al., 2004). RNA Pol III has been shown to transcribe some viral miRNAs (Pfeffer et al., 2005). The biogenesis of miRNA has been classified into two pathways: i) canonical and ii) non-canonical.

1.11.1.1 The Canonical pathway of miRNA biogenesis

This is the dominant pathway by which miRNAs are processed. In this pathway, miRNA genes are transcribed into long primary miRNA (pri-miRNA) and then processed into precursor miRNA (pre-miRNAs) by microprocessor complex, consisting of an RNA binding protein DiGeorge Syndrome Critical Region 8 (DGCR8) and ribonuclease III enzyme, Drosha (Alarcón et al., 2015). Pri-miRNA consists of motifs like N6-methyladenylated GGAC are recognized by DGCR8 (Alarcón et al., 2015), while Drosha binds and cleaves the base of characteristics hairpin loop structure of the pri-miRNA. This results in the formation of a 2 ntd 3' overhang on pre-miRNA in the nucleus (Han et al., 2004). Pre-miRNA generated inside the nucleus has been exported to the cytoplasm using an exportin 5 complex known as XPO5/RanGTP and hence, further processed by RNAse III endonuclease Dicer (Denli et al., 2004; Okada et al., 2009). This processing of pre-miRNA using Dicer involves the removal of the terminal loop structure, resulting in mature miRNA duplex (O'Brien et al., 2018; Zhang et al., 2004). The name of the mature miRNA depends on the directionality of the miRNA strand. 5' end of the pre-miRNA hairpin generates the 5p strand while the 3p strand originates from the 3′ end. The mature miRNA duplex consists of both strands are then loaded by Argonaute (AGO) family of proteins (AGO 1-4 in humans) in an ATP-dependent manner (Yoda et al., 2010). For any given miRNA, depending on the cell type or cellular environment, the proportion of AGO-loaded 5p or 3p strand varies greatly ranging from near equal proportions to predominantly one or the other (Meijer et al., 2014; O'Brien et al., 2018). The 5p or 3p strand selection is based partly on the thermodynamic stability at the 5′ ends of the miRNA duplex or a 5′ U at nucleotide position 1 (Khvorova et al., 2003; O'Brien et al., 2018). Generally, the strand with lower 5′ stability or 5′ uracil is preferentially loaded into AGO, and is considered

as the guide strand. The other unloaded strand is called the passenger strand, which will be separated from the guide strand through various mechanisms based on the degree of complementarity. The passenger strands of miRNA which has no mismatches are cleaved by AGO2 and are degraded by cellular machinery which leads to a strong strand bias, while the miRNA duplexes which have central mismatches or non-AGO2 loaded miRNA are inertly separated and degraded (O'Brien et al., 2018) (Figure 12).

1.11.1.2 The Non-canonical pathway of miRNA biogenesis

Till date, multiple non-canonical miRNA biogenesis pathways have been elucidated, and they use different combinations of the proteins involved in canonical pathways like Drosha, DICER, and AGO2. The non-canonical biogenesis pathway can be Drosha/DGCR8-independent and Dicer-independent pathways. Precursor miRNA which are produced by Drosha/DGCR8 independent pathway resemble Dicer substrates. For example mirtrons, these pre-miRNAs are produced from the introns of mRNA during splicing (Babiarz et al., 2008; O'Brien et al., 2018; Ruby et al., 2007). Another example is one of the nascent RNA called 7-methylguanosine (m7G)-capped pre-miRNA which gets exported directly to cytoplasm without the need of Drosha cleavage through exportin- 1 protein. Due to m7G cap, there is a strong bias for 3p strand selection preventing 5p strand from loading on arganoute (Xie et al., 2013). On the other hand, endogenous short hairpin RNA (shRNA) transcripts are processed by Drosha in Dicer-independent miRNA pathway. Maturation of the pre-miRNAs happens within the cytoplasm with help of AGO2 because they are of insufficient length to be Dicer-substrates (Yang et al., 2010) and in turn promotes loading of pre-miRNA onto AGO2 and slicing of 3p strand. The maturation of pre-miRNA completes with the trimming of 3'-5' of the 5p strand (Cheloufi et al., 2010; O'Brien et al., 2018) (Figure 12).

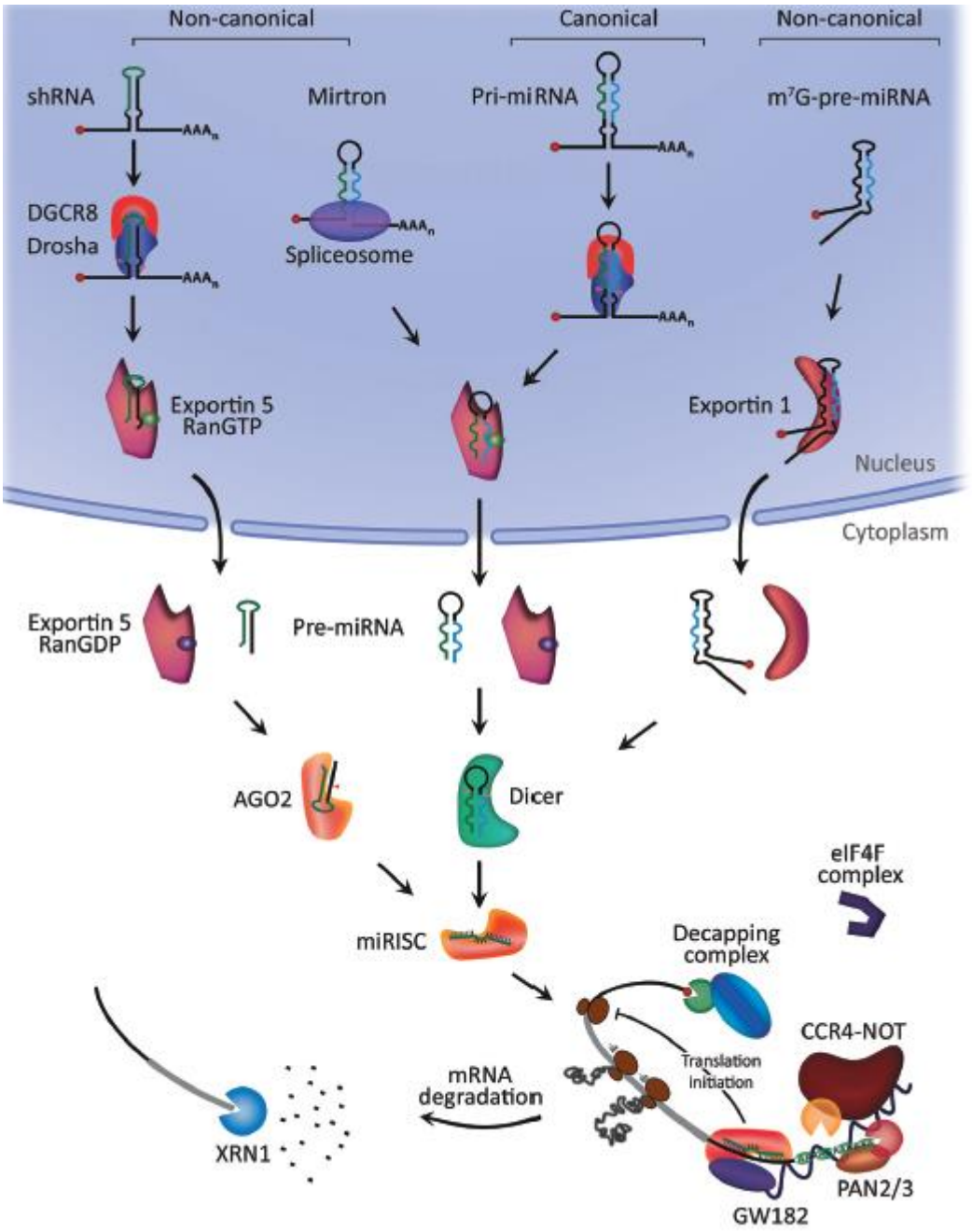

Figure 12: MicroRNA biogenesis and mechanism of action.

In canonical pathway, biogenesis begins with the generation of the pri-miRNA transcript followed by cleavage into pre-miRNA by microprocessor complex. The pre-miRNA exported into the cytoplasm and further processed to produce mature miRNA. In non-canonical pathway, shRNA is initially processed by microprocessor complex and further processed by dicer independent cleavage. Mitrons or 7-methylguanine capped pre-miRNA are dicer independent but they differ in their nucleoplasmic shuttling. Adapted from (O'Brien et al., 2018)

1.12 Transcription of microRNAs

1.12.1 miRNA gene families and nomenclature

miRNA genes composed of abundant gene families, and are broadly distributed in plants, animals and viruses (Kozomara and Griffiths-Jones, 2014). miRNA database (miRbase) has catalogued 466 miRNAs in *Drosophila Melanogaster*, 434 in *Caenorhabditis elegans (C.elegans),* and 2,588 miRNAs in humans. But still these annotated miRNAs need to be functionally verified.

In many species, multiple miRNA gene loci with related sequence arose due to the process of gene duplication and these miRNAs are called paralogues miRNA sequences. Rules for miRNA classification have not yet been unified, but it is considered that miRNA with identical sequences at 2-8 nucleotide of the mature miRNA belongs to the same “miRNA family”. For example, one of the well-studied family of miRNA known as let-7 family (miRNA sisters) is encoded by 14 paralogous loci in the human genome. There are thirty four miRNA families which are phylogenetically conserved from *C.elegans* to humans, and 196 miRNA families are conserved among mammals (Chiang et al., 2010; Wheeler et al., 2009). miRNAs share a common evolutionary origin but diverge in the miRNA seed. For example, miR-200c and miR-141 belongs to a conserved miR-200 superfamily but they differ only by one nucleotide in their miRNA seeds. It has been shown that, deletion of each sister locus causes the targets of both miRNAs to barely overlap, which shows the importance of the miRNA seed sequence in miRNA function and evolution (Kim et al., 2013).

Nomenclature of miRNA genes is somewhat inconsistent. Genes found in early genetic studies were named after their phenotypes (for example, lin-4, and let-7), whereas other miRNAs found from cloning and sequencing received numerical names like lin-4 homologues in other species are called mir-125. Genes which encode for miRNA sisters are indicated with the letter suffixes ‘a’ and ‘b’ (for example, mir-125a and mir-125b). The mature miRNA sequences which are encoded by multiple separate loci, there is addition of numeric suffixes at the end of the names of the miRNA loci (for example, mir-125b-1 and mir-125b-2). miRNAs are derived from stem loop structures and hence encode two mature miRNA one from 5’ strand and the other from 3’ strand of the precursor (for example, miR-125a-5p and miR-125a-3p). However, the prevalence (96-99% of the sum on average) of the one arm (called the guide strand)

is usually more biologically active than the other arm (passenger strand) also known as miRNA*. (Ha and Kim, 2014)

1.13 MicroRNAs in early embryogenesis

MicroRNAs have been involved in many biological processes, including early development and differentiation. Their importance has been demonstrated in many species from C.elegans to mammals. Experiments have been performed to knockout the two enzymes involved in miRNA biogenesis i.e., dicer and dgcr8 in various organisms. C.elegans with dicer homozygous knockout are viable, but infertile and have partial penetrant development abnormalities, such as burst vulva (Grishok et al., 2001; Ketting et al., 2001). Dicer homozygous knockout in zebra fish appears normal during first week after fertilization but then they start showing growth arrest, decrease in activity and eventually die in between 14-21 days after fertilization (Wienholds et al., 2003). Mouse embryo deficient with dicer 1, were 50% fewer in number than expected dicer 1 knockout. During E7.5 stage of development these knockout embryos showed stunted growth and were morphologically abnormal, with lack of expression of both Oct4 and brachyury, which indicates depletion of stem cell pool in the embryos and arrest of development prior to gastrulation (Bernstein et al., 2003). Mouse embryos with dgcr8 knockout were embryonic lethal and showed gross morphological defects during E6.5 stage of development (Wang et al., 2007). There is developmental arrest in all the organism and the impairment occurs at similar time after fertilization, suggesting that the arrest is not stage specific but it depends on the critical threshold of the maternal dicer and dgcr8.In zebra fish embryos, it has been shown that a family of miRNA called mir-430 were highly expressed between 5-48 hrs after fertilization. When family of mir-430 was injected at one-cell stage of embryo deficient with dicer and dgcr8, they were able to rescue the brain morphogenesis defect ((Giraldez et al., 2005). There are very few studies, which has been done on early human development and one of the studies from Rosenbluth and colleagues have shown differentially expressed miRNAs in human blastocyst (Rosenbluth et al., 2013). One of the most abundant miRNAs they identified was miR-372.This is the human homologue of the mir-290-295 cluster in mice, which has been shown to play important role in the survival of embryo (Giraldez et al., 2005).

1.14 MicroRNAs in embryonic stem cells

In ESCs, most of the knowledge of miRNAs have come from knockout studies. Dicer-1 null KO mESC exhibited no morphological change and express pluripotent marker Oct4 but deficient in centrosome silencing. Additionally, these cells displayed low proliferation rate and inability to differentiate, and failed to form teratomas when injected into immunodeficient mice (Kanellopoulou et al., 2005). In addition, Dgcr8 null cells also exhibited defects in differentiation abilities but milder compared to Dicer-1 null mESCs. This might be due to the importance of Dicer for both miRNA and siRNA processing whereas Dgcr8 is important only for miRNA processing. It has also been shown that reintroducing the Dicer gene into dicer null mouse rescued the phenotype for lack of differentiation (Denli et al., 2004; Wang et al., 2007). This suggest that miRNA plays an important role in ESCs self-renewal and differentiation capabilities.

Small RNA sequencing and microRNA profiling from many studies have shown that higher expression of miRNAs like mir-302, mir-17 and mir-519 cluster in undifferentiated ESCs than differentiated samples. miRNA profiling in hESCs showed higher expression of oncogenic miRNAs and downregulation of tumor suppressor miRNAs (Gu et al., 2016). A study in 2008 have shown the chromatin occupancy of miRNA genes using ChIP sequencing in mESCs. H3K4me3 (marks the transcription initiation site) and H3K36me3 (associated with transcription elongation) have been used for mapping the transcripts length of the miRNA genes. Simultaneously, they have also mapped pluripotency associated transcription factors (TFs) and polycomb group protein Suz12. Interestingly, there were co-occupancy of pluripotent TFs at the promoter region of both the pluripotency associated miRNA genes (mir-290 cluster, mir-302 cluster, mir-92 cluster and let-7g) and also the lineage specific miRNA genes (mir-9, mir-124a, mir-708, mir-155). However, the polycomb protein Suz12 was present only on the lineage restricted miRNA genes. This suggest that the pluripotent TFs bind to the promoter regions of the genes which are highly expressed in differentiated and undifferentiated cells. But binding of the polycomb group protein determines the genes which are repressed in PSCs. (Marson et al., 2008)

1.15 miRNAs in NSCs self-renewal, differentiation and fate determinant

1.15.1 Self-renewal and proliferation

NSCs self-renewal and proliferation is regulated by complex regulatory networks comprise of transcription factors, epigenetic modifiers and external signaling cues from the surrounding niche both in embryonic and adult stage. It has been shown that non-coding RNAs (ncRNAs) also play important role in self-renewal by post transcriptional mechanism (Shi et al., 2014).

Studies have been conducted by ablating Dicer enzyme to understand the global role of miRNAs in NSCs development which block the biogenesis of miRNAs in the CNS. To better understand the role of miRNA in CNS, conditional knockout studies were generated. Emx1-Cre and Nes-Cre conditional knockout in mouse cerebral cortex exhibited significant reduction of NSC numbers (depletion of cortical neural progenitor pool) and abnormal differentiation (Andersson et al., 2010; Kawase-Koga et al., 2010; De Pietri Tonelli et al., 2008). When Dicer knockout NSCs were grown in the mitogen deficient culture condition displayed apoptosis (Fukagawa et al., 2004; Kanellopoulou et al., 2005). Individual miRNAs have been studied to understand the role of miRNAs in NSCs proliferation and differentiation, among which some of them are discussed below.

The first identified let-7 miRNA (Reinhart et al., 2000)has been shown to regulate NSC proliferation and differentiation by targeting nuclear receptor TLX and cyclin D1 (Zhao et al., 2010). It has been shown that let-7b overexpression inhibit proliferation and enhance differentiation while the knockdown displayed increased NSC proliferation (Zhao et al., 2010). Let-7 expression in NSCs is controlled by feedback regulation of Lin-28 (RNA binding protein) that controls its processing. Lin-28 binds to the Let-7 precursor and inhibits its processing by Dicer. Alternatively, the expression of Lin-28 is repressed by let-7 and miR-125, allowing the maturation of let-7. This feedback loop reveals autoregulation between let-7 and miR-125, and Lin28 during NSCs development (Rybak et al., 2008).

Another most widely studied miRNA named as miR-124 have been identified as a CNS enriched miRNA and is upregulated during neuronal differentiation (Lagos-Quintana et al., 2002). In adult, NSCs are identified in the SVZ and knocking down of miR-124 *in vivo* and *in vitro* displayed an increase of NSCs proliferation and decrease in differentiation. On the other hand, miR-124 overexpression reduces the number of

dividing NSCs and enhanced differentiation and this is regulated by suppressing Sox9 (Cheng et al., 2009). It has been shown that miR-124 regulate differentiation by modulating a nervous system specific global repressor involved in alternative pre-splicing pathway known as PTBP1 (Makeyev et al., 2007). It appears that miR-124 performs its function through repressing various targets.

One of the other highly expressed miRNAs is miR-9. In xenopus, miR-9 knockdown promotes the proliferation of hindbrain neural progenitors due to increased expression in cyclin D1 and downregulation of p27Xic1 (Bonev et al., 2011). In zebrafish, miR-9 promotes differentiation of neural progenitors (NPs) into neurons of midbrain-hindbrain domain and also controls the boundary between midbrain-hindbrain domain by targeting several genes involved in fgf8 signaling pathway. In mouse brain, double knockout for miR-9-2 and miR-9-3 shown reduced cortical layers, migration defects of interneurons, misrouted thalamocortical axons and cortical axon projections, indicating important role in NSCs proliferation, differentiation and migration. It has been shown that miR-9 regulates many targets like Foxg1, Pax6, Gsh2 which has been shown to be important for cortical development (Shibata et al., 2011). In human ESCs derived NSCs, miR-9 have shown negative effect on migration by inhibiting Stmn1, which causes microtubule instability (Delaloy et al., 2010).

1.15.2 Cell fate determinant

miRNAs are also known to play an important role in cell fate switch between neurons to glia (Davis et al., 2008; Zheng et al., 2010). Kawase-Koga and collegues demonstrated that Dicer knockout in the NSCs displayed anomalous differentiation, with shorter neurites and less processes in glial cells (Kawase-Koga et al., 2010). Studies have shown that conditional dicer ablation in mouse forebrain neurons led to neuronal degeneration and increase in glial fibrillary acidic protein (GFAP) cells (Hébert et al., 2010). It has been shown using miRNA array that specific miRNAs are expressed in neurons and glia. For example, miR-124, miR-128 are enriched in neurons while miR-23 is highly enriched in astrocytes. There are some miRNAs like miR-9 and miR-125 which are evenly enriched in both neurons and astrocytes (Smirnova et al., 2005). Overexpression of miR-124 enhances neuronal differentiation (Cheng et al., 2009). It has also been shown that ectopic expression of miR-124a and miR-9 in neural progenitors derived from ESCs displayed reduction of GFAP positive

cells than controls. While knockout of miR-9, not miR-124a, switches neural progenitors from neurogenic potential to astrogenesis (Krichevsky et al., 2006). They have also shown that one of the potential mechanisms is by targeting phosphorylated STAT3, a transcription factor that promote astrogliogenesis (Bonni et al., 1997; Krichevsky et al., 2006). Loss of function studies of miR-125b (astrocyte specific miRNA) causes impaired proliferation of astrocytes but upregulating cyclin-dependent kinases inhibitor (CDKN2A) which negatively regulates cell proliferation (Pogue et al., 2010) (Figure 13).

Due to lack of availability of human fetal sample and also the difficulty of isolating/obtaining purified population of human neural progenitors, few studies were carried out to study the role of miRNAs in human cells/tissue. Jonsson and collegues did a comprehensive analysis by generating forebrain, midbrain and hindbrain progenitors invitro using chambers et al protocol (Chambers et al., 2009)and performed small RNA sequencing to identify specific miRNAs which are expressed in each progenitor population. They identified miR-10 as one of the hindbrain specific miRNA. They confirmed the region-specific miRNA expression by using miRNA array on sub dissected human foetal brain tissue. The array demonstrated that miRNAs are expressed in stage specific manner. Overexpression of miR-10 in midbrain-patterned neural progenitors leads to caudalization of these neural progenitors into hindbrain progenitors by upregulating hindbrain specific genes suggesting the role of miRNA in cell fate transitions (Jönsson et al., 2015).

Another study on human ESCs derived neuroepithelial like cells (lt-NES) demonstrated that gain and loss of function studies of miRNAs such as miR-153, miR-324-5p/3p and miR-181a/a* contribute to shift of lt-NES cells from self-renewal to neuronal differentiation fate. They also demonstrated that miR-125b and miR-181a promote dopaminergic neurons while miR-181a* inhibits it (Stappert et al., 2013). Although a great detailed characterization of miRNAs in neural stem cells has come from the studies of mouse brain, until now the role of miRNAs in human neural stem cells have been largely unexplored. Here in this study, we have deciphered the role of one of the miRNAs of human neural stem cells i.e., hsa-miR-20b-5p one of the miRNAs from miR-17~92 cluster.

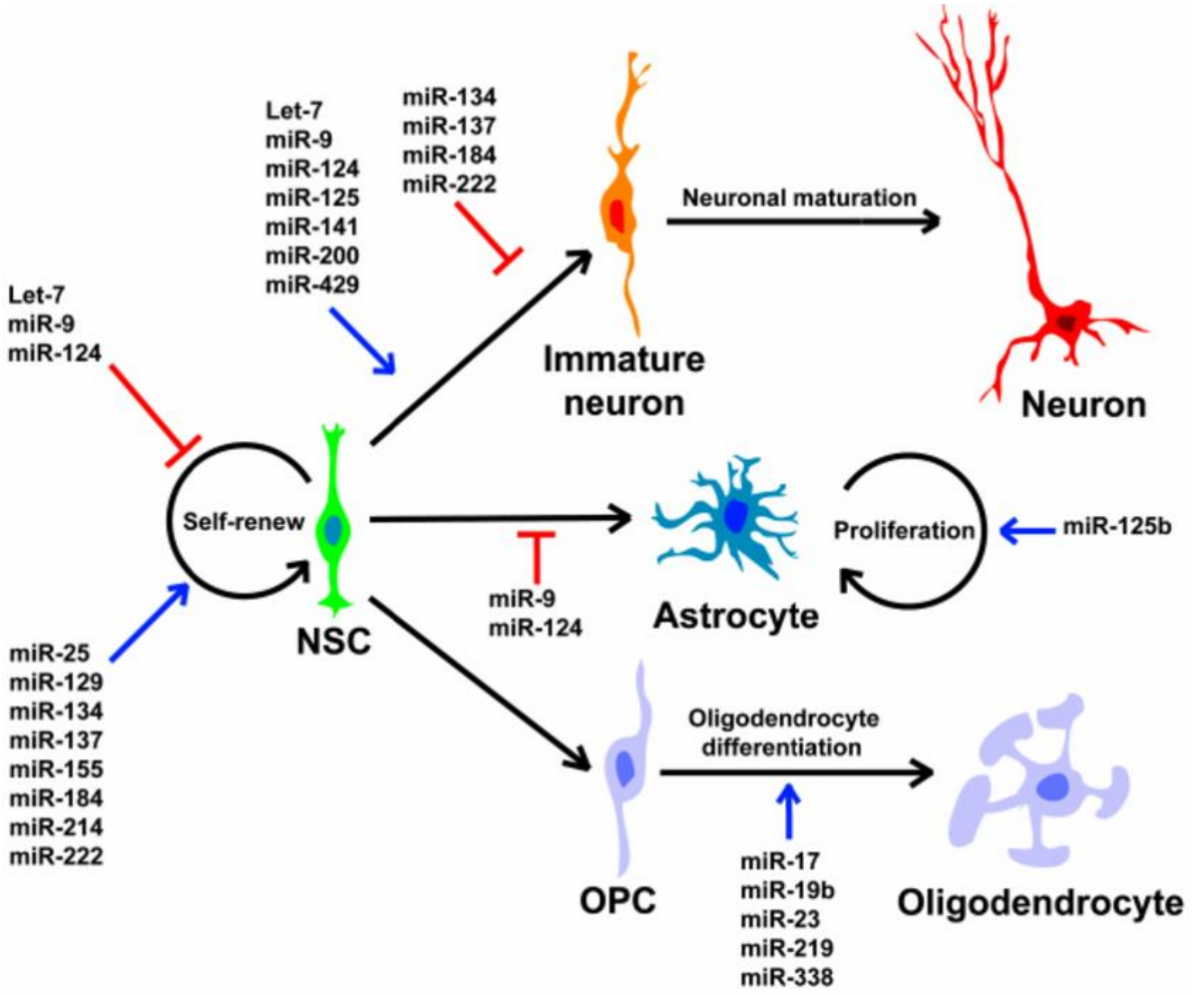

Figure 13: MicroRNAs in self-renewal, proliferation and cell fate determination. MicroRNAs play important role in neural stem cell self-renewal, differentiation such as miR-25, miR-137 and Let-7 respectively. MiRNAs also act as cell fate determinant for generating neurons, astrocytes and oligodendrocytes. Adapted from (Bian and Su, 2012)

1.16 miR17~92 cluster and family

miR 17~92 is one of the best-characterized polycistronic miRNA cluster. This cluster encodes for six individual miRNAs (miR-17, miR-18a, miR-19a, miR-201, miR-19b-1 and miR-92a) and maps to human chromosomes 13. The sequence of the cluster is highly conserved among vertebrates, and in turn gene duplication and deletion events during evolution have resulted in two paralogs: the miR-106~25 cluster and miR-106a~363 (Figure 14a). miR-106~25 cluster is located on human chromosome 7 and resides in the intron of MCM7 gene, while miR-106a~363 is located on chromosomes X. miR-17~92 cluster and miR-106~25b is expressed in ESCs and also in wide array

of mouse tissue. However, miR-106a~363 cluster is expressed at low levels. These three paralogous clusters of miRNAs encode for fifteen miRNAs and can be grouped into four seed families (Figure 14b) (Houbaviy et al., 2003; Suh et al., 2004; Tanzer and Stadler, 2004; Thomson et al., 2004; Ventura et al., 2008).

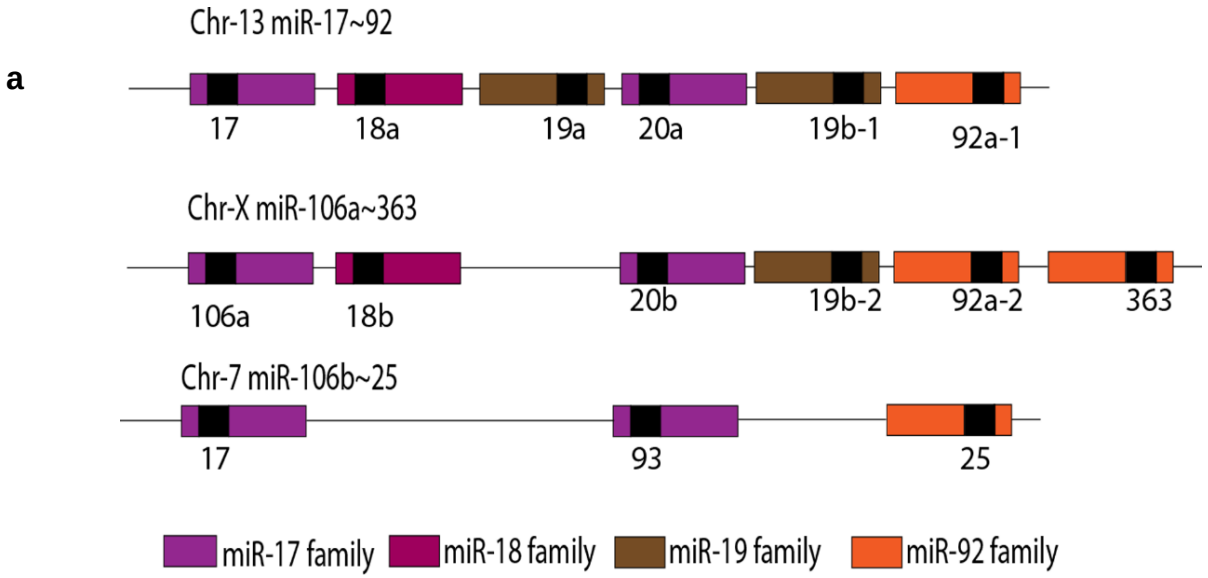

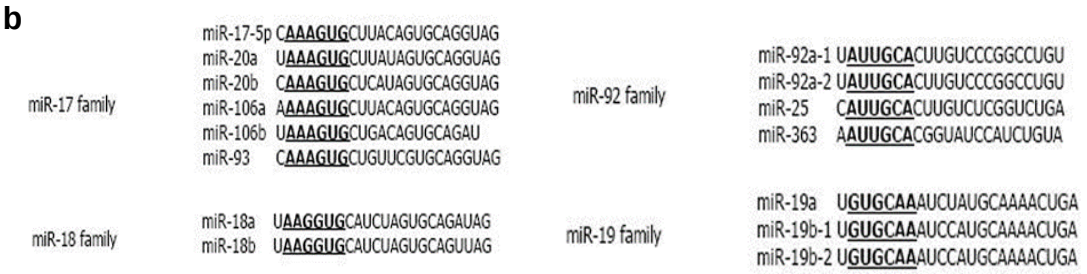

Figure 14: Paralogues sequences of miR-17~92 cluster.

a) Chromosomal location of miR-17~92 cluster which encodes for six individual miRNA family denoted by specific color (miR-17, miR-18, miR-19, miR-92).

b) A family of miRNA targets the same seed sequence and miR-17~92 cluster have four families.

Transcriptional regulation of this cluster demonstrated its functional role as a direct transcriptional target of c-Myc (O' Donnell KA et al., Nature 2005 id 15944709). Consistent with the proliferative role of this cluster due to c-Myc downstream effector, E2F family of transcription factors has also been shown to bind at the promoter of miR-17~92 cluster and regulate its transcription (Sylvestre et al., 2007). miR-17 and miR-20 directly inhibit E2F1/2/3 and act as regulator for cell proliferation. Collectively,

studies have suggested a model system where c-Myc induces cell proliferation while E2F transcription factor expression set the threshold through repression by miR17~92 cluster, in turns maintain the balance between apoptosis and proliferation (Woods et al., 2007).

Studies have shown that according to the cellular context, miRNA processing can be modulated and expression of mature miRNA does not necessarily correlate with that of pri-miRNA (Obernosterer et al., 2006; Thomson et al., 2004; Wulczyn et al., 2007). In case of miR-17~92, the miRNA encoded by this cluster expressed at different levels, which shows that either they are processed with different efficiency or their stability is different. This might be due to the accessibility of microprocessor complex to some miRNAs in a cluster (Chaulk et al., 2011).

Deletion of miR-106~363 and miR-106b~25 cluster does not result in any obvious developmental deformity in mice and the offspring are viable and fertile. However, homozygous deletion of miR-17~92 cluster showed penetrant perinatal lethality (Ventura et al., 2008). This is due to severe lung hypoplasia and cardiac defects. Triple knockouts of the three paralogous cluster simultaneously in the mice showed more severe phenotype with embryonic lethality before E15 due to cardiac problems and apoptosis across the body.

To study the role of this cluster in brain development, Bian S et al used a conditional knockout strategy where they used Emx-cre mice to specifically knockout the cluster in cortex. In this study, they have showed that the miR-17~92 cluster is required for maintaining the pool of radial glial cell (RGs) and intermediate progenitors (IPs) by repressing Pten and Tbr2 protein. Knockout of the paralogs clusters limits NSC proliferation by suppressing RG cells expansion and promoting the transition of RG cells towards IPs. This shows that role of miR-17~92 cluster in promoting proliferation and modulating cell fate decisions of neural progenitors (Bian et al., 2013) (Figure 15). However, individual role of the specific miRNAs from this cluster have not been explored and here in this study we have focused on has-miR-20b-5p which is an early-stage neural stem cell specific miRNA and have elucidated the role of this miRNA in NSCs cell fate transitions, by gain of function studies using brain organoids as model system.

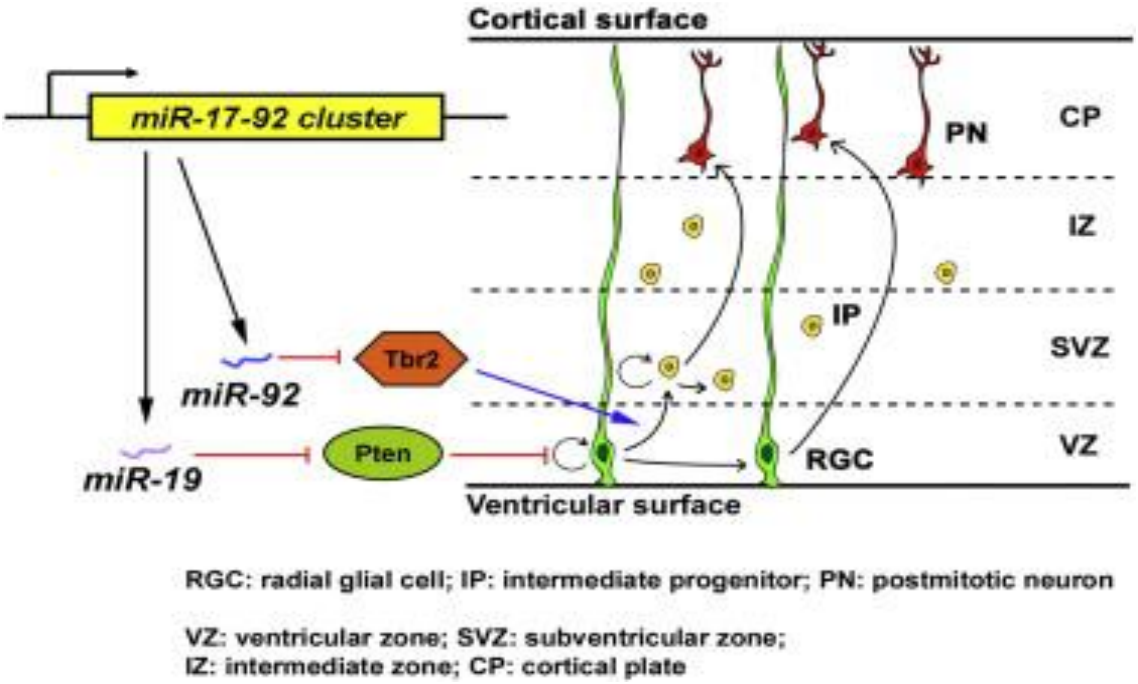

Figure 15: Knockout of miR-17~92 cluster in mice.

Deletion of miR-17~92 cluster and its paralogous sequences from mice cortex showed less radial glial cell proliferation and more of intermediate progenitors. KO of miRNA cluster also effects the upper layer and deep layer neurons of the cortex.

2. MATERIALS AND METHODS

2.1 Reagents

- DMEM/F12 (Gibco)
- Knock-out DMEM (Invitrogen)
- Neurobasal medium (Gibco)
- mTeSR1 medium (Stem Cell Technologies)
- Knockout serum (KSR, Gibco)
- 1mM Glutamine (Gibco)
- GlutaMAX (Invitrogen)
- Penicillin-streptomycin (Gibco)
- MEM non-essential amino acids (MEM-NEAA, Gibco)
- Beta-Mercaptoethanol (Invitrogen)
- Fetal bovine serum heat inactivated (FBS, Gibco)
- Dimethyl sulphoxide (DMSO, Sigma)
- Insulin (Sigma)
- Apotransferin (Sigma)
- Sodium Selenite (Sigma)
- Putrescine (Sigma)
- Progesterone (Sigma)
- D-Glucose (Sigma)
- Sodium bicarbonate (Sigma)
- Gelatin powder (Sigma)
- Matrigel (BD Biosciences)
- Polyornithine (Sigma)
- Fibronectin (BD Biosciences)
- Laminin (BD Biosciences)
- Paraformaldehyde (PFA; Sigma-Aldrich)
- Picric acid
- Sucrose (Sigma-Aldrich)
- Optimal cutting temperature compound (OCT, Tissue-Tek)
- Bovine serum albumin (BSA, Sigma)

- Triton-X100 (Sigma)
- Trypan blue (Gibco)
- DPBS without calcium and magnesium (Gibco)
- Growth factors and small molecule inhibitors
- Basic fibroblast growth factor 2 (bFGF2, R&D)
- Transforming growth factor-β1 (TGF-β1, Peprotech)
- Noggin (R&D)
- SB-431542 (Tocris)
- XAV (Tocris)
- Fibroblast growth factor 8 (FGF8, R&D)
- Brain derived growth factor (BDNF, R&D)
- Epithelial growth factor (EGF, R&D)
- L-Ascorbic acid (Sigma)
- B27 – vitamin A supplement (Gibco)
- B27 + vitamin A supplement (Gibco)
- ROCK inhibitor (Y27632, Tocris)
- Neutral protease (Dispase, Worthington)
- Accutase (Sigma-Aldrich)
- Deoxy ribonuclease (DNase I, Worthington)
- Papain dissociation system (Worthington)
- TrypLE (Gibco)
- 0.5M EDTA (Invitrogen)
- Hank's Balanced Salt Solution (HBSS) (Gibco)

2.2 Molecular biology application kits

- DNeasy Blood & Tissue Kit (Qiagen)
- Plasmid Plus Midi Kit (Qiagen)
- miRNeasy Mini Kit (Qiagen)
- RNase Free DNase Set (Qiagen)
- High-Capacity cDNA Reverse transcription Kit (Applied Biosystems)
- FastStart Universal SYBR Green Master (ROX, Roche)
- Phusion High-Fidelity PCR Kit (New England Biolabs)

- TaqMan Advanced miRNA cDNA synthesis kit (ThermoFischer Scientific)
- miRNA Assay for hsa-miR-20b-5p (ThermoFischer Scientific)
- Papain Dissociation kit (Worthington)

2.3 Cell lines

- HES5::*eGFP* H9 human Embryonic stem cells (hESCs), Wicell Research Institute (WA-09,XX)
- ZIP8K8 induced pluripotent stem cells (gift from F. Muller lab)
- Genetically modified line: LT320b (ZIP8K8 is used as the background line and named as LT3 because the plasmid initials start with LT3)

2.4 Reagents preparation

hESC medium (500 ml)

To 386.5 ml of DMEM/F12, add 100 ml of KSR, 2.5 ml of GlutaMAX, 5 ml of MEM-NEAA, 5 ml of Penicillin-Streptomycin and 0.5 ml of beta-mercaptoethanol. Filter it using a vacuum-driven 0.2-µm filter unit, store at 4°C and use at room temperature (RT).

mTESR1 medium (500 ml)

To 400 ml of mTESR1 basal medium, add 100 ml of mTESR1 5X supplement and 5 ml of Penicillin-Streptomycin. Filter it using a vacuum-driven 0.2-µm filter unit, store at 4°C and use at room temperature (RT).

KSR medium (500 ml)

To 409.5 ml of Knockout DMEM, add 75 ml of KSR, 5 ml of GlutaMAX, 5 ml of MEM-NEAA, 5 ml of Penicillin-Streptomycin and 0.5 ml of beta-mercaptoethanol. Filter it using a vacuum-driven 0.2-µm filter unit, store at 4°C and use at room temperature (RT).

Neurobasal medium (500 ml)

To 484.5 ml of Neurobasal medium, 5 ml of GlutaMAX, 5 ml of MEM-NEAA, 5 ml of Penicillin-Streptomycin and 0.5 ml of beta-mercaptoethanol. Filter it using a vacuum-driven 0.2-µm filter unit, store at 4°C and use at room temperature (RT).

N2 medium (500 ml)

To 490 ml of DDW, add 6.5 g of DMEM/F-12 powder, 0.775 g of D-Glucose, 1 g of Sodium bicarbonate, 5 mg of Apo-transferrin, 12.5 mg of insulin, 30 µl of 500µM Sodium selenite, 100 µl of 830nM Putrescine, 100 µl of 100µM Progesterone and 5 ml of Penicillin-Streptomycin. Filter it using a vacuum-driven 0.2-µm filter unit, store at 4°C and use at room temperature (RT).

Dispase solution

Reconstitute 50 mg of dispase powder with indicated activity of C units/mg dry weight (=50C units) in a desired volume (=50C/4) of hESC medium to get a working activity of 4 units/ml. Filter the solution using a vacuum-driven 0.2-µm filter unit, store at -20°C and use at RT.

EDTA solution

Add 200 µl of 0.5M EDTA to 200 ml of DPBS and filter it using a vacuum-driven 0.2-µm filter unit, store and use at RT

Fixing and staining solutions

4% PFA and 0.15% Picric acid solutions (250 ml)

Heat 200 ml of PBS to 58-60°C in a beaker on a magnetic heating plate and add 10g of PFA with continuous stirring with magnetic stirrer and add few drops of 1N NaOH for complete dissolving of PFA. Once the PFA is dissolved and the solution is clear, make up the rest of the volume to 221 ml with PBS and let it stand to come to room temperature. Add 28.8 ml of 1.3% Picric acid and adjust the pH to 7.4 by using 10N NaOH. Store it at -20°C and use at RT.

PB (PBS/BSA, 500 ml) and PBT (PBS/BSA/Triton X100, 200 ml) solutions

Add 7 g of BSA to 609 ml of DPBS and 70 ml of FBS and stir continuously on a magnetic plate with a magnetic stirrer inside until the solution is completely dissolved and appear clear. Take 194 ml of PB solution, add 6 ml of 10% Triton X100 and mix well. Filter it in to a separate 200 ml bottle using a vacuum-driven 0.2-µm filter unit. Store at 4°C and use at RT. Rest PB solution filter through separate 500ml bottle using vaccum-driven 0.2-µm filter unit and store at 4°C.

HEK medium

To 389.5 ml of DMEM-KO, add 100 ml of FBS, 5 ml of GlutaMAX, 5 ml of Penicillin-Streptomycin and 0.5 ml of beta-mercaptoethanol. Filter it using a vacuum-driven 0.2-µm filter unit, store at 4°C and use at room temperature (RT).

Matrigel Preparation

For maintaining hiPSCs, 0.5ml of Matrigel is diluted in 50 ml of DMEM-KO medium and before splitting plate was coated for 1 hour at 37°C in the incubator. For Matrigel induction experiment, 1 ml of Matrigel is diluted in 19ml of DMEM-KO medium and the plate is coated for 1 hour at RT.

Papain dissociation reagents

Add 32 ml of EBSS to the albumin ovomucoid inhibitor mixture and allow the contents to dissolve and mix before using. Add 5 ml of EBSS to a papain vial and place the vial in a 37°C water bath for ten minutes or until the papain is completely dissolved and the solution appears clear. The solution should be used promptly but can be held at room temperature during the dissection. Add 500 µl of EBSS to a DNase vial and mix gently -- DNase is sensitive to shear denaturation.

2.5 Generation and culturing of hESCs line

The BAC transgenic HES5::eGFP Notch activation human ES cell reporter line has been derived from the H9 (WA-09, XX) human ES cell line (Wicell) and described previously (Placantonakis et al., 2009). Undifferentiated HES5::eGFP hES cell lines were cultured on mitotically inactivated mouse embryonic fibroblasts (Globalstem) and maintained in medium containing DMEM/F12, 20% KSR, 1mM Glutamine, 1% Penicillin/Streptomycin, non-essential amino acids, beta-mercaptoethanol and supplemented daily with 10 ng/ml FGF2 (R&D), and passaged weekly using Dispase (Worthington) to maintain their undifferentiated state.

2.6 Generation and culturing of iPSC line

The ZIP8K8 iPSC line was derived from Human dermal fibroblast (HDF) cells were obtained from a 40-year-old Caucasian male with no history of genetically inherited, neurological or metabolic disorders using a 3 mm punch biopsy. Briefly, biopsy material was segmented into smaller fragments, plated onto tissue culture-treated

plastic dishes and maintained in HDF medium containing DMEM Glutamax, 1% Penicillin/Streptomycin and 20% fetal calf serum at 37°C and 5% CO2. HDF medium was changed every other day to obtain a 90% confluent monolayer until the cells were passaged at a 1:3 ratio using trypsin. PSC line were induced using episomal plasmids following a published protocol with minor modification (Okita et al., 2011). All plasmids were a gift by Shinya Yamanaka and obtained via Addgen (http://www.addgene.org). Briefly, 2 µg of pCXLE-hSK (#27080), pCXLE-hUL (#27078) and pCXLE-hOCT3/4-shp53F (#27077) were transfected into 106 HDFs using the Neon microporator device with 100 µl electroporation tips (Settings: 1.650 V, 10ms, 3 timed pulses; Thermo Fisher Scientific) according to the manufacturer's protocol. Transfected cells were resuspended in 10 ml fibroblast medium containing 90% 1x MEM (Thermo Fisher Scientific) supplemented with 10% FCS, and 2.5x104 HDF/cm2 were reseeded onto Matrigel coated (0.5 mg/ml) six-well plates. Two days post transfection, fibroblast medium was replaced with TeSR-E7 (Stemcell Technologies) and cells were fed every other day with 2 ml TeSR-E7/well. On day 26-30, post transfection emerging hiPSC colonies were picked and transferred onto Matrigel-coated plastic dishes (Corning; 0.5 mg/ml) in TeSR-E8 medium (Stemcell Technologies) for further expansion. Enzyme-free colony expansion using EDTA was performed every 3-4 days at a 1:6 ratio based on a protocol previously described(Beers et al., 2012). Expression of pluripotency markers as well as tri-lineage differentiation markers for this iPSC line was confirmed by qPCR, immunostaining and FACS sorting assays.

The LT320b iPSC line was derived by infecting the ZIP8K8 hiPSC line with 0.2MOI viral particles containing miR-20b-5p cloned in LT3GEPIR vector (gifted by Markus Haffner lab NIH). The genetically modified iPSCs were cultured on feeder-free matrigel coated plates (1:100) and grown in mTeSR™1 medium (Stemcell Technologies). Single cell suspension was made and 10,000 cells were plated in a 60mm dish and clones were picked and expanded. Few cells of the clones we plated in a 24 well plated and induced with doxycycline (2mg/ml) and checked for the percentage of GFP positive cells under the epifluorescence microscope.

For overexpressing CCND1 in miR-20b expressing cells, we took LT320b hiPSC clone and infected these cells at 0.75 MOI with CCND1 virus. The cells were grown in mTesr1 till the colonies become bigger and puromycin selection (2ng/ml) was started

after 48hrs. The selected cells which survived were expanded and some cells were plated in a 24 well plate to check for mCherry expression and we saw the cells were positive for mCherry. Later, after generating organoids from this line we saw the percentage of cells which are double positive for eGFP and mCherry were very low. So, we decided to do induce the dual reporter line for 24 hrs with doxycycline and sorted using FACS the double positive cells and while sorting we observed there were two population one with higher GFP and mCherry and one with medium GFP and mCherry. We collected separately and expanded these cells.

2.7 Neural induction and rosette formation from pluripotent stem cells (EB protocol)

Day 0

For Feeder dependent pluripotent stem cells (PSCs) (hESC growing on MEF feeder layer)

- hESC medium was collected from the confluent hESC culture dish into a 15ml falcon tube.
- 1ml of Dispase (4U/ml) was added to the culture dish and incubated for 10 min at 37°C in the incubator (incubation time could change according to the enzyme activity, so care was taken to not to over digest).
- The culture dish was tapped gently to detach the colonies from MEF and neutralized the dispase by adding 4ml of hESC medium collected in the first step.
- All the colonies were collected into a 15 ml falcon tube and let it wait till all the cells sink to bottom of the tube.
- Supernatant was aspirated and again washed the cells with 5 ml of hESC medium and let the cells to sink down.
- Supernatant was aspirated and 1 ml of accutase was added along with ROCK inhibitor (10µM) and kept in 37°C water bath for 4 min.
- With p1000 pipette, colonies were triturated for 15-20 times and observed for single cells under microscope.

- Neutralized the accutase by adding 10 ml of hESC medium and centrifuged at 1400 rpm for 5 min.
- Aspirated the supernatant and again washed with ½ KSR + ¼ N2 + ¼ NB medium and ROCK inhibitor (10µM) and centrifuged at 1400 rpm for 5 min.
- Aspirated the supernatant, resuspended the pellet in ½ KSR + ¼ N2 + ¼ NB medium with ROCK inhibitor (10µM) and counted the cells with haemocytometer.
- Plated 750K cells per each well of a 6-well low-attachment plate in 2 ml of ½ KSR + ¼ N2 + ¼ NB medium + ROCK inhibitor (10µM) + B27-RA (1%) and kept the plates in incubator at 37 ^{o}C and 5% CO_2.
- Day 0 media: ½ KSR+ ½ (N2+NB) medium + ROCK inhibitor (10µM) + B27-RA (1:100)

For Feeder independent PSC (iPSC growing on matrigel coated plates)

- mTESR1 medium was aspirated from the iPSC culture dish and washed the cells once with 3 ml of EDTA.
- 1ml of EDTA was added to the culture dish and incubated for 3-4 min at 37°C in the incubator.
- EDTA solution was aspirated gently without disturbing the colonies and added 2 ml of accutase and kept in the incubator for another 3 min.
- Cells were triturated 10-15 times and then were collected in a 15 ml tube and 5 ml of mTESR1 was added to neutralize the accutase and checked under the microscope for single cells.
- Cells were centrifuged 270g for 5 min.
- Supernatant was aspirated and washed with 5 ml of ½ KSR+ ½ N2+NB medium with ROCK inhibitor (10 µM) and centrifuged at 270g for 5 min.
- Supernatant was aspirated and resuspended the cells in 2 ml of ½ KSR+ ½ N2+NB medium with ROCK inhibitor (10 µM) and cells were counted.
- Plated 750K cells per each well of a 6-well low-attachment plate in 2 ml of ½ KSR + ¼ N2 + ¼ NB medium + ROCK inhibitor (10 µM) + B27-RA (1%) and kept the plates in incubator at 37 ^{o}C and 5% CO_2.
- Day 0 media: ½ KSR+ ½ (N2+NB) medium + ROCK inhibitor (10 µM) + B27-RA (1%)

Day 1

- EBs were allowed to form and in order for them to not attach to plate, each well was scrapped using cell scraper gently
- For day 3 EB transfer, new 6 cm dishes were coated ahead with 2ml of polyornithine/DPBS solution (15 µg/ ml polyornithine) -- 2 X 6 cm dishes were coated for each well of 6-well plate

Day 2

- EBs were scraped and collected in a 15ml falcon and waited for 15 mins for them to settle down and then centrifuged for 1 min at 200rpm.
- Supernatant was aspirated and then resuspended the EBs in 2ml of day 2 medium with inhibitor molecules SB-431542 (10 µM), Noggin (250 ng/ml) and XAV939 (3.3 µM) as required and replate the EBs in same wells. EBs were treated with SB-431542 and Noggin (denoted dual SMAD-i) and XAV-939 denoted as SBNX.
- Washed the PO plates prepared on Day1 with PBS twice and again coated with Fibronectin (1 µg/ml) and Laminin (1 µg/ml).
- Day 2 medium: ¼ KSR+3/4 (N2 + NB) + Rock inhibitor (10 µm) + 1:100 B27-RA

Day 3

- Laminin plates were dried using 2 ml pipette encircling on the edges of the plate (Just make 1 big drop)
- EBs were scraped in each well using cell scraper, collected and distributed to 2 X 6 cm plates.
- Plates were kept for 10 mins in the incubator for the EBs to attach and then day 3 media was added.
- Medium was not changed for next 4 days.
- Day 3 medium: ¼ KSR+ ¾ (N2 + NB) + Rock inhibitor (10 µm) + B27-RA (1%)

Day 7

- Medium was changed with ½ N2 + ½ NB medium along with inhibitor molecules SB-431542 (5 µM), Noggin (125 ng/ml) and XAV939 (3.3 µM)

Day 9

- Medium was replaced, all inhibitors were omitted and replaced with ½ N2 + ½ NB + FGF8 (100ng/ml) + BDNF (5ng/ml) + B27-RA (1%)

Rosettes were allowed to form till day 12, following which cells were harvested for analysis. Neural induction and direct rosette formation could be also obtained by adherence on Matrigel-coated plates as previously described(Edri et al., 2015), with the modifications defined for this study (such as XAV-939 addition etc.). Long term propagation of cortical neural progenitors was performed by a weekly mechanical harvesting of rosettes followed by re-plating on Po/Lam/FN coated dishes and culture with ½ N2 + ½ NB medium containing 1% B27 without retinoic acid and with either FGF8 and BDNF (till day 28), or 20ng/ml of FGF2, EGF and BDNF (day 28 and on).

2.8 Derivation of cerebral organoids from human pluripotent stem cells

Organoids derivation was performed according to the Lancaster et al. (Lancaster and Knoblich, 2014) protocol with slight modifications as following.

Day 0

For Feeder independent pluripotent stem cells (iPSC growing on matrigel coated plates)

- mTESR1 medium was aspirated from the iPSC culture dish and washed the cells once with 3 ml of EDTA.
- 1ml of EDTA was added to the culture dish and incubated for 3-4 min at 37°C in the incubator.
- EDTA solution was aspirated gently without disturbing the colonies and added 2 ml of accutase and kept in the incubator for another 3 min.
- Cells were triturated 10-15 times and then were collected in a 15 ml tube and 5 ml of mTESR1 was added to neutralize the accutase and checked under the microscope for single cells.
- Cells were centrifuged 270g for 5 min.

- Supernatant was aspirated and washed twice by adding 6-8 ml of hESC medium + FGF2 (4 ng/ml) and centrifuged at 270g for 5 min.
- Aspirated the supernatant and cell pellet was resuspended in hESC medium + FGF2 (4 ng/ml) + ROCK inhibitor (50 µM) and cells were counted using hemocytometer.
- Plated 9000 cells in 150 µl of hESC medium + FGF2 (4 ng/ml) + ROCK inhibitor (50 µM) per each well of a 96-well U-bottom low-attachment plate and kept the plates in incubator at 37^{o}C and 5% CO_2.

Day 1

- Checked the plate under microscope and observed that EBs were started to form at the center of the plate along with some single cells surrounding the EB

Day 2

- 75 µl of medium was gently aspirated without disturbing the EB at the center and 150 µl of fresh hESC medium was added with inhibitor molecules SB-431542 (10 µM), Noggin (250 ng/ml) and XAV939 (3.3 µM). Continued adding FGF2 (4 ng/ml) and ROCK inhibitor (50 µM) until the size of the EBs were around 350-400 µm in diameter. EBs were either untreated (denoted as Inhibitor-free), or treated with SB-431542 and Noggin (denoted dual SMAD-i), or treated with XAV-939 (denoted WNT-i), or their combination (denoted Triple-i).

Day 4

- Organoid size was measured under microscope. If the organoid size is above 350um, FGF2 and ROCK inhibitor were not supplemented to the medium.
- From each well, 150 µl of medium was gently aspirated and 150 µl of fresh hESC medium was added with inhibitor molecules SB-431542 (10 µM), Noggin (250 ng/ml) and XAV939 (3.3 µM).

Day 6

- Organoid size and morphology were checked under microscope. If the organoid size is greater than 400 µm and have brighter and smooth edges, then they

were transferred to N2 neural induction medium. If the organoids were smaller in size, this step should be postponed for one day.

- 500 µl of N2 medium supplemented with the inhibitor molecules (SB-431542 (10 µM), Noggin (250 ng/ml) and XAV939 (3.3 µM)) were pre-added to each well of 24 well low attachment plates and then kept in incubator at 37 ^{o}C for 15-20 minutes.
- Using clipped 200 µl pipette tip, organoids were transferred from each well of 96 well plate to each well of 24 well plates with neural induction medium (one organoid per well).

Day 8

- 300 µl of media was aspirated from each well, and 300 µl of fresh medium, (similar to day 6 medium), was added to each well of 24 well plate.

Day 10

- 300 µl of media was aspirated from each well, and 300 µl of fresh medium, (similar to day 6 medium), was added to each well of 24 well plate.
- Organoid size and morphology were checked under microscope. Observed organoids were brighter on the outside and began to show radial organization of pseudostratified epithelium indicating formation of neuroepithelium.

Day 11

- Matrigel was thawed on ice for about 1 hour for making matrigel droplets.
- Parafilm was cut and sterilized with ethanol and dimples were made using empty 200 µl tip box tray.
- Organoids were transferred into parafilm dimples by looking under the microscope using a clipped 200 µl pipette tip. Excess media was aspirated very gently and 30 µl of matrigel was added on top of each organoid and were gently pushed into the center of matrigel drop with a 10 µl tip to ensure complete embedding.
- Organoids were then kept in incubator at 37 ^{o}C for 30-45 minutes and once the matrigel was solidified (gel), gently transferred using spatula into low

attachment 6-well plate with N2 + NB + B27-RA (1%) medium. 4 organoids were transferred to each well of 6 well plate with 2.5 ml of medium.

Day 12

- Checked the organoids under microscope and neuroepithelial vesicle outgrowths were started to appear.

Day 13

- 1.5 ml of media was aspirated carefully without touching the organoids within in the matrigel droplets and then 1.5 ml of fresh media (similar to day 11 medium) was added.

Day 15

- 1.5 ml of media was aspirated carefully and then 1.5 ml of fresh media now with 1% B27+RA (containing retinoic acid) was given. Plates were now transferred to an orbital shaker shaking with 86 rpm.
- For long term organoid culture, medium was changed every 2 days. Organoids were fixed in 4% paraformaldehyde, 0.15% picric acid for 20-40 minutes (RT) depending on their culture age, and then cryoprotected and processed as described under Immunostaining and confocal imaging section.

2.9 RNA isolation

miRNeasy RNA Mini kit

RNA was isolated using the miRNeasy™ RNA Mini Kit (Qiagene) according to the manufactures protocol briefed below.

- 700 µl of QIAzol lysis reagent was added to the sample and were vortexed for 1 min to get a homogenized mixture.
- Homogenate was then incubated at room temperature (15-25 ^{o}C) for 5 min.
- 140 µl of chloroform was added and shaked vigorously for 15s and incubated at room temperature for 2-3 mins and centrifuged for 15 mins at 12000g at 4^{o}C.
- Sample forms an organic and aqueous phase after centrifugation. 300 µl of aqueous phase was collected without touching the organic phase and

transferred to a new collection tube and 450 µl of 100% ethanol was added and mixed thoroughly by pipetting up and down.

- 700 µl of sample was transferred into RNeasy mini column placed in a 2 ml collection tube. Centrifuged at 8000g for 15 s at room temperature and flow through was discarded.
- 350 µl of buffer RWT (prepared with isopropanol) was added into the RNeasy mini spin column and centrifuged for 15s at 8000g and flow through was discarded.
- 10 µl of DNase I stock solution was added to 70 µl of buffer RDD and mixed gently by inverting the tube.
- DNAse I incubation mix (80 µl) was pipetted directly onto the RNesay mini spin column membrane and incubated for 15 min at room temperature.
- 500 µl of RWT buffer (prepared with iso-propanol) was added into RNeasy mini spin column and centrifuged for 15 s at 8000g. Flow through was kept and reapplied into the RNeasy mini spin column and centrifuged again at 8000g for 15 sec. Flow through was discarded.
- 500 µl of RPE buffer was added to RNeasy mini column. Centrifuged for 15 sec at 8000g. Discarded the flow through.
- Again 500 µl of buffer RPE was added to the column and centrifuged for 2 min at 8000g. Discarded the flow through.
- Transferred the RNeasy mini columns to a new 1.5 ml collection tube and eluted the RNA in 30 µl of RNase free water.
- Eluted RNA quality and concentration was measured using nanodrop.

miRNeasy RNA Micro kit

RNA was isolated with micro kit for the samples with low cell number (less than 10K) and manufactured protocol was followed which is described below.

- 700 µl of QIAzol lysis reagent was added to the sample and were vortexed for 1 min to get a homogenized mixture.
- Homogenate was then incubated at room temperature (15-25 ^{o}C) for 5 min.
- 140 µl of chloroform was added and shaked vigorously for 15s and incubated at room temperature for 2-3 mins and centrifuged for 15 mins at 12000g at 4^{o}C.

- Sample forms an organic and aqueous phase after centrifugation. 300 µl of aqueous phase was collected without touching the organic phase and transferred to a new collection tube and 450 µl of 100% ethanol was added and mixed thoroughly by pipetting up and down.
- 700 µl of sample was transferred into RNeasy mini column placed in a 2 ml collection tube. Centrifuged at 8000g for 15 s at room temperature and flow through was discarded.
- 350 µl of buffer RWT (prepared with isopropanol) was added into the RNeasy mini spin column and centrifuged for 15s at 8000g and flow through was discarded.
- 10 µl of DNase I stock solution was added to 70 µl of buffer RDD and mixed gently by inverting the tube.
- DNAse I incubation mix (80 µl) was pippeted directly onto the RNesay mini spin column membrane and incubated for 15 min at room temperature.
- 500 µl of RWT buffer (prepared with iso-propanol) was added into RNeasy mini spin column and centrifuged for 15 s at 8000g. Flow through was kept and reapplied into the RNeasy mini spin column and centrifuged again at 8000g for 15 sec. Flow through was discarded.
- 500 µl of RPE buffer was added to RNeasy mini column. Centrifuged for 15 sec at 8000g. Discarded the flow through.
- 500ul of 80% ethanol was pipetted to the RNeasy MinElute spin coloumn. Close the lid gently and centrifuged for 2 min at at 8000g to wash the membrane. Flow through was discarded. (carefully remove the filter so that it will not touch the flow through).
- Place the MinElute spin coloumn into a 2 ml collection tube with lid open and centrifuged at full speed for 5 mins to dry the membrane.
- Transferred the RNeasy mini columns to a new 1.5 ml collection tube and eluted the RNA in minimum of 14 µl of RNase free water.
- Eluted RNA quality and concentration was measured using nanodrop.

2.10 Preparation of cDNA

cDNA was prepared using manufacture instruction (Applied biosystems) and written briefly.

Reagents	**Volume (µl) (x1)**
RT buffer x10	2
Random Primers x10	2
dNTPs mix x25 (100mM)	0.8
RNase inhibitor	0.25
RT enzyme	0.25
RNA	50-200ng/ µl
UPW (Ultra-Pure Water)	20-X
Total	20

- Kit and RNA were thawed on ice.
- Buffer, primers and dNTPs should be vortexed and spin down, RNAse inhibitor and RT enzyme should be taken out at the end.

- 96well plate or tube was marked, and UPW was added
- On ice: 5.3µl mix was added to each well, not touching the UPW in the well
- RNA was added to each well and the total volume should be 20µl
- Spin down plate shortly and initiate PCR program as follows:

Kept in the PCR cycler:

Temperature (°C)	Time (min)
25	10
37	120
85	5
4	infinite

2.11 small RNA sequencing

The SMARTer smRNA-Seq Kit for Illumina is used to generate small RNA-seq libraries for sequencing on Illumina platforms. This kit was developed to work directly with total RNA or enriched small RNA (including microRNA), for inputs ranging from 1 ng–2 µg. By incorporating features of the SMARTer Stranded RNA-Seq kits, including our

proprietary SMART (**S**witching **M**echanism **a**t the 5' end of **R**NA **T**emplate) technology, and primers that include locked nucleic acids (LNAs), this kit allows users to analyze a wide range of smRNA species and generate sequencing libraries of considerable complexity from as little as 1 ng of input material. Illumina adapter and index sequences are incorporated in a ligation-free manner during library amplification, ensuring that diverse smRNA species are represented with minimal bias.

2.12 Cloning of hsa-miR-20b-5p into LT3GEPIR plasmid

LT3GEPIR plasmid was a gift from the collaborator in NIH (Markus Hafner) and the plasmid was send on a blotman paper and the part of the paper was cut and dipped into 30 ul of TE buffer and left overnight and following day transformation was done in Stbl3 bacteria as mentioned by the manufacture. Colonies were picked and did plasmid isolation using Qiagen maxiprep kit. The plasmid was double digested using high fidelity Xho1 and EcoR1 restriction enzyme and then gel purified and used for cloning. The insert was ordered from IDT (sequence is mentioned below) as a single strand and then PCR was done to amplify this insert using below mentioned primers and the reaction protocol then the amplified PCR product was gel purified and digested with the same restriction enzyme and then digested product was ligated to the digested LT3GEPIR plasmid. 10 colonies were picked and send for sanger sequencing. The plasmid with no mutation was selected for further process.

miR-20b-5p insert sequence:

gaaggCTCGAGAAGGTATATTGCTGTTGACAGTGAGCGCAAAGUGCUCAUAGUGCAGGUAGCTGTGAAGCCACA
GATGGGCTAACTGCACTAGATGCACCTTATGCCTACTGCCTCGGACTTCAAGGGGCTAGAATTCgagc

CTCGAG: Xho1 restrict site and GAATTC: EcoR1 restriction site

CAAAGUGCUCAUAGUGCAGGUAG: sense strand of human miR-20b-5p

Primers for amplification and sequencing:

Primer name	**Sequence**
miR-E_Xho1_FP	5'-TGAACTCGAGAAGGTATATTGCTGTTGACAGTGAGCG-3'

miR-E_EcoR1_RP	5'-TCTCGAATTCTAGCCCCTTGAAGTCCGAGGCAGTAGGC-3'
LT3_univ-rev seq P1	CTACCCGGTAGAATTACGCG
LT3_univ-rev seq P2	GAATGTGTGCGAGGCCAGAGGC

PCR reagents and program:

Components	**25ul reaction**
Nuclease free water	16.5
5X Phusion GC buffer	5
10mM dNTPs	0.5
10µM Forward primer	1.25
10µM Reverse primer	1.25
Template DNA	0.257
Phusion DNA Polymerase	0.25

Cycle step	**Cycles**	**Temperature (°C)**	**Time**
Initial Denaturation	1	95	5 min
Denaturation Annealing Extension	30	95 54 72	25 sec 25 sec 30 sec
Final Extension	1	72	5 min
Hold	1	4	-

2.13 Cloning of CCND1 in a lentiviral vector

We have used inducible lentiviral based plasmid vector for cloning CCND1 gene. We bought a pDonor plasmid of CCND1 gene without stop codon from addgene (#70302). We did a LR reaction with donor plasmid and the expression plasmid having mCherry as a reporter. After cloning, plasmid was transformed in Stbl3 and kept for 24 hours at 37°C incubator. We picked 5 colonies and grown them in LB broth containing ampicillin (50-100ug/ml) and followed by plasmid isolation and sanger sequencing. Results for

sequencing was matched using snapgene software and we identified the colony which has no mutation in the coding region of gene. After sequencing, the plasmid was isolated at high concentration using midi prep isolation kit from Qiagen according to manufactures protocol. Then the virus was generated as mentioned below.

2.14 Midi Prep Plasmid isolation kit (Qiagen)

100ml bacterial culture was grown for 12-16 hours depending on the plasmid and then midi prep kit was used to isolate the plasmid DNA. The detailed protocol is mentioned below:

- Harvested overnight bacterial culture by centrifuging at 6000 x g for 15 min at 4°C.
- Resuspend the bacterial pellet in 4 ml of Buffer P1 and then added 4 ml Buffer P2, mixed thoroughly by vigorously inverting 4–6 times and incubated at room temperature (15–25°C) for 5 min. If LyseBlue reagent was used, the solution will turn blue.
- 4 ml of prechilled Buffer P3 was added and mixed thoroughly by vigorously inverting 4–6 times. Incubated on ice for □ 15 min. If LyseBlue reagent was used, the solution was mixed until it is colorless.
- Centrifuged at ≥20,000 x g for 30 min at 4°C. Re-centrifuged the supernatant at ≥20,000 x g for 15 min at 4°C.
- Equilibrated a QIAGEN-tip 100 by applying 4 ml of Buffer QBT, and allowed column to empty by gravity flow.
- The supernatant from step 5 was applied to the QIAGEN-tip and allowed it to enter the resin by gravity flow.
- The QIAGEN-tip with 2 x 10 ml was washed with Buffer QC. Allowed Buffer QC to move through the QIAGEN-tip by gravity flow.
- DNA was eluted with 5 ml of Buffer QF into a clean 15 ml falcon. For constructs larger than 45 kb, prewarming the elution buffer to 65°C may help to increase the yield.
- Precipitated the DNA by adding 3.5 ml isopropanol (RT) to the eluted DNA and mixed and then centrifuged at ≥15,000 x g for 30 min at 4°C. Carefully decant the supernatant.

- The DNA pellet was washed with 2 ml 70% ethanol (RT) and centrifuged at ≥15,000 x g for 10 min. Carefully decant supernatant.
- Air-dried the pellet for 5–10 min and redissolved the DNA in a suitable volume of appropriate buffer (e.g., TE buffer, pH 8.0-, or 10-mM Tris·Cl, pH 8.5).

2.15 Virus generation in HEK cells

Day 0: Seeding of HEK293T cells

- HEK293T cells were revived and expanded. Cells were splitted at a density of 4.5*10^6 after they reached 90% confluency.

Day 1: Lipofection of plasmids using lipofectamine 293

- Half an hour before starting the transfection feed the HEK293 cells with fresh medium.
- Made separate DNA eppendorfs:
    - 250 µl DMEM-HG MEDIUM+psPAX2+ pCMV-VSV-G+1ul LT3GEPIR-miR-Ren.713
    - 250 µl DMEM-HG MEDIUM+psPAX2+pCMV-VSV-G+1ul LT3GEPIR-miR-20b-5p

  Note: psPAX2:pCMV-VSV-G:Vector = 1:1:1, psPAX2 = 7µg; pCM-VSV-G = 3.5 µg (Depending on the size of the donor plasmid the concentration of the packaging plasmids was calculated and it is mentioned above)
- Gently mix using pipet 3~4 times.
- Lipofectamine reagent tubes:

For 1 reaction 50 µl of lipo293 + 250 µl of DMEM-HG (high glucose)

So, 2 eppendorfs: 300 µl of lipo+1500µl of DMEM-HG

- Gently mix using pipet 3~4 times.
- Add the diluted lipo solution from step 4 to the DNA eppendorfs. Add 250 µl of lipfectamine solution to 250 µl of DNA Eppendorf. Immediately pipet 3~4 times.
- Incubate for 10 min at RT.
- Add 500 µl from the DNA Eppendorf to the respective HEK293T cells plate. Add drop by drop and gently swirl the plate.
- Carry these plates to S2 lab carefully within the box. Place in incubator

Day 2:

- In the morning, virus plates were checked for the fluorescence. You will observe some cell death.
- Media was aspirated and fresh Hek293 medium was added to each plate.

Day 3 (48 h):

- Medium was collected and filtered using a 0.45-micron filter in a 50 ml falcon and kept it at 4 °C.
- Another 10 ml of HEK293 medium was added gently to the plate.

Day 4 (72 h):

- Virus containing medium was collected in the same 50 ml falcon again after filtering using 0.45 micron filter.
- 5 ml PEG (5X) was for 20 ml viral containing medium.
- Mixed by inverting the tube up and down and keep the falcon at 4°C overnight.

Day 5:

- Centrifuge was pre-cooled at 4°C and virus suspension was spun for 30 min at 1500xg, 4°C.
- The pellet was resuspended in 200 µl of DMEM medium with 25mM Hepes.

2.16 Titer calculation for viral particles and hiPSCs line generation

Titer experiments were done using HEK293 cells. In a 24 well plate, 70k cells were plated and following day by the evening one well was trypsinised and counted. 5 ul of virus was taken along with 495ul of HEK medium and then serial dilution was done from this viral suspension. We next took 50ul and added to another 450ul HEK medium (1:100 dilution). Further from 1:100 diluted viral suspension we again took 50ul of virual suspension and added it to 450ul of medium (1:10000 diluted). Minimum of 3 wells of 24 well plate was done for each condition. When the well was 60-70% confluent, cell were trypsinised and analyzed using FACS for eGFP positive cells. We have chosen, $10^{\wedge -3}$ dilution and 17.2 percent of cells were eGFP positive. Titer was calculated by putting in the below formula:

Titer (per ml) = Percentage of GFP positive cells X No of cells determined at the time of infection/ Dilution factor X Volume of viral inoculum added to the well.
T= 17.2 x 81300/10^-3 x 0.45 = 3.1 x 10^7/ml

For generating the hiPSCs line having miR-20b-5p construct, 4.5 million cells of ZIP8K8 hiPSCs were taken and 30µl of virus was added which is having 9.3x10^5 viral particles (0.2MOI). The cells were grown for some days in mTesR1 medium and then selected with puromycin (2mg/ml). Cells were treated with accutase to make single cell suspension and only 10K single cells were plated in 60mm along with ROCK inhibitor. The cells were grown in mTesr1 medium till colonies were seen and then each clone was picked and expanded. The clones were simultaneously plated in a 96 well plate and induced with doxycycline (2mg/ml) to see the expression of eGFP in the cells. Clones were then tested for making organoid and then the clone where the organoid differentiation was not hampered has been selected for this study.

2.17 Genomic DNA isolation

- Cells were centrifuged for 5 min at 300 x g. Resuspended the pellet in 200 µl PBS along with 20 µl of proteinase K.
- 200 µl Buffer AL (without added ethanol) was added and mixed thoroughly by vortexing, and the tube was then incubated at 56°C for 10 min.
- 200 µl ethanol was added (96–100%) to the sample, and mixed thoroughly by vortexing.
- The mixture was transferred into DNeasy Mini spin column and then centrifuged at 6000g for 1 min. Flow through was discarded.
- DNeasy Mini spin column was placed in a new 2 ml collection tube, and 500 µl Buffer AW1 was added, and centrifuged for 1 min at 6000 x g (8000 rpm). Flow-through and collection tube was discarded.
- Placed the DNeasy Mini spin column in a new 2 ml collection tube, added 500 µl Buffer AW2, and centrifuged for 3 min at 20,000 x g (14,000 rpm) to dry the DNeasy membrane. Flow-through and collection tube was discarded.
- DNeasy Mini spin column was placed in a clean 1.5 ml or 2 ml microcentrifuge tube and 200 µl Buffer AE was transferred directly onto the DNeasy

membrane. Incubated at room temperature for 1 min, and then centrifuge for 1 min at 6000 x g (8000 rpm) to elute.

2.18 Integration copy number analysis

For identifying the number of copies integrated for the miR-20b we have adapted a method which was used to calculate copy number variations in mice. TFRC gene (transferrin receptor) is recommended as the standard reference for copy number variation analysis. In this assay, genomic DNA was isolated from the hiPSCs clone and background line (ZIP8K8). Firstly, a standard curve was generated by taking different concentrations (0.4, 2, 10 and 50ng/ul) of LT320b clone genomic DNA for three set of eGFP primers. Standard program from the applied biosystem qPCR cycler was used. Standard curve was generated and the eGFP primer 2 pair was selected whose sequence has been mentioned below. eGFP primer 2 along with TFRC primer as a control was used for calculating the copy number integration in the clone and qPCR was done using 50ng/ul genomic DNA.

Primers	**Sequences**
eGFP_qPCR_FP2	GAACGGCATCAAGGCGAAC
eGFP_qPCR_RP2	GGTAGTGGTTGTCGGGCAG
hTFRC_qPCR_F1	CAGAGCAGACATAAAGGTGAC
hTFRC_qPCR_R1	CCAACAGGAACACACAGGAAC

2.19 Quantitative PCR (qPCR) analysis

RNA was extracted using miRNeasy kit (Qiagen) followed by cDNA reverse transcription kit (Applied Biosystems). 4-6ng of cDNA was subjected to qPCR using our homemade designed primers (see ‘Primer set list’), FastStart universal SYBR green (Roche) and ViiA-7cycler (ABI). Threshold cycle values were determined in triplicates and presented as average relative fold over those of HPRT. Fold changes were calculated using the 2-ΔΔct method.

Table for qPCR Primer set

Gene	**Sequence**
CTIP2_F	5’-TCCAGAGCAATCTCATCGTG-3’

CTIP2_R	5’-GCATGTGCGTCTTCATGTG-3’
CUX1_F	5′- CAACAAGGAATTTGCTGAAGTG -3′
CUX1_R	5′- CTATGGTTTCGGCTTGGTTC -3′
CUX2_F	5′- GAGCTGAGCATCCTGAAAGC -3′
CUX2_R	5′- AGGCCTCCTTTGCAATAAGC -3′
DCX_F	5’-CATCCCCAACACCTCAGAAGA -3’
DCX_R	5’-CGTTTGCTGAGTCAGCTGGA-3’
EGFR_F	5′- GATAGTCGCCCAAAGTTCCGT -3′
EGFR_R	5′- CTGAATGACAAGGTAGCGCTG -3′
FEZF2_F	5’-CCCAGGAAAAGCCACATAAAT-3’
FEZF2_R	5’-GGATGCGGATATGCGTGTT-3’
FOXG1_F	5’-AGGAGGGCGAGAAGAAGAAC-3’
FOXG1_R	5’-TGAACTCGTAGATGCCGTTG-3’
GFAP_F	5′- AGAGATCCGCACGCAGTATG -3′
GFAP_R	5′- TCTGCAAACTTGGAGCGGTA -3′
GLAST_F	5′-CCCTTGGGTTTTTATTGGAGG-3′
GLAST_R	5′-ATGGGTAGGGTGGCAGAACT-3′
HES5_F	5’-ACCAGCCCAACTCCAAGCT-3’
HES5_R	5’-GGCTTTGCTGTGCTTCAGGTA-3’
HPRT_F	5’-TGACACTGGCAAAACAATGCA-3’
HPRT_R	5’-GGTCCTTTTCACCAGCAAGCT-3’
PAX6_F	5’-CACACCGGTTTCCTCCTTCA-3’
PAX6_R	5’-GGCAGAGCGCTGTAGGTGTTT-3’
S100β_F	5′- GGAAATCAAAGAGCAGGAGGTT -3′
S100β_R	5′- TCCTGGAAGTCACATTCGCC -3′
SATB2_F	5′- TAGCCAAAGAATGCCCTCTC -3′
SATB2_R	5′- AAACTCCTGGCACTTGGTTG -3′
SOX1_F	5’-GCAAGATGGCCCAGGAGAAC-3’
SOX1_R	5’-CGGACATGACCTTCCACTCG-3’
TBR1_F	5’-GTCACCGCCTACCAGAACAC-3’
TBR1_R	5’-ACAGCCGGTGTAGATCGTG-3’
TBR2_F	5’-AACCACTGGCGCTTCCA-3’

TBR2_R	5’-AACATACATTTTGTTGCCCTG-3’

2.20 cDNA prepration for miRNA

Total RNA was used for preparation of cDNA for miRNA quantification. miRNA are small RNA molecules which are 20-21 nucleotides in length so before preparation of cDNA addition steps was done to capture these small molecules. For each sample 1ng/ul of RNA was used. The detailed steps are mentioned below:

Poly(A) tailing reaction

- Samples were thawed on ice and cDNA synthesis reagents were also thawed on ice, gently vortex, then centrifuged briefly. PEG was kept at room temperature
- Poly A reaction mix:

Components	**1 Rxn (µl)**
10X Poly A Buffer	0.5
ATP	0.5
Poly A enzyme	0.3
RNase Free water	1.7
Total	3

- Poly A reaction was vortexed and then centrifuged briefly.
- 2 µl of sample was added to each reaction tube and 3 µl of poly A reaction mix was added, now the total volume was 5 µl.
- Reaction tube was sealed and centrifuged briefly and placed into a thermal cycler, and incubated using the following settings:

Step	Temperature	Time
Polyadenylation	37	45
Stop reaction	65	10
Hold	4	Hold

- Proceeded immediately to the adaptor ligation reaction

Adaptor ligation reaction

- Adaptor ligation reaction:

Components	**1 Reaction (**µl)
5X DNA ligase Buffer	3
50% PEG 8000	4.5
25X ligation Adaptor	0.6
RNA ligase	1.5
RNase free water	0.4
Total	10

- Ligation mixture was vortexed and then centrifuged briefly.
- 10 µl of ligation reaction mix was added to each tube containing 5 µl of poly A reaction product. Now, total its 15 µl volume in the tube.
- Vortexed and centrifuged at 1900rpm for 1 min. Swirling should be done properly to ensure proper mixing.
- Reaction mixture was placed in the thermal cycler and incubated under the mentioned settings:

Step	Temperature(°C)	Time
Ligation	16	60 minutes
Hold	4	Hold

- Proceed immediately to the reverse transcription reaction (RT reaction)

Reverse transcription (RT) reaction

- RT reaction mixture was prepared:

Components	**1 Reaction (µl)**
5X RT Buffer	6
dNTP Mix(25mM each)	1.2
20X Universal RT Primer	1.5
10X RT enzyme mix	3
RNase free water	3.3
Total	15

- RT reaction was vortexed and centrifuged briefly.

- 15 µl of RT reaction was added to each tube containing the adaptor ligation reaction product. Total volume should be 30 µl.
- Reaction tube was vortexed and centrifuged briefly and kept in the thermal cycler on the following settings:

Step	**Temperature** (°C)	**Time**
Reverse transcription	42	15 minutes
Stop reaction	85	5 minutes
Hold	4	Hold

- Proceeded for the miR-Amp reaction (next section) or reaction mixture stored at -20°C.

miR-Amp reaction

- miR-Amp reaction was made as mentioned below:

Components	**1 Reaction (µl)**
2X miR-Amp Master Mix	25
20X miR-Amp Primer Mix	2.5
RNase-free water	17.5
Total	45

- Vortexed and centrifuged briefly.
- 45 µl of the miR-Amp reaction was added to the new reaction tube and to this 5 µl of the RT reaction product was added and now the total volume should be 50 µl.
- Tube was vortexed and centrifuged briefly to mix the contents and then kept at the thermal cycler using the following settings:

Step	**Temperature (°C)**	**Time**	**Cycles**
Enzyme activation	95	5 minutes	1
Denature	95	3 seconds	14
Anneal/Extend	60	30 seconds	
Stop reaction	99	10 minutes	1

Hold	4	Hold	1

- Proceed to perform real time PCR or stored the diluted miR-Amp reaction product at -20°C.

Quantitative real-time PCR

- Thawed the assay on ice, gently vortexed and then centrifuged briefly.
- 1:10 dilution was prepared for the cDNA template.
- Master mix bottle should be gently mixed but do not invert the bottle.
- PCR reaction mix:

Components	**1 Reaction (µl)**
TaqMan® Fast Advanced Master Mix (2X)	10
TaqMan® Advanced miRNA Assay (20X)	1
RNase free water	4
Total	15

- Reaction mixture was vortexed and centrifuged briefly and 15 µl was added to a PCR plate.
- 5 µl of diluted cDNA template was added to each well and then sealed with adhesive cover.
- Vortexed and centrifuge briefly to spin down the contents and kept the plate in a real-time qPCR machine (QuantStudio systems) and the settings were used as mentioned below:

Step	**Temperature (°C)**	**Time**	**Cycles**
Enzyme Activation	95	20 seconds	1
Denature	95	1 second	40
Anneal/Extend	60	20 seconds	

2.21 Matrigel Induction protocol

To understand the role of miR-20b in early neural development we had plated 30,000 cells of LT320b line per 96 well. Till the well were confluent the cells were given mTesR1 and ROCK inhibitor (10uM). The next day when the well was confluent the media was replaced with KSR medium this is known as day 0. On day 2, medium was changed to 3/4 KSR+1/4 N2 i.e untreated (denoted as Inhibitor-free), or treated with SB-431542 and Noggin (denoted dual SMAD-i). Doxycycline (2ug/ml) was added to the respective wells of each treatment to overexpress miR-20b. On day 4, xav was added to the SBN treatment. Doxycycline was administered every day. On day 6 and 8, cells were fixed and immunostained for stem cell, regional markers.

For neural induction we plated ZIP8K8 hiPSCs on 1:20 matrigel coated plates and the confluent cultures were subjected with KSR medium containing SB (10uM) and Noggin (250 ng/ml). On day 2, the cells were scrapped from plates, preincubated with Caþ2/Mgþ2 free HBSS followed by collagenase II (2.5 mg ml/1), Collagenase IV (2.5 mg ml/1) and DNAse (0.5 mg ml/1) solution (all from Worthington; 37°C, 20 min). Cells were then dissociated and replated at high density (100,000 cells per cm^2) on moist matrigel drops along with 0.2MOI of LT320b virus. Next day, the medium was changed to d3 medium along with doxycycline and on day 6 eGFP positive and negative cells were sorted and collected for bulk RNA sequencing. Similarly, on day 4 and day 6 of neural induction cells were scrapped and plated as matrigel drops along with the virus and then induced for then treated for two days with doxycycline. eGFP positive and negative cells were sorted on day 7 and day 10 of neural differentiation and bulk RNA sequencing was done.

2.22 Immunostainings

Cells were fixed with 4% paraformaldehyde, 0.15% picric acid, permeabilized and blocked with PBS, 1% bovine serum albumin (BSA), 10% FBS and 0.3% Triton solution. Organoids were also fixed in the same way, washed, and cryoprotected with 30% sucrose overnight and then embedded in OCT the following day. Fixed cells or sectioned organoids (10uM slices) were stained with indicated primary antibodies (see below) followed by Alexa Fluor secondary antibodies (Invitrogen). Following staining, cells were imaged in PBS, and organoid sections were mounted with Moviol (Sigma). Fluorescence images were obtained using a confocal microscope LSM880 (Carl Zeiss

Micro Imaging, Germany). The confocal images were captured using 10X and 20X objectives (NA=0.3 and 0.8, Plan-Apochromat, respectively). Fluorescence emissions resulting from Ar 488, 543 and 633 nm laser lines for EGFP, CY3 and CY5, respectively, were detected using laser scanning settings and filter sets supplied by the manufacturer. For DAPI detection in all images 405 laser was used. Epi fluorescent and phase contrast images were obtained using Nikon Eclipse Ti-E microscope and Axio stero microscope. Fluorescence emissions results from mercury arc lamp. Images were taken using 10X and 20X objectives. Images were generated and analyzed using either Zeiss ZEN 2011 software (Carl Zeiss, Inc.) or NIS elements software (Nikon). All images were exported in “tif” and their color levels were identically adjusted per each staining procedure.

Table: Antibody list

Antibody name	**Vendor**	**Dilution**
PAX6	DSHB	1:22
SOX2	ABCAM (ab79351)	1:500
SOX1	R and D	1:1000
FOXG1	ABCAM (ab18259)	1:400
LMX1A	ABCAM (ab10533)	1:1000
TTR	Biorad (AHP1837)	1:500
LIFR	Santa cruz biotechnology (sc-515337)	1:100
PTPRZ1	Sigma-Aldrich (HPA015103)	1:500
HOPX	Sigma-Aldrich (HPA030180)	1:500
STMN2	Novus Biologicals (NBP1-49461)	1:1000
DCX	Millipore (AB2253)	1:500
NFIA	Novus Biologicals (NBP1-81406)	1:100 (2ug/ml)

NFIB	Novus Biologicals (NBP1-81000)	1:100 (2ug/ml)
PTN	R & D systems (AF-252-PB)	1:100 (2ug/ml)
TBR1	ABCAM (ab31940)	1:500
TBR2	ABCAM (ab23345)	1:200
N-CADHERIN	Sigma-Aldrich (C2542)	1:200
CAS-3	Cell signaling (#9661)	1:500
SOX10	R & D systems	1:100
FOXA2	Santacruz biotechnology (SC-6554)	1:100
TFAP2A (3B5)	DSHB	1:100
Ki-67	BD Pharmingen (556003)	1:1000
PHH3	ABCAM (ab5176)	1:250
P-VIMENTIN	ABCAM (ab22651)	1:120
TCF7L2	Cell signaling (#2569)	1:500
CCND1(92G2)	Cell Signaling (2978S)	1:200

2.23 Measurements and statistical analysis

For all qPCR gene expression analysis obtained for neural induction, cortical specification, and also the microRNA quantification plots, two-way ANOVA test followed by Tukey's multiple comparison test and t-test were applied repectively. Statistical analysis was performed using GraphPad software.

2.24 Bulk RNA sequencing

For bulk RNA seq, RNA was isolated from NSCs collected at different timepoints during long term differentiation and cDNA was generated and then library was generated and later did PE50 illumina High sequencing. The data was analyzed by Daniel Rosebrock and details are mentioned below.

2.25 Preparation and Sequencing of RNA-Seq Libraries

RNA-seq libraries for human samples were generated using the Illumina TruSeq RNA Library Preparation Kits, and pooled sampled were sequenced on the Illumina HiSeq

2500 sequencer as 50bp paired-end reads for Triple-I (SBNX) organoids and 100bp reads for NT and SBN organoids.

2.26 RNA-Seq datasets processing, normalization and analysis

Raw RNA-Seq reads were first trimmed using Trimmomatic v0.36 (Bolger et al., 2014) using parameters LEADING:3 TRAILING:3 SLIDING WINDOW:4:15 MINLEN:36. The remaining reads were then mapped to the human reference genome hg38 with gencode v29 as a reference transcriptome (https://www.gencodegenes.org/human/release_29.html) using STAR v2.6.1d (Dobin et al., 2013). FPKM values for each gene and corresponding isoforms were estimated with RSEM v1.3.1 (Li and Dewey, 2011) using the STAR aligned bam to the reference transcriptome as input. Principal component analysis was run on the logged FPKM expression values (base 10 with a pseudocount of 1) using the top 10,000 genes with the highest variance. Differential gene expression analysis between mir20b OE and WT organoids at day 13 and day 30 was done using DESeq2 (Love et al., 2014) on the raw gene counts.

2.27 Single cell RNA-Seq procedures

Organoid dissociation Protocol

- Organoids derived under Triple-i (SBNX) protocol were collected on day 13, day 30 and day 50 of differentiation and subjected to papain enzyme dissociation.
    - For Day 13: 10 organoids for WT and 17 organoids for miR-20b OE were taken
    - For Day 30: 3 organoids for WT and 4 organoids for miR-20b OE were taken and the Matrigel was removed with the help of needle.
    - For Day 50: 3 organoids for WT and 4-7 organoids for miR-20b OE were taken and WT organoids were cut into 4 pieces using the needle because they were bigger in size.
- After collecting the respective days organoids in a 6 well of a low attachment plate, 2ml of Papain solution with 100µl of DNases were added and then the organoids were incubated at 37°C for 45 mins in the incubator and were shaken

after every 5 mins. In the meanwhile, in a 15 ml falcon 2 ml of EBSS+2ml of ovomucoid inhibitor+100 µl of DNases+1:1000 ROCK Inhibitor was added.

- After 45 mins of incubation, organoids were triturated 10-15 times and then 1 ml of EBSS medium was added (provided in the kit) and single cell suspension was collected in a 15 ml falcon tube. (EBSS was added to stop the papain activity). To the cell suspension 1:1000 ROCK inhibitor was added.
- Next, the previously made solution containing ovomucoid inhibitor was added to the cell suspension and then centrifuged at 300g for 5 mins.
- Cells were resuspended into HBSS and then passed through a 40-micron filter and then pass through another 40-micron filter of the FACS tube.
- The cell suspension was counted and adjusted to a concentration of 1000 cell/ µl. Total of 17,400 cells were used for library preparation (Love et al., 2014). (recommended in 10X single cell kit).

2.28 Single cell library preparation

- Cell suspension having 1000/µl was taken and extra suspension was taken to lose cell while washing. Two washes with PBS+0.4%BSA was given for 5 mins at 300g.
- Cells were then used to make the GEM beads and then followed by library preparation as suggested by v3.1 single cell kit protocol as mentioned by manufactured.
- Libraries were sequenced using 28/91 high sequencing method as suggested in 10X single cell genomics.

2.29 Single cell RNA-Seq data processing, dataset alignment and cell population identification

Cellranger v3.1.0 software was used to cluster and determine valid cell barcodes, identify unique molecular identifier (UMI) barcodes corresponding to the same RNA molecule across different reads with the same cell barcode, and map reads to the reference genome hg38. Individual cell expression profiles were then clustered using scanpy v1.5.1 (Wolf et al., 2018) and clusters were assigned to biological cell types

based on relative expression levels of specified marker genes for cell type, brain region, and cycling status.

To estimate normalized gene expression values, UMI gene counts per cell were divided by the library size (number of UMIs in each cell), then multiplied by a scaling factor of 10000, and log transformed after adding a pseudocount of 1. In the day 13 single cell RNA experiment, a large discrepancy in the UMI count distribution across cells was detected. In order to remove this source of variation, the total UMI count was regressed from the normalized expression value using scanpy's regress_out function, and the resulting expression values were scaled to unit variance and zero mean. Principal Component Analysis was then performed on the normalized expression values of the top 2,000 highly variable. Clusters were determined using the Louvain clustering procedure on the top 50 principal components with scanpy's louvain function. In the day 13 scRNA-Seq experiment, cells from both mir20b Overepxressing and WT experiments were clustered together, while cmir20b OE and WT cells from day 30 and day 50 experiments were clustered separately. Finally, clusters were assigned to corresponding *in vivo* cell types based on expression levels of known widely used marker genes.

3. RESULTS

3.1 Long term propagation, consecutive isolation and characterization of Neural Stem cells (NSCs) using Triple-i (SBNX) method

We have isolated consecutive stage specific neural rosettes/NSCs using our previously published NSC induction and long-term propagation protocol (SBN) (Edri et al., 2015; Ziller et al., 2015) with the addition of WNT-inhibitor XAV939 (Triple-i/SBNX) to streamline homogenous cortical population from *HES5::eGFP* H9 hESC line (Figure 16a,b). Briefly, PSCs are subjected to a modified protocol of embryoid body 2D differentiation method to generate small EBs formed by aggregation of single cells for three consecutive days. On day 2, small molecule inhibitors for Dual SMAD signalling SB-431542, Noggin along with WNT-i (XAV-939) was added. On day 3, these EBs were plated on laminin/fibronectin coated plates for attachment and continued differentiation as monolayer colonies (Figure 16a). Between day 10-12 of differentiation, neural rosettes were formed which are highly polarized structures containing radially organized cells (Elkabetz et al., 2008). These rosettes are known to be reminiscent of radial glial cells (RGCs) of the developing progenitors of ventricular zone (VZ) as suggested by *in vitro* studies (Gaiano et al., 2000; Götz et al., 1998). According to the nomenclature described by Elkabetz and colleagues, day 10 and day 12 rosettes corresponds to early RGCs stage (Edri et al., 2015). These neural progenitors/NSCs were subsequently cultured and consecutively isolated until day 80 based on their morphology and during progression eventually they lost their rosette cytoarchitecture (Figure 16b). We then tested the developmental potency of consecutively isolated progenitors in culture, similar to the experimental paradigm of our previous work (Edri et al., 2015), Triple-i derived early progenitors retained the potential to execute the timed and ordered cortical lamination throughout long-term progression (Figure 16c). Taken together, these data suggest that we successfully isolated early neural progenitors/NSCs by Triple-i inhibition that gives rise to consecutive progenitors that build the cortex.

a

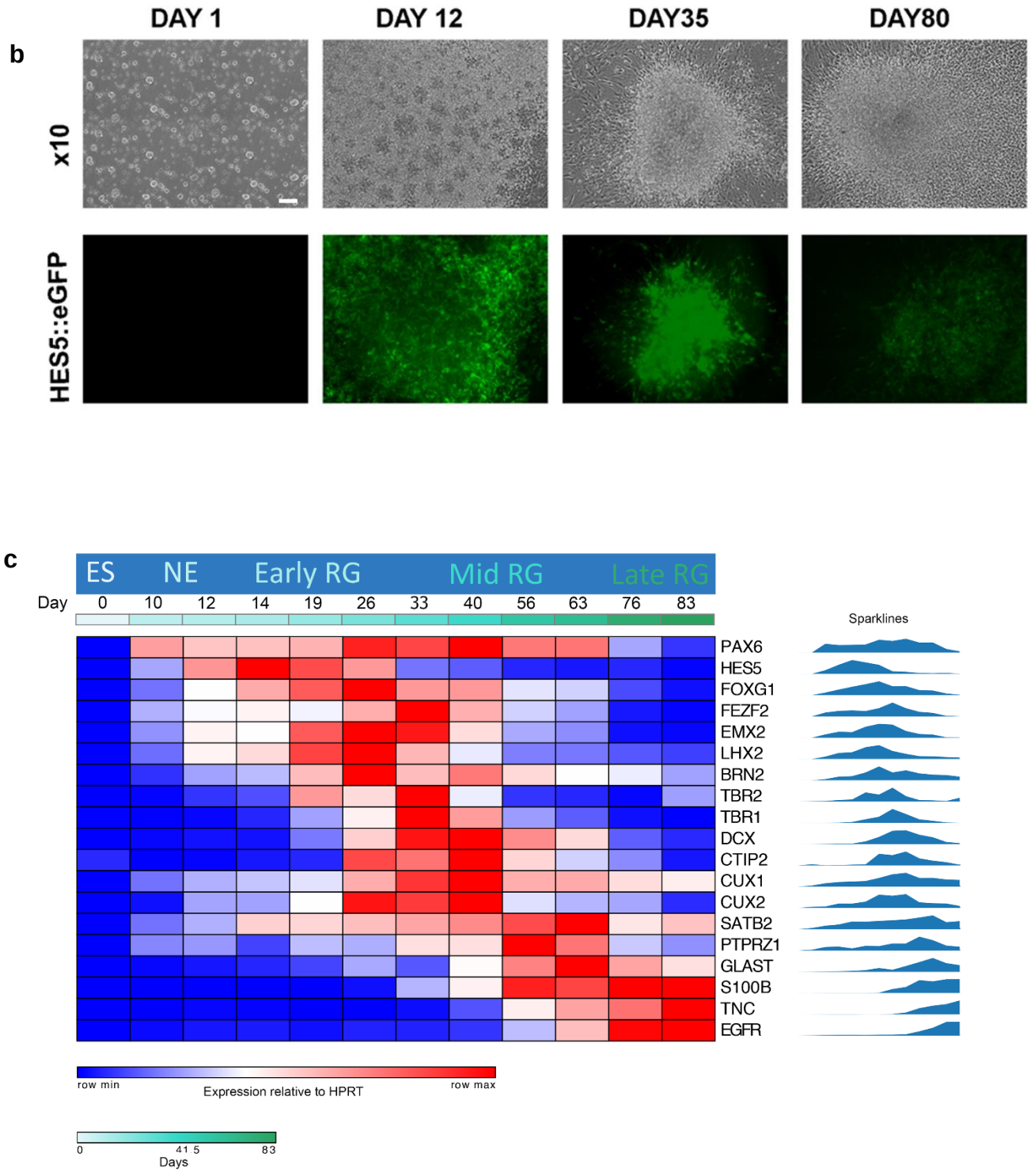

Figure 16: Isolation and characterization of different stages of neural stem cells.

a) Schematic representation for embryoid body differentiation protocol.

b) Phase contrast (top) and HES5::eGFP (bottom) images of long term differentiated neural monolayer progenitors derived from small EBs (sEBs) subjected to neural induction using combined Dual SMAD and WNT inhibition (Triple-i). Scale bar: 50 µm.

c) A heatmap representing expression values for selected genes marking early NE, early radial glial (ERG), mid-radial glial (MRG) and late radial glial (LRG) markers in long term differentiated neural

stem cells. Color-coded scale represents relative expression levels of each gene across row. Note that the early cortical progenitors retained the potential to execute timed and ordered cortical lamination (Blue represent the row minimum and red represent the row maximum expression).

3.2 Identification of stage specific miRNAs in cortical neural progenitors

We were next interested in identifying potential transcriptional regulators in early cortical NSCs that play important roles in shaping regional cell fate composition in the cortex. As a strategy, we chose to profile microRNA expression of early cortical NSCs and their progeny, due to the potential to uncover multiple target genes affecting the early NSC stage. We performed miRNA and mRNA sequencing in Triple-i derived homogenous cortical neural progenitors till 80 days, and identified stage specific miRNAs (Figure 17a) and mRNAs (Figure 17b). Both mRNA and miRNA sequencing exhibited differential expression patterns throughout NSC culture, resulting in identification of stage specific miRNAs classified into three major stages: early (day 10-19), mid (day 26-56) and late (day 63-80). Early neural progenitors expressed microRNAs such as miR-17~92 and its paralogs cluster such as miR-20b/a, miR-92a/b, miR-106 a/b, miR-18, and miR-25. Among them, hsa-miR-20b-5p was found as one of the highest expressed miRNAs in that early stage, with expression as high as threefold upregulation as compared to PSCs at the early stage to as low as three-fold downregulation in late stage NSCs. While it has been shown in mice that miR-17~92 cluster is involved in the proliferation of neural stem cells (Bian et al., 2013), no study in mouse as well as human brain has yet demonstrated the role of individual miRNAs of this miRNA cluster. We have also observed the expression of a specific miRNA known as hsa-miR-449 only in day 35 NSCs which was previously shown to be important for mitotic spindle orientation in the developing cortex in mice. The miR-449 knockout in mouse displayed an upregulation of radial glial population at the expense of intermediate progenitors (IPs), indicating its role in NSC proliferation (Fededa et al., 2016). The microRNAs including let-7 family, miR-137 and miR-181 family are highly expressed in the later days of NSC cultures. It has already been shown that overexpression of let-7b (one of let-7 family members) leads to reduced NSC proliferation and increased differentiation by targeting Tlx and cyclin D1 genes (Zhao et al., 2010). So, in line with previous studies in mouse NSCs, human PSCs derived late NSCs also express let-7 family miRNAs in turn suggesting their role in cortical development (Figure 17a).

a

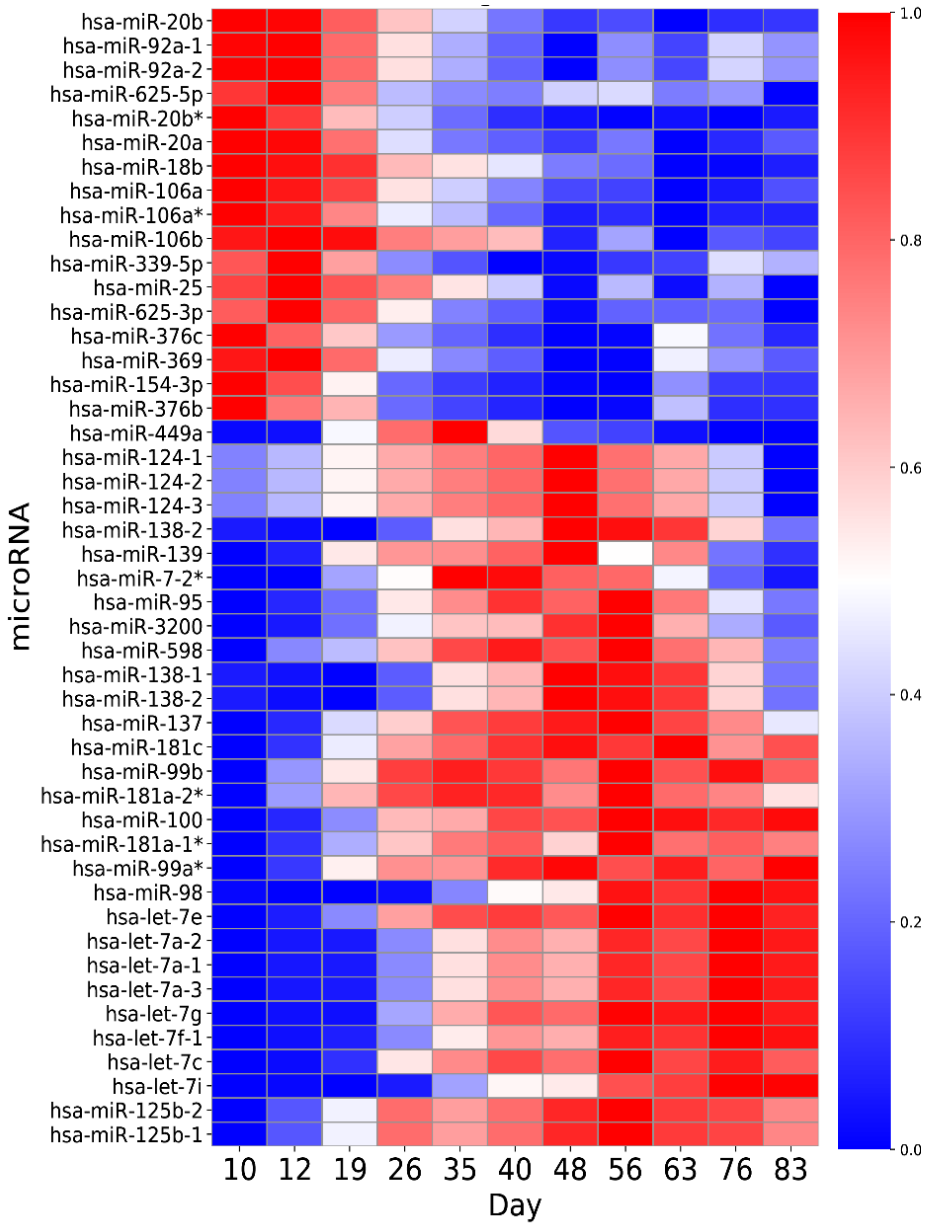
hsa-miR-20b
hsa-miR-92a-1
hsa-miR-92a-2
hsa-miR-625-5p
hsa-miR-20b*
hsa-miR-20a
hsa-miR-18b
hsa-miR-106a
hsa-miR-106a*
hsa-miR-106b
hsa-miR-339-5p
hsa-miR-25
hsa-miR-625-3p
hsa-miR-376c
hsa-miR-369
hsa-miR-154-3p
hsa-miR-376b
hsa-miR-449a
hsa-miR-124-1
hsa-miR-124-2
hsa-miR-124-3
hsa-miR-138-2
hsa-miR-139
hsa-miR-7-2*
hsa-miR-95
hsa-miR-3200
hsa-miR-598
hsa-miR-138-1
hsa-miR-138-2
hsa-miR-137
hsa-miR-181c
hsa-miR-99b
hsa-miR-181a-2*
hsa-miR-100
hsa-miR-181a-1*
hsa-miR-99a*
hsa-miR-98
hsa-let-7e
hsa-let-7a-2
hsa-let-7a-1
hsa-let-7a-3
hsa-let-7g
hsa-let-7f-1
hsa-let-7c
hsa-let-7i
hsa-miR-125b-2
hsa-miR-125b-1
microRNA
10 12 19 26 35 40 48 56 63 76 83
Day
1.0
0.8
0.6
0.4
0.2
0.0

b

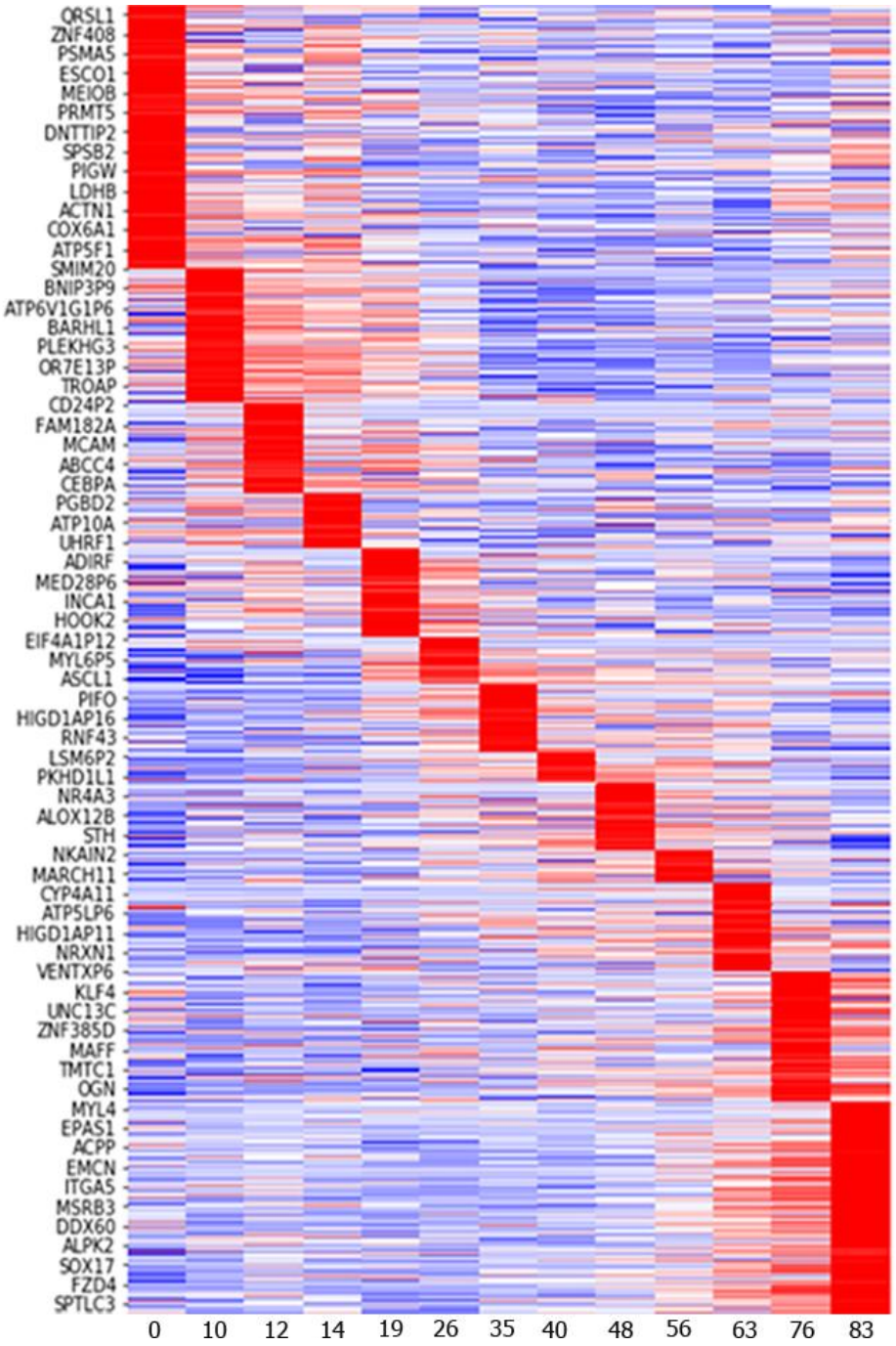
QRSL1
ZNF408
PSMA5
ESCO1
MEIOB
PRMT5
DNTTIP2
SPSB2
PIGW
LDHB
ACTN1
COX6A1
ATP5F1
SMIM20
BNIP3P9
ATP6V1G1P6
BARHL1
PLEKHG3
OR7E13P
TROAP
CD24P2
FAM182A
MCAM
ABCC4
CEBPA
PGBD2
ATP10A
UHRF1
ADIRF
MED28P6
INCA1
HOOK2
EIF4A1P12
MYL6P5
ASCL1
PIFO
HIGD1AP16
RNF43
LSM6P2
PKHD1L1
NR4A3
ALOX12B
STH
NKAIN2
MARCH11
CYP4A11
ATP5LP6
HIGD1AP11
NRXN1
VENTXP6
KLF4
UNC13C
ZNF385D
MAFF
TMTC1
OGN
MYL4
EPAS1
ACPP
EMCN
ITGA5
MSRB3
DDX60
ALPK2
SOX17
FZD4
SPTLC3
0
10
12
14
19
26
35
40
48
56
63
76
83

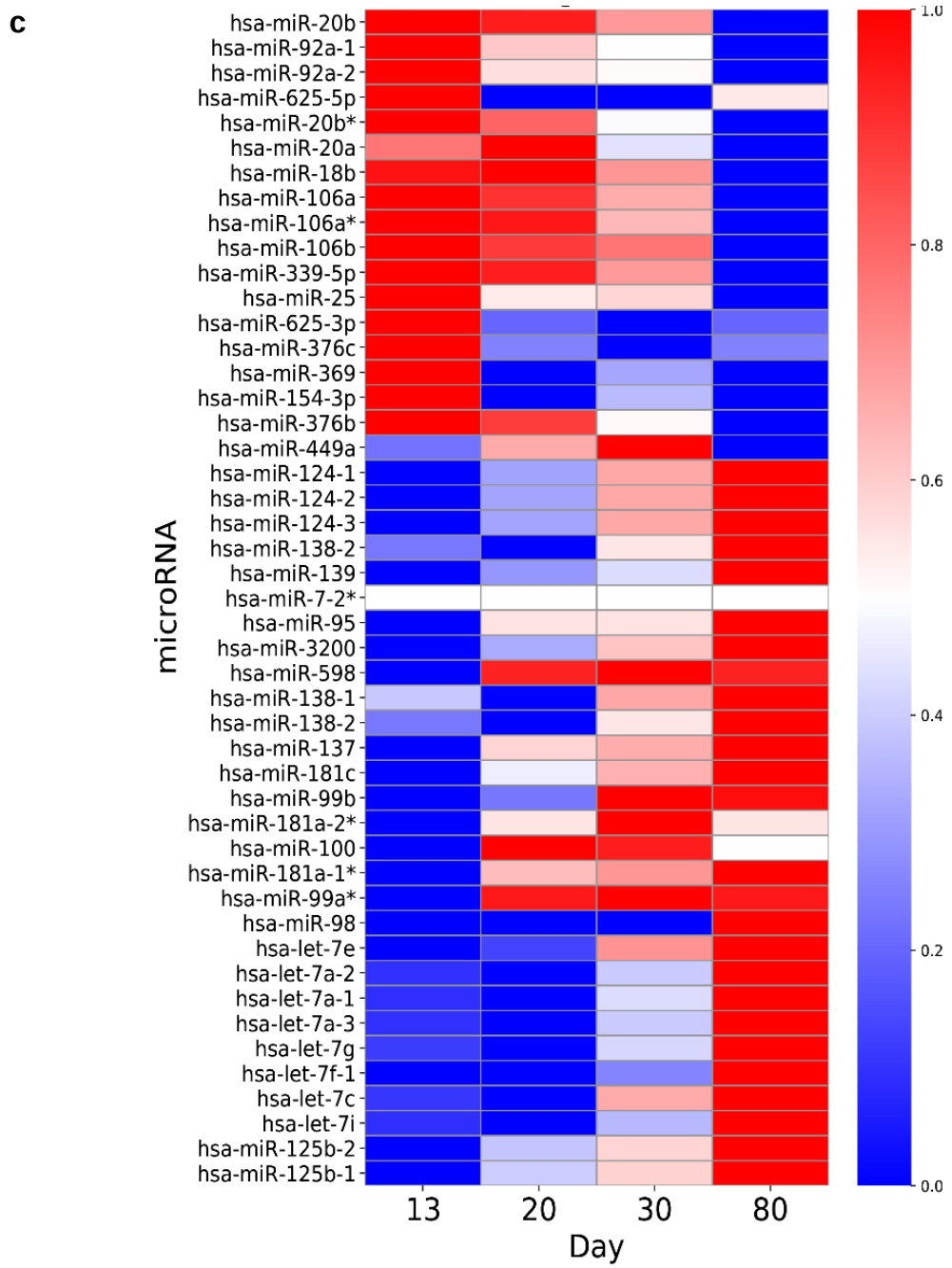

Figure 17: Identification of stage specific miRNAs and genes.

a) A heatmap representing expression values for stage-specific microRNA relative to undifferentiated hES cells (D0) for long-term differentiated NSCs from day 10 to day 80 of neural differentiation. Color code represent the expression level of each microRNA in that row, blue represent the row minimum and red represent the row maximum expression. Note that early, mid and late-stage specific miRNAs has been identified.

b) A heatmap representing expression values for stage specific genes during long term differentiated NSCs from day 0 (D0) untill day 83 (D83). Color-coded scale represents relative expression levels of each gene across row. Note that the neural stem cells derived at each stage (time points) during their

progression have specific set of gene signature. (Blue represent the row minimum and red represent the row maximum expression).

c) A heatmap representing expression values for stage-specific microRNA relative to undifferentiated hES cells (D0) for cortical organoids. Note that has-miR-20b was also highly expressed in early cortical organoids. Color code represent the expression level of each microRNA in that row, blue represent the row minimum and red represent the row maximum expression.

We next validated our stage specific miRs also in our recently developed 3D cerebral organoid system and identified a similar expression pattern of miRNAs in early (day 13), mid (day 30) and late (day 80). The highly differentially expressed hsa-miR20b was also found to be stage specific in organoids (Figure 17c).

It has been shown that deletion of the miR-17~92 cluster and its paralogs containing miR20b, in mouse dorsal cortex results in increase in TBR2+ IP cells and deep layer neurons, suggesting a role for this cluster and its paralogs in promoting NSC progression. However, the role of miR-20b, individual miRNA from miR-17~92, has not yet been studied in early/founder NSCs and organoids *in vitro*. We would like to decipher the role of this early expressed miRNA in early/founder NSCs. First, we validated the expression pattern of miR-20b-5p detected in our hESC derived miRNA profiling also in hiPSC derived neural stem cells in both 2D monolayer cultures and organoids by qPCR quantification. In line with hESC results, we found that hsa-miR-20b is highly expressed at early NSC stages when compared to late NSC stages (Figure 18a,b).

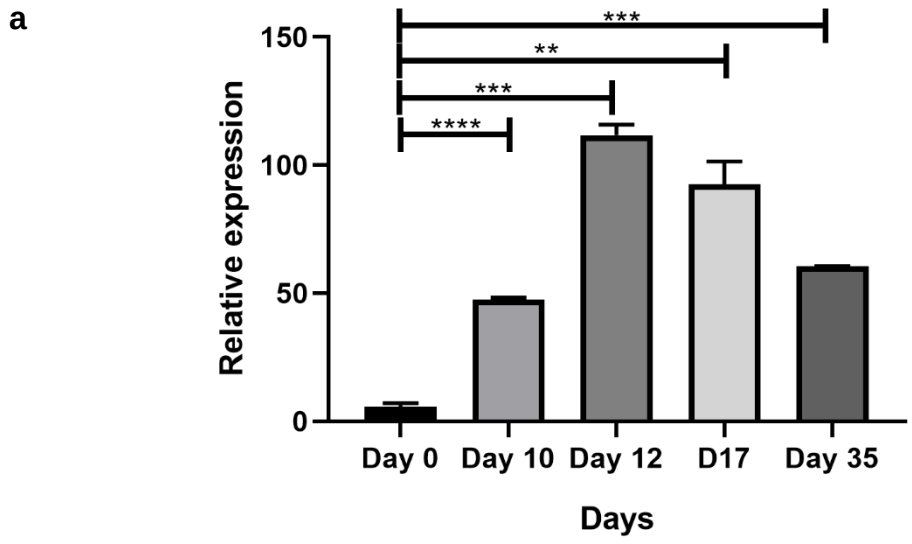

b

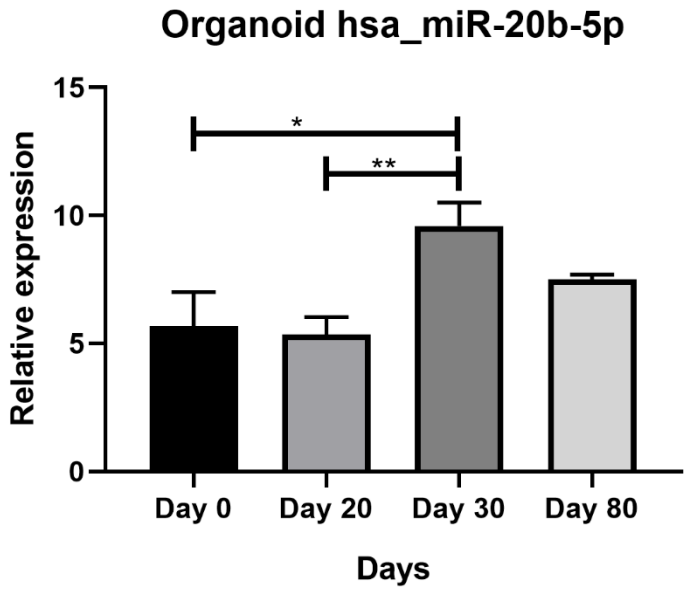

Figure 18: Expression analysis of hsa-miR-20b in neural rosettes and organoids.

a) QPCR analysis of human mature miRNA 20b-5p expression relative to undifferentiated hiPSC cells (D0) for long-term differentiated NSC from day 10 to day 80 of neural differentiation. All transcript levels are normalized to the respective HPRT levels in each sample. Values were obtained from three technical replicates of one reproducible representative experiment. Statistics: Bars represent mean ± S.E. Statistical test: t-test: *P < 0.05; **P < 0.01 ***P < 0.001; ****P < 0.0001.

b) QPCR analysis of transcript levels of human mature miRNA 20b-5p expression relative to undifferentiated hiPSC cells (D0) obtained for D20, D30 and D80 grouped organoids. All transcript levels are normalized to the respective HPRT levels in each sample. Values were obtained from three technical replicates of one reproducible representative experiment, with each sample containing at least 4-5 organoids grouped an analyzed together. Statistics: Bars represent mean ± S.E. Statistical test: one-way ANOVA followed by Tukey's post hoc test: *P < 0.05; **P < 0.01 ***P < 0.001; ****P < 0.0001.

To verify that hsa-miR-20b expression in early stages is within NSCs we performed miRNA-Seq in NSCs and differentiated neurons at different stages generated previously in the lab based on Notch activation stemness hESC reporter (Edri et al., 2015). We found specific expression of miR-20b in early neuroepithelial (NE) and early RGCs, while neurons derived from these early NSC stages exhibited low miR-20b expression. While the mid RG (MRG) and late RG (LRG) derived neurons does not express miR-20b (Figure 19c). We also checked the expression of known neuronal miRNA markers expression such as miR-9 and miR-124 and indeed detected higher in differentiated neurons (Figure 19d). Similarly, let-7 family members known to be

highly expressed in the differentiated cells were expressed in late stage NSCs and their respective derived neurons (Figure 19e).

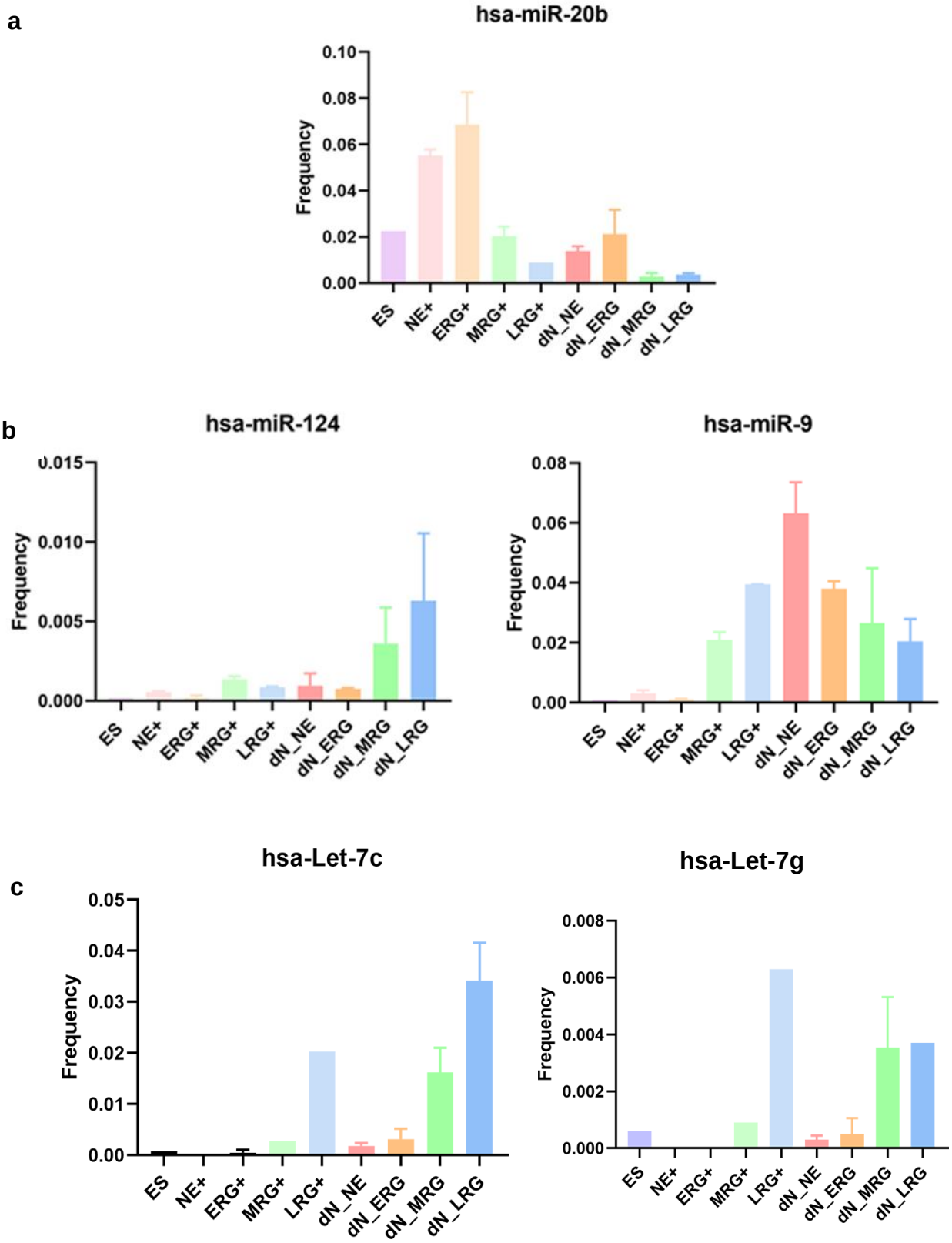

Figure 19: Expression of mature miRNAs in NSCs and their stage derived neurons.

a) Human mature miRNA 20b-5p expression was highly expressed in the neuroepithelial (NE) and early radial glial (ERG) as compared to other NSCs stages. hsa-miR-20b does not express in stage specific derived neurons. Note: dN_NE (differentiated neurons derived from neuroepithelial cells), dN_ERG (differentiated neurons derived from early radial glial), dN_MRG (differentiated neurons derived from mid-radial glial), dN_LRG (differentiated neurons derived from late-radial glial)

b) Mature miRNAs miR-124 seems specific for late stage NSCs derived neurons while miR-9 shown to be expressed in mid and late stage NSCs and in NSCs derived neurons.

c) Another set of miRNAs known to be expressed in differentiated cell types such as Let-7c,7g were expressed in late NSCs and respective stage derived neurons.

3.3 Generation of an inducible stable hsa-miR-20b expressing line

To understand the role of miR-20b in the progression or regionalizing of early NSCs, we overexpressed miR-20b in an inducible manner that will allow us to investigate the effect of miR-20b upregulation throughout the development of NSCs. To this end, we used a LT3GEPIR construct (Fellmann et al., 2013) (kindly given by Markus Haffner, NIH). This lentiviral based Tet-On inducible system contains an eGFP reporter followed by a modified hairpin loop of miR-30 backbone which has been shown to have better efficiency in inducing the expression of shRNA of interest. This plasmid contains both the Tet-responsive element and tetracycline transactivator (rtTa) driven by a constitutive PGK promoter and has puromycin selection marker (Figure 20a). Throughout experiments, miR-20b was induced with doxycycline (2ug/ml) at day 2 of organoid differentiation, and organoids were analyzed at different timepoints (day 13, day 30 and day 50) of development using bulk RNA-Seq, single cell (sc) RNA-Seq, and immunostainings.

First, we validated the inducible system by inducing undifferentiated hiPSCs with doxycycline for 10 days. We found a significant upregulation of miR-20b in the induced hiPSCs (Figure 20c). We similarly validated the system by inducing expression in cerebral organoids at day 2 of differentiation and analyzed them at day 13. We found a significant upregulation of miR-20b in overexpressed organoids as compared to non-induced wild type (WT) organoids (Figure 20d).

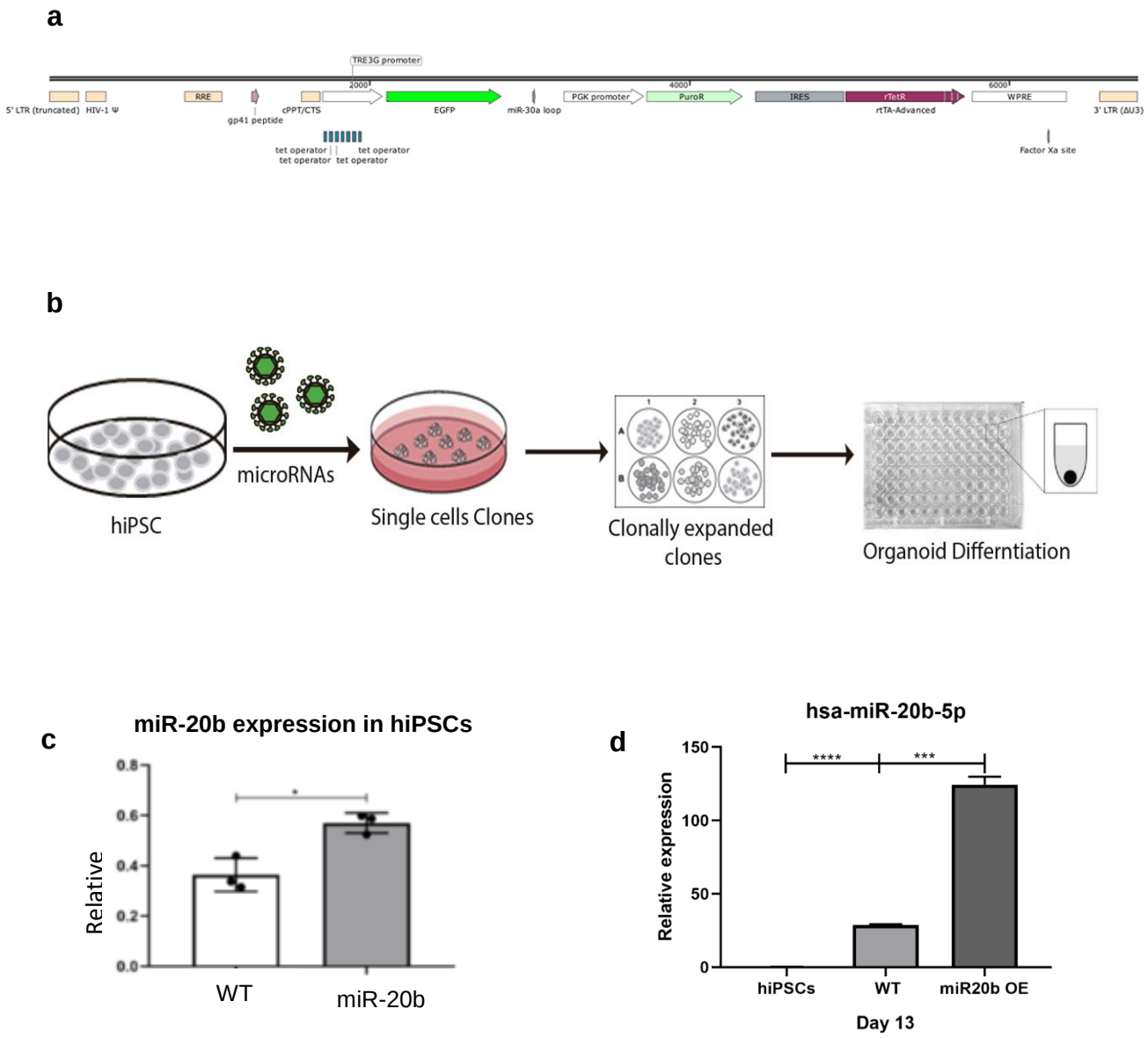

Figure 20: Generation characterization of hsa-miR-20b-5p overexpression line and their derived organoids.

a) Schematic representation of tetracycline inducible LT3GEPIR construct consist of miR-E backbone for overexpressing mature miR-20b at the 3' UTR of eGFP fluorescence reporter gene.

b) Schematic diagram for infecting human iPSc line with lentviral particles and puromycin selected clones for generating the miR-20b overexpressing hiPSC line.

c) QPCR validation of human mature miRNA 20b-5p expression after 10 days of doxcycline induction. All transcript levels are normalized to the respective HPRT levels in each sample. Statistics: Bars represent mean ± S.E. Statistical test: t-test: *$P < 0.05$; **$P < 0.01$ ***$P < 0.001$; ****$P < 0.0001$.

d) QPCR validation of human mature miRNA 20b-5p expression for day 13 obtained organoids for wild type and miR-20b overexpressing organoids. All transcript levels are normalized to the respective HPRT levels in each sample. Note the expression of miR-20b is higher in miR-20b overexpressing

organoids as compared to wild type organoids. Statistics: Bars represent mean ± S.E. Statistical test: t-test: *$P < 0.05$; **$P < 0.01$ ***$P < 0.001$; ****$P < 0.0001$.

3.4 Single Cell RNA Sequencing of day 13 organoids reveals upregulation of WNT family proteins in NSCs of miR-20b overexpressed organoids

To dissect the transcriptomic changes induced by miR-20b overexpression among different cortical cell types, we employed single cell RNA sequencing on day 13, day 30 and day 50 wild type and miR-20b overexpressing organoids. To pinpoint unique and similar cell populations across wild type and miR-20b overexpressing organoids we clustered organoid derived cells together and identified 8 different clusters (Figure 21a). These clusters were then assigned to cortical and non-cortical cell types based on specific marker genes. We identified five clusters of NSCs (C0-C4) based on expression of SOX2, NESTIN, HES5, and FABP7. In addition, we identified non cortical clusters including neural crest (C5), PSCs (C6) and early neurons (C7) (Figure 21b). Interestingly, we observed that there was a suppression of PSCs cluster in miR-20b overexpressing organoids (Figure 21b,c). To further find out the differences between miR-20b overexpressing and wild type NSCs we then employed differential gene expression analysis among NSC clusters (C0-C4). We found an upregulation of cortical NSC markers such as HES5, GLI3, FEZF2, and EMX2, signifying enhanced cortical stemness of more caudal cortical regions. In support, we found a downregulation of anterior telencephalic genes such as SIX3, FZD5, and FZD8 in miR-20b overexpressing organoids (Figure 21e), suggesting posteriorized shift in the telencephalic NSC identity. This was further corroborated by the upregulation of WNT and BMP family genes such as WLS, WNT7B, WNT2B, RSPO2, and BMP7 – signaling molecules involved in caudalization of the telencephalon. The WNT and BMP family genes in particular have been known as morphogens that play an important role in patterning neuroectoderm towards caudal telencephalic structures such as the medial pallium and its derived cortical hem (Grove et al., 1998)

a

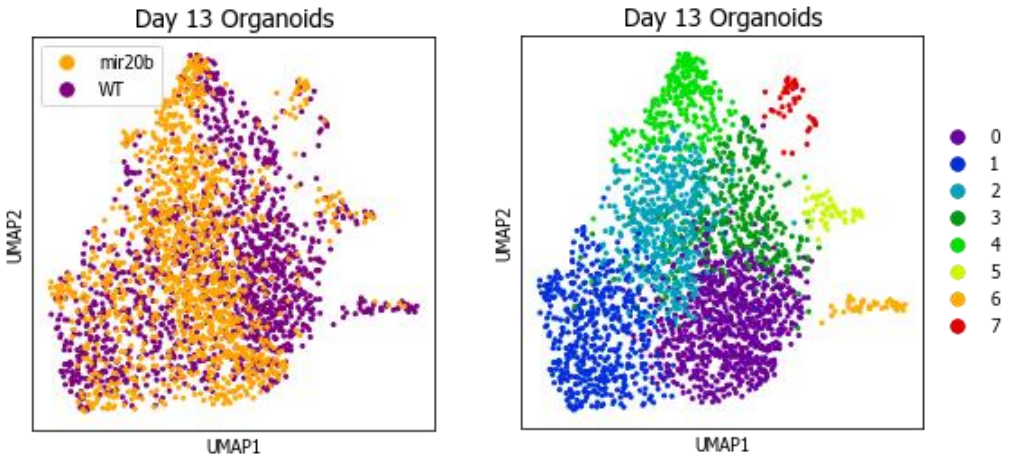
Day 13 Organoids
mir20b
WT
UMAP2
UMAP1
Day 13 Organoids
UMAP2
UMAP1
0
1
2
3
4
5
6
7

b

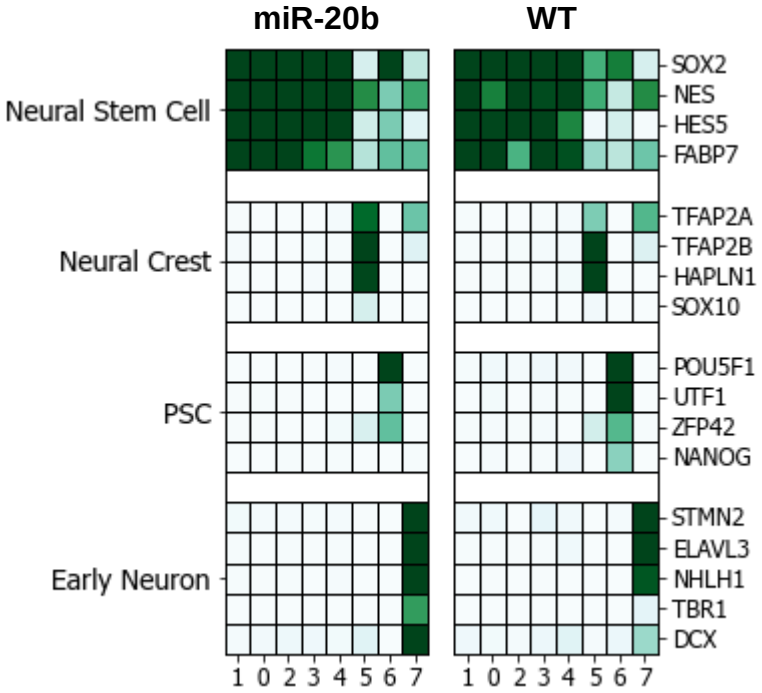
miR-20b
WT
Neural Stem Cell
Neural Crest
PSC
Early Neuron
SOX2
NES
HES5
FABP7
TFAP2A
TFAP2B
HAPLN1
SOX10
POU5F1
UTF1
ZFP42
NANOG
STMN2
ELAVL3
NHLH1
TBR1
DCX
1 0 2 3 4 5 6 7
1 0 2 3 4 5 6 7

c

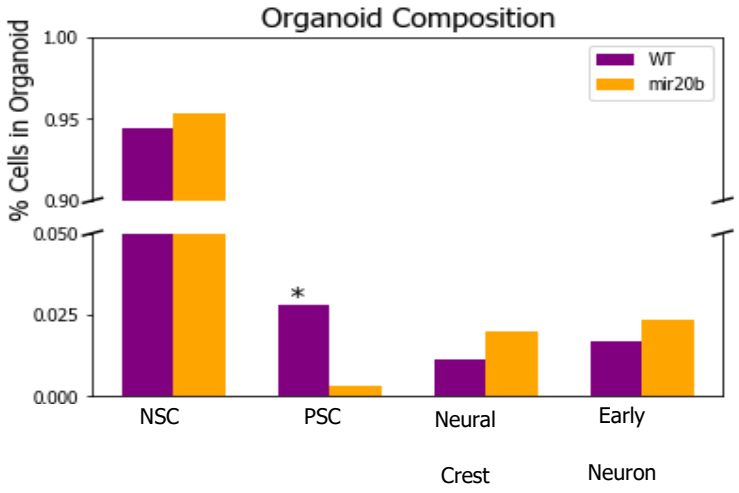
Organoid Composition
% Cells in Organoid
1.00
0.95
0.90
0.050
0.025
0.000
WT
mir20b
*
NSC
PSC
Neural Crest
Early Neuron

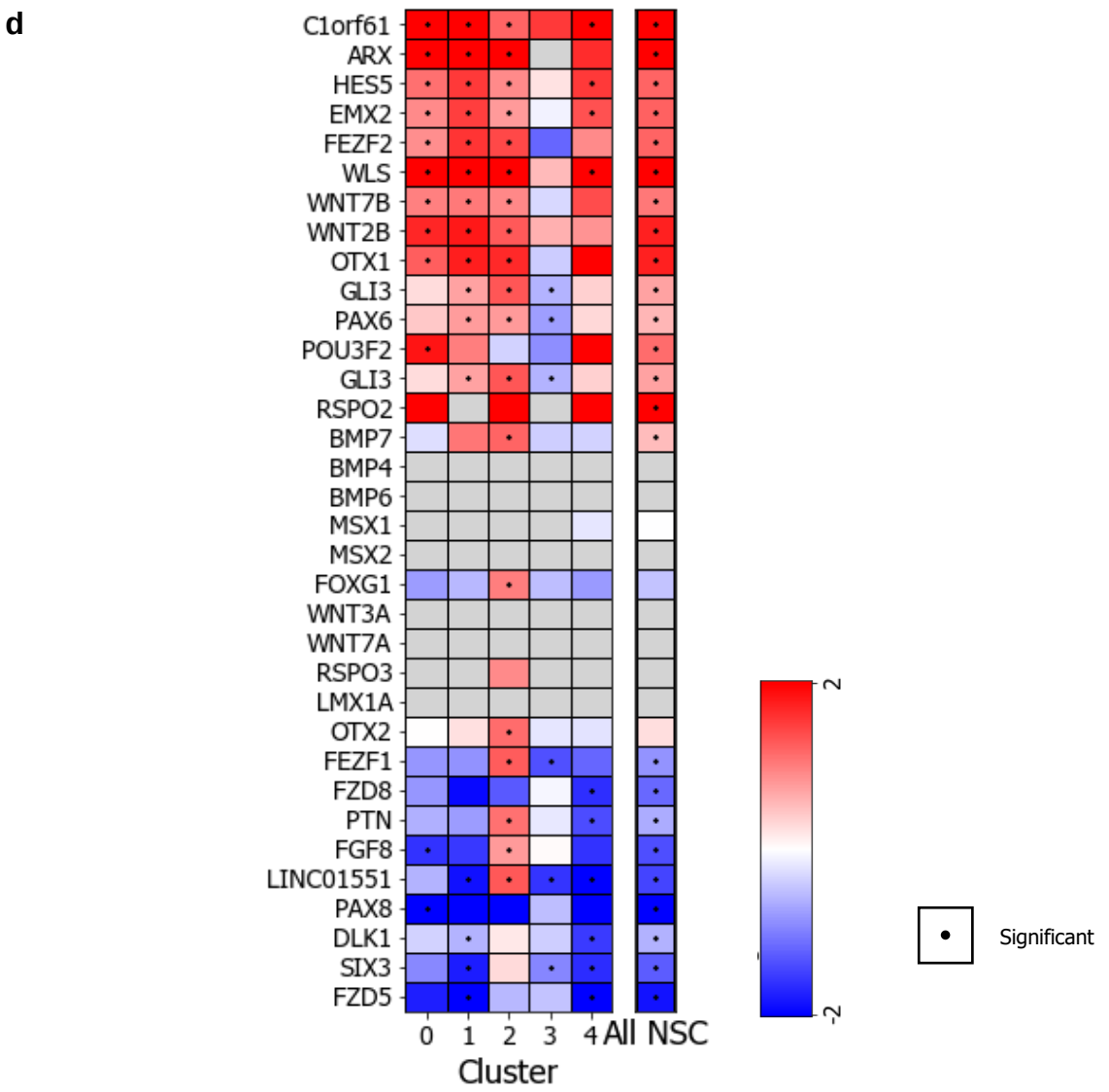

Figure 21: Single cell RNA-Seq reveals lack of PSCs cluster and upregulation of WNT and BMP family molecules in early cortical NSCs.

a) Uniform Manifold Approximation and Projection (UMAP) plot for single cell RNA sequencing data of Day 13 wild type (Purple) and miR-20b overexpressing (orange) organoids derived under Triple-i treatment reveals 8 distinct clusters (C0-C7) highlighted in different colors. WT: Wild type, miR-20b: miR-20b overexpression

b) A heatmap representing expression values for genes marking NSCs and other cell types such as PSCs, neural crest and early neurons for day 13 wild type and miR-20b overexpressing cell clusters. Color-coded scale represents relative expression levels of each genes (row) across clusters. Color code: Dark green (maximum) and white (minimum) across row.

c) Bar plot representing percentage of cells in the wild type (Purple) and miR-20b overexpressing (orange) day 13 organoids according to the cell types present. Note that miR-20b overexpressing organoids displayed significantly smaller number of PSCs.

d) A heatmap representing $\log_2$ fold change differential expression values for selected genes in miR-20b overexpressing NSCs as compared to wild type NSCs, marking for stemness (HES5, and ARX),

WNT molecules (WLS, WNT7B, and WNT2B) and posterior markers (FZD8, and FGF8) in miR-20b overexpressing organoids as compared to wild type organoids. Color-coded scale represents relative expression levels of each genes (row) across NSC clusters. (Blue represent the row minimum and red represent the row maximum expression).

Despite these intriguing molecular changes at the single cell level, cellular characterization of these wild type and miR-20b overexpressing organoids on day 13 revealed similar organoid cytoarchitectural morphology and expression of various stem/progenitor and neuronal cell markers in both wild type and miR-20b overexpressing organoids. This suggested that miR-20b had no major effect on early neuroectodermal development (Figure 22).

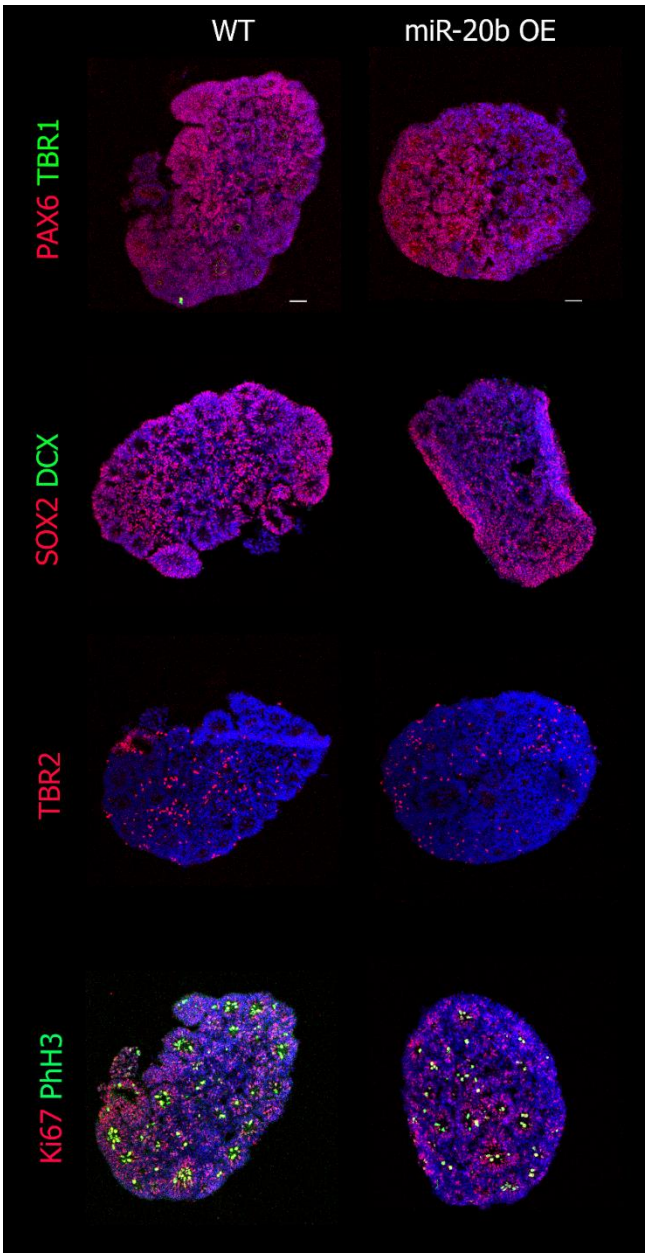

Figure 22: Cellular characterization in day 13 miR-20b overexpressing and wild type organoids displayed no major differences in the morphology.

Immunostaining for NSC and early born neuronal marker such as PAX6 and TBR1 showed no expression in both wild type and miR-20b overexpressing organoids. Immunostaining for stem cell marker SOX2 along with DCX (immature neuronal marker), TBR2 (IP) marker, and proliferating radial glial marker PPH3 in both wild type and miR-20b overexpressing organoids. Scale bar: 50µm.

3.5 Single Cell RNA Sequencing of day 30 mir20b overexpressing organoids revealed inhibition of non-telencephalic fates along with increase in hippocampal NSCs

Next, we analyzed miR-20b induced transcriptional changes in day 30 wild type and miR-20b overexpressing organoids. Clustering wild type and miR-20b overexpressing organoids together revealed no overlap of wild type and miR-20b overexpressing cells, indicating vast transcriptional differences between these populations. We then performed clustering separately and identified 25 and 18 clusters in wild type and miR-20b overexpressing organoids respectively (Figure 23a,b). We assigned these clusters to respective cell types and brain regions based on specific marker gene expression (Figure 23c,d). While wild type organoids exhibited both telencephalic and posterior fates, miR-20b overexpressing organoids were comprised of telencephalic identities only. Posterior brain regions cell types appearing in wild type organoids included diencephalic stem cells (TCF7L2, FZD10, IRX2, IRX3, PROX1 and OLIG3, mid/hindbrain stem cells (PAX3, DMBX1, HOXA2, HOXB2, HOXB3, PAX7, PHOX2B, and BARHL1) and their posterior neurons (PAX3, HOXB3/2, TCF7L2, NTRF1, and SCNG), PNS neurons (POU4F1, NTRK1, NEFL and SNCG), as well as schwann cells (MPZ, S100B, SOX10, and NGFR) (Figure 23e,f). The telencephalic population observed in both wild type and miR-20b organoids consisted of cortical stem cells (FOXG1, EMX1, LHX2, PAX6, and SFRP1) and their respective neurons (FOXG1, TBR1, and DCX),hippocampal stem cells (TCF4, LFE1, LMX1A, and WNT2B), and sub-pallium neurons (DLX1, DLX2, DLX5, ELVA3/2, and DCX) (Figure 23c-f). Most importantly, among telencephalic identities, we found a 60% increase in the number of hippocampal stem cells in miR-20b overexpressing organoids compared to wild type organoids. Lastly, we also found 80% increase in the cajal-retzius neurons in miR-20b overexpressing organoids as compared to wild type. Together these data suggested

enhancement of caudal telencephalic cell types (hippocampal NSCs) along with decrease in the non-cortical cell types in miR-20b overexpressing organoids.

3.6 miR-20b overexpressing organoids on day 30 exhibit reduced number of cortical NSCs and IP populations, while showing an increase in cortical neurons

We next looked into the cortical cell types in both wild type and miR-20b overexpressing organoids. We identified decrease in the number of NSC cluster types in miR-20b overexpressing organoids (4 clusters) as compared to wild type organoids (6 clusters). Overall, we also observed 33% reduction in the cortical NSC population in miR-20b overexpressing organoids. Next, we looked at the IPs and observed decrease in the IP clusters in miR-20b overexpressing organoids (2 clusters) as compared to 4 clusters in wild type organoids. Interestingly, we identified 66% decrease in the IP population in the miR-20b overexpressing organoids as compared to wild type. Altogether these data suggest that the stem cell and progenitor populations are lessened in the miR-20b overexpressing organoids (Figure 23g,h).

Next, we looked into the differentiated progenies of these NSC and progenitor cell populations. We identified 6 clusters of cortical neurons in miR-20b overexpressing organoids as compared to 1 cluster in the wild type organoids. We also observed an 89% increase in the cortical neuronal population in miR-20b overexpressing organoids as compared to wild type organoids. This suggests precocious differentiation of cortical NSCs and progenitor cells towards cortical neurons (Figure 23c-g). We next focused on the cortical neuronal clusters in both wild type and overexpressing organoids. We observed that wild type organoids consist of only one cluster of TBR1+ neurons while miR-20b overexpressing organoids consisted of different cluster types of neurons. We next used published mouse cortical brain datasets and identified the type of neurons which are enriched in our miR-20b overexpressing organoids (Lodato and Arlotta, 2015). We identified that cluster 5 and 8 in miR-20b overexpressing organoids resembles layer 6 of corticothalamic projection neurons based on high expression of FOXP2 and TLE4 and low expression of BCL11B. While cluster 0, 1, and 2 expressed high TBR1 and BCL11B and were negative for FOXP2 and CUX1, cluster 1 specifically expressed FEZF2 along with the aforementioned genes, suggesting that these clusters belong to layer 5 cortical neurons. Altogether this data

suggests that miR-20b overexpression causes differentiation of cortical NSCs towards deep layer neurons (layer 5 and 6) in miR-20b overexpressing organoids.

a

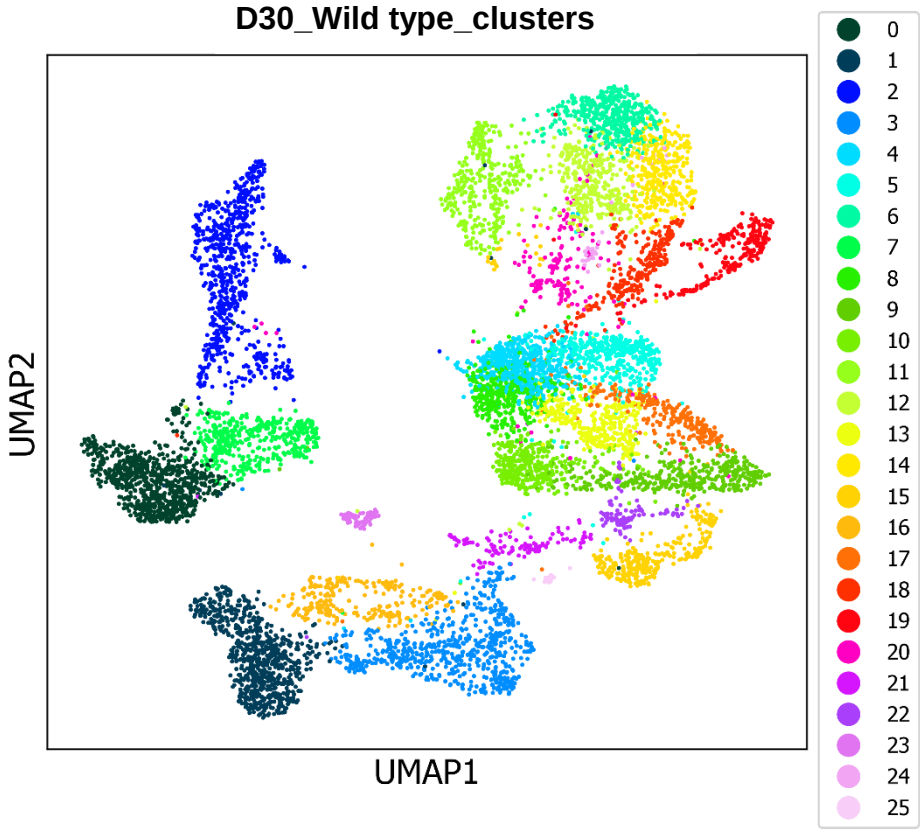

b

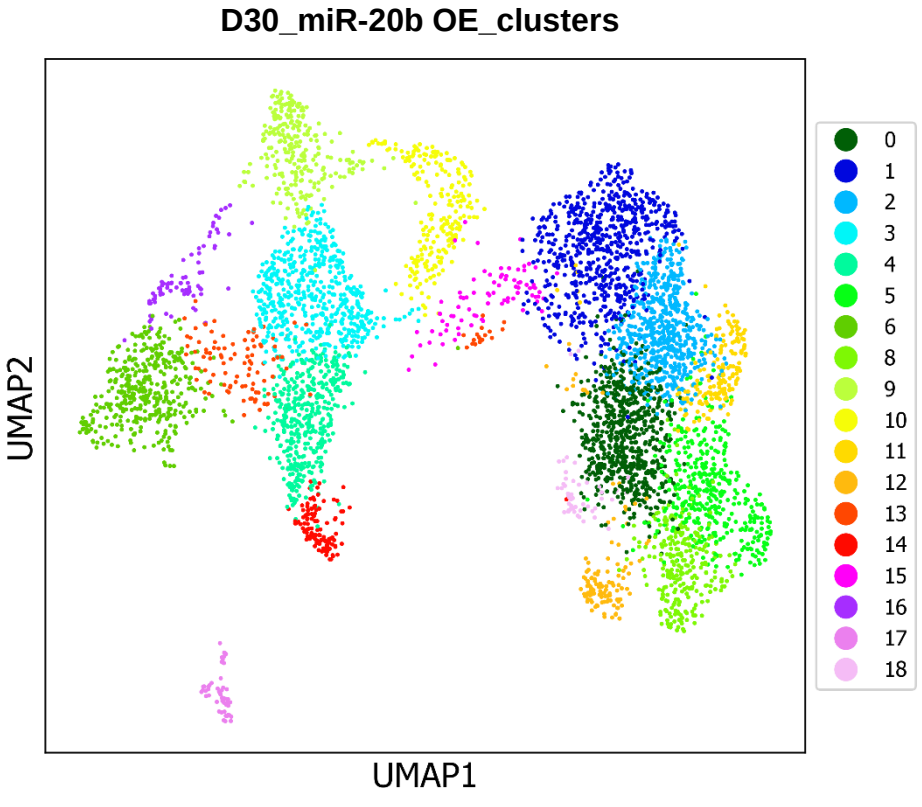

c

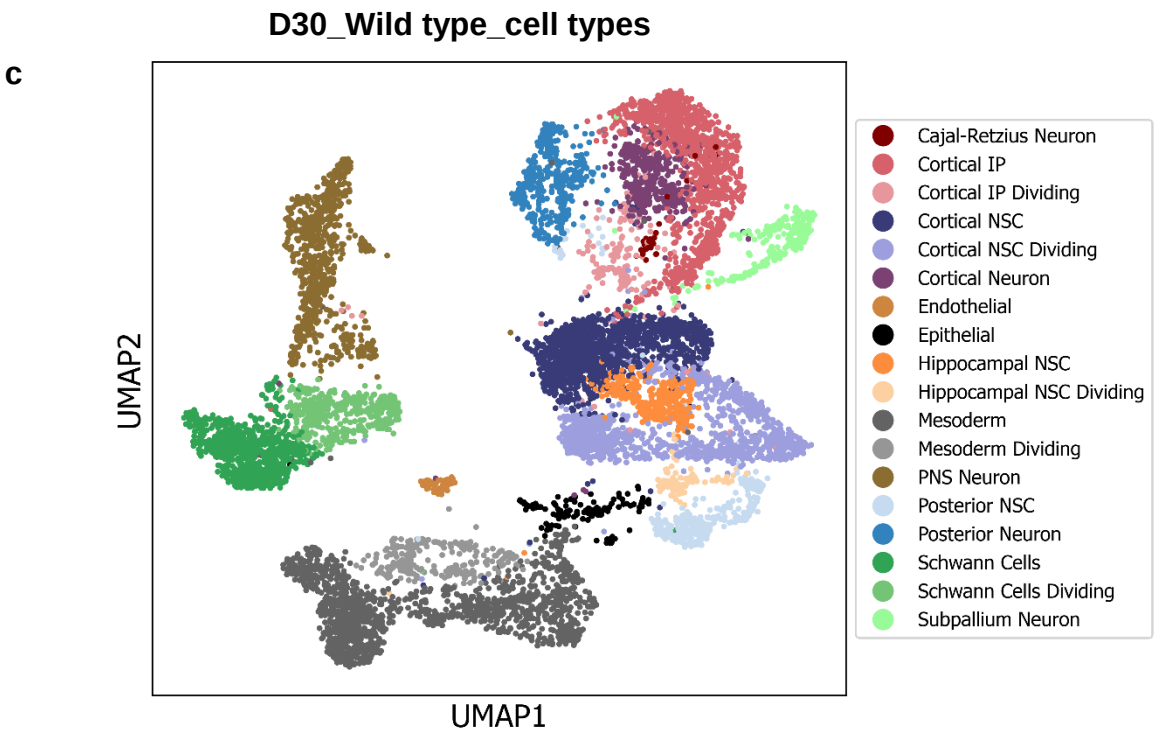
D30_Wild type_cell types
UMAP2
UMAP1
Cajal-Retzius Neuron
Cortical IP
Cortical IP Dividing
Cortical NSC
Cortical NSC Dividing
Cortical Neuron
Endothelial
Epithelial
Hippocampal NSC
Hippocampal NSC Dividing
Mesoderm
Mesoderm Dividing
PNS Neuron
Posterior NSC
Posterior Neuron
Schwann Cells
Schwann Cells Dividing
Subpallium Neuron

d

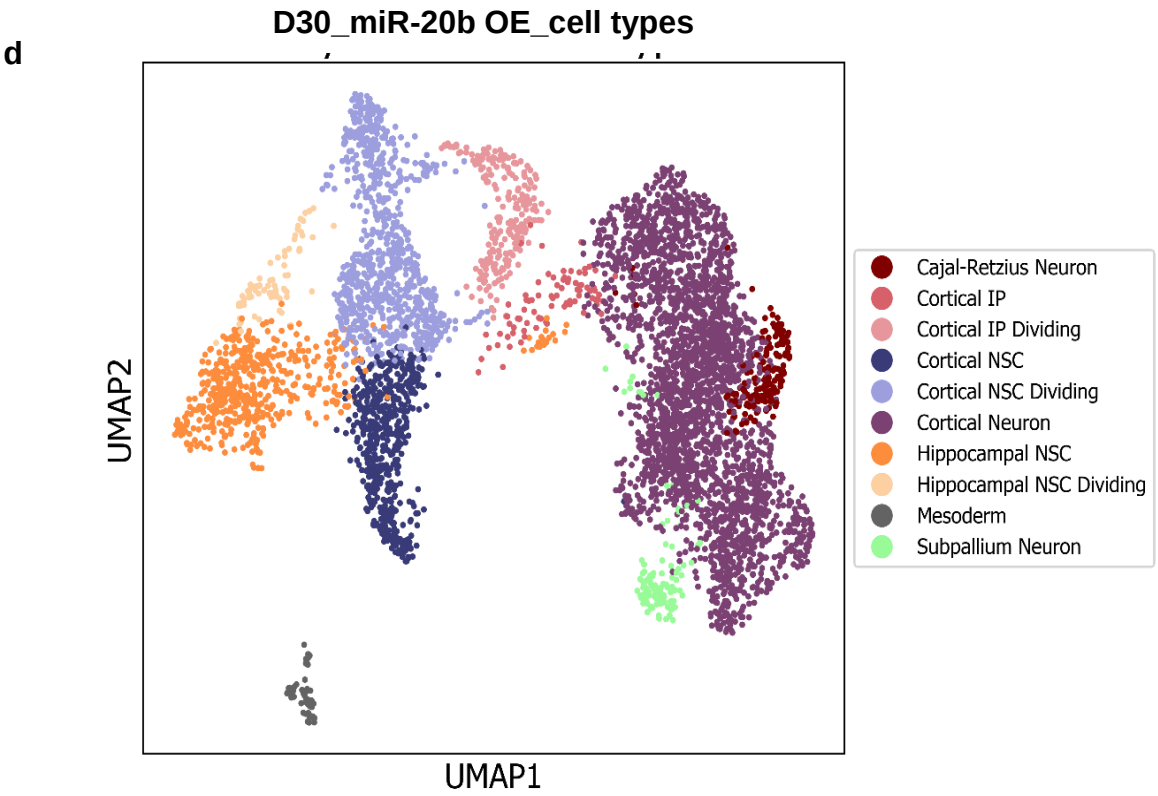
D30_miR-20b OE_cell types
UMAP2
UMAP1
Cajal-Retzius Neuron
Cortical IP
Cortical IP Dividing
Cortical NSC
Cortical NSC Dividing
Cortical Neuron
Hippocampal NSC
Hippocampal NSC Dividing
Mesoderm
Subpallium Neuron

e

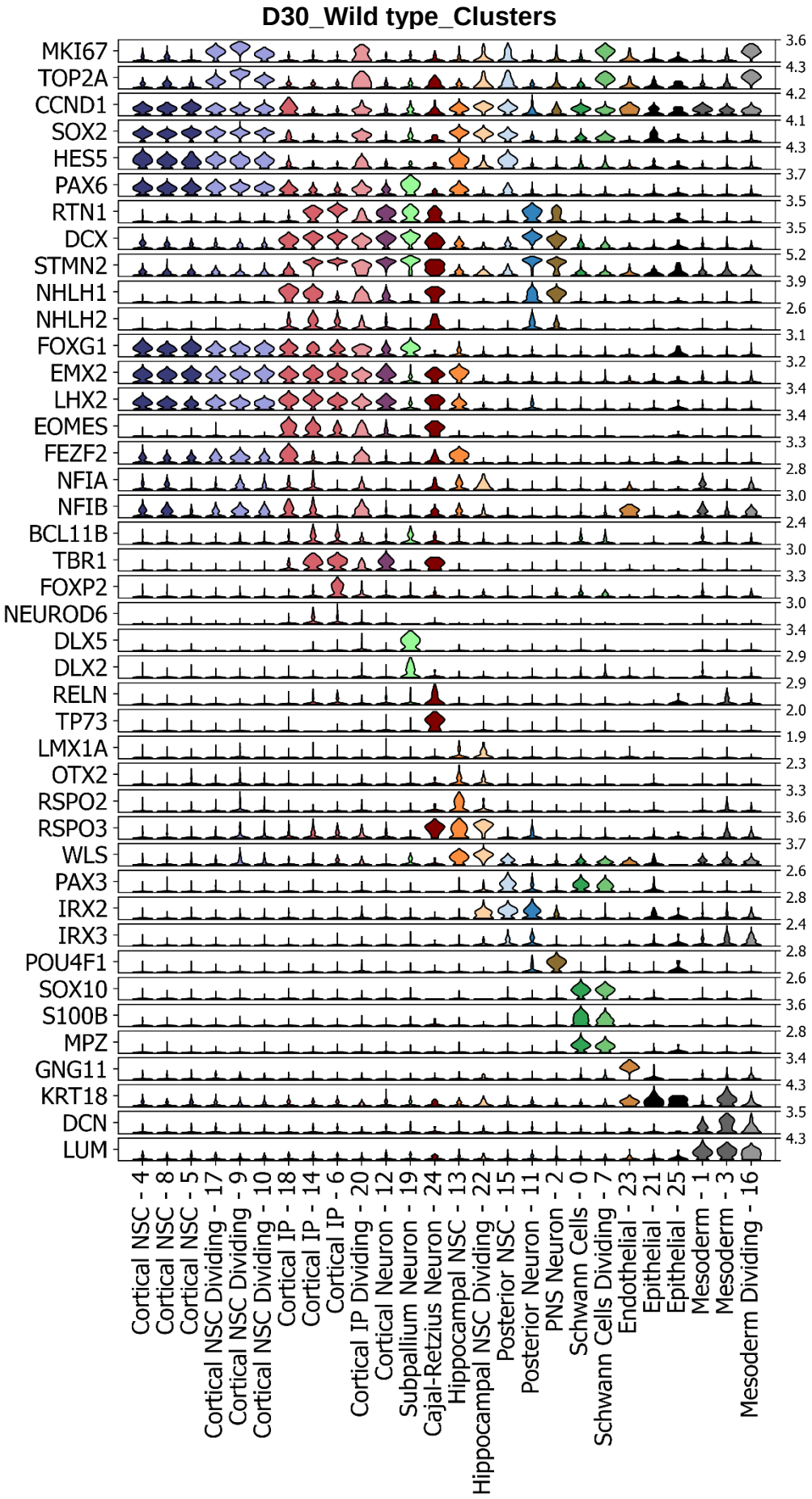
D30_Wild type_Clusters
MKI67
TOP2A
CCND1
SOX2
HES5
PAX6
RTN1
DCX
STMN2
NHLH1
NHLH2
FOXG1
EMX2
LHX2
EOMES
FEZF2
NFIA
NFIB
BCL11B
TBR1
FOXP2
NEUROD6
DLX5
DLX2
RELN
TP73
LMX1A
OTX2
RSPO2
RSPO3
WLS
PAX3
IRX2
IRX3
POU4F1
SOX10
S100B
MPZ
GNG11
KRT18
DCN
LUM
3.6
4.3
4.2
4.1
4.3
3.7
3.5
3.5
5.2
3.9
2.6
3.1
3.2
3.4
3.4
3.3
2.8
3.0
2.4
3.0
3.3
3.0
3.4
2.9
2.9
2.0
1.9
2.3
3.3
3.6
3.7
2.6
2.8
2.4
2.8
2.6
3.6
2.8
3.4
4.3
3.5
4.3
Cortical NSC - 4
Cortical NSC - 8
Cortical NSC - 5
Cortical NSC Dividing - 17
Cortical NSC Dividing - 9
Cortical NSC Dividing - 10
Cortical IP - 18
Cortical IP - 14
Cortical IP - 6
Cortical IP Dividing - 20
Cortical Neuron - 12
Subpallium Neuron - 19
Cajal-Retzius Neuron - 24
Hippocampal NSC - 13
Hippocampal NSC Dividing - 22
Posterior NSC - 15
Posterior Neuron - 11
PNS Neuron - 2
Schwann Cells - 0
Schwann Cells Dividing - 7
Endothelial - 23
Epithelial - 21
Epithelial - 25
Mesoderm - 1
Mesoderm - 3
Mesoderm Dividing - 16

f

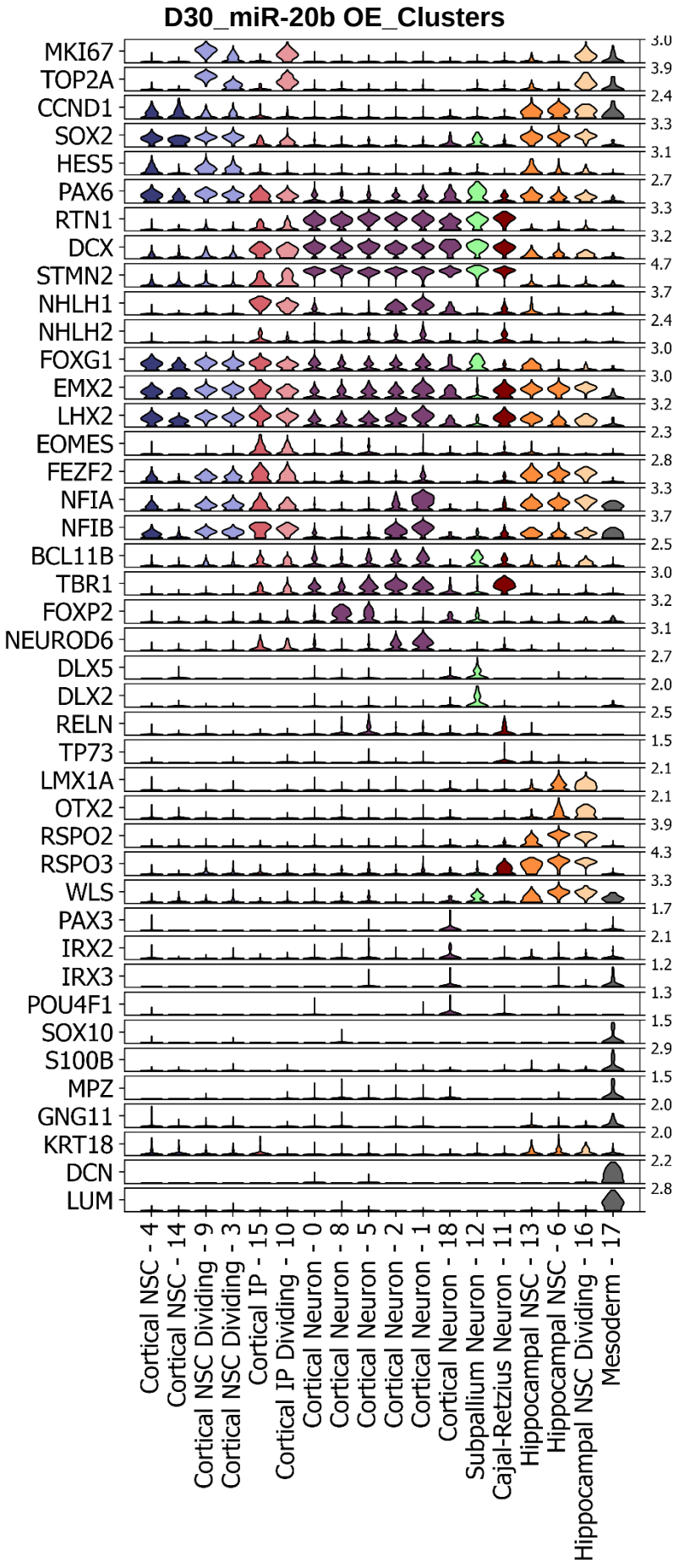
D30_miR-20b OE_Clusters
MKI67
TOP2A
CCND1
SOX2
HES5
PAX6
RTN1
DCX
STMN2
NHLH1
NHLH2
FOXG1
EMX2
LHX2
EOMES
FEZF2
NFIA
NFIB
BCL11B
TBR1
FOXP2
NEUROD6
DLX5
DLX2
RELN
TP73
LMX1A
OTX2
RSPO2
RSPO3
WLS
PAX3
IRX2
IRX3
POU4F1
SOX10
S100B
MPZ
GNG11
KRT18
DCN
LUM
3.0
3.9
2.4
3.3
3.1
2.7
3.3
3.2
4.7
3.7
2.4
3.0
3.0
3.2
2.3
2.8
3.3
3.7
2.5
3.0
3.2
3.1
2.7
2.0
2.5
1.5
2.1
2.1
3.9
4.3
3.3
1.7
2.1
1.2
1.3
1.5
2.9
1.5
2.0
2.0
2.2
2.8
Cortical NSC - 4
Cortical NSC - 14
Cortical NSC Dividing - 9
Cortical NSC Dividing - 3
Cortical IP - 15
Cortical IP Dividing - 10
Cortical Neuron - 0
Cortical Neuron - 8
Cortical Neuron - 5
Cortical Neuron - 2
Cortical Neuron - 1
Cortical Neuron - 18
Subpallium Neuron - 12
Cajal-Retzius Neuron - 11
Hippocampal NSC - 13
Hippocampal NSC - 6
Hippocampal NSC Dividing - 16
Mesoderm - 17

g

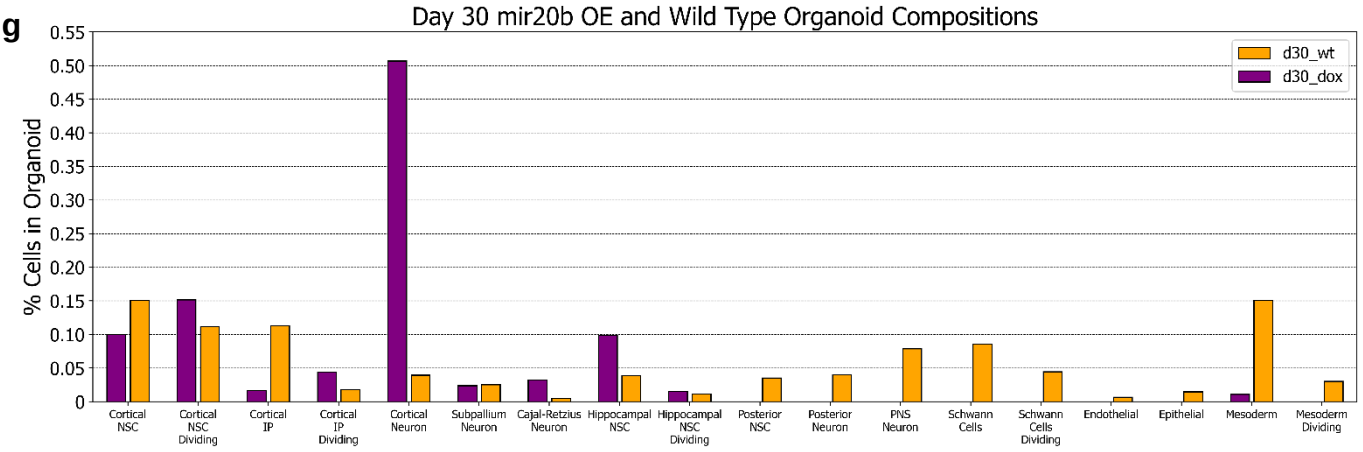
Day 30 mir20b OE and Wild Type Organoid Compositions
% Cells in Organoid
d30_wt
d30_dox
Cortical NSC
Cortical NSC Dividing
Cortical IP
Cortical IP Dividing
Cortical Neuron
Subpallium Neuron
Cajal-Retzius Neuron
Hippocampal NSC
Hippocampal NSC Dividing
Posterior NSC
Posterior Neuron
PNS Neuron
Schwann Cells
Schwann Cells Dividing
Endothelial
Epithelial
Mesoderm
Mesoderm Dividing

Wild type

h

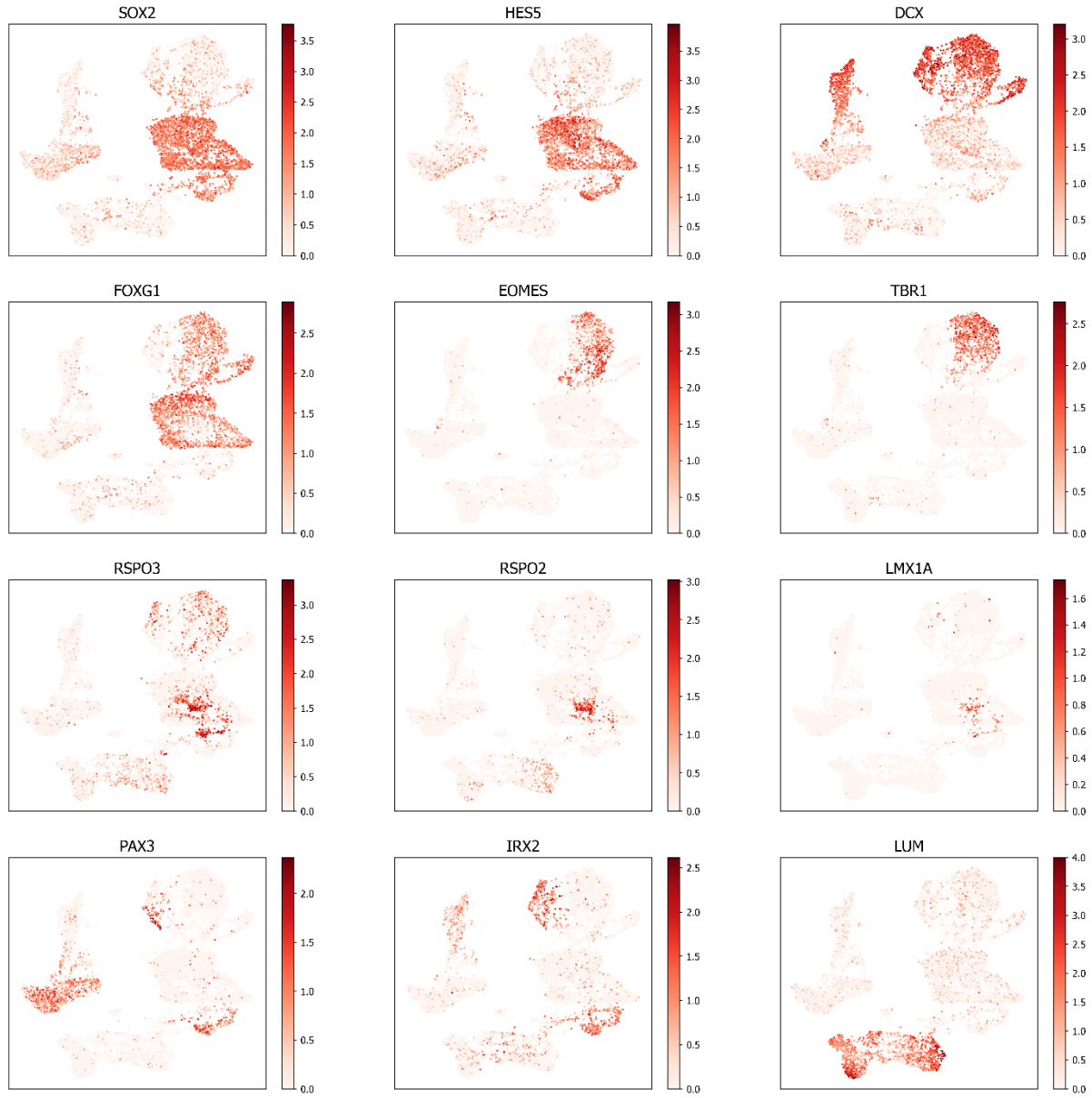
SOX2
HES5
DCX
FOXG1
EOMES
TBR1
RSPO3
RSPO2
LMX1A
PAX3
IRX2
LUM

miR-20b OE

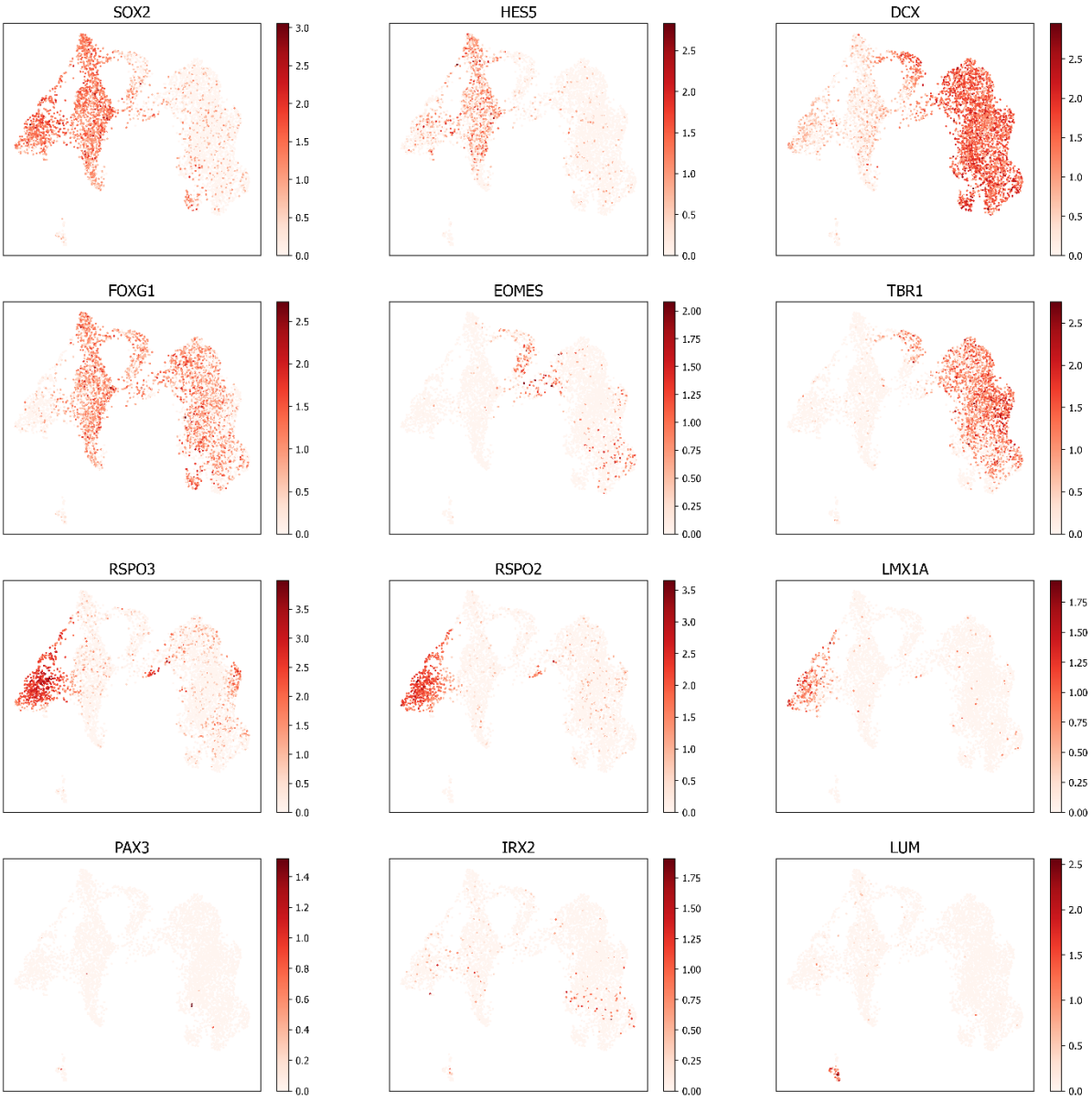
SOX2
HES5
DCX
FOXG1
EOMES
TBR1
RSPO3
RSPO2
LMX1A
PAX3
IRX2
LUM

i

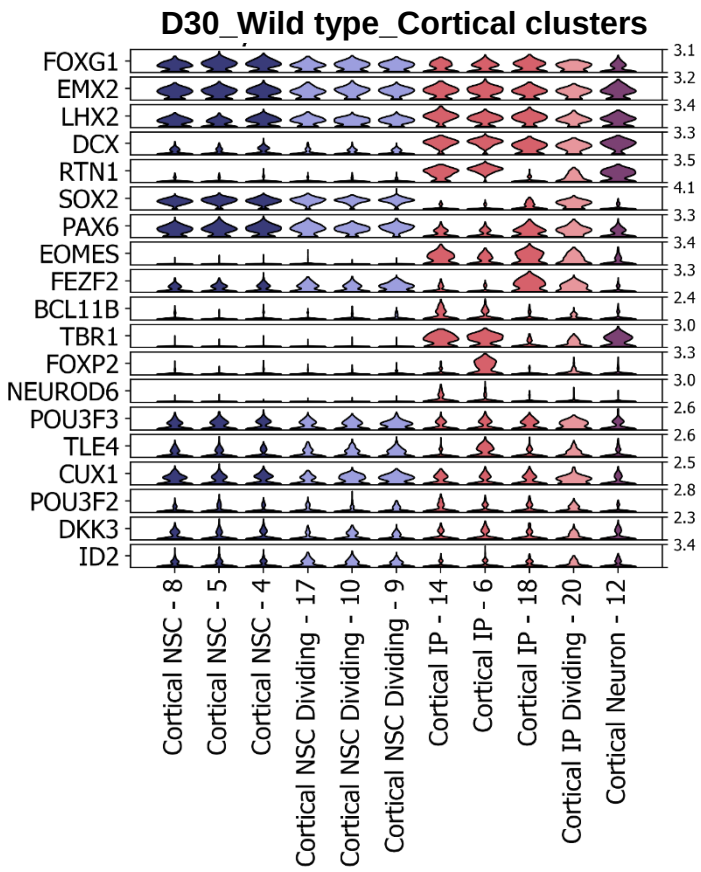
D30_Wild type_Cortical clusters
FOXG1
EMX2
LHX2
DCX
RTN1
SOX2
PAX6
EOMES
FEZF2
BCL11B
TBR1
FOXP2
NEUROD6
POU3F3
TLE4
CUX1
POU3F2
DKK3
ID2
3.1
3.2
3.4
3.3
3.5
4.1
3.3
3.4
3.3
2.4
3.0
3.3
3.0
2.6
2.6
2.5
2.8
2.3
3.4
Cortical NSC - 8
Cortical NSC - 5
Cortical NSC - 4
Cortical NSC Dividing - 17
Cortical NSC Dividing - 10
Cortical NSC Dividing - 9
Cortical IP - 14
Cortical IP - 6
Cortical IP - 18
Cortical IP Dividing - 20
Cortical Neuron - 12

j

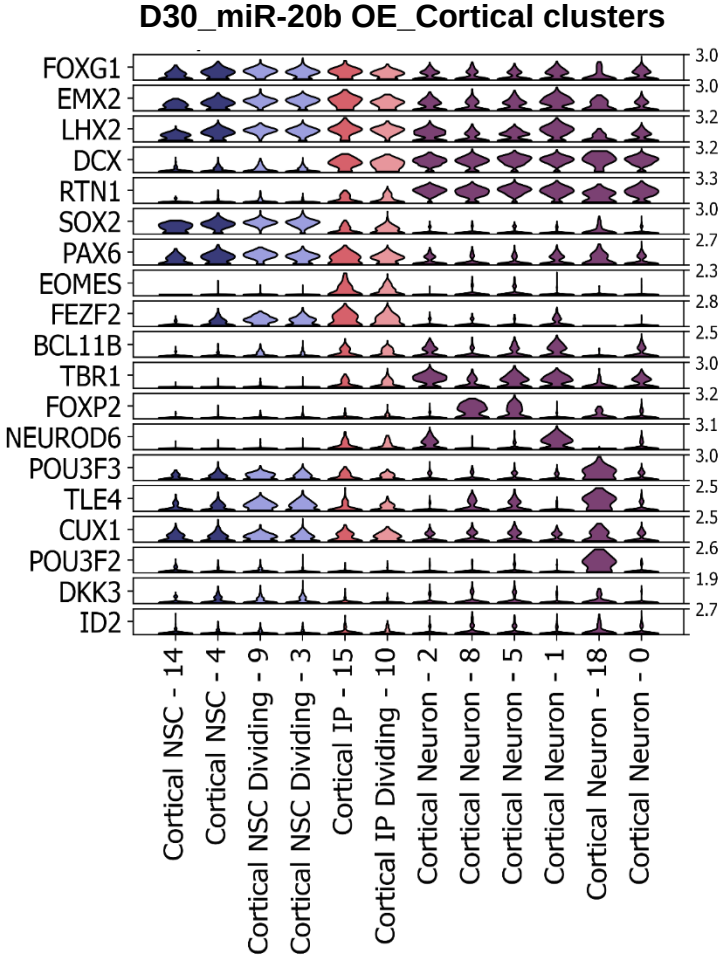
D30_miR-20b OE_Cortical clusters
FOXG1
EMX2
LHX2
DCX
RTN1
SOX2
PAX6
EOMES
FEZF2
BCL11B
TBR1
FOXP2
NEUROD6
POU3F3
TLE4
CUX1
POU3F2
DKK3
ID2
3.0
3.0
3.2
3.2
3.3
3.0
2.7
2.3
2.8
2.5
3.0
3.2
3.1
3.0
2.5
2.5
2.6
1.9
2.7
Cortical NSC - 14
Cortical NSC - 4
Cortical NSC Dividing - 9
Cortical NSC Dividing - 3
Cortical IP - 15
Cortical IP Dividing - 10
Cortical Neuron - 2
Cortical Neuron - 8
Cortical Neuron - 5
Cortical Neuron - 1
Cortical Neuron - 18
Cortical Neuron - 0

Figure 23: Single cell analysis reveals decrase in NSCs, IPs, and increase in cortical neurons in miR-20b overexpressing organoids

a) Uniform Manifold Approximation and Projection (UMAP) plot for single cell RNA sequencing data of day 30 wild type organoids with distinct clusters highlighted in different colors.
b) Uniform Manifold Approximation and Projection (UMAP) plot for single cell RNA sequencing data of day 30 miR-20b overexpressing organoids with distinct clusters highlighted in different colors.
c) Uniform Manifold Approximation and Projection (UMAP) plot for single cell RNA sequencing data of day 30 wild type organoids with distinct clusters and associated cell types defined based on specific marker genes highlighted in different colors.
d) Uniform Manifold Approximation and Projection (UMAP) plot for single cell RNA sequencing data of day 30 miR-20b overexpressing organoids with distinct clusters and associated cell types defined based on specific marker genes highlighted in different colors.
e) A violin plot representing distribution and expression for selected genes categorized according to NSC markers and additional groups of regional markers (neocortex, medial pallium, diencephalon, midbrain-hindbrain and other non-neural cell types) in day 30 wild type organoids.
f) A violin plot representing distribution and expression for selected genes categorized according to NSC markers and additional groups of regional markers (neocortex, medial pallium, diencephalon, midbrain-hindbrain and other non-neural cell types) in day 30 miR-20b overexpressing organoids.
g) Bar plot showing percentage of cells in wild type and miR-20b overexpressing organoids for different cell types. Colour code: Wild type (orange) and miR-20b overexpressing (purple).
h) Uniform Manifold Approximation and Projection (UMAP) plots depicting expression of selected marker genes for brain regions such as cortical (PAX6, and FOXG1), hippocampal markers (RSPO2/3, and LMX1A) and non-cortical cell types (PAX3, IRX2 and LUM).
i) A violin plot representing distribution and expression for selected neuronal genes from published dataset in day 30 wild type organoids.
j) A violin plot representing distribution and expression for selected neuronal genes from published dataset in day 30 miR-20b overexpressing organoids.

3.7 miR-20b overexpressing organoids exhibited a decrease in ventricular zone (VZ) expansion and poorly defined sub-ventricular zone (SVZ)

We next looked at the cellular cytoarchitecture of wild type and miR-20b overexpressing organoids using immunostainings. We first stained for NSC markers, early and immature neuronal markers such as SOX2, PAX6, TBR1 and DCX. We observed similar level of expression of SOX2 in both conditions, while the expression of the immature neuronal marker DCX was slightly higher in miR-20b overexpressing organoids (Figure 24a). Morphologically, wild type organoids displayed thick pseudostratified vesicles consisting of RG stem cells resembling ventricular zone-like regions while overexpressing organoids contained small rosettes similar to early day

13 organoids along with slightly larger (thin layer) rosettes that consisted of short radial fibres, indicating a hampered development and lack of expansion of ventricular zone regions in miR-20b overexpressing organoids – potentially reflecting that cells remained in their early neuroepithelial morphology. We quantified the area of VZ positive for SOX2 in both wild type and miR-20b overexpressing organoids and observed significant expansion of VZ area in wild type organoids (Figure 24f). In addition, we also stained for the NSC marker PAX6 and observed lower expression in miR-20b overexpressing organoids as compared to the wild type. We then found significant increase in the deep layer neuronal marker TBR1 in miR-20b overexpressing organoids as compared to wild type organoids, suggesting precocious differentiation of NSCs and progenitor cells in miR-20b overexpressing organoids. (Figure 24b,g). We found decrease in the expression of cortical marker FOXG1 in the overexpressing organoids (Figure 24c), in-turn validating our scRNA sequencing results (Figure 23f). We observed significant decrease in the TBR2+ IP cells in miR-20b overexpressing organoids (Figure 24b,h). To understand whether the lack of VZ expansion is due to impaired proliferation we next stained for dividing markers (PHH3) and found decrease in PHH3 positive cells, though not significant in miR-20b overexpressing organoids compared to wild type organoids (Figure 24d,g). We next asked whether the reason for smaller neural rosettes and lower percentage of dividing RG cells in overexpressing organoids are due to the death of NSCs, we stained organoids with activated caspase CAS-3 and found no significant difference between the wild type and overexpressing organoids (Figure 24d). Altogether these results suggest impaired/decrease cortical fate specification in miR-20b overexpressing organoids.

Additionaly, we also validated some of the upregulated markers from our scRNA seq dataset such as NF1A and PTN which has been previously shown to play important role in hippocampus development (González-Castillo et al., 2015) and observed upregulation of both genes in miR-20b overexpressing organoids as compared to wild type (Figure 24e), indicating potential expansion of hippocampal primordial cells, as shown by our scRNA-Seq analysis.

a

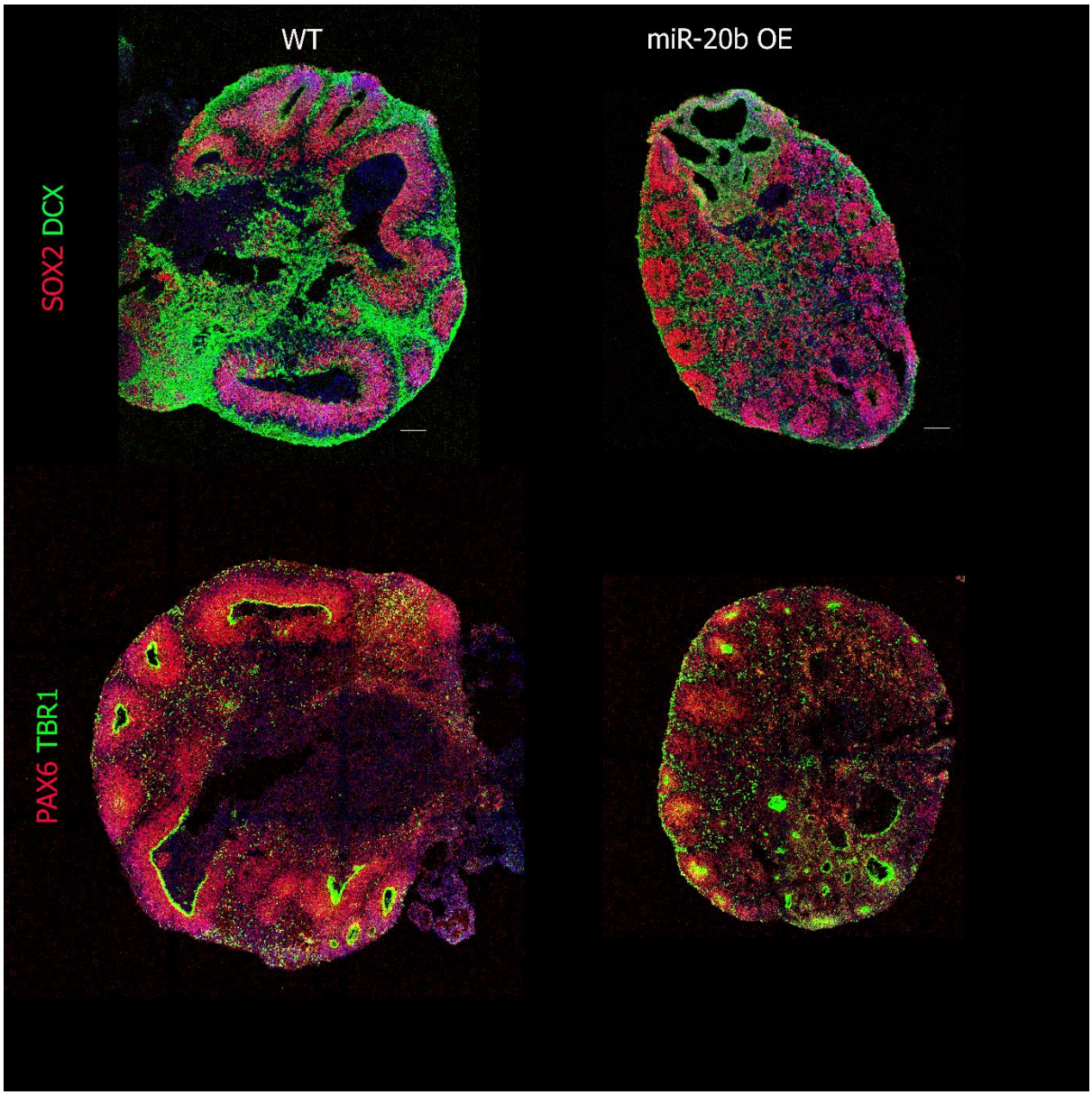

b

c

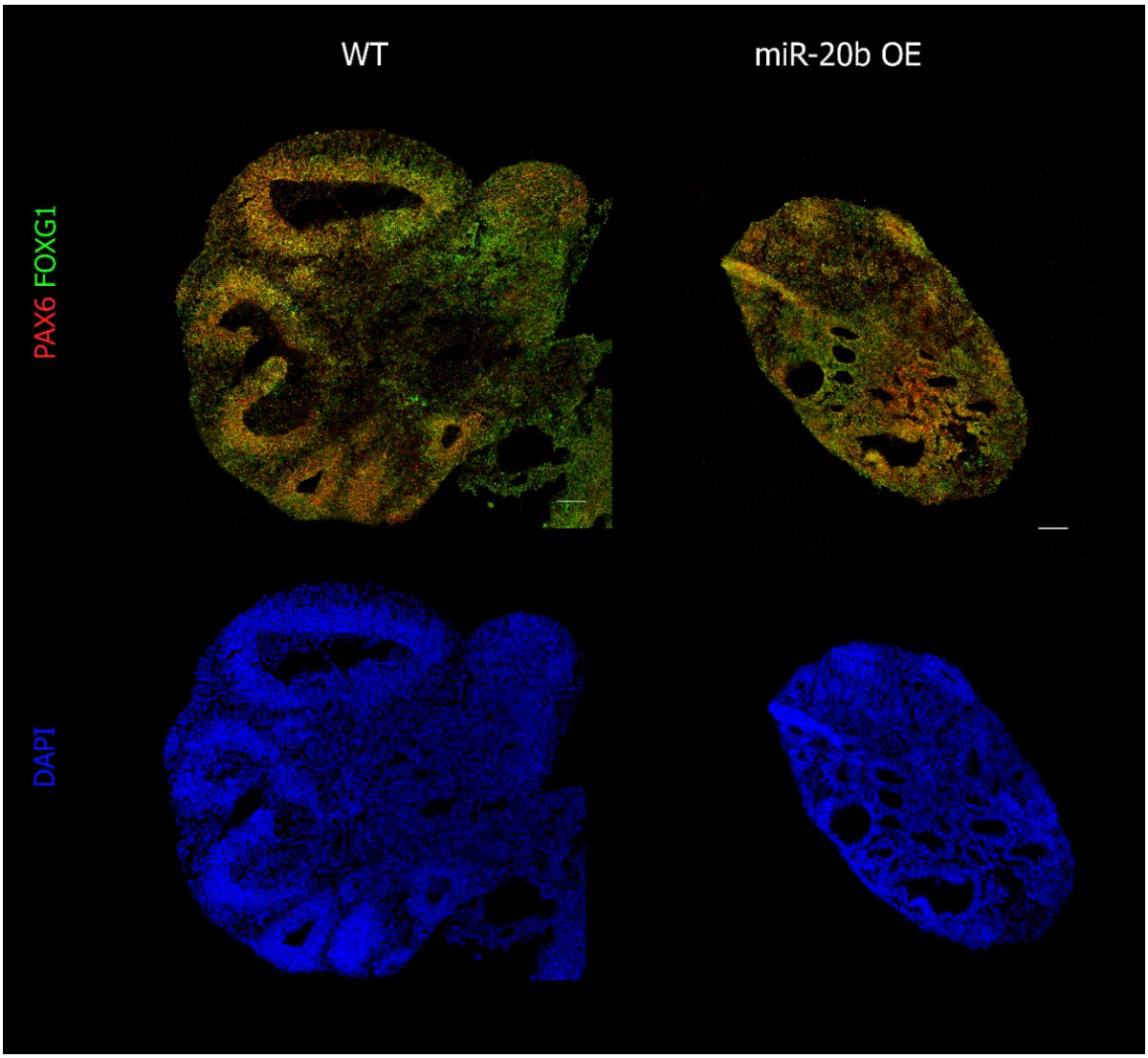

d

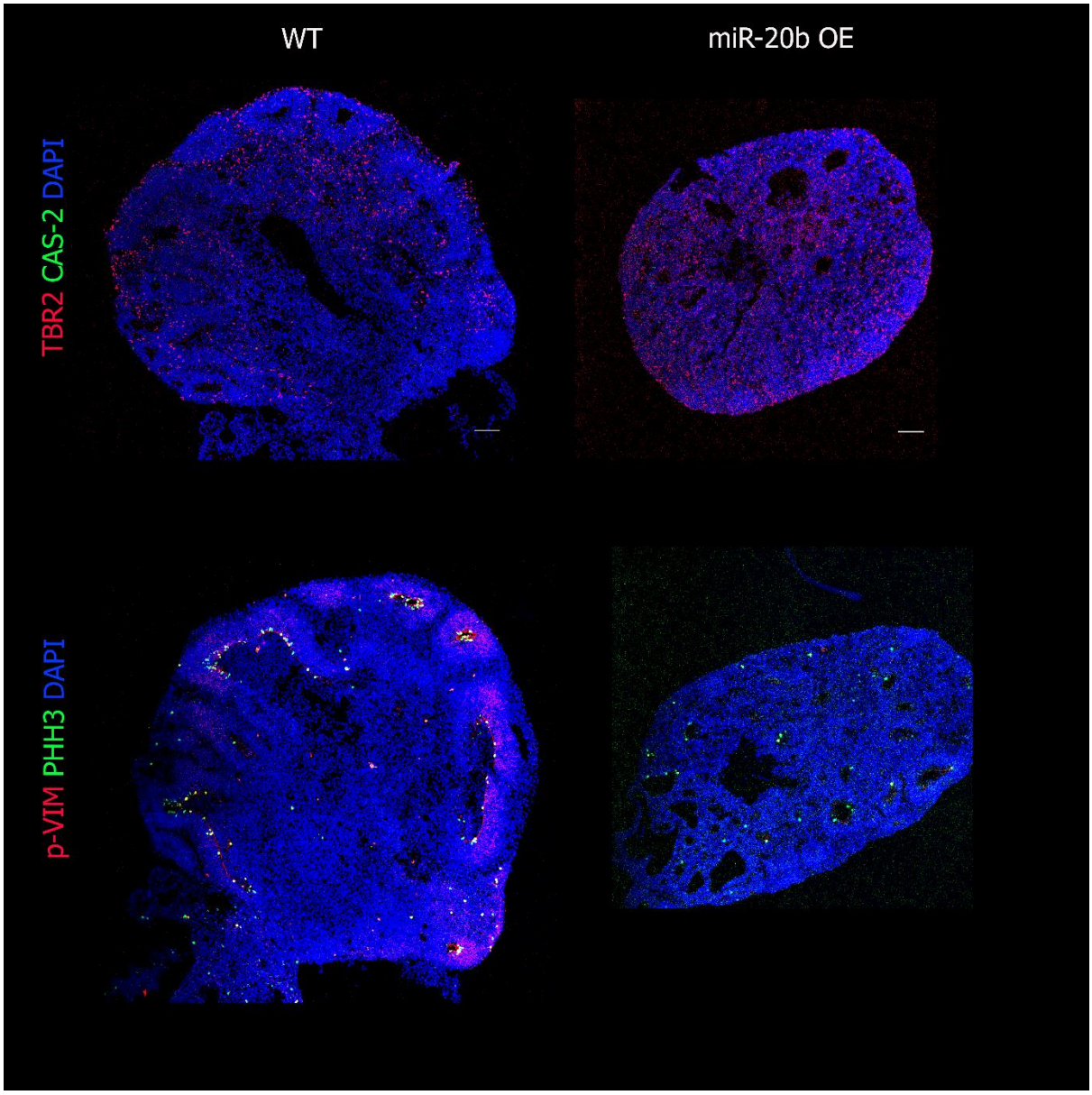

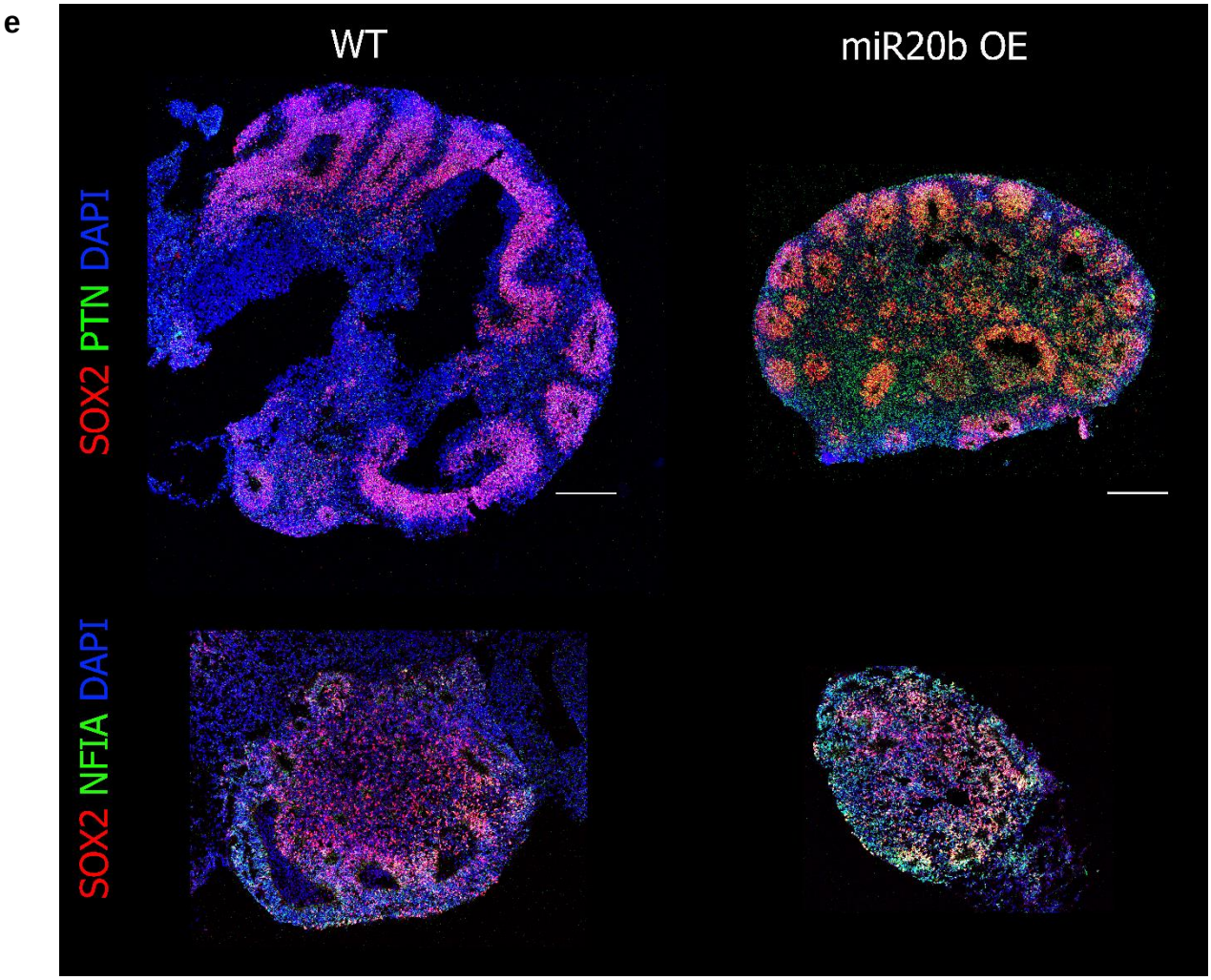
e
WT
miR20b OE
SOX2 PTN DAPI
SOX2 NFIA DAPI

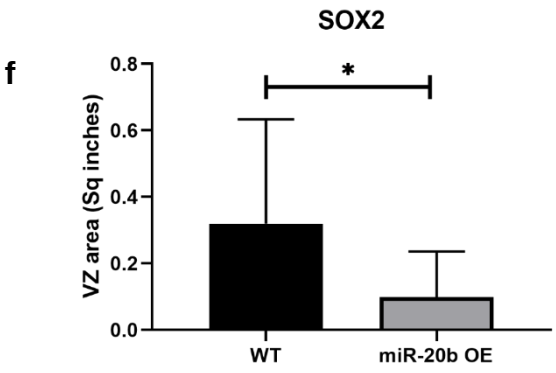
f
SOX2
VZ area (Sq inches)
0.8
0.6
0.4
0.2
0.0
*
WT
miR-20b OE

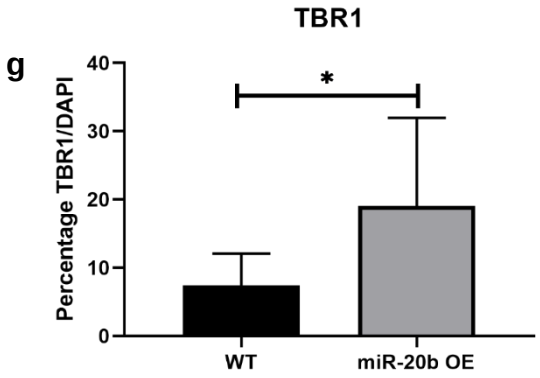
g
TBR1
Percentage TBR1/DAPI
40
30
20
10
0
*
WT
miR-20b OE

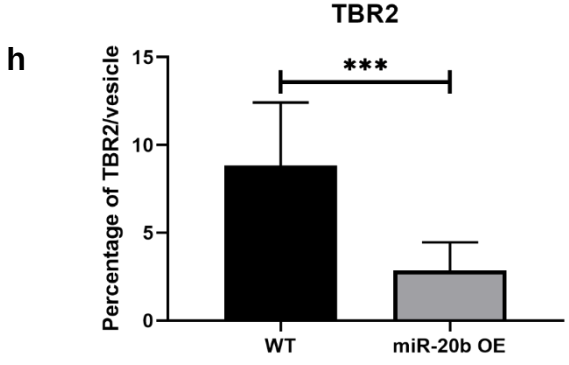
h
TBR2
Percentage of TBR2/vesicle
15
10
5
0
***
WT
miR-20b OE

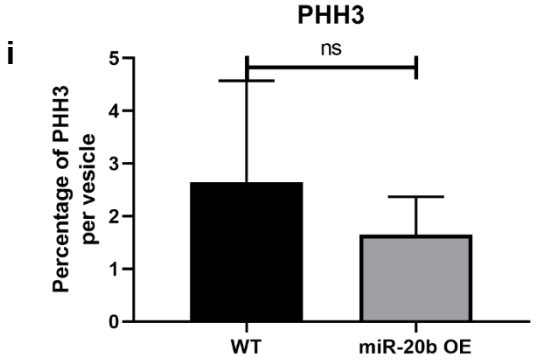
i
PHH3
Percentage of PHH3 per vesicle
5
4
3
2
1
0
ns
WT
miR-20b OE

Figure 24: Cytoarchitectural differences among NSCs/ IPs, and neurons in wildtype and overexpressing organoids.

a) Immunostaining images of SOX2/DCX in day 30 wild type and miR-20b overexpressing organoids. Note that the expression of stem cell marker (SOX2) is unaffected but there is a clear cytoarchitecture difference as wild type organoids displayed large vesicles while the overexpressing organoids have shown rosettes and larger vesicles. Immature neuron marker DCX expression is upregulate but not significant in overexpressing organoids. (Scale bar:100µm)
b) Immunostaining images of PAX6/TBR1 (bottom) in day 30 organoids. Note expression of PAX6 is lower in miR-20b overexpressing organoids while there is an increase in early born TBR1+ neurons (Scale bar:100µm)
c) Immunostaining images of PAX6/FOXG1 (top) along with their respective DAPI (bottom) as a separate channel for both wild type and miR-20b overexpressing organoids (Scale bar: 100 µm). Note that the expression of PAX6 and FOXG1 is mostly cytoplasmic in overexpressing organoids so for better visualization DAPI is kept as a separate channel.
d) Immunostained images of TBR2/CAS (top), and P-VIM/PHH3 (bottom) expression in day 30 WT and overexpressing organoids. Note the number of TBR positive basal intermediate population diminishes in miR-20b overexpressing organoids along with decrease in the proliferation markers. (Scale bar:100µm)
e) Immunostaining images for SOX2/PTN (top) and SOX2/NFIA (bottom), upregulated genes in the miR-20b overexpressing organoids using molecular analysis. (Scale bar:200µm)
f) Quantitative analysis of area of SOX2+ ventricular zone (VZ) in both wild type and miR-20b overexpressing organoids. Note: miR-20b overexpressing organoids have smaller area of ventricular zone as compared to wild type. Statistics: Bars represent mean ± S.E. Statistical test: t-test: *$P < 0.05$; **$P < 0.01$ ***$P < 0.001$; ****$P < 0.0001$.
g) Quantitative analysis of percentage of deep layer neurons TBR1+ cells per vesicle in both wild type and miR-20b overexpressing organoids. Note: miR-20b overexpressing organoids have more percentage of TBR1+ neurons as compared to wild type. Statistics: Bars represent mean ± S.E. Statistical test: t-test: *$P < 0.05$; **$P < 0.01$ ***$P < 0.001$; ****$P < 0.0001$.
h) Quantitative analysis of percentage of TBR2+ cells per vesicle in both wild type and miR-20b overexpressing organoids. Note: miR-20b overexpressing organoids showed decrease in the percentage of TBR2+ population as compared to wild type. Statistics: Bars represent mean ± S.E. Statistical test: t-test: *$P < 0.05$; **$P < 0.01$ ***$P < 0.001$; ****$P < 0.0001$.
i) Quantitative analysis of percentage of PHH3+ cells per vesicle in both wild type and miR-20b overexpressing organoids. Note: No significant change in the percentage of PHH3 in both miR-20b overexpressing and wild type organoids.

3.8 Single cell transcriptome analysis of day 50 miR-20b overexpressing organoids display emergence of caudal cortical fates such as cortical hem derived hippocampal as well as choroid plexus fates

To further comprehend the long-term effect of over represented WNT and BMP signalling molecules in day 13 cortical organoids we analysed day 50 organoids using scRNA sequencing for both wild type and miR-20b overexpression. First, we identified a greater number of clusters in miR-20b overexpressing organoids (15 clusters) as compared to wild type (10 clusters). We then assigned these clusters based on specific set of marker genes. In wild type organoids, we found a majority of FOXG1 expressing telencephalic cell types (~80%) as well as non-telencephalic, posterior brain regional cell types (5%), which included NSCs expressing IRX2 and PAX3, and posterior neurons (10%) expressing TCF7L2, PAX3 and DCX. We also found one mesenchymal cluster with cells expressing DCN and LUM as well as schwann cells expressing SOX10, MPZ and S100B. Furthermore, among the telencephalic brain regional cells, we found both cortical (~76%) and hippocampal (~4%) cell types representing dorsal and medial pallium, respectively. Within FOXG1 expressing cortical cell types, we found ~40% of NSCs and 25% of cortical neurons. Among cortical NSCs, both dividing (PAX6, SOX2, HES5, CCND1, TOP2A, and MKI67) and non-dividing (PAX6, SOX2, HES5) NSCs were identified. In addition to NSCs we also found basal intermediate cell populations expressing TBR2/EOMES (5%) as well as different cortical neuronal types (20%) such as TBR1 expressing deep layer neurons, TP73 and REELIN expressing Cajal-Retzius neurons (5%) belonging to the marginal zone (Figure 25a,b,e). Finally, we also found hippocampal stem cells (~4%) marked by the presence of genes such as RSPO2, RSPO3, WLS and OTX2.

In contrast, in miR-20b overexpressing organoids we observed a dramatic decrease in the number of cortical cells (~4%). Among them, we found 1 cluster only representing NSCs (~2% only), compared to 7 in wild type, and another single IP cell cluster (1% only), compared to 2 clusters in wild type. Additionally, there was also decrease in the cortical neuronal cluster (<1% only), as compared to 4 clusters in wild type. Furthermore, we observed 6 clusters of posterior NSCs (26%) as compared to one cluster in wild type organoids. Interestingly, we identified one cluster of hippocampal intermediate progenitor (LMX1A and TBR2) cluster only in miR-20b overexpressing organoids. Finally, we strikingly identified 9 clusters of choroid plexus (35%) populations marked by TTR, RSPO3, OTX2, EMX2, WLS, FOXJ1, PIFO and

CLIC6 in miR-20b overexpressing organoids (Figure 25b,d,e). Taken together, these results indicate that the wild type organoids are cortical in identity while miR-20b overexpressing organoids largely consist of choroid plexus (ChP) and hippocampal cell populations along with other posterior cell types.

We next looked deeper into these sparse group of cortical NSC population and observed an upregulation of cortical hem/hippocampal (RSPO3/2, WLS, and WNT7B) and choroid plexus marker genes such as TTR and OTX2, along with approximately 2-fold reduction of cortical genes such as FOXG1, PAX6, HES5, and LHX2. (Figure 25c,d,and f), suggesting presence of confused NSC population consisting of mixed identity of cortical and caudal cortical (hippocampal and choroid plexus) fates, in turn might be a source for choroid plexus cell types in miR-20b overexpressing organoids.

a

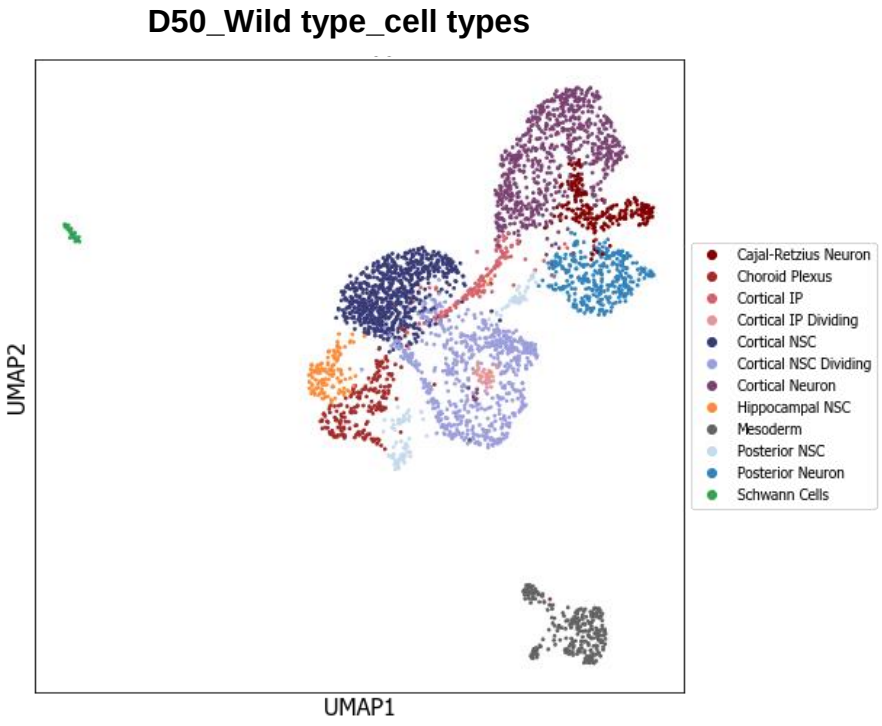

b

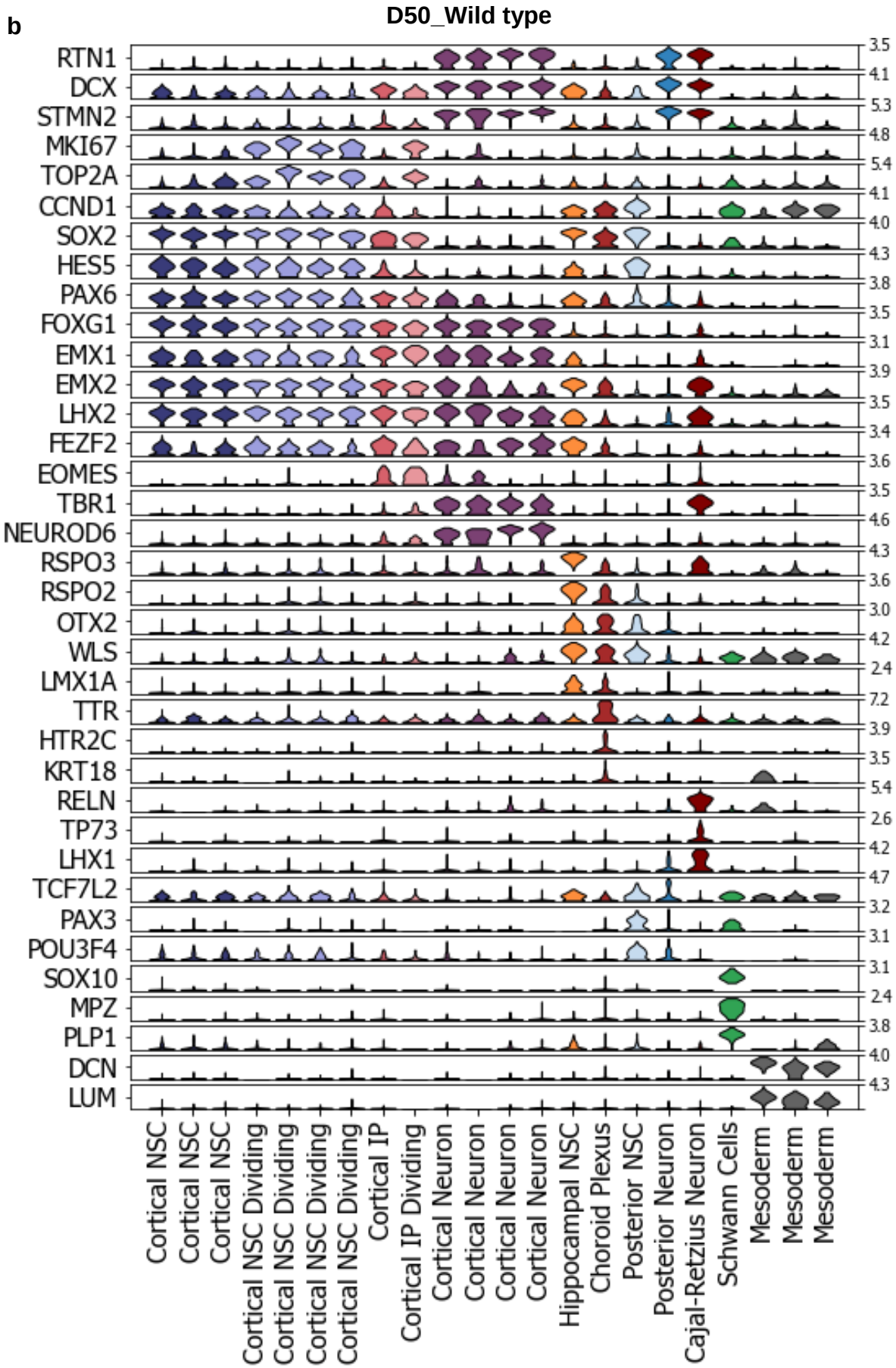
D50_Wild type
RTN1
DCX
STMN2
MKI67
TOP2A
CCND1
SOX2
HES5
PAX6
FOXG1
EMX1
EMX2
LHX2
FEZF2
EOMES
TBR1
NEUROD6
RSPO3
RSPO2
OTX2
WLS
LMX1A
TTR
HTR2C
KRT18
RELN
TP73
LHX1
TCF7L2
PAX3
POU3F4
SOX10
MPZ
PLP1
DCN
LUM
3.5
4.1
5.3
4.8
5.4
4.1
4.0
4.3
3.8
3.5
3.1
3.9
3.5
3.4
3.6
3.5
4.6
4.3
3.6
3.0
4.2
2.4
7.2
3.9
3.5
5.4
2.6
4.2
4.7
3.2
3.1
3.1
2.4
3.8
4.0
4.3
Cortical NSC
Cortical NSC
Cortical NSC
Cortical NSC Dividing
Cortical NSC Dividing
Cortical NSC Dividing
Cortical NSC Dividing
Cortical IP
Cortical IP Dividing
Cortical Neuron
Cortical Neuron
Cortical Neuron
Cortical Neuron
Hippocampal NSC
Choroid Plexus
Posterior NSC
Posterior Neuron
Cajal-Retzius Neuron
Schwann Cells
Mesoderm
Mesoderm
Mesoderm

c

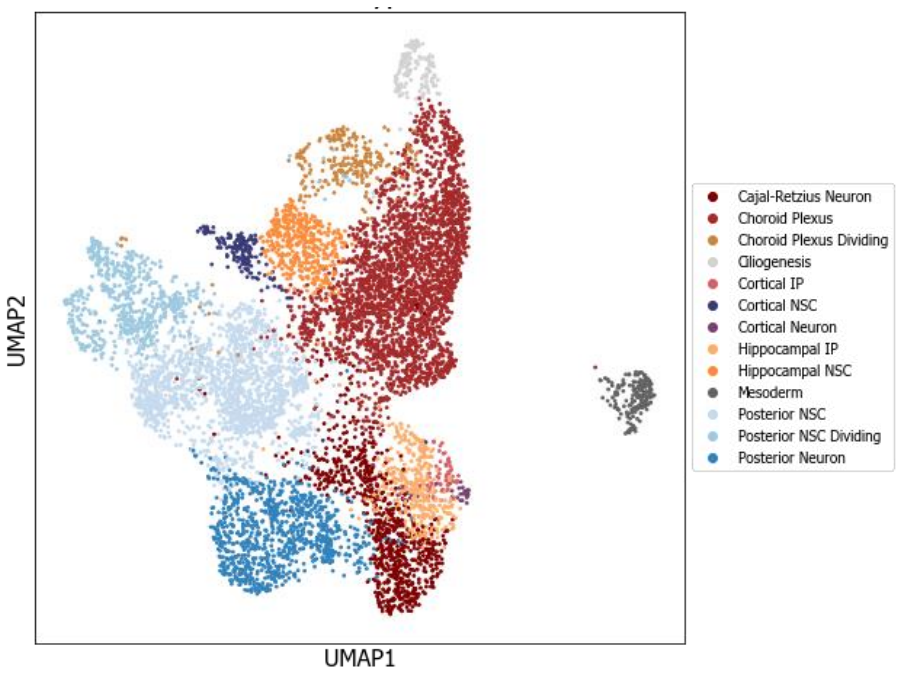
D50_miR-20b OE_cell types
UMAP2
UMAP1
Cajal-Retzius Neuron
Choroid Plexus
Choroid Plexus Dividing
Ciliogenesis
Cortical IP
Cortical NSC
Cortical Neuron
Hippocampal IP
Hippocampal NSC
Mesoderm
Posterior NSC
Posterior NSC Dividing
Posterior Neuron

D50_miR-20b OE

d

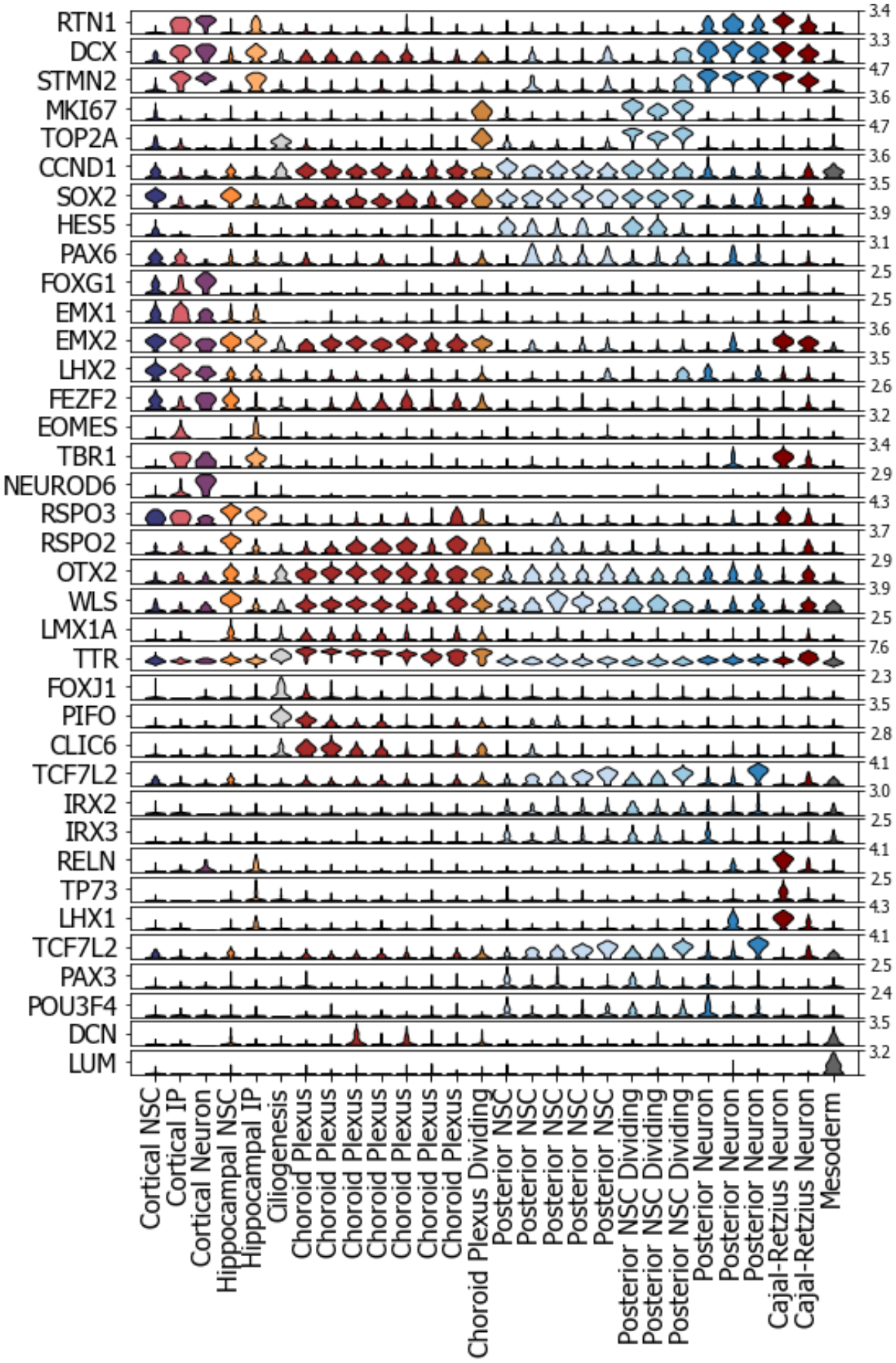

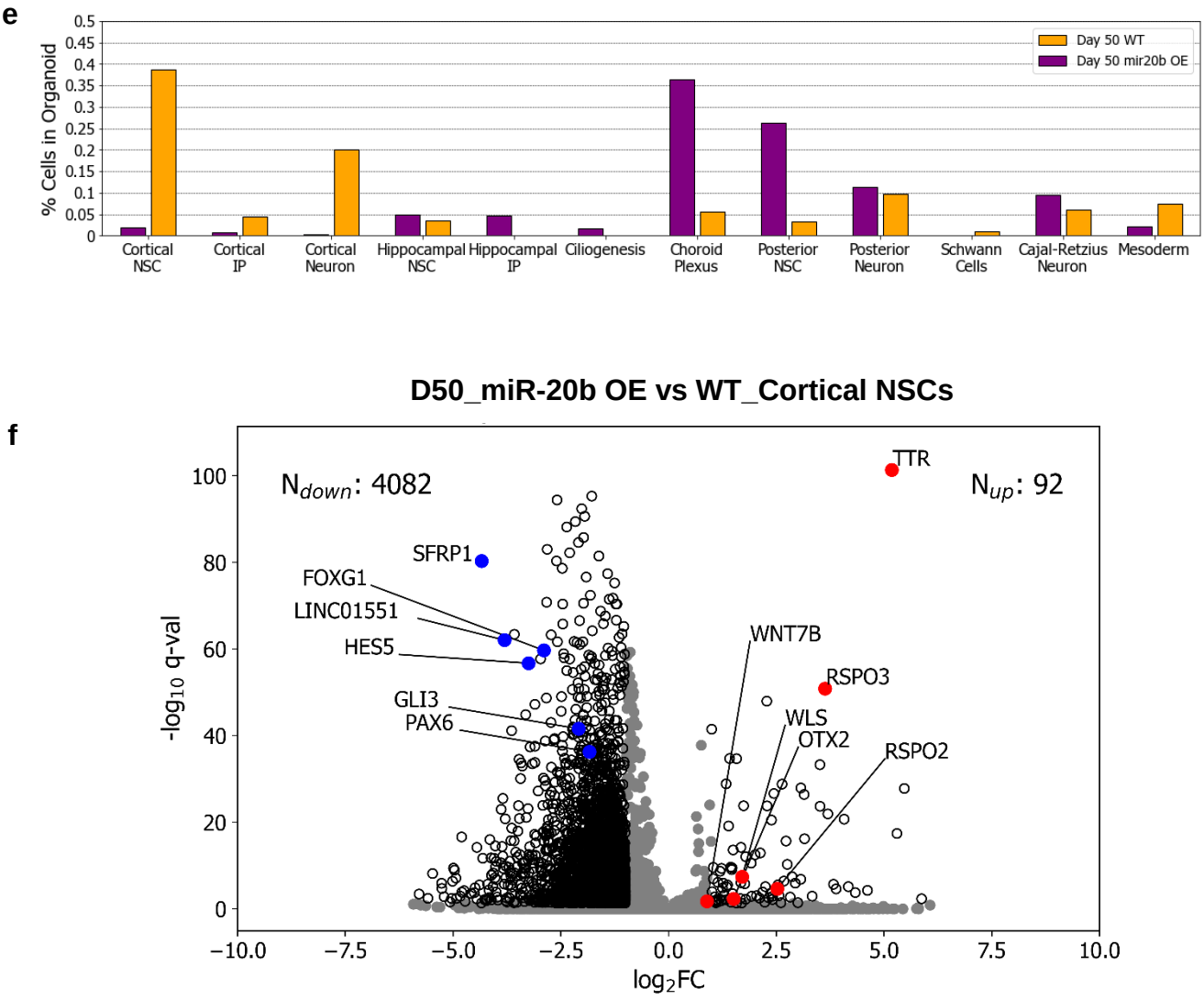

Figure 25: **Single cell RNA Sequencing reveals caudalization of miR-20b overexpressing towards hippocampal and Choroid plexus fates**

a) Uniform Manifold Approximation and Projection (UMAP) plot for single cell RNA sequencing data of day 50 wild type organoids with distinct clusters and associated cell types defined based on specific marker genes highlighted in different colors.

b) Stacked violent plot showing relative expression of selected differentially expressed genes across different cell types in wild type day 50 organoids.

c) Uniform Manifold Approximation and Projection (UMAP) plot for single cell RNA sequencing data of Day 50 miR-20b overexpressing organoids with distinct clusters and associated cell types defined based on specific marker genes highlighted in different colors.

d) A violin plot depicting relative expression of selected differentially expressed genes across different cell types in miR-20b overexpressing organoids.

e) Bar plot-showing percentage of cells in wild type and miR-20b overexpressing organoids for different cell types. Note emergence of choroid plexus identity cells in miR-20b overexpressing organoids.
f) Volcano plot depicting the upregulated caudal genes (red) and downregulated cortical genes (blue) in cortical NSCs for miR-20b overexpressing as compared to wild type organoids.

3.9 miR-20b overexpressing organoids exhibited an emergence of choroid plexus and hippocampal cell types in later stage of development

To gain insight into the cytoarchitecture of these organoids we performed a series of immunostainings. First, we stained for cortical marker combination PAX6 and FOXG1 and found a few cells expressing PAX6 alongside many cells displaying background levels of FOXG1 and/or PAX6 (Figure 26), indicating the absence of cortical cells. We stained with the stem cell marker SOX2, the hippocampal stem cell marker LMX1A and the Choroid plexus marker TTR. We found one rosette-like population expressing high levels of SOX2 together with LMX1A, potentially marking medial telencephalic NSCs, while another population expressing low SOX2/high LMX1A together with TTR appeared along expanded single cell layer vesicles, marking developing choroid plexus cells (Figure 26), and in agreement with the expression of these markers *in vivo* from mouse Allen brain atlas. Interestingly, we observed that thick vesicles (SOX2+/LMX1A+) present at the core of the thin single layer epithelial cells (LMX1A+/TTR+) (Figure 26), mimicking the *in vivo* cytoarchitecture from mouse brain. Altogether, these immunostainings confirmed our transcriptomic data showing the emergence of choroid plexus (ChP) and hippocampal populations in the miR-20b overexpressing organoids.

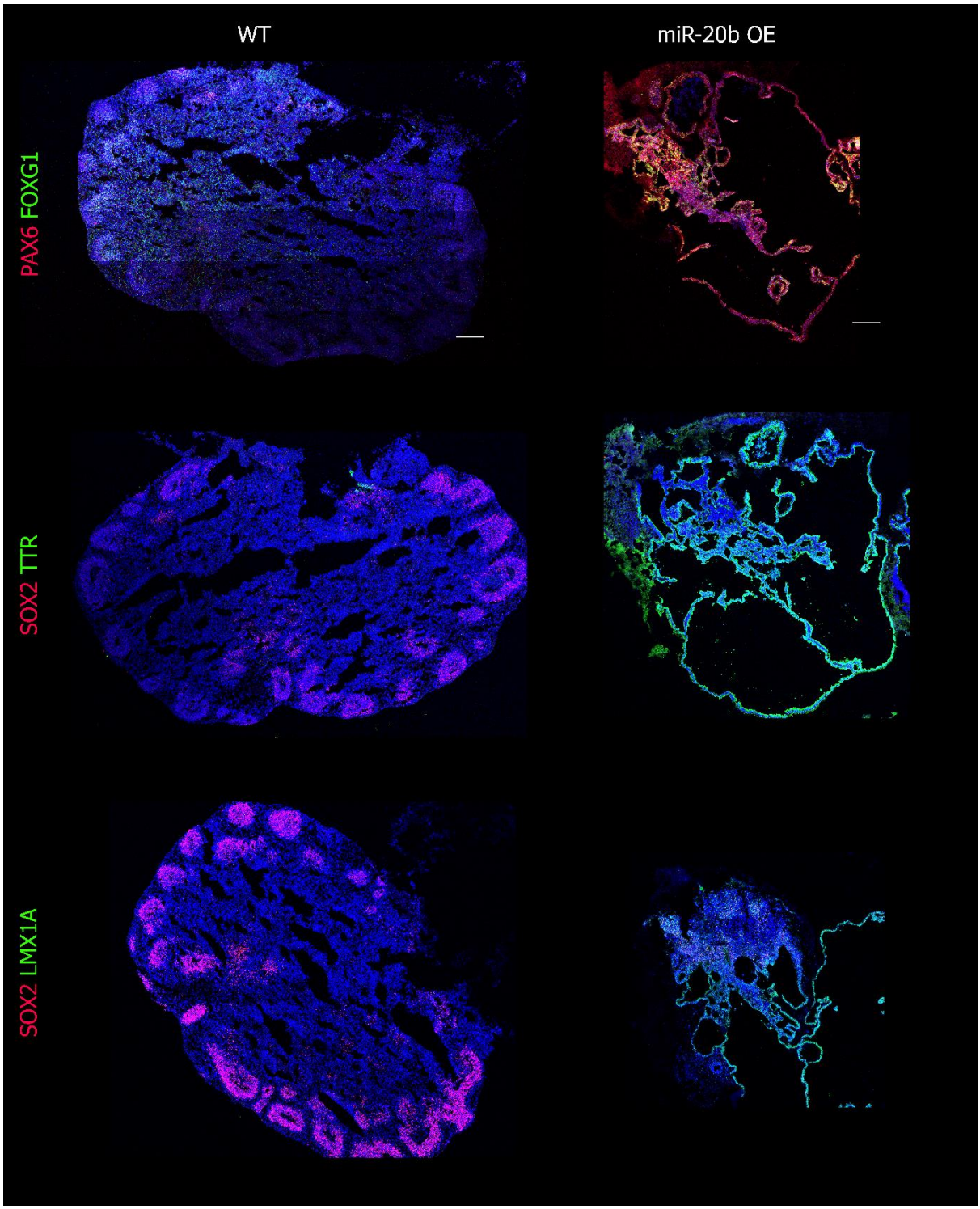

Figure 26: Emergence of choroid plexuses cells in overexpressing organoids

Immunostaining images of PAX6/FOXG1 (top) in day 50 wild type and miR-20b overexpressing organoids. Note that wild type organoids displayed vesicles positive for PAX6/FOXG1 while the miR-20b overexpressing organoids displayed few PAX6+ cells and FOXG1 expression was cytosolic (background). Immunostaining images of SOX2/TTR (middle) and SOX2/LMX1A (bottom) in day 50 WT and miR-20b overexpressing organoids, which are the markers genes for choroid plexus and

hippocampal stem cells respectively. Note that single layer think vesicle is positive for TTR and LMX1A.Scale bar: 200µm.

3.10 Overexpression of miR-20b causes downregulation of its target gene CCND1 in cortical NSCs and IPs

We hypothesised that decrease in cortical NSCs and IPs are due to impairment in cell cycle kinetics, therefore we looked for miR-20b targets and found CCND1 as one of the main targets. In addition to that we looked at the CCND1 (Cyclin D1) expression in both NSCs and IPs and observed threefold downregulation in miR-20b overexpressing organoids as compared to wild type organoids (Figure 27a). It has been shown in mice that cyclin D1 plays an important role in the progression of cortical progenitors by regulating G1 cell cycle phase (Lange et al., 2009; Pilaz et al., 2009). Decrease in CCND1 expression leads to lengthening of G1 phase of cell cycle and leads to differentiation of cortical NSCs (Dehay and Kennedy, 2007; Salomoni and Calegari, 2010). To gain further insights we first looked for the correlation of CCND1 expression in different stem cells/progenitors in our wild type and miR-20b overexpressing organoids. We observed that wild type cortical NSC (dividing and non-dividing) express high levels of CCND1 along with stem cells markers such as SOX2, and HES5, while there is decrease in the CCND1 expression in miR-20b overexpressing organoids. Together with NSCs, we also checked CCND1 expression in IPs and observed very low expression in both dividing and non-dividing IPs in miR-20b overexpressing organoids as compared to wild type. There is no expression of CCND1 in cortical neurons, indicating the post-mitotic terminally differentiated nature of these cell types (Figure 27b). To confirm the transcriptional results, we then performed immunostainings of CCND1 in the miR-20b overexpressing and wild type organoids, and in turn found a global decrease in the expression of CCND1 in the miR-20b overexpressing organoids (Figure 28a).

We next decided to compensate the expression of CCND1 in these miR-20b overexpressing organoids to give them the proliferative advantage and to check whether we can revert the cell fate change observed in miR-20b overexpressing organoids. To achieve this, we generated an inducible dual expression line of miR-20b and CCND1.

a

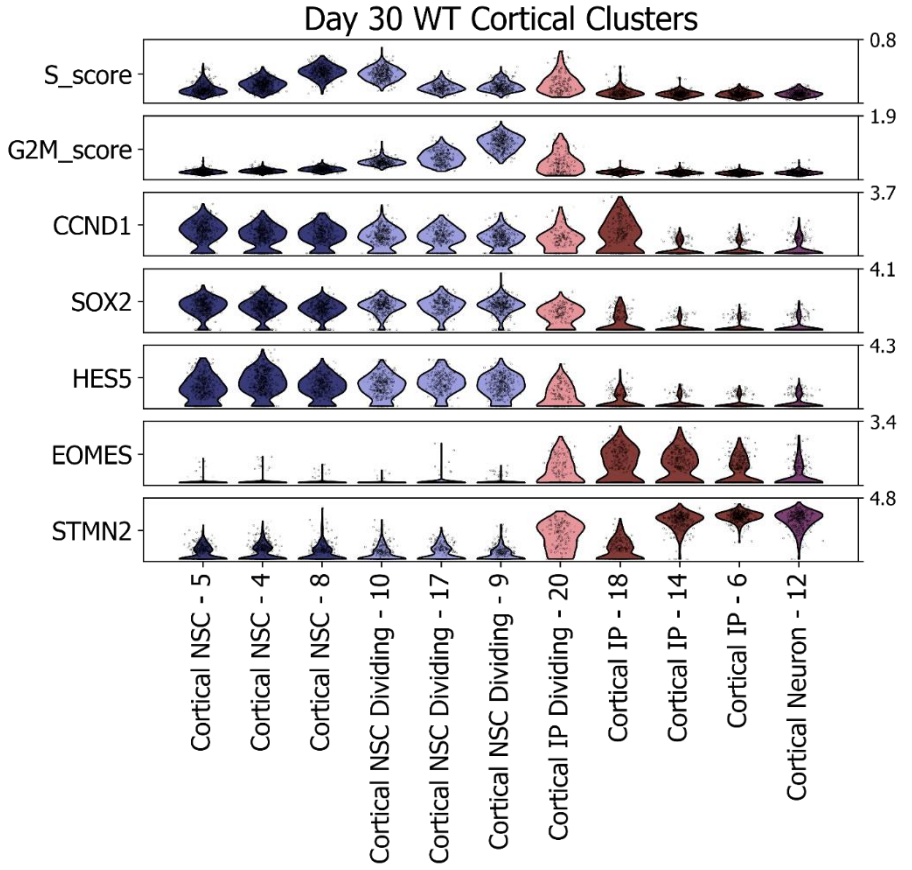
Day 30 WT Cortical Clusters
S_score
G2M_score
CCND1
SOX2
HES5
EOMES
STMN2
0.8
1.9
3.7
4.1
4.3
3.4
4.8
Cortical NSC - 5
Cortical NSC - 4
Cortical NSC - 8
Cortical NSC Dividing - 10
Cortical NSC Dividing - 17
Cortical NSC Dividing - 9
Cortical IP Dividing - 20
Cortical IP - 18
Cortical IP - 14
Cortical IP - 6
Cortical Neuron - 12

b

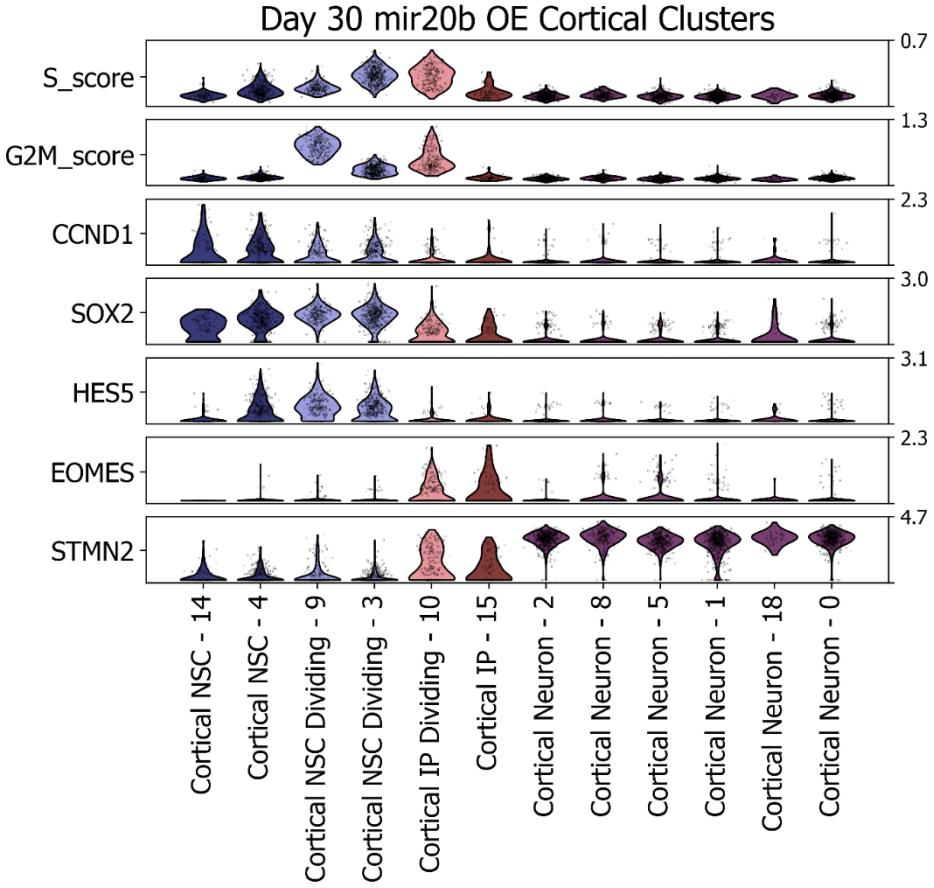
Day 30 mir20b OE Cortical Clusters
S_score
G2M_score
CCND1
SOX2
HES5
EOMES
STMN2
0.7
1.3
2.3
3.0
3.1
2.3
4.7
Cortical NSC - 14
Cortical NSC - 4
Cortical NSC Dividing - 9
Cortical NSC Dividing - 3
Cortical IP Dividing - 10
Cortical IP - 15
Cortical Neuron - 2
Cortical Neuron - 8
Cortical Neuron - 5
Cortical Neuron - 1
Cortical Neuron - 18
Cortical Neuron - 0

Figure 27: Single cell RNA-Seq analysis reveals downregulation of target gene (CCND1) of miR-20b in overexpressing organoids.

a) Violin plots depicting the expression of CCND1 along with stem cell markers (SOX2, and HES5), IPs (EOMES) and neuronal marker (STMN2) in cortical cell types for wild type day 30 organoids.
b) Violin plots depicts the expression of CCND1 along with stem cell markers (SOX2, HES5), IPs (EOMES) and neuronal marker (STMN2) genes in cortical cell types in day 30 miR-20b overexpressing organoids. Note that downregulation of CCND1 in NSCs and IPs in overexpressing organoids

3.11 Generation of inducible stable hsa-miR-20b and CCND1 expressing line

For compensating the CCND1 expression in miR-20b overexpressing cells, we used LT3-20b hiPSC line and infected them with CCND1 virus. The cells were selected and expanded and then checked for mCherry expression. We then generated organoids from this dual hiPSC line and found the percentage of cells that are double positive for eGFP and mCherry were very low. Therefore, we then decided to do induce the dual reporter line for 24 hrs with doxycycline and using FACS, we sorted two populations—one with higher GFP and mCherry, and the other with medium GFP and mCherry expression.

3.12 Rescue of the cytoarchitectural phenotype along with change in identity towards hippocampal fates in CCND1-compensating, miR-20b overexpressing organoids

We generated organoids from both of the dual reporter lines i.e., high green/mCherry, and medium green/mCherry. At day 30, organoids were fixed, cut and immunostained. We observed the rescue of rosette cytoarchitecture in medium green/mCherry CCND1-compensating, miR-20b overexpressing organoids (named as MGMM miR-20b+CCND1). These organoids consist mostly of thick vesicles/rosettes compared to the miR-20b only overexpressing organoids, which consisted of mostly single layer thin epithelial vesicles and small rosettes. Simultaneously, we analysed the high green/mCherry line (HGHM miR-20b+CCND1) and observed many single-layer thin epithelial vesicles alongside one giant pseudo-stratified vesicle. Since the HGHM miR-20b+ CCND1 overexpressing organoids cytoarchitecture resemble more closely to the mir-20b only overexpressing organoids, suggesting the dominant effect of mir-20b

over CCND1 (Figure 28a), we decided to use the MGMM miR-20b+CCND1 line for further study.

We next stained both wild type and MGMM miR-20b+CCND1 overexpressing organoids for basic markers including the neural stem cell markers SOX2 and PAX6, the immature neuronal marker DCX, as well as the early-born neuronal marker TBR1. We found no significant difference in the expression of SOX2, DCX, and TBR1 in both wild type and MGMM miR-20b+CCND1 overexpressing organoids, while the expression of PAX6 was lower in the miR-20b+CCND1 overexpressing organoids as compared to wild type (Figure 28b). To check for other telencephalic identities we then stained for FOXG1 and LMX1A, marking cortical and medial pallium cells respectively (Figure 28c). The cortical marker FOXG1 was absent in MGMM miR-20b+CCND1 overexpressing organoids compared to widespread expression in wild type organoids, whereas the hippocampal marker LMX1A was highly expressed in MGMM miR-20b+ CCND1 organoids compared to wild type, which only expressed LMX1A in a few vesicles. Next, we checked for the choroid plexus marker TTR and observed its expression only in MGMM miR-20b+CCND1 overexpressing organoids (Figure 28b). Taken together, these results indicate the presence of cortical hem/hippocampal identity in MGMM miR-20b+CCND1 overexpressing organoids.

a

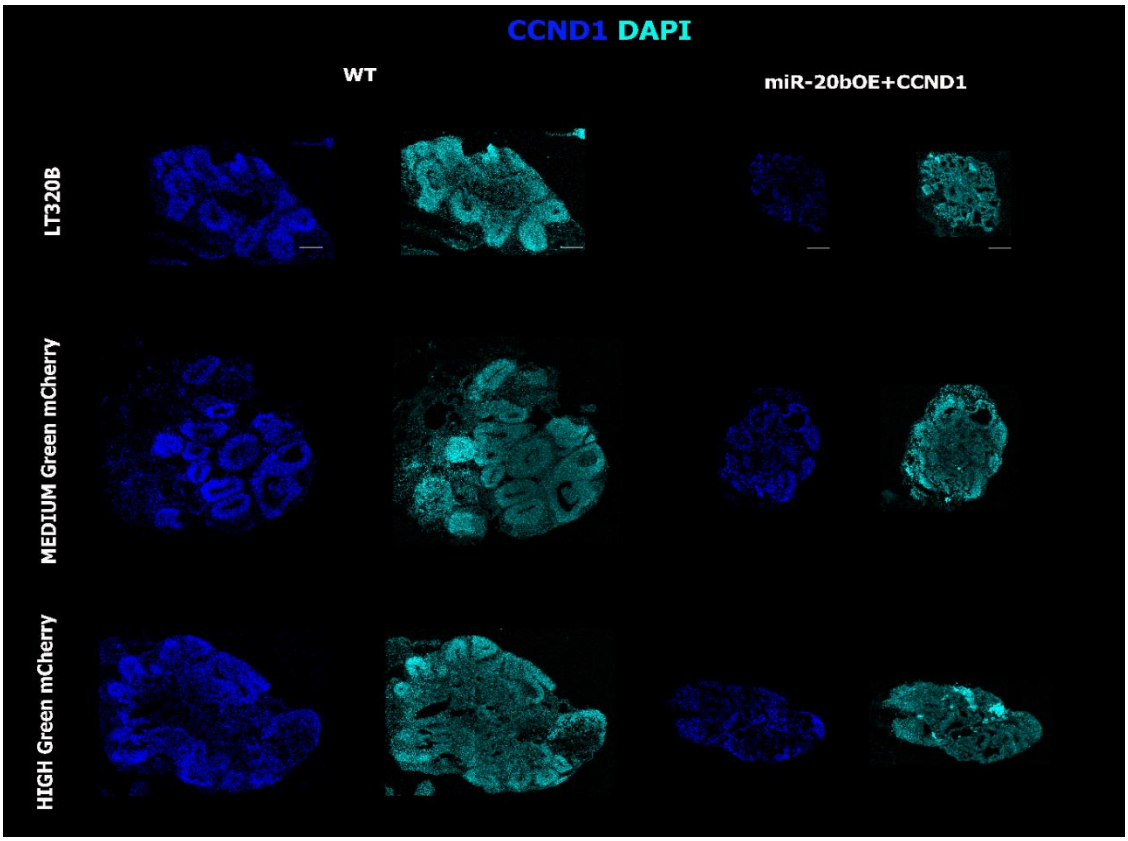

b

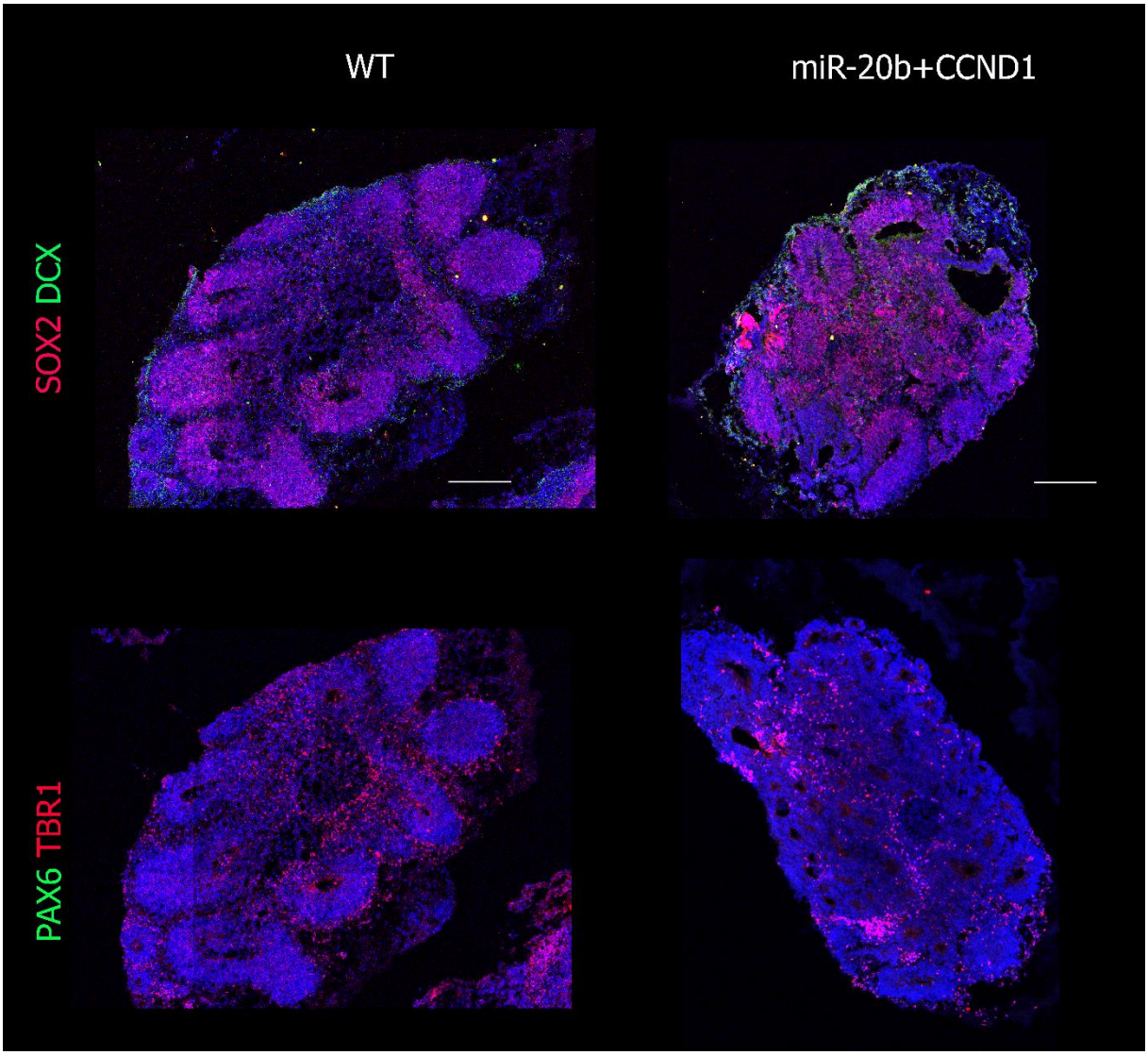

c

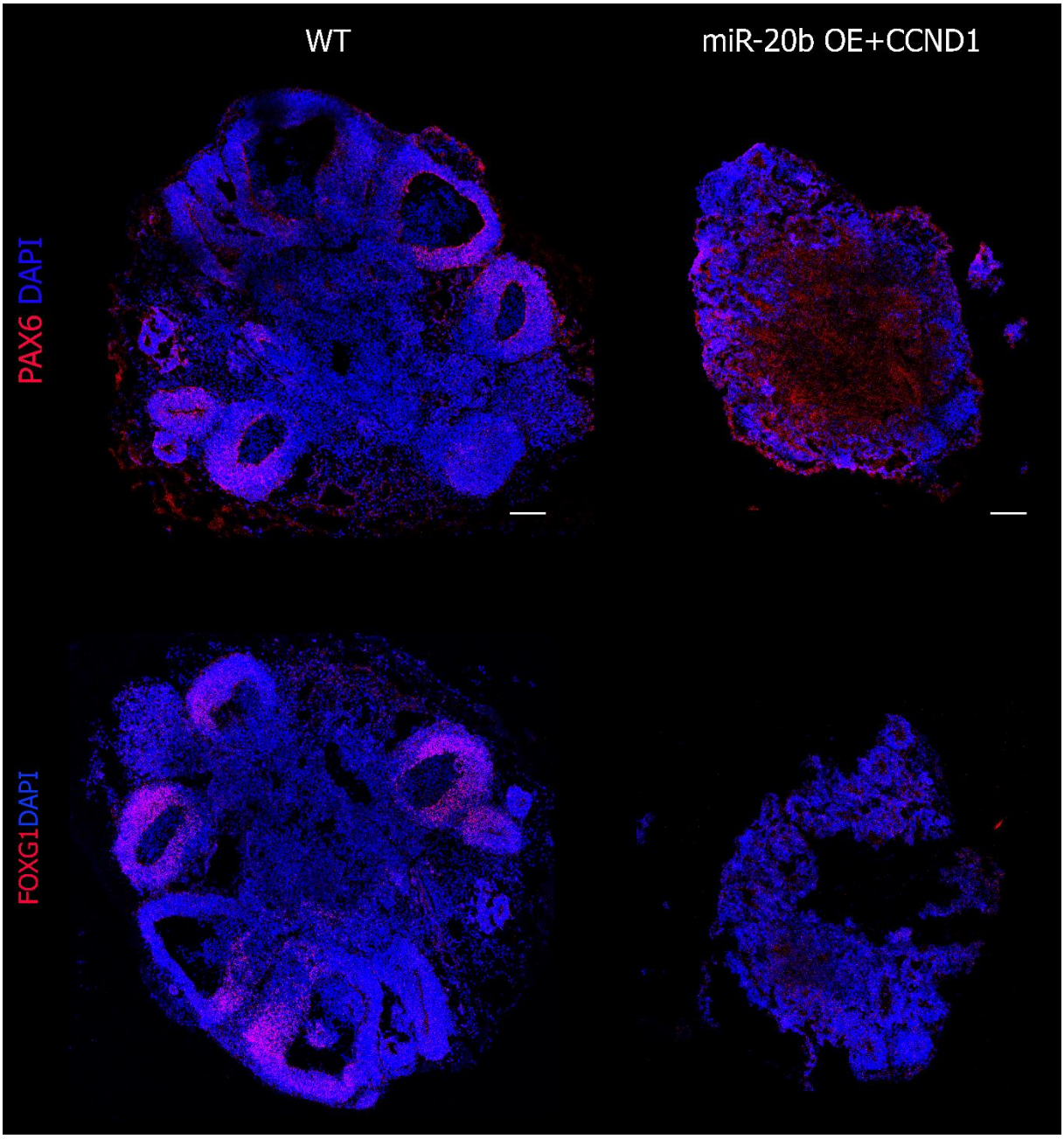

d

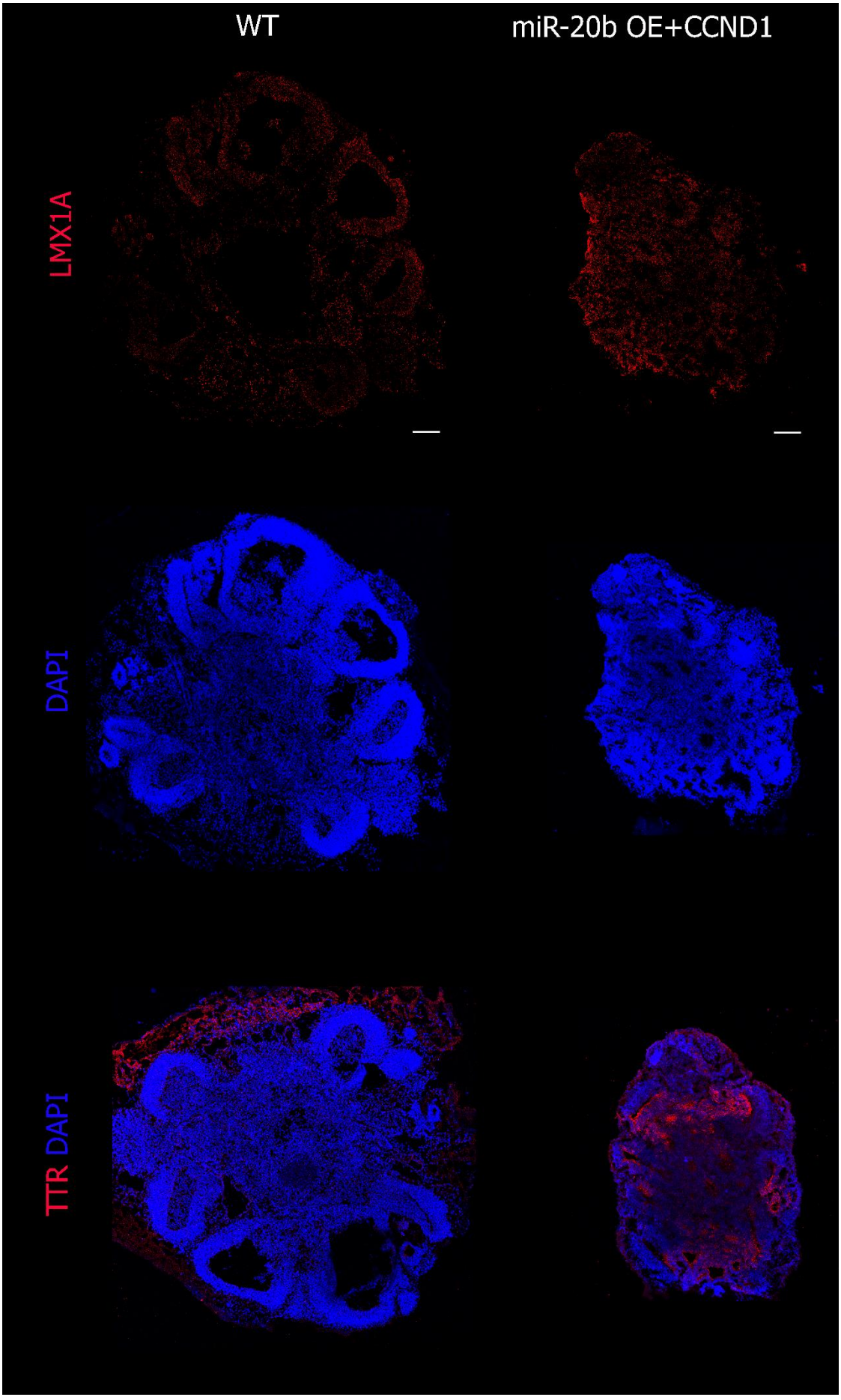
e
WT
miR-20b OE+CCND1
LMX1A
DAPI
f
TTR DAPI

Figure 28: Phenotypical rescue of the radial glial vesicles in CCND1 compensate miR-20b overexpressing organoids along with change in the identity towards hippocampal fates.

a) Immunostaining images for CCND1 marker gene along with the miR-20b reporter (green channel) and CCND1 reporter (red channel) in day 30 organoids derived under LT320b wild type and overexpressing organoids (top), MGMM miR20b+CCND1 (middle), HGMM miR20b+CCND1 organoids (low). (Scale bar: 200µm)
b) Immunostaining images for stem cell marker SOX2/DCX (top), and PAX6/TBR1 (bottom) for day 30 wild type and MGMM miR-20b+CCND1 overexpressing organoids. (Scale bar: 200µm)
c) Immunostaining images of NSC marker PAX6 in day 30 wild type and miR-20b+CCND1 overexpressing organoids. Note that wild type organoids were PAX6+ while overexpressing organoids only displayed background staining but have vesicles similar to wild type organoids.
d) Immunostaining for cortical marker FOXG1 in day 30 wild type and miR-20b+CCND1 overexpressing organoids. Note that wild type organoids were only FOXG1+.
e) Immunostaining images of hippocampal marker LMX1A (top) and respective DAPI (middle) in day 30 WT and miR-20b+CCND1 overexpressing organoids. Note that there is upregulation of LMX1A in the overexpressing organoids as compared to wild type. (Scale bar: 200µm)
f) Immunostaining images of choroid plexus marker TTR in day 30 wild type and miR-20b+CCND1 overexpressing organoids. (Scale bar: 200µm)

3.13 Single Cell RNA sequencing reveals significant increase in hippocampal stem cell populations in CCND1-compensating miR-20b overexpressing organoids

Next, we employed single cell RNA sequencing for MGMM miR-20b+CCND1 overexpressing and wildtype organoids in better understand the phenotypic changes. We clustered the cells of both wild type and miR20b+CCND1 overexpressing organoids separately and assigned these clusters to a biological cell type based on marker gene expression. In total, we found 10 cell types in wild type organoids and 7 cell types in MGMM miR-20b+CCND1 organoids (Figure 29 a,c). We found 5 cortical NSC clusters in wild type organoids, comprising 40% of all cells, whereas we found only 1 cortical NSC cluster comprising merely 2% of all cells in MGMM miR-20b+CCND1 organoids (Figure 29 b,d,e,and f). Moreover, cortical IPs and cortical neurons were exclusively present in wild type organoids (Figure 29b). This suggests that compensation of CCND1 halts precocious differentiation of cortical NSCs towards neurons, which is in line with previous studies. For example, Ghosh and colleagues demonstrated that overexpression of cyclin D1 in cortical progenitors inhibits the

transition of NSCs from proliferation to neuronal differentiation in the mouse brain (Ghosh et al., 2014).

Additionally, we also found other cell types exclusive to wild type such as posterior NSCs (mid/hindbrain), schwann cells and mesodermal cells similar to what we have observed previously with miR-20b wildtype organoids. Interestingly, we observed an enormous increase in the number of hippocampal NSC clusters expressing RSPO3, LMX1A and OTX2 and their relative percentage in MGMM miR-20b+CCND1 overexpressing organoids (8 clusters, 68% population) compared to wild type organoids (1 cluster, 2% population) (Figure 29 b,c,e,and f). Alongside the increased hippocampal NSC populations in MGMM miR-20b+CCND1 organoids, we also observed the presence of choroid plexus cells expressing TTR and LMX1A, which were absent in wild type organoids. Taken together, these findings indicate the overwhelming enrichment of a hippocampal identity in MGMM miR-20b+CCND1 organoids.

a

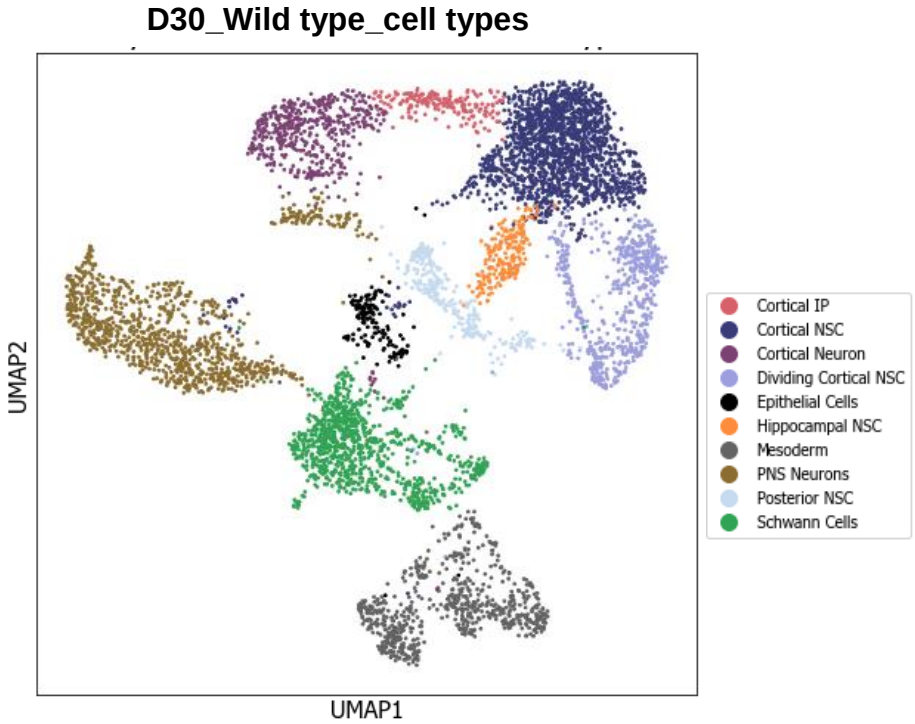

b

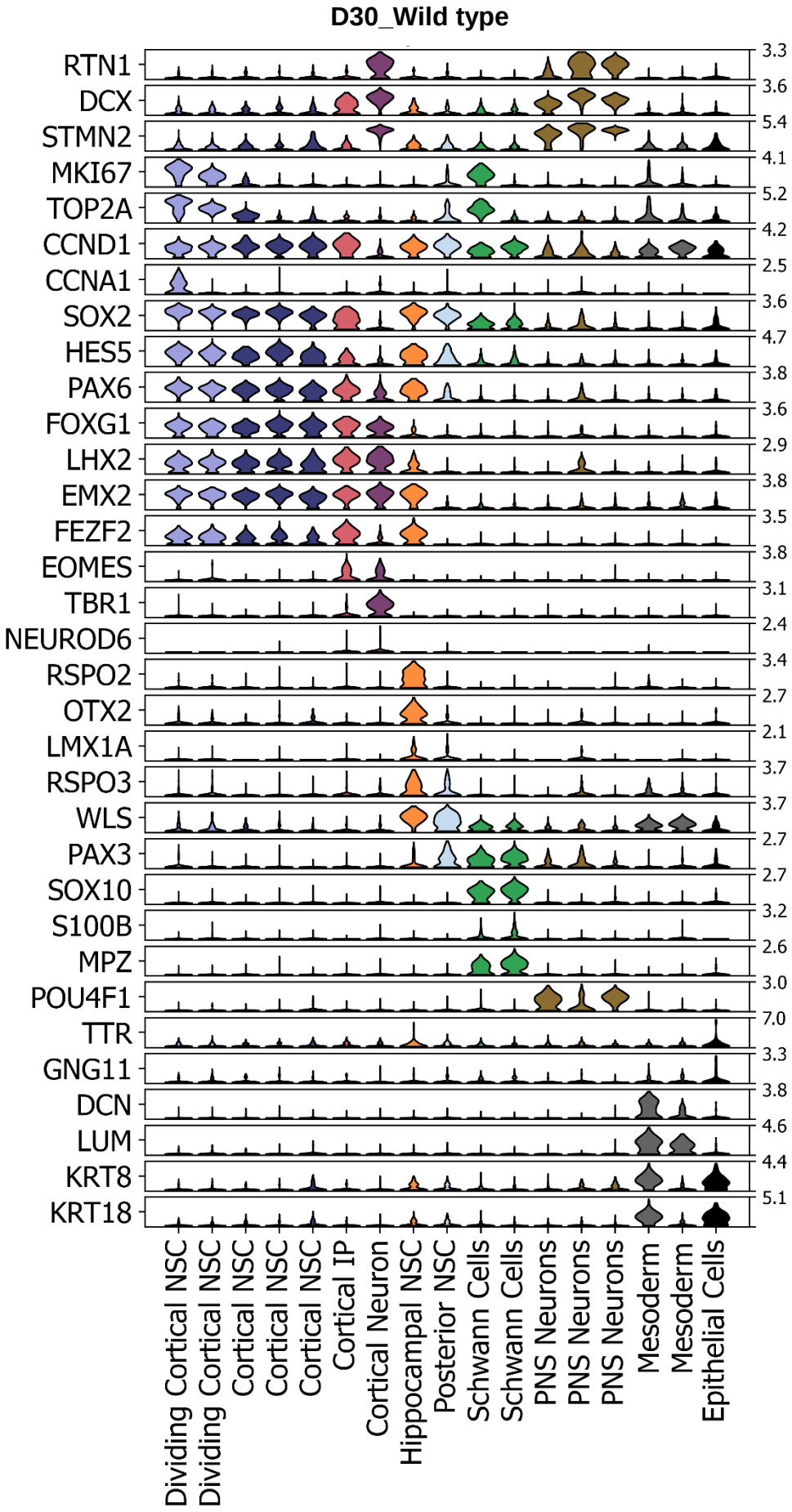
D30_Wild type
RTN1
DCX
STMN2
MKI67
TOP2A
CCND1
CCNA1
SOX2
HES5
PAX6
FOXG1
LHX2
EMX2
FEZF2
EOMES
TBR1
NEUROD6
RSPO2
OTX2
LMX1A
RSPO3
WLS
PAX3
SOX10
S100B
MPZ
POU4F1
TTR
GNG11
DCN
LUM
KRT8
KRT18
3.3
3.6
5.4
4.1
5.2
4.2
2.5
3.6
4.7
3.8
3.6
2.9
3.8
3.5
3.8
3.1
2.4
3.4
2.7
2.1
3.7
3.7
2.7
2.7
3.2
2.6
3.0
7.0
3.3
3.8
4.6
4.4
5.1
Dividing Cortical NSC
Dividing Cortical NSC
Cortical NSC
Cortical NSC
Cortical NSC
Cortical IP
Cortical Neuron
Hippocampal NSC
Posterior NSC
Schwann Cells
Schwann Cells
PNS Neurons
PNS Neurons
PNS Neurons
Mesoderm
Mesoderm
Epithelial Cells

c

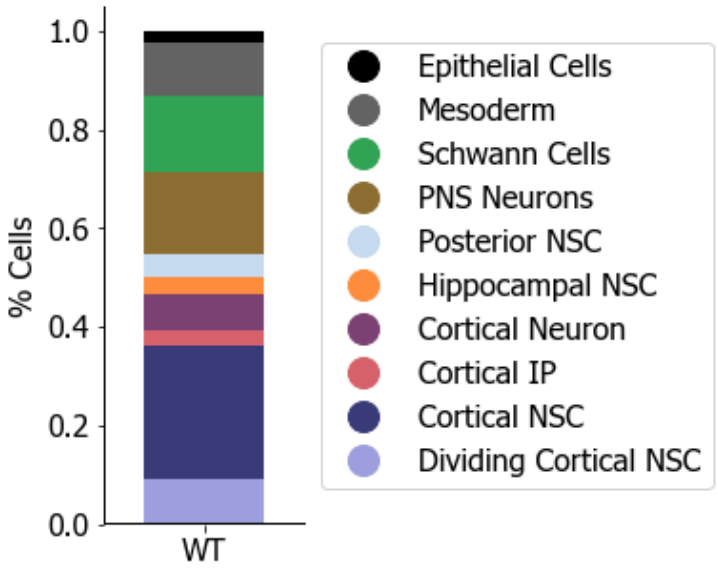
1.0
0.8
0.6
0.4
0.2
0.0
% Cells
WT
Epithelial Cells
Mesoderm
Schwann Cells
PNS Neurons
Posterior NSC
Hippocampal NSC
Cortical Neuron
Cortical IP
Cortical NSC
Dividing Cortical NSC

d

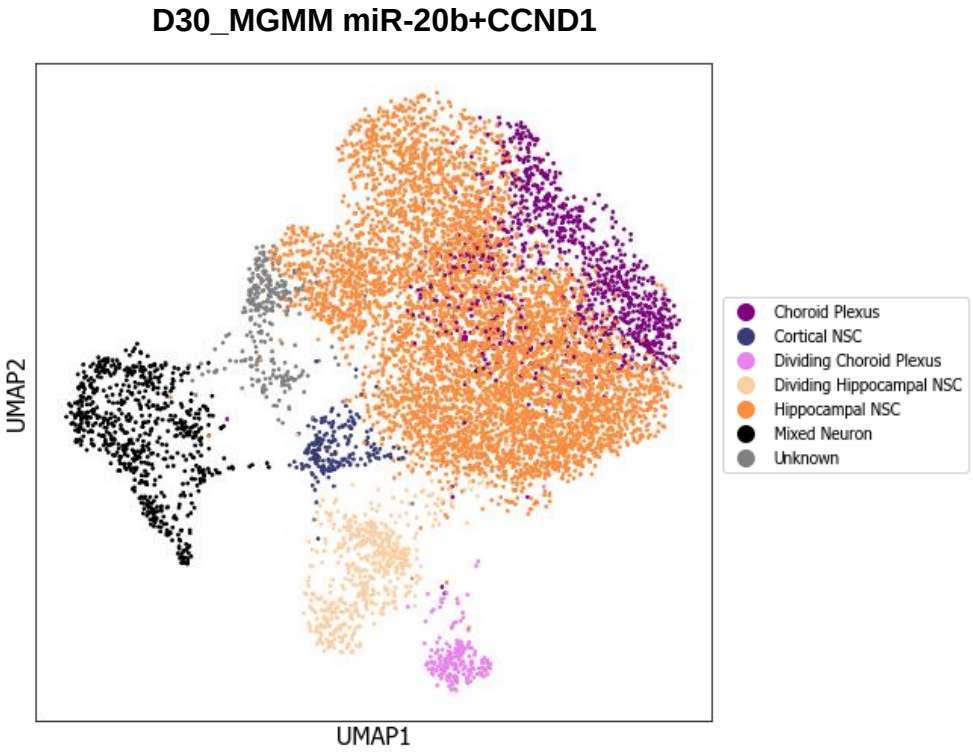
D30_MGMM miR-20b+CCND1
UMAP2
UMAP1
Choroid Plexus
Cortical NSC
Dividing Choroid Plexus
Dividing Hippocampal NSC
Hippocampal NSC
Mixed Neuron
Unknown

e

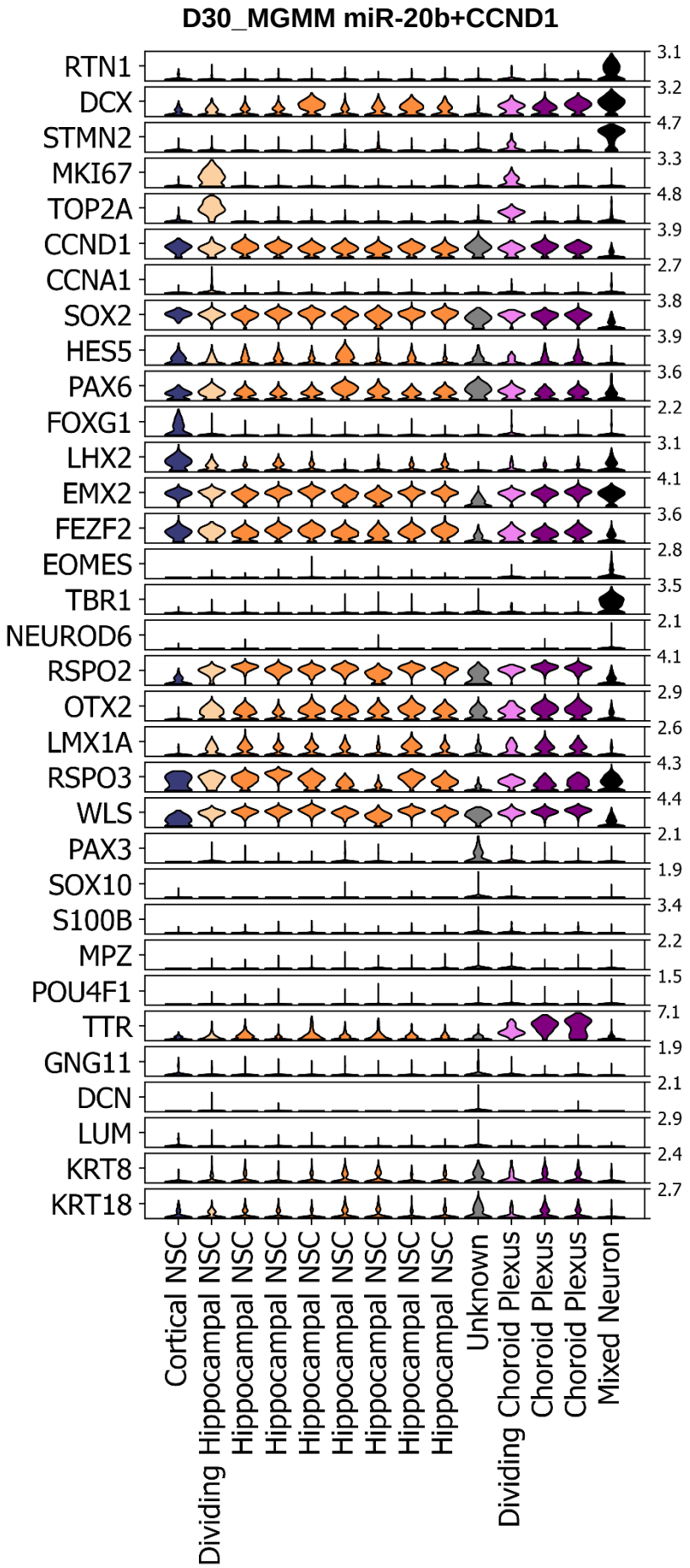
D30_MGMM miR-20b+CCND1
RTN1 3.1
DCX 3.2
STMN2 4.7
MKI67 3.3
TOP2A 4.8
CCND1 3.9
CCNA1 2.7
SOX2 3.8
HES5 3.9
PAX6 3.6
FOXG1 2.2
LHX2 3.1
EMX2 4.1
FEZF2 3.6
EOMES 2.8
TBR1 3.5
NEUROD6 2.1
RSPO2 4.1
OTX2 2.9
LMX1A 2.6
RSPO3 4.3
WLS 4.4
PAX3 2.1
SOX10 1.9
S100B 3.4
MPZ 2.2
POU4F1 1.5
TTR 7.1
GNG11 1.9
DCN 2.1
LUM 2.9
KRT8 2.4
KRT18 2.7
Cortical NSC
Dividing Hippocampal NSC
Hippocampal NSC
Hippocampal NSC
Hippocampal NSC
Hippocampal NSC
Hippocampal NSC
Hippocampal NSC
Hippocampal NSC
Unknown
Dividing Choroid Plexus
Choroid Plexus
Choroid Plexus
Mixed Neuron

f

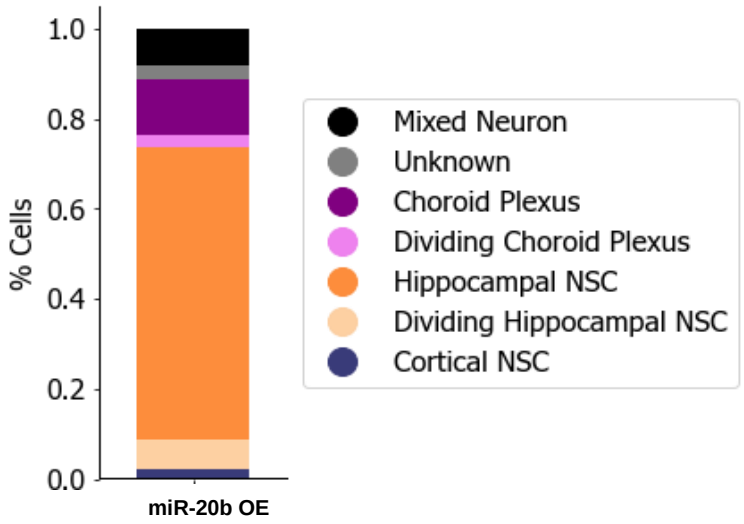

Figure 29: Single cell RNA Sequencing displayed the emergence of hippocampus stem cell population in day 30 CCND1 compensating miR20b overexpressing organoids

a) Uniform Manifold Approximation and Projection (UMAP) plot for single cell RNA sequencing data of day 30 wild type organoids with distinct clusters and associated cell types defined based on specific marker genes highlighted in different colors.

b) Stacked violin plot showing relative expression of selected differentially expressed genes across different cell types in wild type day 30 organoids.

c) Stacked bar plot showing percentage of cells in wild type organoids. Note wild type organoids contains both cortical and non-cortical fates.

d) Uniform Manifold Approximation and Projection (UMAP) plot for single cell RNA sequencing data of day 30 MGMM miR-20b+CCND1 overexpressing organoids with distinct clusters and associated cell types defined based on specific marker genes highlighted in different colors.

e) Stacked violin plot depicting relative expression of selected differentially expressed genes across different cell types in miR-20b overexpressing organoids.

f) Stacked bar plot showing percentage of cells in miR-20b+CCND1 overexpressing organoids. Note emergence of hippocampus stem cell identity in miR-20b overexpressing organoids.

3.14 Over expression of miR-20b induces an early ectoderm fate in 2D monolayer neural differentiation system

Along with cerebral organoids, we used 2D monolayer matrigel platform to understand the role of miR-20b in early neural differentiation. We induced the miR-20b expression at early days (d2) of neural induction using inhibitor-free (No treatment) and Triple-i (SBNX) paradigms, and then analyzed these cells at day 6 and day 8 of neural induction. We then performed immunostainings for early ectoderm markers of both No treatment (NT) and SBNX induced neural differentiation cells. We first co-stained for

stem cell marker SOX2 along with the early ectoderm marker TFAP2A. We observed that NT wildtype condition consists of two kinds of population islands with SOX2+/TFAP2A- and SOX2-/TFAP2A+ expression pattern, while the miR-20b overexpressing consists of homogenous double positive population without any isolated island like population (Figure 30a). In Triple-i, we observed only SOX2+ cells but not TFAP2A+ cells. This might be due to the addition of inhibitors (SBNX) which caused the cells to directly differentiate into cortical fates. To check whether these cells are cortical in identity we next stained for PAX6 marker in both NT and SBNX derived cultures. We found that in NT both wild type and miR-20b overexpressing cells does not have PAX6 expression while in SBNX condition wild type has stronger PAX6 expression as compared to its respective miR-20b overexpressing cells. This indicates that in SBNX, at day 6 of differentiation cells were already attained cortical identity. Then, we checked for the expression of PAX6 in day 8 of differentiation under NT and observed that wild type cells have shown PAX6 expression while miR-20b overexpressing cells does not have any expression suggesting non-neural identities (Figure 30b). Therefore, these staining suggests that miR-20b overexpression causes the cells to stuck in early stage of ectoderm differentiation as they are indeed positive for both SOX2 and TFAP2A and negative for neural PAX6. These results suggest that during differentiation towards neural lineage, there might be a stage where the progenitors are both SOX2 and TFAP2A positive and have the bi-potential to become SOX2+/TFAP2A- (neuroectoderm) or TFAP2A+/SOX2- (Neural crest and non-neural ectoderm) cell types. Further experiments are required to prove the presence of SOX2/TFAP2A progenitor cell population.

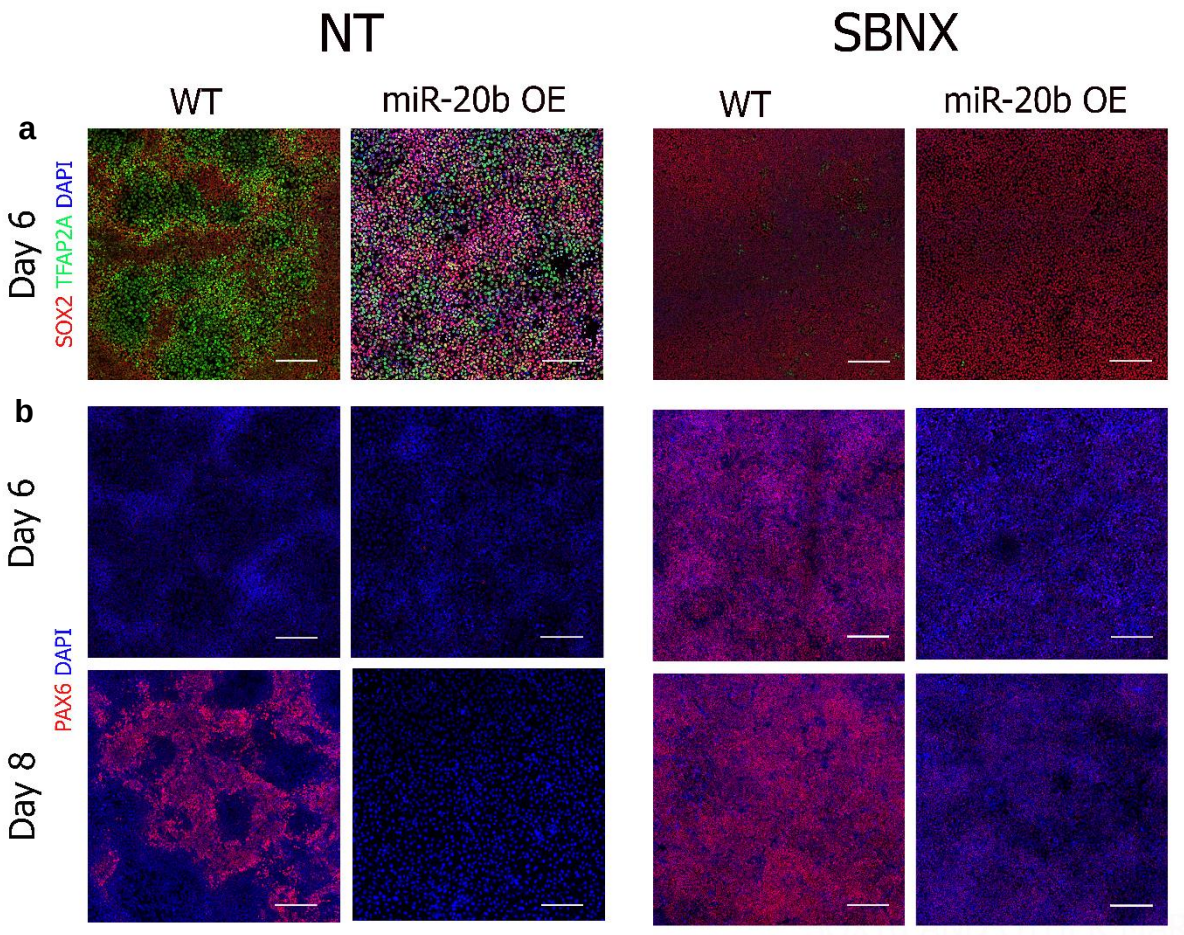

Figure 30: Overexpression of miR-20b in early days of differentiation identified a unique progenitor population

a) Immunostaining images of SOX2/TFAP2A in day 6 neural differentiated cells for wild type and miR-20b overexpressing cells under inhibitor free (NT) and Triple-i (SBNX) differentiation paradigm (Scale bar: 200µm)
b) Immunostaining images of PAX6 in day 6 (top) and day 8 (bottom) neural differentiated cells for wild type and miR-20b OE cells under inhibitor free and triple-I differentiation paradigm (Scale bar: 200µm)

4. DISCUSSION

Pluripotent stem cells (PSCs) serve as an unlimited homogenous cell source for the production of different cell types of interest because of their enormous ability to self-replicate indefinitely *in vitro* while retaining the potential for multi-lineage differentiation. The immense capacity of PSCs to maintain differentiation potential towards distinct cell types makes them an indispensable tool for developmental studies, disease modelling and regenerative medicine applications (Ebert et al., 2012; Keller, 2005; Sterneckert et al., 2014). However, one of the major challenges is to device differentiation schemes that can generate homogenous cell types of interest *in vitro* using PSCs.

The advent of PSCs has revolutionized our understandings of brain development and modelling neurodegenerative disorders that are otherwise hard to access and model. Brain development is a protracted process that starts with a simple tube-like structure known as neural tube consisting of a single layer of epithelial cells called neuroepithelial cells—founder neural stem cells (NSCs). Neural stem cells are building blocks of brain development that can be isolated from the embryonic neural tube *in vivo* as well as can also be derived from PSCs *in vitro*. Similar to PSCs, NSCs are also known to hold high proliferative capacity while retaining multipotency – that is the potential to differentiate into three neural lineages – neurons, astrocytes and oligodendrocytes. However, these founder NSCs are heterogeneous with respect to different brain regions including cerebral cortex, archicortex, hypothalamus, mid-brain and hind-brain.

This study has been aimed to identify early signals—miRNAs that modulate temporal and regional fates within this early founder NSCs populations. To achieve this, we first derived neural stem cells from PSCs *in vitro* and propagated them long-term in culture in both 2D monolayer and 3D organoids model systems and then identified early neural stem stage-specific microRNAs using microRNA sequencing. We next identified hsa-miR-20b as one of the highest differentially expressed microRNAs in early NSCs as compared to late NSCs.

To know whether hsa-miR-20b plays an important role in either temporal progression or regionalization of cortex, we employed an inducible model system to overexpress this microRNA at early days of organoid differentiation and analysed them at different

time points of organoid development. Single cell RNA-Sequencing at early day 13 of organoid development revealed early exit from pluripotency in miR-20b over expressed organoids. In addition, we found an enhanced caudal cortical brain regional fates in neural stem cell clusters with an upregulation of genes such as HES5, GLI3, EMX2, and FEZF2. Simultaneously, we observed a down regulation of anterior/rostral cortical specific genes such as FZD5, FZD8, SIX3 in miR-20b overexpressed organoids, suggesting miR-20b over expression favors the caudal cortical fates (Lagutin et al., 2003). This finding was further supported by an upregulation of genes such as WNT2B, WLS, WNT7B, and BMP7 that were known to be involved in posteriorizing of the telencephalon. The WNT and BMP family genes in particular have been known as morphogens that play an important role in patterning neuroectoderm towards caudal telencephalic structures such as the archi cortex consisting of cortical hem, hippocampus and choroid plexus (Grove et al., 1998). Altogether, the upregulation of WNT/BMP signaling molecules and simultaneous downregulation of anterior telencephalic genes in early NSCs, indicates the regionalization of early cortical NSCs towards more caudal telencephalic NSCs.

To further probe in development, we next analysed day 30 wildtype and miR-20b overexpressing organoids through single cell RNA-Sequencing. It has been shown by different labs that day 30 of organoid development corresponds to 21 post conception weeks (PCW) brain of human gestation. At this stage of development, organoids already establish different cell types/zones including VZ consisting of apical radial glial cells, SVZ consisting of intermediate progenitors (IPs) and cortical plate with deep layer neurons such as TBR1 and CTIP2 neurons. Firstly, we confirmed that day 30 wildtype organoids were more developed as compared to day 13 with the presence of additional cell types including clusters (25 clusters in day 30 Vs 7 clusters in day 13) of cortical NSCs, emergence of IPs, early neurons, and even some non-neural cell identities. When compared to wildtype, miR-20b overexpressed organoids displayed a decrease in cortical NSCs and IPs while increase in neuronal populations such as layer 5 (TBR1+, CTIP2/BCL11B+, FOXP2-), and layer 6 (TBR1+ FOXP2+ TLE4+) suggesting precocious differentiation of miR-20b overexpressed NSC/progenitor cells. Interestingly, FOXP2 specific neurons have never been observed *in vitro* wildtype organoids even in later days of development, suggesting miR-20b improved *in vitro* neuronal differentiation signals. It has previously been shown that blockade of Wnt

pathway promotes self-renewal capacity of neural progenitor cells (NPCs) and inhibition of neural differentiation *in vitro* as well as in the developing mouse neocortex (Hirabayashi et al., 2004; Lie et al., 2005; Muroyama et al., 2004). Nevertheless, the precise mechanism of how the Wnt pathway induces neural differentiation has not been elucidated yet (Muroyama et al., 2004). In addition, it has also been shown in rat NPCs that miR-20b overexpression leads to downregulation of REST protein which in turn activate WNT pathway leading to differentiation of NPCs towards neurons (Cui et al., 2016). In the context of posterior cortical/telencephalic fates, we have identified an increase in the percentage of hippocampal NSCs and emergence of cajal-retzius neurons which are known to be derived from hippocampal NSCs (Frotscher, 1998; Marín-Padilla, 1998; Del Río et al., 1997) in miR-20b overexpressing organoids. Altogether, miR-20b overexpression resulted in the depletion of cortical NSC and IP pool by precociously differentiating them towards deep layer neurons, along with an increase in the percentage of hippocampal NSCs, suggesting a shift in the regional identity from rostral cortical cell types to caudal cortical fates.

Cytoarchitectural studies using immunofluorescence revealed that wildtype organoids display profuse, bulk vesicles consisting of multiple zones including ventricular zone—positive for neural stem cell marker-SOX2, sub-ventricular zone marked by TBR2, and cortical plate with early cortical neuro-TBR1, and thus recapitulating *in vivo* cortical cytoarchitecture. While in miR-20b overexpressing organoids we found small rosettes, and distorted vesicles along with drastic decrease in the IP population suggesting lacking lateral expansion of ventricular zone. Moreover, cellular analyses confirm the earlier transcriptome results displaying increased neuronal population over cortical progenitors and a shift in caudal cortical fates in miR-20b overexpressed organoids.

To further delineate the long-term effect of miR-20b with respect to telencephalic/cortex regionalization. We next analysed mirR-20b overexpressing day 50 organoids and observed a marked decrease in cortical fates as evident by downregulation of genes such as PAX6, and FOXG1 and a concomitant upregulation of cortical hem, hippocampal and choroid plexus populations marked by genes such as WLS, RSPO3, and TTR in cortical NSCs. These findings in turn could be directly due to the continuous overexpression of mir-20b resulted in regulating the gene networks that promotes the shift in cell identities towards more caudal telencephalon

i.e., hippocampal and choroid plexus fates or indirectly due to the enhanced WNT and BMP pathways in earlier days of organoid resulted in progressive downregulation of cortical fates and a stepwise concomitant upregulation of caudal telencephalic fates. This is in line with a previous finding which has shown that the downregulation of cortical specific gene Foxg1 expression leads to a simultaneous upregulation of hippocampal genes in mouse cortex (Godbole et al., 2018). Another reason might be the conversion of hippocampal population towards choroid plexus tissue in the presence of WNT and BMP signalling molecules. Further experimental evidence through lineage tracing might be required to prove which hypothesis can be correct. Cellular analyses revealed a striking appearance of giant thin single layered like vesicles co-expressing with choroid plexuses markers such as LMX1A and TTR in miR-20b organoids as opposed to bulk cortical vesicles with pseudostratified VZ, SVZ and cortical plate in wildtype organoids. Surprisingly, we found a decreased cortical neuronal population in day 50 miR-20b organoids contrary to day 30 miR-20b organoids and supposed to be continued in later days of organoids. Further experimental evidence is required to know whether the cortical neuronal cell type underwent apoptosis and lost or a change in their cell identity occurred with the appearance of a simultaneous favourable niche that helped choroid plexus lineages to populate and thus overtaking the entirety of organoid.

We next looked for what targets of miR-20b be responsible for the decreased cortical NSCs and IPs and an increase in posterior telencephalic fates in miR-20b overexpressed organoids. We then found CCND1 as one of its main cell cycle related targets and indeed its levels are decreased in both NSCs and IPs of miR-20b overexpressed organoids. Therefore, we decided to compensate the CCND1 expression levels in these miR-20b overexpressing cell types to give a proliferative advantage to these effected cell types. Interestingly, we observed the re-appearance of thick layered neuroepithelial vesicles in CCND1 compensated miR20b overexpressing organoids similar to wild type. Surprisingly, we observed the presence of enormous cortical hem/hippocampal stem cell populations in CCND1 compensate miR-20b organoids while the cortical NSCs are still scarce and not rescued. This could be due to CCND1 may not be the only target of miR-20b but just a part of a regulatory cascade of cell identity change which thus may be insufficient to bring a shift in cell identity back to cortical fates. The second reason could be the levels of CCND1

compensation gave a proliferative advantage to hippocampal stem cells to over populate in organoids leaving the cortical stem cells untouched. Another reason might be due to the existence of a feedback regulation between cyclin D1 and miR-20b which reveals that the expression levels of CCND1 is sensitive to miRNA dosage (Ghosh et al., 2014). Cyclin D1 binds to the promoter of miR-20b and induces the expression of miR-20b and in turn miR-20b binding to CCND1 3' UTR and decreases its level (Ghosh et al., 2014). The CCND1 cDNA used in this study for the generation of CCND1 compensating miR-20b overexpressing cell line is without the 3' UTR and therefore, it will not undergo the miR-20b mediated degradation. Thus, in the CCND1 compensate miR-20b overexpressing organoids, an upregulation of CCND1 (without the 3'UTR) eventually induces the higher levels of expression of miR-20b breaking the feedback loop. Thus, there is a cumulative increase in the expression of miR-20b which in turn could lead to an increase in the WNT and BMP signalling molecules much more than what is observed earlier in miR-20b only overexpressing organoids. Hence, this increased miR-20b ultimately prompted to the emergence of higher percentage of hippocampal stem cells and choroid plexus cells in CCND1 compensated miR-20b overexpressing organoids.

In line, a recent study published by Lancaster and colleagues shown the generation of choroid plexus (ChP) organoids by using a pulse of BMP-4 and CHIR small molecule activators which enhance BMP and WNT signalling (Pellegrini et al., 2020). These human ChP organoids mimicked *in vivo* choroid plexus tissue including selective barrier permeability to small molecules and cerebral-spinal fluid (CSF) like secretions. Transcriptomic and proteomic signature of these human ChP organoids displayed much similarities to its *in vivo* counterpart. Nonetheless, the knowledge of prominent transcription factors, and transcriptional regulators such as miRNAs that are significant for the formation of Choroid plexus (ChP) is still underway. In this study, we have advanced a step and identified an early-stage neural stem cell specific miRNA 20b-5p, when continuously expressed in cortical organoids for long-term (at least till day50) eventually converts them into choroid plexus tissue like identity. This could be due to the generation of NSCs of day 13 miR-20b overexpressing organoids with significantly higher level of WLS, WNT7B, WNT2B and BMP7, in turn acting as a progenitor source for generating the choroid plexus tissue identity at later stage of organoid development. This suggest that miR-20b role in upregulation of WNT and

BMP signalling inherently causing the caudalization of the cortical organoids to choroid plexus identity. In line with this notion, we have found that Sakaguchi H and colleagues have previously generated a hippocampus, and choroid plexus structures by using a hESC-FOXG1 reporter line. First, they have generated cortical spheroids using TGF-beta and WNT-inhibition conditions for 18 days and then cultured these cortical spheroids with small molecule activators like BMP-4 and CHIR from day 18 onwards till late days (at least till day42). This led to an eventual shift in cortical identity towards the choroid plexus tissue identity. They have demonstrated the downregulation of FOXG1 expression among these cortical spheroids with the simultaneous generation of a single thin neuroepithelial layer of choroid plexus structures indicating the caudalization of cortical fate to choroid plexus fate (Sakaguchi et al., 2015). Similarly, in my study, we have observed that the cortical NSCs present in earlier day 30 of miR-20b organoids are plastic enough to change their fate from cortical towards caudal cortical regions such as choroid plexus and hippocampus fates in later days of organoid development.

To conclude, this study delineates miR-20b as one of the important regulatory elements involved in the induction of choroid plexus tissue—a critical brain structure that secretes cerebrospinal fluid (CSF) and acts as a blood brain barrier for selective transport of substances in the brain (Liddelow, 2015). Hence, the knowledge about the induction of this important brain structures *in vitro* as ChP organoids will help us to screen already known and novel drug compounds with differential CNS permeability and thus are indispensable to develop effective drug therapeutics against neurodegenerative diseases like Alzheimer’s, Parkinson’s, and Schizophrenia etc. This model system can also be used to identify specific early biomarkers for neuropsychiatric diseases such as schizophrenia, where choroid plexus structure is affected and the patients release neuroinflammatory molecules in to cerebrospinal fluid. In addition, this platform could be used to model diseases caused by FOXP2 mutation leading to cognitive dysfunctions and autism like phenotypes (Gong et al., 2004; Li et al., 2005) as well as to study genetic variation/mutation that causes changes in hippocampus size/volume eventually leading to neuropsychiatric disorders.

5. REFERENCES

1. Aaku-Saraste, E., Hellwig, A., and Huttner, W.B. (1996). Loss of occludin and functional tight junctions, but not ZO-1, during neural tube closure--remodeling of the neuroepithelium prior to neurogenesis. Dev Biol *180*, 664–679.
2. Acampora, D., Avantaggiato, V., Tuorto, F., Briata, P., Corte, G., and Simeone, A. (1998). Visceral endoderm-restricted translation of Otx1 mediates recovery of Otx2 requirements for specification of anterior neural plate and normal gastrulation. Development *125*, 5091–5104.
3. Alarcón, C.R., Lee, H., Goodarzi, H., Halberg, N., and Tavazoie, S.F. (2015). N6-methyladenosine marks primary microRNAs for processing. Nature *519*, 482–485.
4. Andersson, T., Rahman, S., Sansom, S.N., Alsiö, J.M., Kaneda, M., Smith, J., O'Carroll, D., Tarakhovsky, A., and Livesey, F.J. (2010). Reversible block of mouse neural stem cell differentiation in the absence of dicer and microRNAs. PLoS One *5*, e13453.
5. Babiarz, J.E., Ruby, J.G., Wang, Y., Bartel, D.P., and Blelloch, R. (2008). Mouse ES cells express endogenous shRNAs, siRNAs, and other Microprocessor-independent, Dicer-dependent small RNAs. Genes Dev *22*, 2773–2785.
6. Bachiller, D., Klingensmith, J., Kemp, C., Belo, J.A., Anderson, R.M., May, S.R., McMahon, J.A., McMahon, A.P., Harland, R.M., Rossant, J., et al. (2000). The organizer factors Chordin and Noggin are required for mouse forebrain development. Nature *403*, 658–661.
7. Baghbaderani, B.A., Syama, A., Sivapatham, R., Pei, Y., Mukherjee, O., Fellner, T., Zeng, X., and Rao, M.S. (2016). Detailed Characterization of Human Induced Pluripotent Stem Cells Manufactured for Therapeutic Applications. Stem Cell Rev *12*, 394–420.
8. Bartel, D.P. (2004). MicroRNAs: genomics, biogenesis, mechanism, and function. Cell *116*, 281–297.
9. Beddington, R.S. (1994). Induction of a second neural axis by the mouse node. Development *120*, 613–620.
10. Beddington, R.S., and Robertson, E.J. (1998). Anterior patterning in mouse. Trends Genet *14*, 277–284.
11. Beers, J., Gulbranson, D.R., George, N., Siniscalchi, L.I., Jones, J., Thomson, J.A., and Chen, G. (2012). Passaging and colony expansion of human pluripotent stem cells by enzyme-free dissociation in chemically defined culture conditions. Nat Protoc *7*, 2029–2040.
12. Bernstein, E., Kim, S.Y., Carmell, M.A., Murchison, E.P., Alcorn, H., Li, M.Z., Mills, A.A., Elledge, S.J., Anderson, K. V, and Hannon, G.J. (2003). Dicer is essential for mouse development. Nat Genet *35*, 215–217.

13. Bhaskaran, M., and Mohan, M. (2014). MicroRNAs: History, Biogenesis, and Their Evolving Role in Animal Development and Disease. Vet. Pathol. *51*, 759–774.
14. Bian, S., and Su, T. (2012). Noncoding RNAs in Neural Stem Cell Development. In Neural Stem Cells and Therapy, (InTech), p.
15. Bian, S., Hong, J., Li, Q., Schebelle, L., Pollock, A., Knauss, J.L., Garg, V., and Sun, T. (2013). MicroRNA cluster miR-17-92 regulates neural stem cell expansion and transition to intermediate progenitors in the developing mouse neocortex. Cell Rep *3*, 1398–1406.
16. Bilic, J., and Izpisua Belmonte, J.C. (2012). Concise review: Induced pluripotent stem cells versus embryonic stem cells: close enough or yet too far apart? Stem Cells *30*, 33–41.
17. Biology, B. Developmental Biology 3230.
18. Blauwkamp, T.A., Nigam, S., Ardehali, R., Weissman, I.L., and Nusse, R. (2012). Endogenous Wnt signalling in human embryonic stem cells generates an equilibrium of distinct lineage-specified progenitors. Nat Commun *3*, 1070.
19. Bolger, A.M., Lohse, M., and Usadel, B. (2014). Trimmomatic: a flexible trimmer for Illumina sequence data. Bioinformatics *30*, 2114–2120.
20. Bonev, B., Pisco, A., and Papalopulu, N. (2011). MicroRNA-9 reveals regional diversity of neural progenitors along the anterior-posterior axis. Dev Cell *20*, 19–32.
21. Bonni, A., Sun, Y., Nadal-Vicens, M., Bhatt, A., Frank, D.A., Rozovsky, I., Stahl, N., Yancopoulos, G.D., and Greenberg, M.E. (1997). Regulation of gliogenesis in the central nervous system by the JAK-STAT signaling pathway. Science (80-.). *278*, 477–483.
22. Bouwmeester, T., Kim, S., Sasai, Y., Lu, B., and De Robertis, E.M. (1996). Cerberus is a head-inducing secreted factor expressed in the anterior endoderm of Spemann's organizer. Nature *382*, 595–601.
23. Cai, X., Hagedorn, C.H., and Cullen, B.R. (2004). Human microRNAs are processed from capped, polyadenylated transcripts that can also function as mRNAs. Rna *10*, 1957–1966.
24. Campbell, K., and Gotz, M. (2002). Radial glia: multi-purpose cells for vertebrate brain development. Trends Neurosci *25*, 235–238.
25. Camus, A., Perea-Gomez, A., Moreau, A., and Collignon, J. (2006). Absence of Nodal signaling promotes precocious neural differentiation in the mouse embryo. Dev Biol *295*, 743–755.
26. Cattaneo, E., and McKay, R. (1990). Proliferation and differentiation of neuronal stem cells regulated by nerve growth factor. Nature *347*, 762–765.
27. Chambers, S.M., Fasano, C.A., Papapetrou, E.P., Tomishima, M., Sadelain, M., and Studer, L. (2009). Highly efficient neural conversion of human ES and iPS cells by dual inhibition of SMAD signaling. Nat. Biotechnol. *27*, 275–280.

28. Chaulk, S.G., Thede, G.L., Kent, O.A., Xu, Z., Gesner, E.M., Veldhoen, R.A., Khanna, S.K., Goping, I.S., MacMillan, A.M., Mendell, J.T., et al. (2011). Role of pri-miRNA tertiary structure in miR-17~92 miRNA biogenesis. RNA Biol. *8*.
29. Cheloufi, S., Dos Santos, C.O., Chong, M.M., and Hannon, G.J. (2010). A dicer-independent miRNA biogenesis pathway that requires Ago catalysis. Nature *465*, 584–589.
30. Cheng, L.C., Pastrana, E., Tavazoie, M., and Doetsch, F. (2009). miR-124 regulates adult neurogenesis in the subventricular zone stem cell niche. Nat Neurosci *12*, 399–408.
31. Chiang, H.R., Schoenfeld, L.W., Ruby, J.G., Auyeung, V.C., Spies, N., Baek, D., Johnston, W.K., Russ, C., Luo, S., Babiarz, J.E., et al. (2010). Mammalian microRNAs: experimental evaluation of novel and previously annotated genes. Genes Dev *24*, 992–1009.
32. Cooper, J.A. (2008). A mechanism for inside-out lamination in the neocortex. Trends Neurosci. *31*, 113–119.
33. Cowan, C.A., Atienza, J., Melton, D.A., and Eggan, K. (2005). Nuclear reprogramming of somatic cells after fusion with human embryonic stem cells. Science (80-.). *309*, 1369–1373.
34. Cox, W.G., and Hemmati-Brivanlou, A. (1995). Caudalization of neural fate by tissue recombination and bFGF. Development *121*, 4349–4358.
35. Cui, Y., Han, J., Xiao, Z., Chen, T., Wang, B., Chen, B., Liu, S., Han, S., Fang, Y., Wei, J., et al. (2016). The miR-20-Rest-Wnt signaling axis regulates neural progenitor cell differentiation. Sci Rep *6*, 23300.
36. D'Arcangelo, G., Miao, G.G., Chen, S.C., Soares, H.D., Morgan, J.I., and Curran, T. (1995). A protein related to extracellular matrix proteins deleted in the mouse mutant reeler. Nature *374*, 719–723.
37. Davis, T.H., Cuellar, T.L., Koch, S.M., Barker, A.J., Harfe, B.D., McManus, M.T., and Ullian, E.M. (2008). Conditional loss of Dicer disrupts cellular and tissue morphogenesis in the cortex and hippocampus. J Neurosci *28*, 4322–4330.
38. Dehay, C., and Kennedy, H. (2007). Cell-cycle control and cortical development. Nat Rev Neurosci *8*, 438–450.
39. Delaloy, C., Liu, L., Lee, J.A., Su, H., Shen, F., Yang, G.Y., Young, W.L., Ivey, K.N., and Gao, F.B. (2010). MicroRNA-9 coordinates proliferation and migration of human embryonic stem cell-derived neural progenitors. Cell Stem Cell *6*, 323–335.
40. Delaunay, D., Kawaguchi, A., Dehay, C., and Matsuzaki, F. (2017). Division modes and physical asymmetry in cerebral cortex progenitors. Curr Opin Neurobiol *42*, 75–83.
41. Denli, A.M., Tops, B.B., Plasterk, R.H., Ketting, R.F., and Hannon, G.J. (2004). Processing of primary microRNAs by the Microprocessor complex. Nature *432*, 231–235.

42. Desbaillets, I., Ziegler, U., Groscurth, P., and Gassmann, M. (2000). Embryoid bodies: an in vitro model of mouse embryogenesis. Exp Physiol *85*, 645–651.
43. Di-Gregorio, A., Sancho, M., Stuckey, D.W., Crompton, L.A., Godwin, J., Mishina, Y., and Rodriguez, T.A. (2007). BMP signalling inhibits premature neural differentiation in the mouse embryo. Development *134*, 3359–3369.
44. Dobin, A., Davis, C.A., Schlesinger, F., Drenkow, J., Zaleski, C., Jha, S., Batut, P., Chaisson, M., and Gingeras, T.R. (2013). STAR: ultrafast universal RNA-seq aligner. Bioinformatics *29*, 15–21.
45. Durston, A.J., Timmermans, J.P., Hage, W.J., Hendriks, H.F., de Vries, N.J., Heideveld, M., and Nieuwkoop, P.D. (1989). Retinoic acid causes an anteroposterior transformation in the developing central nervous system. Nature *340*, 140–144.
46. Ebert, A.D., Liang, P., and Wu, J.C. (2012). Induced pluripotent stem cells as a disease modeling and drug screening platform. J Cardiovasc Pharmacol *60*, 408–416.
47. Edri, R., Yaffe, Y., Ziller, M.J., Mutukula, N., Volkman, R., David, E., Jacob-Hirsch, J., Malcov, H., Levy, C., Rechavi, G., et al. (2015). Analysing human neural stem cell ontogeny by consecutive isolation of Notch active neural progenitors. Nat Commun *6*, 6500.
48. Eiraku, M., Watanabe, K., Matsuo-Takasaki, M., Kawada, M., Yonemura, S., Matsumura, M., Wataya, T., Nishiyama, A., Muguruma, K., and Sasai, Y. (2008). Self-organized formation of polarized cortical tissues from ESCs and its active manipulation by extrinsic signals. Cell Stem Cell *3*, 519–532.
49. Elkabetz, Y., and Studer, L. (2008). Human ESC-derived neural rosettes and neural stem cell progression. Cold Spring Harb Symp Quant Biol *73*, 377–387.
50. Elkabetz, Y., Panagiotakos, G., Al Shamy, G., Socci, N.D., Tabar, V., and Studer, L. (2008). Human ES cell-derived neural rosettes reveal a functionally distinct early neural stem cell stage. Genes Dev *22*, 152–165.
51. Englund, C., Fink, A., Lau, C., Pham, D., Daza, R.A., Bulfone, A., Kowalczyk, T., and Hevner, R.F. (2005). Pax6, Tbr2, and Tbr1 are expressed sequentially by radial glia, intermediate progenitor cells, and postmitotic neurons in developing neocortex. J Neurosci *25*, 247–251.
52. Evans, M.J., and Kaufman, M.H. (1981). Establishment in culture of pluripotential cells from mouse embryos. Nature *292*, 154–156.
53. Eyal-Giladi, H. (1954). Dynamic aspects of neural induction in amphibia. Arch Biol *65*, 179–259.
54. Fededa, J.P., Esk, C., Mierzwa, B., Stanyte, R., Yuan, S., Zheng, H., Ebnet, K., Yan, W., Knoblich, J.A., and Gerlich, D.W. (2016). MicroRNA-34/449 controls mitotic spindle orientation during mammalian cortex development. Embo J *35*, 2386–2398.

55. Fellmann, C., Hoffmann, T., Sridhar, V., Hopfgartner, B., Muhar, M., Roth, M., Lai, D.Y., Barbosa, I.A., Kwon, J.S., Guan, Y., et al. (2013). An optimized microRNA backbone for effective single-copy RNAi. Cell Rep *5*, 1704–1713.
56. Fietz, S.A., Kelava, I., Vogt, J., Wilsch-Bräuninger, M., Stenzel, D., Fish, J.L., Corbeil, D., Riehn, A., Distler, W., Nitsch, R., et al. (2010). OSVZ progenitors of human and ferret neocortex are epithelial-like and expand by integrin signaling. Nat Neurosci *13*, 690–699.
57. Florio, M., and Huttner, W.B. (2014). Neural progenitors, neurogenesis and the evolution of the neocortex. Development *141*, 2182–2194.
58. Florio, M., Heide, M., Pinson, A., Brandl, H., Albert, M., Winkler, S., Wimberger, P., Huttner, W.B., and Hiller, M. (2018). Evolution and cell-type specificity of human-specific genes preferentially expressed in progenitors of fetal neocortex. Elife *7*.
59. Foley, A.C., Skromne, I., and Stern, C.D. (2000). Reconciling different models of forebrain induction and patterning: a dual role for the hypoblast. Development *127*, 3839–3854.
60. Frantz, G.D., and McConnell, S.K. (1996). Restriction of late cerebral cortical progenitors to an upper-layer fate. Neuron *17*, 55–61.
61. Fraser, S.E. a. . (2004). Early rostrocaudal patterning of the mesoderm and neural plate. In: Gastrulation: from cells to embryo. (ed. C.D. Stern). Cold Spring Harb. Press 389–402.
62. Frotscher, M. (1998). Cajal-Retzius cells, Reelin, and the formation of layers. Curr. Opin. Neurobiol. *8*, 570–575.
63. Fukagawa, T., Nogami, M., Yoshikawa, M., Ikeno, M., Okazaki, T., Takami, Y., Nakayama, T., and Oshimura, M. (2004). Dicer is essential for formation of the heterochromatin structure in vertebrate cells. Nat Cell Biol *6*, 784–791.
64. Gadue, P., Huber, T.L., Paddison, P.J., and Keller, G.M. (2006). Wnt and TGF-beta signaling are required for the induction of an in vitro model of primitive streak formation using embryonic stem cells. Proc Natl Acad Sci U S A *103*, 16806–16811.
65. Gage, F.H. (2000). Mammalian neural stem cells. Science (80-.). *287*, 1433–1438.
66. Gage, F.H., and Temple, S. (2013). Neural stem cells: generating and regenerating the brain. Neuron *80*, 588–601.
67. Gaiano, N., Nye, J.S., and Fishell, G. (2000). Radial glial identity is promoted by Notch1 signaling in the murine forebrain. Neuron *26*, 395–404.
68. Gammill, L.S., and Bronner-Fraser, M. (2003). Neural crest specification: migrating into genomics. Nat Rev Neurosci *4*, 795–805.
69. Gerhart, J. (1999). Pieter Nieuwkoop's contributions to the understanding of meso-endoderm induction and neural induction in chordate development. Int J Dev Biol *43*, 605–613.
70. Ghildiyal, M., and Zamore, P.D. (2009). Small silencing RNAs: an expanding universe.

Nat Rev Genet *10*, 94–108.

71. Ghosh, T., Aprea, J., Nardelli, J., Engel, H., Selinger, C., Mombereau, C., Lemonnier, T., Moutkine, I., Schwendimann, L., Dori, M., et al. (2014). MicroRNAs establish robustness and adaptability of a critical gene network to regulate progenitor fate decisions during cortical neurogenesis. Cell Rep *7*, 1779–1788.
72. Giraldez, A.J., Cinalli, R.M., Glasner, M.E., Enright, A.J., Thomson, J.M., Baskerville, S., Hammond, S.M., Bartel, D.P., and Schier, A.F. (2005). MicroRNAs regulate brain morphogenesis in zebrafish. Science (80-.). *308*, 833–838.
73. Godbole, G., Shetty, A.S., Roy, A., D'Souza, L., Chen, B., Miyoshi, G., Fishell, G., and Tole, S. (2018). Hierarchical genetic interactions between FOXG1 and LHX2 regulate the formation of the cortical hem in the developing telencephalon. Dev. *145*.
74. Gong, X., Jia, M., Ruan, Y., Shuang, M., Liu, J., Wu, S., Guo, Y., Yang, J., Ling, Y., Yang, X., et al. (2004). Association between the FOXP2 gene and autistic disorder in Chinese population. Am J Med Genet B Neuropsychiatr Genet *127b*, 113–116.
75. González-Castillo, C., Ortuño-Sahagún, D., Guzmán-Brambila, C., Pallàs, M., and Rojas-Mayorquín, A.E. (2015). Pleiotrophin as a central nervous system neuromodulator, evidences from the hippocampus. Front. Cell. Neurosci. *8*, 443.
76. Götz, M., Stoykova, A., and Gruss, P. (1998). Pax6 controls radial glia differentiation in the cerebral cortex. Neuron *21*, 1031–1044.
77. Graus-Porta, D., Blaess, S., Senften, M., Littlewood-Evans, A., Damsky, C., Huang, Z., Orban, P., Klein, R., Schittny, J.C., and Müller, U. (2001). Beta1-class integrins regulate the development of laminae and folia in the cerebral and cerebellar cortex. Neuron *31*, 367–379.
78. Greig, L.C., Woodworth, M.B., Galazo, M.J., Padmanabhan, H., and Macklis, J.D. (2013). Molecular logic of neocortical projection neuron specification, development and diversity. Nat Rev Neurosci *14*, 755–769.
79. Grishok, A., Pasquinelli, A.E., Conte, D., Li, N., Parrish, S., Ha, I., Baillie, D.L., Fire, A., Ruvkun, G., and Mello, C.C. (2001). Genes and mechanisms related to RNA interference regulate expression of the small temporal RNAs that control C. elegans developmental timing. Cell *106*, 23–34.
80. Grove, E.A., Tole, S., Limon, J., Yip, L., and Ragsdale, C.W. (1998). The hem of the embryonic cerebral cortex is defined by the expression of multiple Wnt genes and is compromised in Gli3-deficient mice. Development *125*, 2315–2325.
81. Gu, K.L., Zhang, Q., Yan, Y., Li, T.T., Duan, F.F., Hao, J., Wang, X.W., Shi, M., Wu, D.R., Guo, W.T., et al. (2016). Pluripotency-associated miR-290/302 family of microRNAs promote the dismantling of naive pluripotency. Cell Res *26*, 350–366.
82. Guo, H., Ingolia, N.T., Weissman, J.S., and Bartel, D.P. (2010). Mammalian microRNAs

predominantly act to decrease target mRNA levels. Nature *466*, 835–840.

83. Gurdon, J.B. (1962). The developmental capacity of nuclei taken from intestinal epithelium cells of feeding tadpoles. J Embryol Exp Morphol *10*, 622–640.
84. Ha, M., and Kim, V.N. (2014). Regulation of microRNA biogenesis. Nat Rev Mol Cell Biol *15*, 509–524.
85. Hadjantonakis, A.-K. The MAmmalian Blastocyst: Development and Stem Cells.
86. Hafner, M., Landthaler, M., Burger, L., Khorshid, M., Hausser, J., Berninger, P., Rothballer, A., Ascano Jr., M., Jungkamp, A.C., Munschauer, M., et al. (2010). Transcriptome-wide identification of RNA-binding protein and microRNA target sites by PAR-CLIP. Cell *141*, 129–141.
87. Hamazaki, T., El Rouby, N., Fredette, N.C., Santostefano, K.E., and Terada, N. (2017). Concise Review: Induced Pluripotent Stem Cell Research in the Era of Precision Medicine. Stem Cells *35*, 545–550.
88. Han, J., Lee, Y., Yeom, K.H., Kim, Y.K., Jin, H., and Kim, V.N. (2004). The Drosha-DGCR8 complex in primary microRNA processing. Genes Dev *18*, 3016–3027.
89. Hansen, D. V, Lui, J.H., Parker, P.R., and Kriegstein, A.R. (2010). Neurogenic radial glia in the outer subventricular zone of human neocortex. Nature *464*, 554–561.
90. Hébert, S.S., Papadopoulou, A.S., Smith, P., Galas, M.C., Planel, E., Silahtaroglu, A.N., Sergeant, N., Buée, L., and de Strooper, B. (2010). Genetic ablation of dicer in adult forebrain neurons results in abnormal tau hyperphosphorylation and neurodegeneration. Hum. Mol. Genet. *19*, 3959–3969.
91. Heisenberg, C.P., Houart, C., Take-Uchi, M., Rauch, G.J., Young, N., Coutinho, P., Masai, I., Caneparo, L., Concha, M.L., Geisler, R., et al. (2001). A mutation in the Gsk3-binding domain of zebrafish Masterblind/Axin1 leads to a fate transformation of telencephalon and eyes to diencephalon. Genes Dev *15*, 1427–1434.
92. Helwak, A., Kudla, G., Dudnakova, T., and Tollervey, D. (2013). Mapping the human miRNA interactome by CLASH reveals frequent noncanonical binding. Cell *153*, 654–665.
93. Hemmati-Brivanlou, A., and Melton, D.A. (1994). Inhibition of activin receptor signaling promotes neuralization in Xenopus. Cell *77*, 273–281.
94. Hirabayashi, Y., Itoh, Y., Tabata, H., Nakajima, K., Akiyama, T., Masuyama, N., and Gotoh, Y. (2004). The Wnt/beta-catenin pathway directs neuronal differentiation of cortical neural precursor cells. Development *131*, 2791–2801.
95. Hiramatsu, R., Matsuoka, T., Kimura-Yoshida, C., Han, S.W., Mochida, K., Adachi, T., Takayama, S., and Matsuo, I. (2013). External mechanical cues trigger the establishment of the anterior-posterior axis in early mouse embryos. Dev Cell *27*, 131–144.
96. Houbaviy, H.B., Murray, M.F., and Sharp, P.A. (2003). Embryonic stem cell-specific

MicroRNAs. Dev Cell *5*, 351–358.

97. Inui, M., Montagner, M., Ben-Zvi, D., Martello, G., Soligo, S., Manfrin, A., Aragona, M., Enzo, E., Zacchigna, L., Zanconato, F., et al. (2012). Self-regulation of the head-inducing properties of the Spemann organizer. Proc Natl Acad Sci U S A *109*, 15354–15359.
98. Ishikawa, Y., Yamamoto, N., Yoshimoto, M., and Ito, H. (2012). The primary brain vesicles revisited: are the three primary vesicles (forebrain/midbrain/hindbrain) universal in vertebrates? Brain Behav Evol *79*, 75–83.
99. Itskovitz-Eldor, J., Schuldiner, M., Karsenti, D., Eden, A., Yanuka, O., Amit, M., Soreq, H., and Benvenisty, N. (2000). Differentiation of human embryonic stem cells into embryoid bodies compromising the three embryonic germ layers. Mol Med *6*, 88–95.
100. Jönsson, M.E., Nelander Wahlestedt, J., Åkerblom, M., Kirkeby, A., Malmevik, J., Brattaas, P.L., Jakobsson, J., and Parmar, M. (2015). Comprehensive analysis of microRNA expression in regionalized human neural progenitor cells reveals microRNA-10 as a caudalizing factor. Development *142*, 3166–3177.
101. Kadoshima, T., Sakaguchi, H., Nakano, T., Soen, M., Ando, S., Eiraku, M., and Sasai, Y. (2013). Self-organization of axial polarity, inside-out layer pattern, and species-specific progenitor dynamics in human ES cell-derived neocortex. Proc Natl Acad Sci U S A *110*, 20284–20289.
102. Kanellopoulou, C., Muljo, S.A., Kung, A.L., Ganesan, S., Drapkin, R., Jenuwein, T., Livingston, D.M., and Rajewsky, K. (2005). Dicer-deficient mouse embryonic stem cells are defective in differentiation and centromeric silencing. Genes Dev *19*, 489–501.
103. Kawase-Koga, Y., Low, R., Otaegi, G., Pollock, A., Deng, H., Eisenhaber, F., Maurer-Stroh, S., and Sun, T. (2010). RNAase-III enzyme Dicer maintains signaling pathways for differentiation and survival in mouse cortical neural stem cells. J Cell Sci *123*, 586–594.
104. Keller, G. (2005). Embryonic stem cell differentiation: emergence of a new era in biology and medicine. Genes Dev *19*, 1129–1155.
105. Kelly, O.G., Pinson, K.I., and Skarnes, W.C. (2004). The Wnt co-receptors Lrp5 and Lrp6 are essential for gastrulation in mice. Development *131*, 2803–2815.
106. Ketting, R.F., Fischer, S.E., Bernstein, E., Sijen, T., Hannon, G.J., and Plasterk, R.H. (2001). Dicer functions in RNA interference and in synthesis of small RNA involved in developmental timing in C. elegans. Genes Dev *15*, 2654–2659.
107. Khvorova, A., Reynolds, A., and Jayasena, S.D. (2003). Functional siRNAs and miRNAs exhibit strand bias. Cell *115*, 209–216.
108. Kiecker, C., and Niehrs, C. (2001). A morphogen gradient of Wnt/beta-catenin signalling regulates anteroposterior neural patterning in Xenopus. Development *128*, 4189–4201.
109. Kim, Y.K., and Kim, V.N. (2007). Processing of intronic microRNAs. Embo J *26*, 775–783.
110. Kim, V.N., Han, J., and Siomi, M.C. (2009). Biogenesis of small RNAs in animals. Nat

Rev Mol Cell Biol *10*, 126–139.

111. Kim, Y.K., Wee, G., Park, J., Kim, J., Baek, D., Kim, J.S., and Kim, V.N. (2013). TALEN-based knockout library for human microRNAs. Nat Struct Mol Biol *20*, 1458–1464.
112. Kozomara, A., and Griffiths-Jones, S. (2014). miRBase: annotating high confidence microRNAs using deep sequencing data. Nucleic Acids Res *42*, D68-73.
113. Krichevsky, A.M., Sonntag, K.C., Isacson, O., and Kosik, K.S. (2006). Specific microRNAs modulate embryonic stem cell-derived neurogenesis. Stem Cells *24*, 857–864.
114. Kumamoto, T., and Hanashima, C. (2014). Neuronal subtype specification in establishing mammalian neocortical circuits. Neurosci. Res. *86*, 37–49.
115. Kwan, K.Y., Sestan, N., and Anton, E.S. (2012). Transcriptional co-regulation of neuronal migration and laminar identity in the neocortex. Development *139*, 1535–1546.
116. Lagos-Quintana, M., Rauhut, R., Yalcin, A., Meyer, J., Lendeckel, W., and Tuschl, T. (2002). Identification of tissue-specific microRNAs from mouse. Curr Biol *12*, 735–739.
117. Laguesse, S., Peyre, E., and Nguyen, L. (2015). Progenitor genealogy in the developing cerebral cortex. Cell Tissue Res *359*, 17–32.
118. Lagutin, O. V., Zhu, C.C., Kobayashi, D., Topczewski, J., Shimamura, K., Puelles, L., Russell, H.R.C., McKinnon, P.J., Solnica-Krezel, L., and Oliver, G. (2003). Six3 repression of Wnt signaling in the anterior neuroectoderm is essential for vertebrate forebrain development. Genes Dev. *17*, 368–379.
119. Lamb, T.M., and Harland, R.M. (1995). Fibroblast growth factor is a direct neural inducer, which combined with noggin generates anterior-posterior neural pattern. Development *121*, 3627–3636.
120. Lancaster, M.A., and Knoblich, J.A. (2014). Generation of cerebral organoids from human pluripotent stem cells. Nat Protoc *9*, 2329–2340.
121. Lancaster, M.A., Renner, M., Martin, C.A., Wenzel, D., Bicknell, L.S., Hurles, M.E., Homfray, T., Penninger, J.M., Jackson, A.P., and Knoblich, J.A. (2013). Cerebral organoids model human brain development and microcephaly. Nature *501*, 373–379.
122. Lange, C., Huttner, W.B., and Calegari, F. (2009). Cdk4/cyclinD1 overexpression in neural stem cells shortens G1, delays neurogenesis, and promotes the generation and expansion of basal progenitors. Cell Stem Cell *5*, 320–331.
123. Lee, R.C., Feinbaum, R.L., and Ambros, V. (1993). The C. elegans heterochronic gene lin-4 encodes small RNAs with antisense complementarity to lin-14. Cell *75*, 843–854.
124. Lee, Y., Kim, M., Han, J., Yeom, K.H., Lee, S., Baek, S.H., and Kim, V.N. (2004). MicroRNA genes are transcribed by RNA polymerase II. Embo J *23*, 4051–4060.
125. Levine, A.J., and Brivanlou, A.H. (2007). Proposal of a model of mammalian neural induction. Dev Biol *308*, 247–256.

126. Li, B., and Dewey, C.N. (2011). RSEM: accurate transcript quantification from RNA-Seq data with or without a reference genome. BMC Bioinformatics *12*, 323.
127. Li, H., Yamagata, T., Mori, M., and Momoi, M.Y. (2005). Absence of causative mutations and presence of autism-related allele in FOXP2 in Japanese autistic patients. Brain Dev *27*, 207–210.
128. Li, L., Liu, C., Biechele, S., Zhu, Q., Song, L., Lanner, F., Jing, N., and Rossant, J. (2013). Location of transient ectodermal progenitor potential in mouse development. Development *140*, 4533–4543.
129. Liddelow, S.A. (2015). Development of the choroid plexus and blood-CSF barrier. Front. Neurosci. *9*.
130. Lie, D.-C., Colamarino, S.A., Song, H.-J., Désiré, L., Mira, H., Consiglio, A., Lein, E.S., Jessberger, S., Lansford, H., Dearie, A.R., et al. (2005). Wnt signalling regulates adult hippocampal neurogenesis. Nature *437*, 1370–1375.
131. Liguori, G.L., Echevarria, D., Improta, R., Signore, M., Adamson, E., Martinez, S., and Persico, M.G. (2003). Anterior neural plate regionalization in cripto null mutant mouse embryos in the absence of node and primitive streak. Dev Biol *264*, 537–549.
132. Lodato, S., and Arlotta, P. (2015). Generating Neuronal Diversity in the Mammalian Cerebral Cortex. Annu. Rev. Cell Dev. Biol. *31*, 699–720.
133. Love, M.I., Huber, W., and Anders, S. (2014). Moderated estimation of fold change and dispersion for RNA-seq data with DESeq2. Genome Biol *15*, 550.
134. Lu, C.C., Brennan, J., and Robertson, E.J. (2001). From fertilization to gastrulation: axis formation in the mouse embryo. Curr Opin Genet Dev *11*, 384–392.
135. Lui, J.H., Hansen, D. V, and Kriegstein, A.R. (2011). Development and evolution of the human neocortex. Cell *146*, 18–36.
136. Lumsden, A., and Krumlauf, R. (1996). Patterning the vertebrate neuraxis. Science (80-.). *274*, 1109–1115.
137. Makarova, J.A., Shkurnikov, M.U., Wicklein, D., Lange, T., Samatov, T.R., Turchinovich, A.A., and Tonevitsky, A.G. (2016). Intracellular and extracellular microRNA: An update on localization and biological role. Prog Histochem Cytochem *51*, 33–49.
138. Makeyev, E. V, Zhang, J., Carrasco, M.A., and Maniatis, T. (2007). The MicroRNA miR-124 promotes neuronal differentiation by triggering brain-specific alternative pre-mRNA splicing. Mol Cell *27*, 435–448.
139. Malatesta, P., Hartfuss, E., and Götz, M. (2000). Isolation of radial glial cells by fluorescent-activated cell sorting reveals a neuronal lineage. Development *127*, 5253–5263.
140. Manabe, N., Hirai, S., Imai, F., Nakanishi, H., Takai, Y., and Ohno, S. (2002). Association of ASIP/mPAR-3 with adherens junctions of mouse neuroepithelial cells. Dev Dyn *225*,

61–69.

141. Mangold, O. (1933). ?ber die Induktionsf?higkeit der verschiedenen Bezirke der Neurula von Urodelen. Naturwissenschaften *21*, 761–766.
142. Mariani, J., Simonini, M. V, Palejev, D., Tomasini, L., Coppola, G., Szekely, A.M., Horvath, T.L., and Vaccarino, F.M. (2012). Modeling human cortical development in vitro using induced pluripotent stem cells. Proc Natl Acad Sci U S A *109*, 12770–12775.
143. Marikawa, Y. (2006). Wnt/β-catenin signaling and body plan formation in mouse embryos. Semin. Cell Dev. Biol. *17*, 175–184.
144. Marikawa, Y., and Alarcon, V.B. (2009). Establishment of trophectoderm and inner cell mass lineages in the mouse embryo. Mol Reprod Dev *76*, 1019–1032.
145. Marín-Padilla, M. (1998). Cajal-Retzius cells and the development of the neocortex. Trends Neurosci. *21*, 64–71.
146. Marson, A., Levine, S.S., Cole, M.F., Frampton, G.M., Brambrink, T., Johnstone, S., Guenther, M.G., Johnston, W.K., Wernig, M., Newman, J., et al. (2008). Connecting microRNA genes to the core transcriptional regulatory circuitry of embryonic stem cells. Cell *134*, 521–533.
147. Martin, G.R. (1981). Isolation of a pluripotent cell line from early mouse embryos cultured in medium conditioned by teratocarcinoma stem cells. Proc Natl Acad Sci U S A *78*, 7634–7638.
148. McMahon, A.P., Joyner, A.L., Bradley, A., and McMahon, J.A. (1992). The midbrain-hindbrain phenotype of Wnt-1-/Wnt-1- mice results from stepwise deletion of engrailed-expressing cells by 9.5 days postcoitum. Cell *69*, 581–595.
149. Megason SG, M.A. A mitogen gradient of dorsal midline Wnts organizes growth in the CNS. Development *129*, 2087–08.
150. Meijer, H.A., Smith, E.M., and Bushell, M. (2014). Regulation of miRNA strand selection: follow the leader? Biochem Soc Trans *42*, 1135–1140.
151. Mitsui, K., Tokuzawa, Y., Itoh, H., Segawa, K., Murakami, M., Takahashi, K., Maruyama, M., Maeda, M., and Yamanaka, S. (2003). The homeoprotein Nanog is required for maintenance of pluripotency in mouse epiblast and ES cells. Cell *113*, 631–642.
152. Miura, S., Singh, A.P., and Mishina, Y. (2010). Bmpr1a is required for proper migration of the AVE through regulation of Dkk1 expression in the pre-streak mouse embryo. Dev Biol *341*, 246–254.
153. Miyata, T., Kawaguchi, A., Saito, K., Kawano, M., Muto, T., and Ogawa, M. (2004). Asymmetric production of surface-dividing and non-surface-dividing cortical progenitor cells. Development *131*, 3133–3145.
154. Mukhopadhyay, M., Shtrom, S., Rodriguez-Esteban, C., Chen, L., Tsukui, T., Gomer, L., Dorward, D.W., Glinka, A., Grinberg, A., Huang, S.P., et al. (2001). Dickkopf1 is required

for embryonic head induction and limb morphogenesis in the mouse. Dev Cell *1*, 423–434.

155. Muroyama, Y., Kondoh, H., and Takada, S. (2004). Wnt proteins promote neuronal differentiation in neural stem cell culture. Biochem Biophys Res Commun *313*, 915–921.
156. Mutukula N*, R.R. (2021). Emergence of outer sub-ventricular zone cells in cerebral organoids exhibiting homogeneous cortical NSC identity. Commun. with Nat. Cell Biol.
157. Nieuwkoop, P.D. (1952). Activation and organization of the central nervous system in amphibians. Part II. Differentiation and organization. J. Exp. Zool. *120*, 33–81.
158. Nieuwkoop, P.D. (1952). No TitleActivation and organization of the central nervous system in amphibians. Part I. Induction and activation. J. Exp. Zool. *120*, 1–31.
159. Nikolopoulou, E., Galea, G.L., Rolo, A., Greene, N.D., and Copp, A.J. (2017). Neural tube closure: cellular, molecular and biomechanical mechanisms. Development *144*, 552–566.
160. Niwa, H., Burdon, T., Chambers, I., and Smith, A. (1998). Self-renewal of pluripotent embryonic stem cells is mediated via activation of STAT3. Genes Dev. *12*, 2048–2060.
161. Noctor, S.C., Flint, A.C., Weissman, T.A., Dammerman, R.S., and Kriegstein, A.R. (2001). Neurons derived from radial glial cells establish radial units in neocortex. Nature *409*, 714–720.
162. Nordstrom, U., Jessell, T.M., and Edlund, T. (2002). Progressive induction of caudal neural character by graded Wnt signaling. Nat Neurosci *5*, 525–532.
163. O'Brien, J., Hayder, H., Zayed, Y., and Peng, C. (2018). Overview of MicroRNA Biogenesis, Mechanisms of Actions, and Circulation. Front Endocrinol *9*, 402.
164. Obernosterer, G., Leuschner, P.J.F., Alenius, M., and Martinez, J. (2006). Post-transcriptional regulation of microRNA expression. RNA *12*, 1161–1167.
165. Okada, C., Yamashita, E., Lee, S.J., Shibata, S., Katahira, J., Nakagawa, A., Yoneda, Y., and Tsukihara, T. (2009). A high-resolution structure of the pre-microRNA nuclear export machinery. Science (80-.). *326*, 1275–1279.
166. Okita, K., Matsumura, Y., Sato, Y., Okada, A., Morizane, A., Okamoto, S., Hong, H., Nakagawa, M., Tanabe, K., Tezuka, K.I., et al. (2011). A more efficient method to generate integration-free human iPS cells. Nat. Methods *8*, 409–412.
167. Ozsolak, F., Poling, L.L., Wang, Z., Liu, H., Liu, X.S., Roeder, R.G., Zhang, X., Song, J.S., and Fisher, D.E. (2008). Chromatin structure analyses identify miRNA promoters. Genes Dev. *22*, 3172–3183.
168. Parthasarathy, S., Srivatsa, S., Nityanandam, A., and Tarabykin, V. (2014). Ntf3 acts downstream of Sip1 in cortical postmitotic neurons to control progenitor cell fate through feedback signaling. Development *141*, 3324–3330.
169. Pasca, A.M., Sloan, S.A., Clarke, L.E., Tian, Y., Makinson, C.D., Huber, N., Kim, C.H., Park, J.Y., O'Rourke, N.A., Nguyen, K.D., et al. (2015). Functional cortical neurons and

astrocytes from human pluripotent stem cells in 3D culture. Nat Methods *12*, 671–678.

170. Pellegrini, L., Bonfio, C., Chadwick, J., Begum, F., Skehel, M., and Lancaster, M.A. (2020). Human CNS barrier-forming organoids with cerebrospinal fluid production. Science (80-.). *369*.

171. Perea-Gomez, A., Vella, F.D., Shawlot, W., Oulad-Abdelghani, M., Chazaud, C., Meno, C., Pfister, V., Chen, L., Robertson, E., Hamada, H., et al. (2002). Nodal antagonists in the anterior visceral endoderm prevent the formation of multiple primitive streaks. Dev Cell *3*, 745–756.

172. Pfeffer, S., Sewer, A., Lagos-Quintana, M., Sheridan, R., Sander, C., Grässer, F.A., van Dyk, L.F., Ho, C.K., Shuman, S., Chien, M., et al. (2005). Identification of microRNAs of the herpesvirus family. Nat Methods *2*, 269–276.

173. De Pietri Tonelli, D., Pulvers, J.N., Haffner, C., Murchison, E.P., Hannon, G.J., and Huttner, W.B. (2008). miRNAs are essential for survival and differentiation of newborn neurons but not for expansion of neural progenitors during early neurogenesis in the mouse embryonic neocortex. Development *135*, 3911–3921.

174. Pilaz, L.J., Patti, D., Marcy, G., Ollier, E., Pfister, S., Douglas, R.J., Betizeau, M., Gautier, E., Cortay, V., Doerflinger, N., et al. (2009). Forced G1-phase reduction alters mode of division, neuron number, and laminar phenotype in the cerebral cortex. Proc Natl Acad Sci U S A *106*, 21924–21929.

175. Placantonakis, D.G., Tomishima, M.J., Lafaille, F., Desbordes, S.C., Jia, F., Socci, N.D., Viale, A., Lee, H., Harrison, N., Tabar, V., et al. (2009). BAC Transgenesis in Human Embryonic Stem Cells as a Novel Tool to Define the Human Neural Lineage. Stem Cells *27*, 521–532.

176. Pogue, A.I., Cui, J.G., Li, Y.Y., Zhao, Y., Culicchia, F., and Lukiw, W.J. (2010). Micro RNA-125b (miRNA-125b) function in astrogliosis and glial cell proliferation. Neurosci. Lett. *476*, 18–22.

177. Pollen, A.A., Nowakowski, T.J., Chen, J., Retallack, H., Sandoval-Espinosa, C., Nicholas, C.R., Shuga, J., Liu, S.J., Oldham, M.C., Diaz, A., et al. (2015). Molecular identity of human outer radial glia during cortical development. Cell *163*, 55–67.

178. Qian, X., Nguyen, H.N., Song, M.M., Hadiono, C., Ogden, S.C., Hammack, C., Yao, B., Hamersky, G.R., Jacob, F., Zhong, C., et al. (2016). Brain-Region-Specific Organoids Using Mini-bioreactors for Modeling ZIKV Exposure. Cell *165*, 1238–1254.

179. Quadrato, G., Nguyen, T., Macosko, E.Z., Sherwood, J.L., Min Yang, S., Berger, D.R., Maria, N., Scholvin, J., Goldman, M., Kinney, J.P., et al. (2017). Cell diversity and network dynamics in photosensitive human brain organoids. Nature *545*, 48–53.

180. Radakovits, R., Barros, C.S., Belvindrah, R., Patton, B., and Müller, U. (2009). Regulation of radial glial survival by signals from the meninges. J Neurosci *29*, 7694–7705.

181. Rakic, P. (2009). Evolution of the neocortex: a perspective from developmental biology. Nat Rev Neurosci *10*, 724–735.
182. Reinhart, B.J., Slack, F.J., Basson, M., Pasquienelll, A.E., Bettlnger, J.C., Rougvle, A.E., Horvitz, H.R., and Ruvkun, G. (2000). The 21-nucleotide let-7 RNA regulates developmental timing in Caenorhabditis elegans. Nature *403*, 901–906.
183. Rhinn, M., Dierich, A., Le Meur, M., and Ang, S. (1999). Cell autonomous and non-cell autonomous functions of Otx2 in patterning the rostral brain. Development *126*, 4295–4304.
184. de Rie, D., Abugessaisa, I., Alam, T., Arner, E., Arner, P., Ashoor, H., Åström, G., Babina, M., Bertin, N., Burroughs, A.M., et al. (2017). An integrated expression atlas of miRNAs and their promoters in human and mouse. Nat Biotechnol *35*, 872–878.
185. Del Río, J.A., Heimrich, B., Borrell, V., Förster, E., Drakew, A., Alcántara, S., Nakajima, K., Miyata, T., Ogawa, M., Mikoshiba, K., et al. (1997). A role for Cajal-retzius cells and reelin in the development of hippocampal connections. Nature *385*, 70–74.
186. Robinton, D.A., and Daley, G.Q. (2012). The promise of induced pluripotent stem cells in research and therapy. Nature *481*, 295–305.
187. Rodriguez, A., Vigorito, E., Clare, S., Warren, M. V, Couttet, P., Soond, D.R., van Dongen, S., Grocock, R.J., Das, P.P., Miska, E.A., et al. (2007). Requirement of bic/microRNA-155 for normal immune function. Science (80-.). *316*, 608–611.
188. Romero, D.M., Bahi-Buisson, N., and Francis, F. (2018). Genetics and mechanisms leading to human cortical malformations. Semin. Cell Dev. Biol. *76*, 33–75.
189. Rosenbluth, E.M., Shelton, D.N., Sparks, A.E., Devor, E., Christenson, L., and Van Voorhis, B.J. (2013). MicroRNA expression in the human blastocyst. Fertil Steril *99*, 855-861.e3.
190. Roush, S., and Slack, F.J. (2008). The let-7 family of microRNAs. Trends Cell Biol *18*, 505–516.
191. Ruby, J.G., Jan, C.H., and Bartel, D.P. (2007). Intronic microRNA precursors that bypass Drosha processing. Nature *448*, 83–86.
192. Rybak, A., Fuchs, H., Smirnova, L., Brandt, C., Pohl, E.E., Nitsch, R., and Wulczyn, F.G. (2008). A feedback loop comprising lin-28 and let-7 controls pre-let-7 maturation during neural stem-cell commitment. Nat Cell Biol *10*, 987–993.
193. Sakaguchi, H., Kadoshima, T., Soen, M., Narii, N., Ishida, Y., Ohgushi, M., Takahashi, J., Eiraku, M., and Sasai, Y. (2015). Generation of functional hippocampal neurons from self-organizing human embryonic stem cell-derived dorsomedial telencephalic tissue. Nat Commun *6*, 8896.
194. Salomoni, P., and Calegari, F. (2010). Cell cycle control of mammalian neural stem cells: putting a speed limit on G1. Trends Cell Biol *20*, 233–243.

195. Sauer, F.C. (1935). Mitosis in the neural tube. J. Comp. Neurol. *62*, 377–405.
196. Sauer, M.E., and Walker, B.E. (1959). Radioautographic study of interkinetic nuclear migration in the neural tube. Proc Soc Exp Biol Med *101*, 557–560.
197. Seuntjens, E., Nityanandam, A., Miquelajauregui, A., Debruyn, J., Stryjewska, A., Goebbels, S., Nave, K.A., Huylebroeck, D., and Tarabykin, V. (2009). Sip1 regulates sequential fate decisions by feedback signaling from postmitotic neurons to progenitors. Nat Neurosci *12*, 1373–1380.
198. Shi, Y., Wang, Y., Luan, W., Wang, P., Tao, T., Zhang, J., Qian, J., Liu, N., and You, Y. (2014). Long non-coding RNA H19 promotes glioma cell invasion by deriving miR-675. PLoS One *9*.
199. Shibata, M., Nakao, H., Kiyonari, H., Abe, T., and Aizawa, S. (2011). MicroRNA-9 regulates neurogenesis in mouse telencephalon by targeting multiple transcription factors. J Neurosci *31*, 3407–3422.
200. Singh S.;, R.. M. (2020). Embryology, Neural Tube. (Treasure Island (Florida): STARPEARLS), p.
201. Slack, F.J., Basson, M., Liu, Z., Ambros, V., Horvitz, H.R., and Ruvkun, G. (2000). The lin-41 RBCC gene acts in the C. elegans heterochronic pathway between the let-7 regulatory RNA and the LIN-29 transcription factor. Mol Cell *5*, 659–669.
202. Smirnova, L., Gräfe, A., Seiler, A., Schumacher, S., Nitsch, R., and Wulczyn, F.G. (2005). Regulation of miRNA expression during neural cell specification. Eur. J. Neurosci. *21*, 1469–1477.
203. Sousa, A.M.M., Meyer, K.A., Santpere, G., Gulden, F.O., and Sestan, N. (2017). Evolution of the Human Nervous System Function, Structure, and Development. Cell *170*, 226–247.
204. Srinivas, S. (2006). The anterior visceral endoderm-turning heads. Genesis *44*, 565–572.
205. Stappert, L., Borghese, L., Roese-Koerner, B., Weinhold, S., Koch, P., Terstegge, S., Uhrberg, M., Wernet, P., and Brüstle, O. (2013). MicroRNA-based promotion of human neuronal differentiation and subtype specification. PLoS One *8*, e59011.
206. Sterneckert, J.L., Reinhardt, P., and Schöler, H.R. (2014). Investigating human disease using stem cell models. Nat Rev Genet *15*, 625–639.
207. Strominger, N.L., Demarest, R.J., and Laemle, L.B. (2012). Cerebral Cortex. In Noback's Human Nervous System, Seventh Edition, (Humana Press), pp. 429–451.
208. Suh, M.R., Lee, Y., Kim, J.Y., Kim, S.K., Moon, S.H., Lee, J.Y., Cha, K.Y., Chung, H.M., Yoon, H.S., Moon, S.Y., et al. (2004). Human embryonic stem cells express a unique set of microRNAs. Dev Biol *270*, 488–498.
209. Suzuki, I.K., Gacquer, D., Van Heurck, R., Kumar, D., Wojno, M., Bilheu, A., Herpoel, A., Lambert, N., Cheron, J., Polleux, F., et al. (2018). Human-Specific NOTCH2NL Genes

Expand Cortical Neurogenesis through Delta/Notch Regulation. Cell *173*, 1370-1384.e16.

210. Sylvestre, Y., De Guire, V., Querido, E., Mukhopadhyay, U.K., Bourdeau, V., Major, F., Ferbeyre, G., and Chartrand, P. (2007). An E2F/miR-20a autoregulatory feedback loop. J Biol Chem *282*, 2135–2143.
211. Tada, M., Takahama, Y., Abe, K., Nakatsuji, N., and Tada, T. (2001). Nuclear reprogramming of somatic cells by in vitro hybridization with ES cells. Curr Biol *11*, 1553–1558.
212. Takahashi, K., and Yamanaka, S. (2006). Induction of Pluripotent Stem Cells from Mouse Embryonic and Adult Fibroblast Cultures by Defined Factors. Cell *126*, 663–676.
213. Takaoka, K., Yamamoto, M., and Hamada, H. (2007). Origin of body axes in the mouse embryo. Curr Opin Genet Dev *17*, 344–350.
214. Tam, P.P., and Behringer, R.R. (1997). Mouse gastrulation: the formation of a mammalian body plan. Mech Dev *68*, 3–25.
215. Tam, P.P., and Steiner, K.A. (1999). Anterior patterning by synergistic activity of the early gastrula organizer and the anterior germ layer tissues of the mouse embryo. Development *126*, 5171–5179.
216. Tanzer, A., and Stadler, P.F. (2004). Molecular evolution of a microRNA cluster. J Mol Biol *339*, 327–335.
217. Taverna, E., Götz, M., and Huttner, W.B. (2014). The cell biology of neurogenesis: toward an understanding of the development and evolution of the neocortex. Annu Rev Cell Dev Biol *30*, 465–502.
218. Tchieu, J., Zimmer, B., Fattahi, F., Amin, S., Zeltner, N., Chen, S., and Studer, L. (2017). A Modular Platform for Differentiation of Human PSCs into All Major Ectodermal Lineages. Cell Stem Cell *21*, 399-410.e7.
219. Temple, S. (2001). The development of neural stem cells. Nature *414*, 112–117.
220. Thomas, K.R., and Capecchi, M.R. (1990). Targeted disruption of the murine int-1 proto-oncogene resulting in severe abnormalities in midbrain and cerebellar development. Nature *346*, 847–850.
221. Thomas P. Naidich Pedro Pasik, E.A.N. Cerebral Cortex (Radiology Key).
222. Thomson, J.A. (1998). Embryonic stem cell lines derived from human blastocysts. Science (80-.). *282*, 1145–1147.
223. Thomson, J.M., Parker, J., Perou, C.M., and Hammond, S.M. (2004). A custom microarray platform for analysis of microRNA gene expression. Nat Methods *1*, 47–53.
224. Toma, K., and Hanashima, C. (2015). Switching modes in corticogenesis: mechanisms of neuronal subtype transitions and integration in the cerebral cortex. Front Neurosci *9*, 274.
225. Treutlein, B., Lee, Q.Y., Camp, J.G., Mall, M., Koh, W., Shariati, S.A., Sim, S., Neff, N.F.,

Skotheim, J.M., Wernig, M., et al. (2016). Dissecting direct reprogramming from fibroblast to neuron using single-cell RNA-seq. Nature *534*, 391–395.

226. Tropepe, V., Hitoshi, S., Sirard, C., Mak, T.W., Rossant, J., and van der Kooy, D. (2001). Direct neural fate specification from embryonic stem cells: a primitive mammalian neural stem cell stage acquired through a default mechanism. Neuron *30*, 65–78.
227. Vasudevan, S. (2012). Posttranscriptional upregulation by microRNAs. Wiley Interdiscip Rev RNA *3*, 311–330.
228. Ventura, A., Young, A.G., Winslow, M.M., Lintault, L., Meissner, A., Erkeland, S.J., Newman, J., Bronson, R.T., Crowley, D., Stone, J.R., et al. (2008). Targeted Deletion Reveals Essential and Overlapping Functions of the miR-17~92 Family of miRNA Clusters. Cell *132*, 875–886.
229. Visvanathan, J., Lee, S., Lee, B., Lee, J.W., and Lee, S.K. (2007). The microRNA miR-124 antagonizes the anti-neural REST/SCP1 pathway during embryonic CNS development. Genes Dev *21*, 744–749.
230. Waddington, C.H. (1933). Induction by coagulated organisers in the chick embryo [6]. Nature *131*, 275–276.
231. Wang, Y., Medvid, R., Melton, C., Jaenisch, R., and Blelloch, R. (2007). DGCR8 is essential for microRNA biogenesis and silencing of embryonic stem cell self-renewal. Nat Genet *39*, 380–385.
232. Watanabe, K., Kamiya, D., Nishiyama, A., Katayama, T., Nozaki, S., Kawasaki, H., Watanabe, Y., Mizuseki, K., and Sasai, Y. (2005). Directed differentiation of telencephalic precursors from embryonic stem cells. Nat Neurosci *8*, 288–296.
233. Wheeler, B.M., Heimberg, A.M., Moy, V.N., Sperling, E.A., Holstein, T.W., Heber, S., and Peterson, K.J. (2009). The deep evolution of metazoan microRNAs. Evol Dev *11*, 50–68.
234. Wienholds, E., Koudijs, M.J., van Eeden, F.J., Cuppen, E., and Plasterk, R.H. (2003). The microRNA-producing enzyme Dicer1 is essential for zebrafish development. Nat Genet *35*, 217–218.
235. Wightman, B., Ha, I., and Ruvkun, G. (1993). Posttranscriptional regulation of the heterochronic gene lin-14 by lin-4 mediates temporal pattern formation in C. elegans. Cell *75*, 855–862.
236. Wilmut, I., Schnieke, A.E., McWhir, J., Kind, A.J., and Campbell, K.H. (1997). Viable offspring derived from fetal and adult mammalian cells. Nature *385*, 810–813.
237. Wolf, F.A., Angerer, P., and Theis, F.J. (2018). SCANPY: Large-scale single-cell gene expression data analysis. Genome Biol. *19*.
238. Woods, K., Thomson, J.M., and Hammond, S.M. (2007). Direct regulation of an oncogenic micro-RNA cluster by E2F transcription factors. J Biol Chem *282*, 2130–2134.
239. Wulczyn, F.G., Smirnova, L., Rybak, A., Brandt, C., Kwidzinski, E., Ninnemann, O.,

Strehle, M., Seiler, A., Schumacher, S., and Nitsch, R. (2007). Post-transcriptional regulation of the let-7 microRNA during neural cell specification. Faseb J *21*, 415–426.

240. Xie, M., Li, M., Vilborg, A., Lee, N., Shu, M.D., Yartseva, V., Šestan, N., and Steitz, J.A. (2013). Mammalian 5'-capped microRNA precursors that generate a single microRNA. Cell *155*, 1568–1580.
241. Yamamoto, M., Saijoh, Y., Perea-Gomez, A., Shawlot, W., Behringer, R.R., Ang, S.L., Hamada, H., and Meno, C. (2004). Nodal antagonists regulate formation of the anteroposterior axis of the mouse embryo. Nature *428*, 387–392.
242. Yang, J.S., Maurin, T., Robine, N., Rasmussen, K.D., Jeffrey, K.L., Chandwani, R., Papapetrou, E.P., Sadelain, M., O'Carroll, D., and Lai, E.C. (2010). Conserved vertebrate mir-451 provides a platform for Dicer-independent, Ago2-mediated microRNA biogenesis. Proc Natl Acad Sci U S A *107*, 15163–15168.
243. Ying, Q.L., Stavridis, M., Griffiths, D., Li, M., and Smith, A. (2003). Conversion of embryonic stem cells into neuroectodermal precursors in adherent monoculture. Nat Biotechnol *21*, 183–186.
244. Yoda, M., Kawamata, T., Paroo, Z., Ye, X., Iwasaki, S., Liu, Q., and Tomari, Y. (2010). ATP-dependent human RISC assembly pathways. Nat Struct Mol Biol *17*, 17–23.
245. Yoo, A.S., Sun, A.X., Li, L., Shcheglovitov, A., Portmann, T., Li, Y., Lee-Messer, C., Dolmetsch, R.E., Tsien, R.W., and Crabtree, G.R. (2011). MicroRNA-mediated conversion of human fibroblasts to neurons. Nature *476*, 228–231.
246. Zhadanov, A.B., Provance Jr., D.W., Speer, C.A., Coffin, J.D., Goss, D., Blixt, J.A., Reichert, C.M., and Mercer, J.A. (1999). Absence of the tight junctional protein AF-6 disrupts epithelial cell-cell junctions and cell polarity during mouse development. Curr Biol *9*, 880–888.
247. Zhang, Y.E., and Newfeld, S.J. (2013). Meeting report - TGF-β superfamily: Signaling in development and disease. J. Cell Sci. *126*, 4809–4813.
248. Zhang, H., Kolb, F.A., Jaskiewicz, L., Westhof, E., and Filipowicz, W. (2004). Single processing center models for human Dicer and bacterial RNase III. Cell *118*, 57–68.
249. Zhang, S.C., Wernig, M., Duncan, I.D., Brüstle, O., and Thomson, J.A. (2001a). In vitro differentiation of transplantable neural precursors from human embryonic stem cells. Nat Biotechnol *19*, 1129–1133.
250. Zhang, S.C., Wernig, M., Duncan, I.D., Brüstle, O., and Thomson, J.A. (2001b). In vitro differentiation of transplantable neural precursors from human embryonic stem cells. Nat. Biotechnol. *19*, 1129–1133.
251. Zhao, C., Sun, G., Li, S., Lang, M.F., Yang, S., Li, W., and Shi, Y. (2010). MicroRNA let-7b regulates neural stem cell proliferation and differentiation by targeting nuclear receptor TLX signaling. Proc Natl Acad Sci U S A *107*, 1876–1881.

252. Zheng, K., Li, H., Zhu, Y., Zhu, Q., and Qiu, M. (2010). MicroRNAs are essential for the developmental switch from neurogenesis to gliogenesis in the developing spinal cord. J Neurosci *30*, 8245–8250.
253. Ziller, M.J., Edri, R., Yaffe, Y., Donaghey, J., Pop, R., Mallard, W., Issner, R., Gifford, C.A., Goren, A., Xing, J., et al. (2015). Dissecting neural differentiation regulatory networks through epigenetic footprinting. Nature *518*, 355–359.
254. Zimmer, B., Piao, J., Ramnarine, K., Tomishima, M.J., Tabar, V., and Studer, L. (2016). Derivation of Diverse Hormone-Releasing Pituitary Cells from Human Pluripotent Stem Cells. Stem Cell Reports *6*, 858–872.
255. Ziv, O., Zaritsky, A., Yaffe, Y., Mutukula, N., Edri, R., and Elkabetz, Y. (2015). Quantitative Live Imaging of Human Embryonic Stem Cell Derived Neural Rosettes Reveals Structure-Function Dynamics Coupled to Cortical Development. PLoS Comput Biol *11*, e1004453

6. ABBREVIATIONS

ICM — Inner cell mass

TE — Trophoectoderm

PSC — Pluripotent stem cells

BBB— Blood Brain Barrier

A-P — Anterior-Posterior

TGF-β— Transforming growth factor-beta

BMP— Bone Morphogenetic Protein

APC/C — Anaphase promoting complex / cyclosome

AVE — Anterior visceral endoderm

bHLH — Basic helix-loop-helix

BMP — Bone morphogenetic protein

hESCs —human Embryonic stem cells

TF— Transcription factor

SCNT— somatic cell nuclear transfer

aRG — Apical radial glial

bRG/Cs— Basal radial glial Cells

CC — Coiled coil

CNS — Central nervous system

CP — Cortical plate

DL — Deep layers

UL — Upper layers

CR— Cajal-Retzius

Dkk1 — Dickkopf 1

D-V — Dorso-ventral

EB — Embryoid body

SFEB— Serum free culture of embryoid bodies like culture

ESC — Embryonic stem cells

piRNA— PIWI-interacting RNAs

AGO— Argonaute proteins

L1/L2— First/Second larval Stage

Chip-seq—Chromatin immunoprecipitation

Pri-miRNA—Primary microRNA

Pre-miRNA—Precursor microRNA

DGCR8— DiGeorge Syndrome Critical Region 8

M7G— 7-methylguanosine

shRNA— short hairpin RNA

ncRNAs—Non-coding RNAs

lt-NES— Neuroepithelial like cells

KO— Knockout

HBSS— Hank's Balanced Salt Solution

FACS — Fluorescence activated cell sorting

FGF — Fibroblast growth factor

BDNF—Brain derived growth factor

EGF— Epithelial growth factor

hESC — Human embryonic stem cells

INM — Interkinetic nuclear migration

IP — Intermediate progenitors

iPSC — Induced pluripotent stem cell

MEF — Mouse embryonic fibroblast

mESC — Mouse embryonic stem cells

mPSC — Mouse pluripotent stem cell

NE — Neuroepithelial

ERG — Early Radial Glial

MRG — Mid Radial Glial

LRG — Late Radial Glial

NECD — Notch extracellular domain

NICD — Notch intra cellular domain

NPC — Neural progenitor cell

NSC — Neural stem cells

OSVZ — Outer sub-ventricular zone

RA — Retinoic acid

RG — Radial glial

R-NSC — Rosette neural stem cell

SHH — Sonic Hedgehog

SVZ — Sub-ventricular zone

TM — Transmembrane domain

VZ — Ventricular zone

UPW— Ultra Pure water

SMART— Switching Mechanism at the 5' end of RNA Template

LNA—Locked Nucleic Acid

UMAP—Uniform Manifold Approximation and Projection

7. List of Publications

- **Arora S***, Rosbrock D*, Mutukula N, Haffner M, Elkabetz Y. “Role of early microRNA in cortical development and differentiation”. (Manuscript in preparation)

- Mutukula N*, Rosebrock D*, **Arora S****, Elzbieta G**, Vidal R, Brändl B, Börno S, Timmermann B, Müller FJ, Sauer S, Vingron M and Elkabetz Y “-Combinatorial Pathway Inhibition in Brain Organoids Dictates Distinct Regional, Stem Cell and Cytoarchitectural Signatures in Health and Disease” (in revision Nature *Cell Biology*)

- **Arora S**, Saha S, Roy S, Das M, Jana SS, Malancha Ta “Role of Non-Muscle Myosin II in Human Wharton’s Jelly derived Mesenchymal Stem Cells”. (*Stem Cells Dev*, 2015 Sep DOI: 10.1089/scd.2015.0095).

- Roy S, **Arora S**, Kumari P, Ta M “A simple and Serum-free protocol for Cryopreservation of Human Umbilical Cord as Source of Wharton’s jelly Mesenchymal Stem Cells”. (*Cryobiology*, 2014, DOI: 10.1016/j.cryobiol.2014.03.010)

8. Declaration of Independence

Name: Arora
First name: Sneha

I declare to the Freie Universität Berlin that I have completed the submitted dissertation independently and without the use of sources and aids other than those indicated. The present thesis is free of plagiarism. I have marked as such all statements that are taken literally or in content from other writings. This dissertation has not been submitted in the same or similar form in any previous doctoral procedure.

I agree to have my thesis examined by a plagiarism examination software.

Date: _____ Signature: _____